LONDON'S GLOBAL UNIVERSITY

Retinal bioimaging for neurodegenerative and cardiovascular diseases

Siegfried Karl Wagner

University College London

This thesis is submitted for the degree of

Doctor of Philosophy

July 2023

Supervisors

Professor Pearse Keane

Professor Jugnoo Rahi

Dr Axel Petzold

Professor Mario Cortina-Borja

I, Siegfried Karl Wagner, confirm that the work presented in this thesis is my own. Where information has been derived from other sources, I confirm that this has been indicated in the thesis.

Abstract

Imaging of the retina using new high-resolution techniques enables in-vivo and minimally invasive assessment of the body's cardiovascular, neurological, and metabolic systems. The ability to interrogate these imaging-derived data using advanced statistical and computational approaches has significantly improved in the past 15 years. While retinal signatures of systemic disease ('oculomics') from in-vivo imaging are increasingly postulated, our understanding of the cardiometabolic and neurodegenerative associations with ocular phenotype has been hampered by a lack of large labeled retinal imaging datasets.

In this thesis, I report methods and findings from my analysis of clinical and retinal imaging data from two health datasets – UK Biobank, a prospective cohort study of >500,000 volunteers residing in the UK, and AlzEye, where ophthalmic data from 353,157 patients attending Moorfields Eye Hospital has been deterministically linked with hospital admissions data across England.

I report that acute conditions affecting the retinal vessels (retinal artery occlusion), optic nerve (non-arteritic ischaemic optic neuropathy) and cranial nerves (third, fourth and sixth palsies) represent sentinel events for cardiovascular dysfunction and all-cause mortality bearing implications for the interdisciplinary management of these conditions.

I show that differences in retinal morphology, resembling cardiometabolic, neurodegenerative and inflammatory dysfunction are seen in individuals with

schizophrenia and periodontitis. The observation that individuals with Parkinson's disease exhibit thinner inner nuclear layers, the retinal niche of dopaminergic activity, and that these differences are detectable, on average, seven years prior to clinical diagnosis warrants further attention. Retinal imaging can also reveal insights into the mechanisms of systemic disease - bilateral retinal structural differences in individuals with unilateral amblyopia in childhood has informed a novel finding of heightened cardiometabolic dysfunction in these individuals.

Finally, I demonstrate that while group-level differences exist, individual-level prediction of all-cause dementia using retinal imaging remains challenging and does not confer improved performance beyond sociodemographic and clinical risk factors. Future work should consider high-dimensional modelling approaches, alternative imaging modalities, and more granular case definitions of dementia.

Impact statement

This project leverages local and national health data resources to investigate the relationship between retinal structure and leading causes of morbidity and mortality. At the outset of this project, large scale investigator-led linkage between national hospital admissions data and medical imaging was rare and, at the scale undertaken in this doctoral research (>6 million images), unprecedented. The learnings and experience from establishing AlzEye have been published and informed an NHSx case-study, a trusted research environment development for both academic and non-academic organisations, reviews of UK health research regulation and the work of multiple other local and national research groups. Indeed, the NHS Digital Independent Group Advising on the Release of Data suggested this project could act as “as an exemplar by NHS Digital to help other researchers with their applications”. In an environment increasingly influenced by big data and artificial intelligence, this project has also highlighted several non-technical themes pivotal to any similar project – from privacy-by-design principles to Confidential Advisory Group approvals.

This thesis describes several novel findings linking retinal anatomy and systemic health, using exemplar conditions that include schizophrenia to Parkinson’s disease and periodontal disease. Showcasing the value of eye health biomarkers across the landscape of life sciences has bolstered arguments for the use of retinal imaging in clinical trials and other deep phenotyping studies in these diseases. It has also fostered the development of several new collaborations at the local, national, and international level. Findings from this study have been disseminated widely in both scientific and

non-scientific outlets, including peer-reviewed academic publications, conference presentations, national news media, and public engagement events. Vision is consistently ranked the most treasured sense and the public are naturally fascinated by the prospect of eye scans revealing signs of heart disease, inflammation, and dementia. Feedback from several public engagement activities have highlighted newfound motivation to attend for regular eye checks and participate in prospective observational research involving retinal imaging.

Publications related to this thesis

Kleerekooper I, **Wagner SK**, Trip SA, Plant GT, Petzold A, Keane PA, Khawaja AP. Differentiating glaucoma from chiasmal compression using optical coherence tomography: the macular naso-temporal ratio. Br J Ophthalmol. 2023 Jun 28:bjo-2023-323529. doi: 10.1136/bjo-2023-323529. Epub ahead of print. PMID: 37385651.

Wagner SK, Zhou Y, O'Byrne C, Khawaja AP, Petzold A, Keane PA. Comment on "Race distribution in non-arteritic anterior ischemic optic neuropathy". Am J Ophthalmol. 2023 May 4:S0002-9394(23)00179-4. doi: 10.1016/j.ajo.2023.04.009.

Hannaway N, Zarkali A, Leyland LA, Bremner F, Nicholas JM, **Wagner SK**, Roig M, Keane PA, Toosy A, Chataway J, Weil RS. Visual dysfunction is a better predictor than retinal thickness for dementia in Parkinson's disease. J Neurol Neurosurg Psychiatry. 2023 Apr 20:jnnp-2023-331083. doi: 10.1136/jnnp-2023-331083.

Wagner SK, Cortina-Borja M, Silverstein SM, Zhou Y, Romero-Bascones D, Struyven RR, Trucco E, Mookiah MRK, MacGillivray T, Hogg S, Liu T, Williamson DJ, Pontikos N, Patel PJ, Balaskas K, Alexander DC, Stuart KV, Khawaja AP, Denniston AK, Rahi JS, Petzold A, Keane PA. Association Between Retinal Features From Multimodal Imaging and Schizophrenia. JAMA Psychiatry. 2023 Mar 22:e230171. doi: 10.1001/jamapsychiatry.2023.0171.

Zhou Y, **Wagner SK**, Chia MA, Zhao A, Woodward-Court P, Xu M, Struyven R, Alexander DC, Keane PA. AutoMorph: Automated Retinal Vascular Morphology Quantification Via a Deep Learning Pipeline. Transl Vis Sci Technol. 2022 Jul 8;11(7):12. doi: 10.1167/tvst.11.7.12.

Wagner SK, Hughes F, Cortina-Borja M, Pontikos N, Struyven R, Liu X, Montgomery H, Alexander DC, Topol E, Petersen SE, Balaskas K, Hindley J, Petzold A, Rahi JS, Denniston AK, Keane PA. AlzEye: longitudinal record-level linkage of ophthalmic imaging and hospital admissions of 353 157 patients in London, UK. BMJ Open. 2022 Mar 16;12(3):e058552. doi: 10.1136/bmjopen-2021-058552.

Balal S, J'Bari AS, Hassan A, Sharma A, **Wagner SK**, Pasu S. Capturing the Occult Central Retinal Artery Occlusion Using Optical Coherence Tomography. Curr Eye Res. 2021 Nov;46(11):1762-1767. doi: 10.1080/02713683.2021.1921219. Epub 2021 Apr 30. PMID: 33882770.

Petzold A, Albrecht P, Balcer L, Bekkers E, Brandt AU, Calabresi PA, Deborah OG, Graves JS, Green A, Keane PA, Nij Bijvank JA, Sander JW, Paul F, Saidha S, Villoslada P, **Wagner SK**, Yeh EA; IMSVISUAL, ERN-EYE Consortium. Artificial intelligence extension of the OSCAR-IB criteria. Ann Clin Transl Neurol. 2021 Jul;8(7):1528-1542. doi: 10.1002/acn3.51320.

Chopra R, **Wagner SK**, Keane PA. Optical coherence tomography in the 2020s-outside the eye clinic. Eye (Lond). 2021 Jan;35(1):236-243. PMID: 33168975.

Huemer J, **Wagner SK**, Sim DA. The Evolution of Diabetic Retinopathy Screening Programmes: A Chronology of Retinal Photography from 35 mm Slides to Artificial Intelligence. Clin Ophthalmol. 2020 Jul 20;14:2021-2035. doi: 10.2147/OPTH.S261629. PMID: 32764868; PMCID: PMC7381763.

Wagner SK, Fu DJ, Faes L, Liu X, Huemer J, Khalid H, Ferraz D, Korot E, Kelly C, Balaskas K, Denniston AK, Keane PA. Insights into Systemic Disease through Retinal Imaging-Based Oculomics. Transl Vis Sci Technol. 2020 Feb 12;9(2):6. doi: 10.1167/tvst.9.2.6.

Wagner SK, Romero-Bascones D, Cortina-Borja M, Williamson DJ, Struyven RR, Zhou Y, Patel S, Weil RS, Antoniades CA, Topol EJ, Korot E, Foster PJ, Balaskas K, Ayala U, Barrenechea M, Gabilondo I, Schapira AHV, Khawaja AP, Patel PJ, Rahi JS, Denniston AK, Petzold A, and Keane PA. Retinal optical coherence tomography features associated with incident and prevalent Parkinson's disease. 2023. *Accepted.*

Acknowledgements

The work presented in this thesis has only been possible due to the support, kindness and contribution of many friends, colleagues, mentors, and organisations. I am grateful to the Medical Research Council for granting me a clinical research training fellowship to conduct this work and the Moorfields Biomedical Research Centre, Fight for Sight UK and the National Institute for Health and Care Research for project support.

Learning from each of my four supervisors has been one of life's great privileges, especially during the tempest that was the COVID-19 pandemic. Pearse Keane and I 'built' AlzEye together along with the extraordinary student (and now budding anaesthetist), Fintan Hughes. Since meeting him when I was a medical student and he a registrar, Pearse has provided unwavering support, guidance and cultivated my development as a researcher. Thank you to Jugnoo Rahi, who taught me what it truly means to be an epidemiologist, for honing my critical thinking and for reminding me never to lose sight of our ultimate goal in research, that of public and patient benefit. I also thank Mario Cortina Borja and Axel Petzold for catalysing my scientific interest and recharging my motivation throughout the PhD – from Mueller's findings on axonal degeneration to the artistic hyperbola of Cotán, their passion and research values will resonate with me throughout my career. I am also grateful to two 'informal' supervisors whose mentorship I have benefitted enormously from - Alastair Denniston and Anthony Khawaja. They represent true lodestars for any aspiring clinician academic.

One of the most enjoyable aspects of this PhD has been interdisciplinary collaboration and, I see, as one of the project's greatest successes, the development of new relationships with experts in fields outside ophthalmology, such as Steve Silverstein, Rimona Weil, Chrystalina Antoniades, Iain Chapple and Thomas Dietrich. Each has patiently guided me through their own scientific fields and given me academic sustenance during the PhD.

Special thanks must go to my friends and colleagues in the AlzEye research team, particularly Robbert Struyven, Dom Williamson, Yukun Zhou, David Romero-Bascones and Mateo Gende. None of the work presented here would have been possible without their support. I feel extremely lucky to be a small part of a wonderful group united by a shared ambition to combine ophthalmic and computer science for improving public health.

There are also those 'behind the scenes', but at the forefront of my mind, who have supported me throughout my PhD, especially my partner, Michelle, and my family.

Last but certainly not least, thank you to the patients and members of the public who contribute to health research. It is only because of them that this work has been possible and indeed worth doing.

Research Paper Declarations

UCL Research Paper Declaration Form
referencing the doctoral candidate's own published work(s)

Please use this form to declare if parts of your thesis are already available in another format, e.g. if data, text, or figures:

- *have been uploaded to a preprint server*
- *are in submission to a peer-reviewed publication*
- *have been published in a peer-reviewed publication, e.g. journal, textbook.*

This form should be completed as many times as necessary. For instance, if you have seven thesis chapters, two of which containing material that has already been published, you would complete this form twice.

1. **For a research manuscript that has already been published** (if not yet published, please skip to section 2)

   a) **What is the title of the manuscript?**

   AlzEye: longitudinal record-level linkage of ophthalmic imaging and hospital admissions of 353 157 patients in London, UK

   b) **Please include a link to or doi for the work**

   doi: 10.1136/bmjopen-2021-058552.

   c) **Where was the work published?**

   BMJ Open

   d) **Who published the work?** (e.g. OUP)

   BMJ

   e) **When was the work published?**

   March 16nd 2022

   f) **List the manuscript's authors in the order they appear on the publication**

   Wagner SK, Hughes F, Cortina-Borja M, Pontikos N, Struyven R, Liu X, Montgomery H, Alexander DC, Topol E, Petersen SE, Balaskas K, Hindley J, Petzold A, Rahi JS, Denniston AK, Keane PA.

   g) **Was the work peer reviewed?**

   Yes

   h) **Have you retained the copyright?**

   CC BY-NC License

   i) **Was an earlier form of the manuscript uploaded to a preprint server?** (e.g. medRxiv). If 'Yes', please give a link or doi)

   No

   If 'No', please seek permission from the relevant publisher and check the box next to the below statement:

   ☒

   *I acknowledge permission of the publisher named under **1d** to include in this thesis portions of the publication named as included in **1c**.*

2. **For a research manuscript prepared for publication but that has not yet been published** (if already published, please skip to section 3)

a) **What is the current title of the manuscript?**

Click or tap here to enter text.

b) **Has the manuscript been uploaded to a preprint server?** (e.g. medRxiv; if 'Yes', please give a link or doi)

Click or tap here to enter text.

c) **Where is the work intended to be published?** (e.g. journal names)

Click or tap here to enter text.

d) **List the manuscript's authors in the intended authorship order**

Click or tap here to enter text.

e) **Stage of publication** (e.g. in submission)

Click or tap here to enter text.

3. **For multi-authored work, please give a statement of contribution covering all authors** (if single-author, please skip to section 4)

SKW, AKD and PAK wrote the first draft of the manuscript, which was critically revised by FH, MCB, RS, NP, XL, HM, DCA, ET, SEP, KB, JH, AP and JSR. Authors SKW, FH, NP, HM, JH, AP, JSR, AKD and PAK were involved in the original design of the study. RS, NP and DCA: computer science expertise. JH: information governance. MCB, AP, JSR and AKD provided statistical and epidemiological guidance.

4. **In which chapter(s) of your thesis can this material be found?**

Chapter 4.1 and Chapter 5.1

5. **e-Signatures confirming that the information above is accurate** (this form should be co-signed by the supervisor/ senior author unless this is not appropriate, e.g. if the paper was a single-author work)

Candidate
Siegfried Wagner
Date:
1st May 2023

Supervisor/ Senior Author (where appropriate)
Pearse Keane
Date
1st May 2023

UCL Research Paper Declaration Form

referencing the doctoral candidate's own published work(s)

Please use this form to declare if parts of your thesis are already available in another format, e.g. if data, text, or figures:

- *have been uploaded to a preprint server*
- *are in submission to a peer-reviewed publication*
- *have been published in a peer-reviewed publication, e.g. journal, textbook.*

This form should be completed as many times as necessary. For instance, if you have seven thesis chapters, two of which containing material that has already been published, you would complete this form twice.

1. **For a research manuscript that has already been published** (if not yet published, please skip to section 2)

   j) **What is the title of the manuscript?**

   Association Between Retinal Features From Multimodal Imaging and Schizophrenia

   k) **Please include a link to or doi for the work**

   doi:10.1001/jamapsychiatry.2023.0171

   l) **Where was the work published?**

   JAMA Psychiatry

   m) **Who published the work?** (e.g. OUP)

   JAMA Network

   n) **When was the work published?**

   March 22nd 2023

   o) **List the manuscript's authors in the order they appear on the publication**

   Wagner SK, Cortina-Borja M, Silverstein SM, Zhou Y, Romero-Bascones D, Struyven RR, Trucco E, Mookiah MRK, MacGillivray T, Hogg S, Liu T, Williamson DJ, Pontikos N, Patel PJ, Balaskas K, Alexander DC, Stuart KV, Khawaja AP, Denniston AK, Rahi JS, Petzold A, Keane PA.

   p) **Was the work peer reviewed?**

   Yes

   q) **Have you retained the copyright?**

   No

   r) **Was an earlier form of the manuscript uploaded to a preprint server?** (e.g. medRxiv). If 'Yes', please give a link or doi)

   No

   If 'No', please seek permission from the relevant publisher and check the box next to the below statement:

   ☒

   *I acknowledge permission of the publisher named under **1d** to include in this thesis portions of the publication named as included in **1c**.*

2. **For a research manuscript prepared for publication but that has not yet been published** (if already published, please skip to section 3)

   f) **What is the current title of the manuscript?**

Click or tap here to enter text.

g) **Has the manuscript been uploaded to a preprint server?** (e.g. medRxiv; if 'Yes', please give a link or doi)

Click or tap here to enter text.

h) **Where is the work intended to be published?** (e.g. journal names)

Click or tap here to enter text.

i) **List the manuscript's authors in the intended authorship order**

Click or tap here to enter text.

j) **Stage of publication** (e.g. in submission)

Click or tap here to enter text.

3. **For multi-authored work, please give a statement of contribution covering all authors** (if single-author, please skip to section 4)

Concept and design: Wagner, Struyven, Patel, Balaskas, Denniston, Petzold, Keane.
Acquisition, analysis, or interpretation of data: Wagner, Cortina-Borja, Silverstein, Zhou, Romero-Bascones, Struyven, Trucco, Mookiah, MacGillivray, Hogg, Liu, Williamson, Pontikos, Alexander, Stuart, Khawaja, Denniston, Rahi, Keane.
Drafting of the manuscript: Wagner, Silverstein, Liu, Patel, Rahi.
Critical revision of the manuscript for important intellectual content: Wagner, Cortina-Borja, Silverstein, Zhou, Romero-Bascones, Struyven, Trucco, Mookiah, MacGillivray, Hogg, Liu, Williamson, Pontikos, Balaskas, Alexander, Stuart, Khawaja, Denniston, Rahi, Petzold, Keane.
Statistical analysis: Wagner, Cortina-Borja, Silverstein, Liu, Pontikos.
Obtained funding: Wagner, Rahi, Keane.
Administrative, technical, or material support: Wagner, Silverstein, Zhou, Struyven, Mookiah, MacGillivray, Hogg, Balaskas, Alexander, Denniston.
Supervision: Cortina-Borja, Pontikos, Patel, Khawaja, Denniston, Rahi, Petzold, Keane.

4. **In which chapter(s) of your thesis can this material be found?**

Chapter 6.1

5. **e-Signatures confirming that the information above is accurate** (this form should be co-signed by the supervisor/ senior author unless this is not appropriate, e.g. if the paper was a single-author work)

Candidate
Siegfried Wagner
Date:
1st May 2023

Supervisor/ Senior Author (where appropriate)
Pearse Keane
Date
1st May 2023

UCL Research Paper Declaration Form

referencing the doctoral candidate's own published work(s)

Please use this form to declare if parts of your thesis are already available in another format, e.g. if data, text, or figures:

- *have been uploaded to a preprint server*
- *are in submission to a peer-reviewed publication*
- *have been published in a peer-reviewed publication, e.g. journal, textbook.*

This form should be completed as many times as necessary. For instance, if you have seven thesis chapters, two of which containing material that has already been published, you would complete this form twice.

1. **For a research manuscript that has already been published** (if not yet published, please skip to section 2)

   s) **What is the title of the manuscript?**

   Click or tap here to enter text.

   t) **Please include a link to or doi for the work**

   Click or tap here to enter text.

   u) **Where was the work published?**

   Click or tap here to enter text.

   v) **Who published the work?** (e.g. OUP)

   Click or tap here to enter text.

   w) **When was the work published?**

   Click or tap here to enter text.

   x) **List the manuscript's authors in the order they appear on the publication**

   Click or tap here to enter text.

   y) **Was the work peer reviewed?**

   Click or tap here to enter text.

   z) **Have you retained the copyright?**

   Click or tap here to enter text.

   aa) **Was an earlier form of the manuscript uploaded to a preprint server?** (e.g. medRxiv). If 'Yes', please give a link or doi)

   Click or tap here to enter text.

   If 'No', please seek permission from the relevant publisher and check the box next to the below statement:

   ☐

   *I acknowledge permission of the publisher named under **1d** to include in this thesis portions of the publication named as included in **1c**.*

2. **For a research manuscript prepared for publication but that has not yet been published** (if already published, please skip to section 3)

   k) **What is the current title of the manuscript?**

Retinal optical coherence tomography features associated with incident and prevalent Parkinson disease

l) **Has the manuscript been uploaded to a preprint server?** (e.g. medRxiv; if 'Yes', please give a link or doi)

No

m) **Where is the work intended to be published?** (e.g. journal names)

Neurology

n) **List the manuscript's authors in the intended authorship order**

Siegfried K Wagner, David Romero-Bascones, Mario Cortina-Borja, Dominic J Williamson, Robbert R Struyven, Yukun Zhou, Salil Patel, Rimona S Weil, Chrystalina A Antoniades, Eric J Topol, Edward Korot, Paul J Foster, Konstantinos Balaskas, Unai Ayala, Maitane Barrenechea, Iñigo Gabilondo, Anthony HV Schapira, Anthony P Khawaja, Praveen J Patel, Jugnoo S Rahi, Alastair K Denniston, Axel Petzold, Pearse A Keane

o) **Stage of publication** (e.g. in submission)

Accepted

3. **For multi-authored work, please give a statement of contribution covering all authors** (if single-author, please skip to section 4)

Concept and design: Wagner, Cortina-Borja, Khawaja, Denniston, Rahi, Petzold, Keane
Acquisition, analysis or interpretation of data: All authors
Drafting of the manuscript: Wagner, Denniston, Petzold
Critical revision of the manuscript for important intellectual content: All authors
Statistical analysis: Wagner, Cortina-Borja
Obtaining funding: Wagner, Keane
Supervision: Cortina-Borja, Rahi, Denniston, Petzold, Keane

4. **In which chapter(s) of your thesis can this material be found?**

Chapter 6.2

5. **e-Signatures confirming that the information above is accurate** (this form should be co-signed by the supervisor/ senior author unless this is not appropriate, e.g. if the paper was a single-author work)

Candidate
Siegfried Wagner
Date:
1st June 2023

Supervisor/ Senior Author (where appropriate)
Pearse Keane
Date
1st June 2023

Table of Contents

List of Tables

List of Figures

Abbreviations

AD: Alzheimer's Disease

AIC: Akike Information Criterion

AMD: Age-related macular degeneration

APOSTEL: Advised Protocol for OCT Study Terminology and Elements

ARIC: Atherosclerosis Risk in Communities study

ATET: Estimated treated effect of the treated

AUC: Area under the curve

AVR: Arteriolar-to-Venule ratio

BIC: Bayesian Information Criterion

BMI: Body mass index

BRAO: Branch retinal arterial occlusion

CDR: Cup-to-disc ratio

CEA: Carotid endarterectomy

CFP: Colour fundus photography

CHD: Coronary heart disease

cHR: Cause-specific hazard ratio

CI: Confidence interval

CN3: Third cranial nerve palsy

CN4: Fourth cranial nerve palsy

CN6: Sixth cranial nerve palsy

CPRD: Clinical Practice Research Datalink

CRAE: Central retinal artery equivalent

CRVE: Central retinal vein equivalent

CVD: Cardiovascular disease

DARS: Data Access Request Service

DAT: Dopamine transport scan

DICOM: Digital Imaging and Communications in Medicine

ETDRS: Early Treatment of Diabetic Retinopathy study

EHR: Electronic health record

FD: Fractal dimension

GCC: Ganglion cell complex

GC-IPL: Ganglion cell-inner plexiform layer

GCL: Ganglion cell layer

GoDARTS: Genetics of Diabetes Audit and Research Tayside Scotland

HES: Hospital episode statistics

HR: Hazard ratio

ICD: International Classification of Diseases

IGARD: Independent Group Advising on the Release of Data

IMD: Index of multiple deprivation

INL: Inner nuclear layer

IPL: Inner plexiform layer

IVAN: Interactive Vessel Analysis software

MACE: major adverse cardiovascular event

MCI: Mild cognitive impairment

MEH: Moorfields Eye Hospital

mGCIPL: macular ganglion cell-inner plexiform layer

MLE: Maximum likelihood estimation

mRNFL: macular retinal nerve fibre layer

NAION: Non-arteritic anterior ischaemic optic neuropathy

NCD: Non-communicable disease

NHS: National Health Service

OCP: Ocular cranial palsy

OCT: Optical coherence tomography

OCTA: Optical coherence tomography angiography

OPCS: Operating Procedure Code Supplement

OR: Odds ratio

PAS: Patient administration system

PDR: Proliferative diabetic retinopathy

PET: Positron emission topography

png: Portable network graphics

PPIE: Patient and Public Involvement and Engagement

PROGRESS: Prognosis Research Strategy Framework

PSM: Propensity score matching

PYAR: Person-years at risk

QUARTZ: Quantitative Analysis of Retinal Vessel Topology and Size

RA: Retinal analysis software

RAO: Retinal arterial occlusion

RECORD: REporting of studies Conducted using Observational Routinely-Collected health Data

RNFL: Retinal nerve fibre layer

RR: Risk ratio

RTSD: Retrograde trans-synaptic degeneration

SD: Standard deviation

SES: Socioeconomic status

sHR: Subdistribution hazard ratio

SIR: Standardised incidence ratio

SIVA: Singapore Vessel Assessment System

SLMS: School of Life and Medical Sciences

sOR: Summary odds ratio

sRR: Summary risk ratio

SSD: Schizophrenia spectrum disorders

STROBE: Strengthening the Reporting of Observational Studies in Epidemiology

TMVL: Transient monocular visual loss

TRF: Traditional risk factors

TRIPOD: Transparent Reporting of a Multivariable Prediction Model for Individual Prognosis or Diagnosis

UCL: University College London

UKBB: UK Biobank

VAMPIRE: Vessel Assessment and Measurement Platform for Images of the Retina

1. Introduction

The retina, a thin neurosensory tissue lining the back of the eye, is the only organ allowing direct non-invasive visualisation of the central nervous system and microvasculature. Advances in imaging hardware coupled with increasingly sophisticated statistical approaches have enabled the discovery of retinal signatures of systemic disease ('oculomics'). However, further understanding and discovery of eye-body links have been hampered by a lack of large labeled retinal imaging datasets. Given the importance that the public places on their vision and thus interest in taking up the increasing offer of retinal imaging hardware in the community setting, oculomics potentially provides an attractive scalable substrate for identifying those at risk of non-communicable disease.

Through three complementary strands, the research reported in this thesis seeks to further our understanding of retinal signatures of systemic disease using a purpose-designed health dataset, AlzEye, which links ophthalmic data from >350,000 users of the UK National Health Service with national hospital admissions data on systemic disease. In this thesis, I assert firstly that certain ocular phenotypes represent sentinel events for emerging systemic disease (*Description*). Secondly, quantitative retinal features not only associate with but can reveal novel mechanistic insights into the biology of systemic disease (*Discovery*). Thirdly, retinal morphology may provide useful variables for individual-level prediction of non-communicable diseases, such as dementia (*Prediction)*.

2. Background

Derived from the same tissue as the primitive brain, the retina is the only human tissue allowing direct non-invasive visualisation of the central nervous system and small blood vessels (microvasculature). While ophthalmic manifestations of systemic disease have been described since antiquity[1], recent advances in high-resolution retinal imaging coupled with modern computational approaches have enabled the fully automated and reproducible extraction of clinically relevant features at scale. Furthering our understanding of how these features associate with systemic dysfunction can afford insights into the biological mechanisms of disease as well and the utility of retinal feature-based risk prediction for incident life-threatening events.

This chapter begins with an overview of the rationale for using the eye as a surrogate marker of systemic disease. The broad focus is on cardiovascular and neurodegenerative diseases (background on and rationale for specific diseases, such as schizophrenia and Parkinson's disease, for *Discovery* are presented in later chapters). Retinal imaging modalities and relevant clinical features are then discussed finishing with a review of the health informatic repository central to this project, Hospital Episode Statistics. A list of search strategies informing the project's background can be found in Appendix 1: Search strategies.

2.1 The eye and systemic health

Relationship with the central nervous system

There are several scientific justifications for the ability of the eye to illustrate systemic health and disease in humans. Firstly, as a part of the central nervous system, the development of the eye occurs in tandem with the brain in utero. The primitive eyes originate as paired outpouchings from the lateral aspect of the forebrain at around Day 22 post fertilization (Figure *1*)[2]. Progressive dilation of this outpouching, termed the optic vesicle, is twinned with constriction of the proximal portion (the optic stalk), which will eventually house the optic nerve. The optic nerve conveys the products of retinal phototransduction (the conversion of the 'analogue' light signal from the photoreceptors to the 'digital' electrical impulses in the ganglion cells) to the brain.

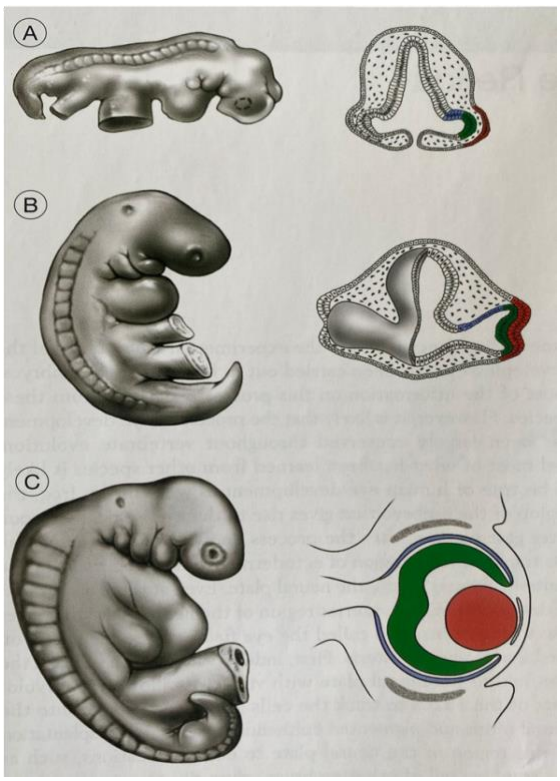

Figure 1: Development of the eye.

A: Around day 13, the optic vesicles begin to invaginate forming paired outpouchings from the central nervous system. B: At day 26, caudal displacement of the vesicles results from closed and continued growth of the primitive forebrain. C: By day 34, the neural retina and pigment epithelial layers (green) are seen as distinct layers. *(From Chapter 13 - The Development of the Retina,Editor(s): Stephen J. Ryan, SriniVas R. Sadda, David R. Hinton, Andrew P. Schachat, SriniVas R. Sadda, C.P. Wilkinson, Peter Wiedemann, Andrew P. Schachat*[3]*)* Reproduced with permission from Elsevier.

Retinal nerve fibres have a relatively long course, passing from the retina through the optic nerve, the nasal retinal fibres then crossing at the optic chiasm before continuing their journey onto the midbrain where they finally synapse either in the dorsal lateral geniculate nucleus or superior colliculus. As with other neuron tracts in the central nervous system, they are surrounded by an oligodendrocytic myelin sheath. Given that damage along anywhere along this path can potentially induce changes within the retinal nerve fibre layer (termed trans-synaptic retrograde degeneration, Figure *2*)[4] and that the retinal nerve fibre layer and the optic nerve can be directly visualized through clinical ophthalmic examination and imaging, some conditions of the brain may present with abnormal retinal features. For example, multiple sclerosis, ischaemic stroke and compression of the chiasm secondary to pituitary tumours lead to thinning of the retinal nerve fibre layer through this mechanism[4–6]. Further details of this anterior visual pathway are given in Section 2.2.2 Neurodegenerative disease and Section 2.3.2 Optical coherence tomography.

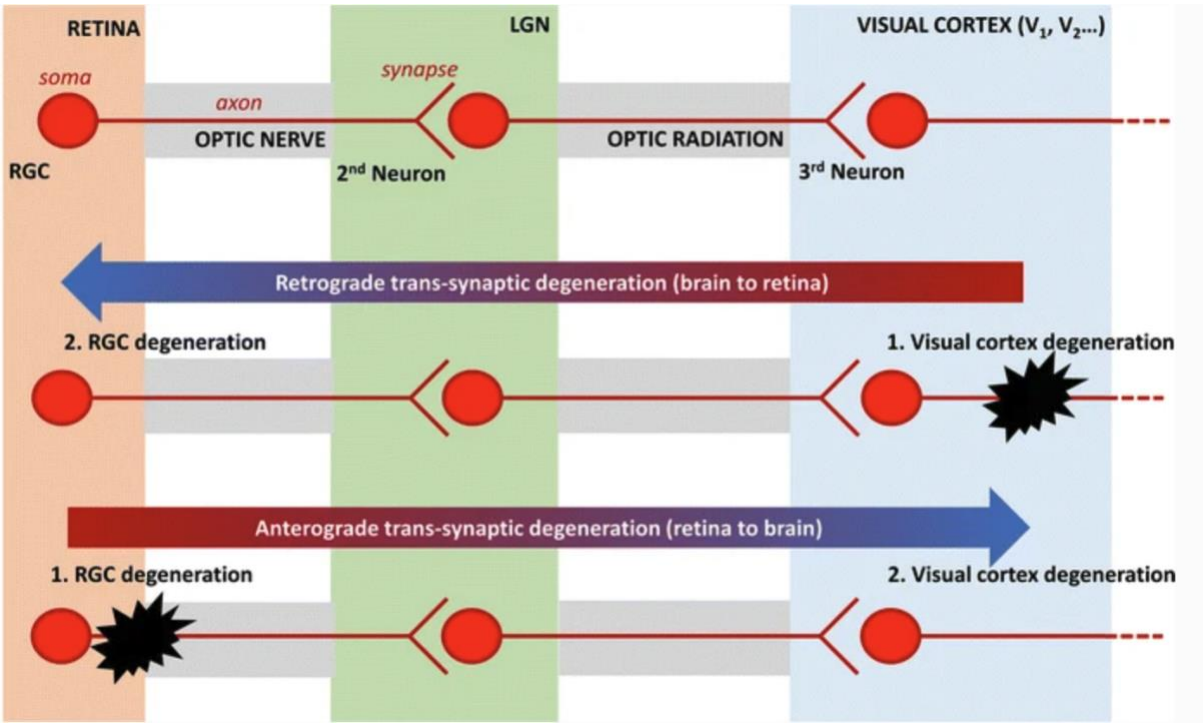

Figure 2: Schematic of anterograde and retrograde trans-synaptic degeneration between the retina and brain.

LGN: lateral geniculate nucleus; RGC: retinal ganglion cell

*From Davis, B.M., Crawley, L., Pahlitzsch, M. et al. Glaucoma: the retina and beyond. Acta Neuropathol **132**, 807–826 (2016)[7], figure available under CC license, no changes made).*

Ocular vascular architecture

The anatomy of the microvascular system of the posterior segment of the eye including the retina and choroid, is highly analogous to those of other microvascular organ systems. The lumina of retinal vessels (100-300 microns) and choroidal endothelial fenestrations have similar diameters (~80 nanometres) to their respective counterparts in the heart, brain and kidney and have exceptional perfusion per area. Behaviour of the retinal vasculature is akin to other vascular networks conforming to Murray's law of minimal work, which describes the relationship of the trunk and branch radii of transport systems[8,9]. Compartmentalisation through the presence of

specialised barriers, such as the blood-retinal barrier, blood-kidney barrier, and blood-brain-barrier, is another shared characteristic. Therefore, the broad similarities in architecture suggest that atherosclerotic disease processes may present similarly across microvascular organ systems. Interestingly however, the retinal vasculature consist of end-arterioles without anastomoses while microvascular systems of the heart and brain are richly supplied with collateral vessels[10].

The eye additionally exhibits other features that make it uniquely equipped for conveying information about systemic health. The eye is one of few organs that exhibits so-called immune privilege, a term first coined by Peter Medawar in 1948 when he noted that foreign skin tissue placed within the anterior chamber of the eye failed to elicit a rejection response[11]. Accordingly, the presence of intraocular inflammation may be a harbinger of systemic diseases characterised by abnormal immunoregulation[12]. Moreover, it lacks a lymphatic system. Also, as a by-product of the metabolically active retinal photoreceptors, the retina has the highest consumption of oxygen per volume of any tissue in the body and accordingly the choroid the highest blood flow volume of the body per volume justifying the disproportionately frequent involvement of the retina, optic nerve and extraocular muscles in diseases where metabolic activity is dysregulated, such as mitochondrial disorders or thyrotoxicosis.

2.2 The eye and systemic disease

Some systemic diseases harbour manifestations, which are unique to that condition, such as the Lisch nodules seen on the iris of people with neurofibromatosis type 1[13] or the Elschnig spots of hypertensive choroidopathy[14]. However, most features within cardiovascular and neurodegenerative diseases involve non-specific progressive changes in retinal morphology, which occur to a lesser extent with healthy ageing. Examples of this include thinning of the inner retinal layers on OCT or dilation of the retinal venules[15,16].

2.2.1 Cardiovascular disease

Cardiovascular diseases (CVD), including both ischaemic heart disease and stroke, account for more than a quarter of deaths worldwide and are the globally leading cause of mortality[17]. It is therefore unsurprising that some of the earliest literature on the ophthalmic manifestations of systemic disease relate mostly to hypertension. In 1836, Richard Bright, who many consider the founder of modern nephrology, described a series of patients presenting with a constellation of nausea, peripheral oedema, headache and seizures. Several of these patients also exhibited unexplained complete visual loss, often shortly before their death[18]. However, the answer as to the cause of mortality as well as vision loss had to wait nearly 50 years. In 1881, von Basch invented the sphygmomanometer which uncovered the cause of this constellation of symptoms to be severe hypertension and, contemporaneously, von Helmholtz and Babbage invented the ophthalmoscope which revealed the first features of hypertensive retinopathy as described by Marcus Gunn[19]. A half-century later, Keith, Wagener and Barker first proposed a risk-stratification index of

hypertensive retinopathy – a system of four distinct grades of severity of hypertensive changes within the retina with reasonable prognostic accuracy for mortality (Figure *3*)[20]. They were:

Grade 1: Mild generalised arteriolar retinal narrowing

Grade 2: Definite focal narrowing and arteriovenous nicking

Grade 3: Signs of grade 2 retinopathy, retinal haemorrhages, cotton wool spots, exudates

Grade 4: Grade 3 plus papilloedema

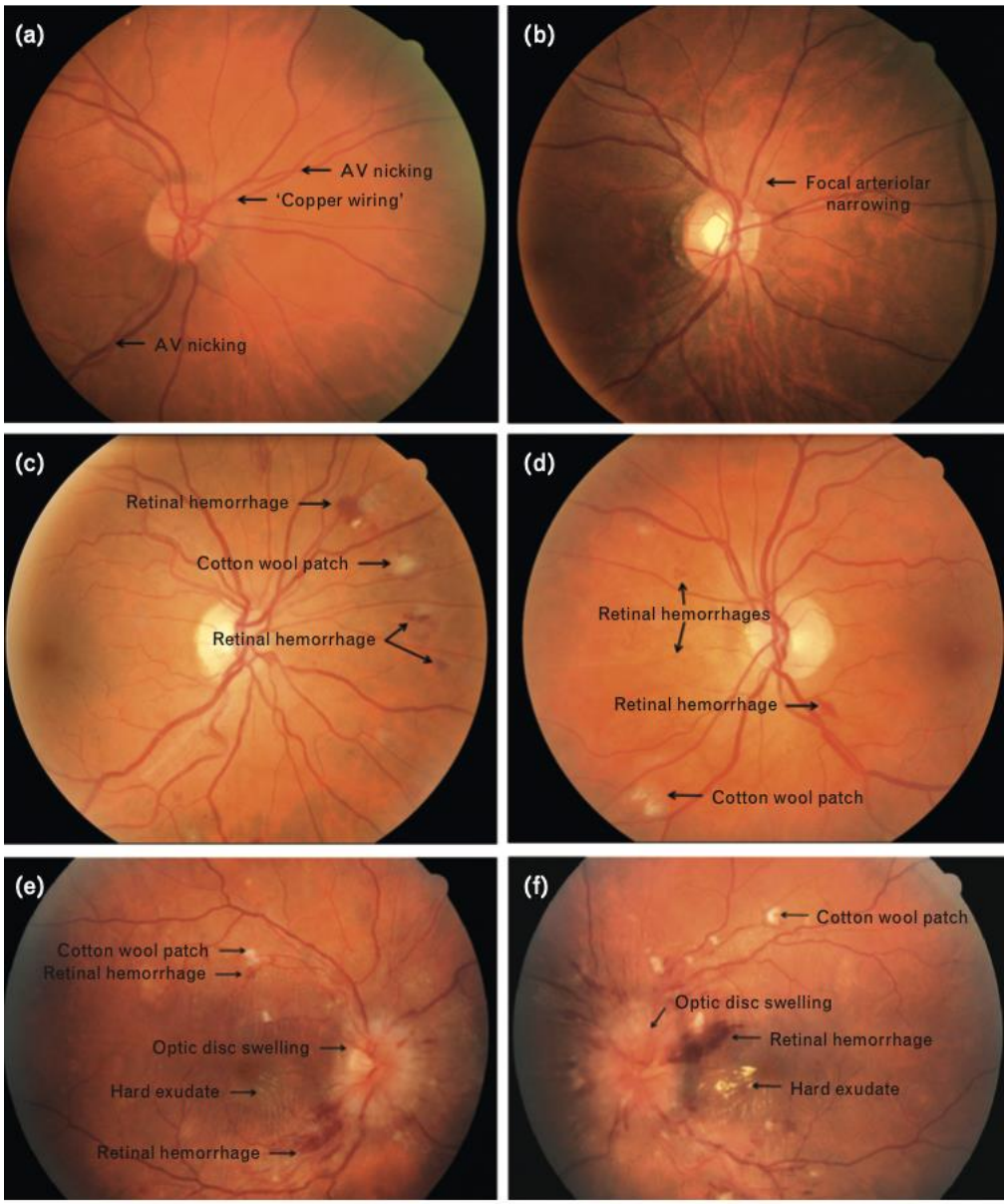

Figure 3: Stages of hypertensive retinopathy.

(a) and (b) show features of Grade I and Grade 2, (c) and (d) Grade 3, and (e) and (f) Grade 4. From Downie, L et al[21] Reproduced with permission from Lippincott Williams & Wilkins.

However, these qualitative features, while of prognostic value, are of limited population-based utility in risk-stratification today as it is uncommon to note features beyond mild hypertensive retinopathy due to effective anti-hypertensive therapy, appropriate cardiovascular risk-stratification and screening, and other public health

programmes. However, discrimination can be found even among those with mild hypertension using the quantifiable features of retinal vascular morphometry in particular retinal vascular calibre, tortuosity and fractal dimension[22 23]. Retinal vascular morphometry will be discussed in Section 2.3.1.2 Retinal vascular morphometry.

2.2.2 Neurodegenerative disease

Neurodegenerative diseases are a group of disorders characterised by a progressive loss of neurons of either the peripheral or central nervous system. Neurodegenerative diseases may manifest with different symptoms and signs (e.g. movement abnormalities) depending on the predominant site of degeneration. Dementia is an umbrella term of a group of symptoms resulting from predominant impairment of higher-order cerebral functions, such as memory, executive function and language[24]. Alzheimer's disease (AD) and vascular dementia are the two leading causes of dementia, collectively accounting for approximately 80% of all cases. In 2015, dementia overtook cardiovascular diseases as the leading cause of death in the UK and yet around 50-80% of affected people in high-income countries are estimated to be undiagnosed[25,26]. However, the utility of screening for dementia is questionable. Some advocate that the lack of benefit of early intervention coupled with a lower reported quality of life when diagnosed with AD or mild cognitive impairment suggests minimal benefit with screening[27–29]. On the other hand, AD research has garnered increasing funding (the US National Institute of Health increased federal funding into AD to 3.1 billion US dollars in 2020), auspicious results from the humanised IgG1 monoclonal antibody lecanemab have led to the

first AD drug approved by the Food and Drug Administration in many years, and the *Lancet Commission* on dementia concluded that around 40% of dementia globally could be prevented or delayed through addressing twelve modifiable risk factors [30–32]. While the identified risk factors, such as smoking or limiting alcohol use, may not be particularly sophisticated, recognition of the impact of current behavioural patterns can promote health-enhancing activities (e.g. physical exercise) and limit health-compromising behaviours (e.g. smoking and excess alcohol consumption)[33,34].

While vascular dementia is typically characterised by the presence of cerebrovascular disease, the neuropathological hallmarks of AD include deposition of amyloid-beta plaques and neurofibrillary tangles within the central nervous system as well as progressive degeneration of the limbic system[35]. Prompted by the finding that sufferers of AD exhibited visual deficits unexplained by ophthalmic examination[36,37], Hinton et al were the first to histologically demonstrate the loss of retinal ganglion cells and reduction in RNFL thickness in the optic nerve of those with AD (Figure *4*)[38].

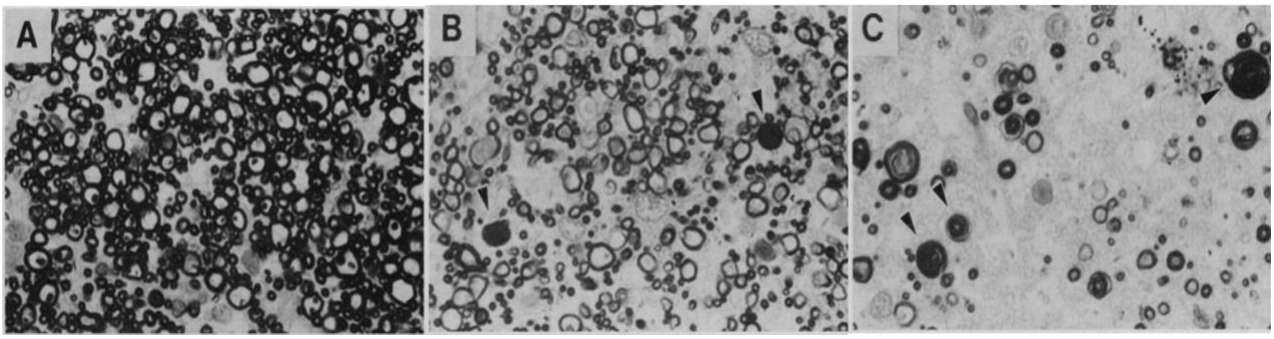

Figure 4: Original histological observations stained with *p*-Phenylenediamine by Hinton et al demonstrating normal optic nerve axons in healthy controls (A) but reduced axon number with differing morphology in those with moderate (B) and severe Alzheimer's disease (C).

The origin of retinal and optic nerve changes in AD remains unclear but two potential mechanisms have been proposed. Firstly, given their shared embryological origin and anatomical makeup, the disease process underlying AD within the brain may similarly and simultaneously be occurring within the eye. Supporting this hypothesis is the finding of amyloid and neurofibrillary tangles within the retina of those with AD observed either non-invasively or using curcumin fluorescence[39,40]. However, as highlighted by Alber et al in their systematic review of 2019, most work has not reliably identified amyloid-beta in human retina[41]. A second hypothesis relates to the principle that, as mentioned in Section 2.1 The eye and systemic health, damage anywhere along the visual pathway may result in trans-synaptic retrograde degeneration with resulting atrophy in retinal ganglion cell axons, such as that seen in multiple sclerosis[42,43]. The finding that post-chiasmal ischaemic events may impact

on retinal nerve fibre layer, and that many people with AD demonstrate changes within their visual cortex (although reverse causality cannot be excluded) support this theory[4,44]. Evidence therefore exists that both hypotheses may be true to some extent.

Pathophysiological overlap between vascular and Alzheimer's-type dementia is increasingly recognised by the scientific community[45]. Postmortem analysis suggests the majority of individuals with dementia exhibit features of both AD and vascular dementia[46,47] and, in one large report, over 70% of patients with AD had features of cerebrovascular disease on brain autopsy[48]. Conversely, individuals with vascular dementia harbour increased amyloid positivity compared to healthy controls[49]. Moreover, optimisation of vascular risk factors reduces the risk of AD[50]. Given this, it is biologically plausible that imaging investigations which incorporate both retinal neurodegeneration and cerebrovascular disease may provide enhanced performance beyond either in isolation.

While most work has involved histopathological analysis to reveal the thinning of the inner retinal layers, characteristic of neurodegeneration, most of these can now be quantitatively analysed using non-invasive in vivo retinal imaging techniques. The most widely leveraged modality for visualising and measuring the inner retinal sublayers is OCT, which will be described further along with the characteristic changes seen in dementia in Section 2.3.2 Optical coherence tomography. Visualisation and feature extraction of the retinal vessels is typically with CFP, which will be described in Section 2.3.1 Retinal colour fundus photography (CFP).

2.3. Retinal imaging modalities

Vision science and ophthalmology benefit from a rich and diverse catalogue of retinal imaging modalities, each one providing a unique illustration of the posterior segment. Most are minimally invasive, carry minimal risks, and often require only nominal expertise for acquisition. This project will focus on two imaging techniques – retinal colour fundus photography (CFP) and optical coherence tomography (OCT). After a brief description of each, the corresponding features which they reveal in the context of CVD and dementia are discussed.

2.3.1 Retinal colour fundus photography (CFP)

The most widely and commonly used ophthalmic imaging modality is retinal CFP which has undergone a number of key developments including improved resolution, less requirement for pupil-dilating drops (mydriatics), and greater portability starting with the work by Jackman and Webster in 1886[51]. The ability to digitise images with the permeation of computers in the 1990s allowed the eventual development of automated image analysis systems, which reduced the variability in measurement and segmentation (classifying each pixel of an image)[52]. Also emerging in the last couple of decades has been the delivery of CFP through different spectral channels (e.g. red, green blue), digital true colour and pseudocolour, each with its own suitability to the detection of certain lesions. For example, a red-free channel provides greatest contrast for detecting haemorrhage. While certain “ultra-widefield” devices may capture up to 200 degrees of the retina, most cameras currently available provide fields of view between 25 and 45 degrees, which is sufficient to capture the macula, optic nerve and major retinal vessels of the posterior pole (Figure 5)[53]. Retinal CFP can reveal both qualitative features, such as those

attributed to hypertensive retinopathy and discussed in Section 2.3.1.1 Retinopathy, and quantitative features, such as the calibre, tortuosity and fractal dimension of retinal vessels (Section 2.3.1.2 Retinal vascular morphometry).

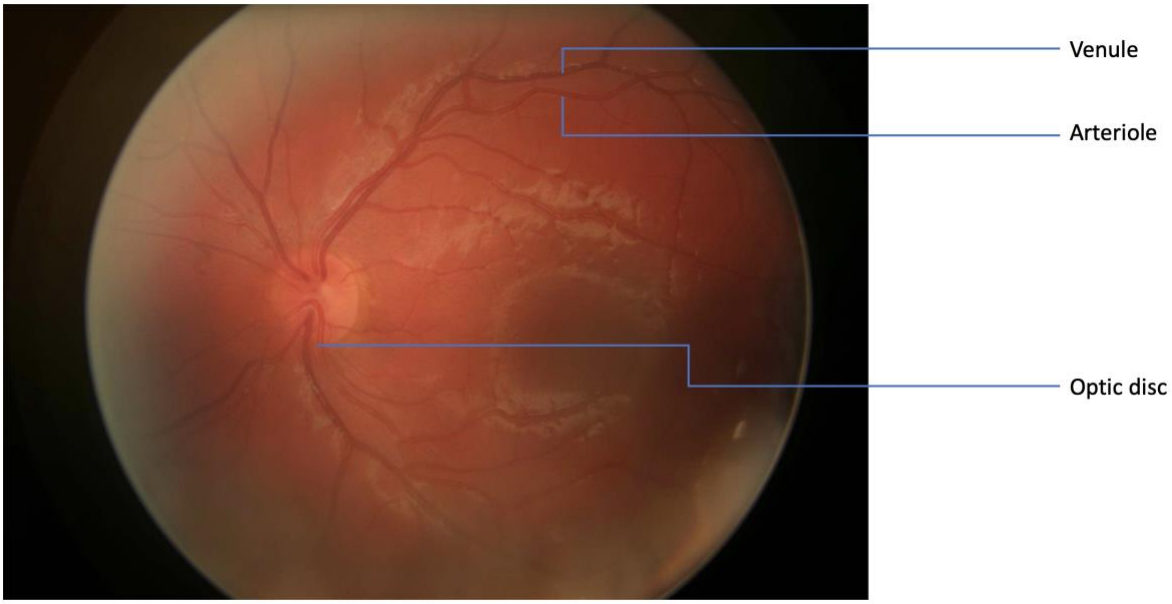

Figure 5: Retinal colour fundus photograph.

Venules tend to have greater calibre and exhibit a deeper red colour.

2.3.1.1 Retinopathy

Retinopathy describes any discrete feature of retinal disease but is traditionally reserved for those of retinal vascular origin[54]. Signs of retinopathy, including hard exudates (lipid deposition in the outer retina), haemorrhage, microaneurysms and cotton wool spots (infarcted retinal nerve fibres) are most recognised in association with diabetic eye disease and their severity and distribution account for the major triaging criteria within diabetic screening programmes[55] (Figure *6*). However, they are also seen in hypertensive retinopathy. While the retinopathy of hypertensive eye disease has clear prognostic utility for mortality when considering all 4 grades of the

classic Keith-Wagener-Bark classification[56], the majority of patients in modern practice are skewed towards the milder stages of disease. For example, among the 3654 people recruited to the Blue Mountains Eye Study, the prevalence of retinal haemorrhages and microaneurysms were 4.6% (95% CI: 3.9, 5.4%) and 6.4% (95% CI: 5.5, 7.2%) in non-diabetic people[57]. This is a consistent finding among similar reports assessing hypertensive study populations with the proportion affected in more recent studies by Grade 3 or more retinopathy approximating 2%[58–61].

Nonetheless, when present, qualitative features of retinopathy are strongly associated with incident CVD events, particularly cerebrovascular events. The summary risk ratio (sRR) derived from eight studies, including five population-based analyses covering 25,324 participants for incident stroke was 2.1 (95% CI: 1.7, 2.6) for those with retinopathy versus those without[62]. For prevalent stroke, this increases to 2.5 (95% CI: 1.4, 4.3). Most of these studies recruited participants aged 45 years and above who were from White or Black backgrounds. Rather than use distinct stroke episodes, a recent meta-analysis looked at the association of retinopathy with different cerebrovascular disease subtypes[63]. Summary odds ratios (sOR) for the presence of any retinopathy were 1.94 (95% CI: 1.30, 2.70) for white matter hyperintensities, 1.99 (95% CI: 1.21, 3.25) for lacunar infarcts and 1.96 (95% CI: 1.53, 2.50) for subclinical cerebral infarction. In terms of coronary heart disease (CHD) events, such as myocardial infarction, it can be challenging to disentangle their association with retinopathy as they are often aggregated with cerebrovascular events as seen in the study of Wong et al using data from the Beaver Dam Eye study. Following adjustment for vascular risk factors, those with retinopathy had 1.8 times the odds (95% CI: 1.2, 2.7) of those without for cardiovascular mortality

consisting of those secondary to either CHD and stroke[64]. Within the Atherosclerosis Risk in Communities (ARIC) study population, presence of any retinopathy had an adjusted risk ratio (RR) of 1.83 (95% CI: 1.00, 3.38) for women and 0.84 (95% CI: 0.46, 1.52) for men though no statistical evidence of interaction was found with sex and retinopathy[65].

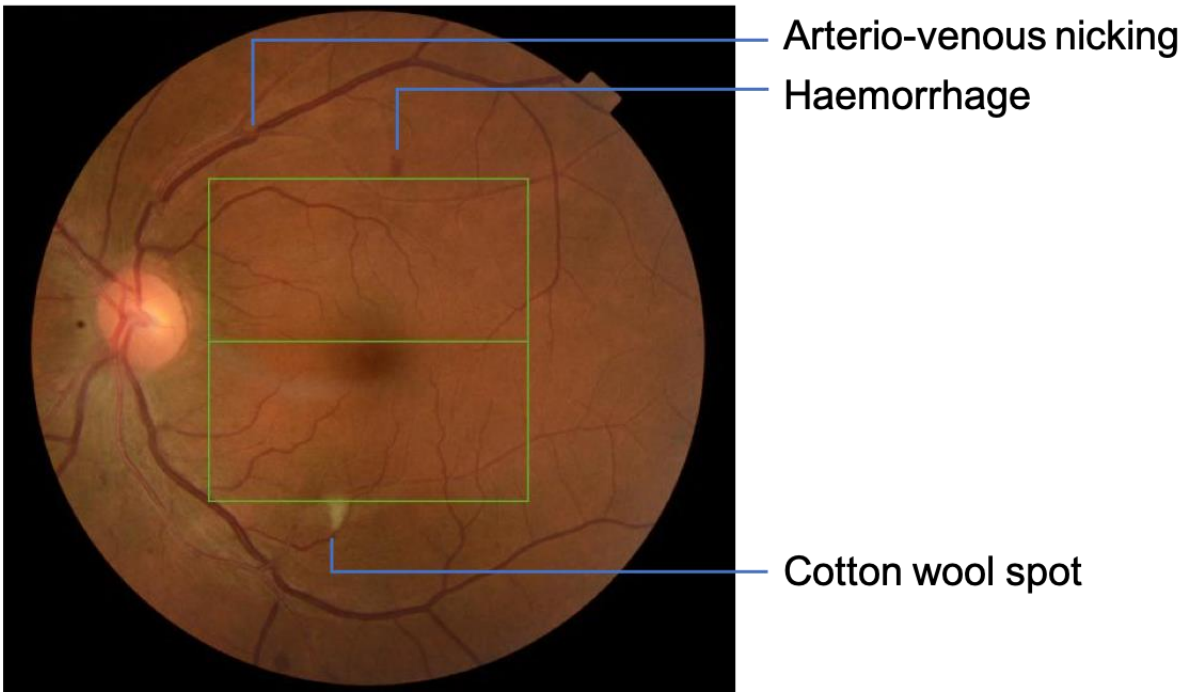

Figure 6: Features of retinopathy on a colour fundus photograph of the retina.

In arterio-venous nicking, compression of the underlying venule can be seen with an evident prominence of the venule on either side of the crossing.

Given the aforementioned links between retinopathy and cerebrovascular disease and the latter's contribution to cognitive impairment[66], retinopathy has also been assessed in those with dementia however OCT has superseded CFP as the imaging modality of choice for investigation retinal associations with dementia in the last

decade (Section 2.3.2 Optical coherence tomography). After age and sex adjustment and at mean follow-up of 11.4 years, retinopathy was associated with prevalent (odds ratio [OR] 2.04, 95% CI: 1.34, 3.09) but not incident (OR 1.15, 95% CI: 0.88, 1.48) dementia (defined using cognitive questionnaires and neuropsychology assessment) in the Rotterdam Study although this did not adjust for diabetes mellitus, which notably affected 10% of controls but 23% of those with dementia[67]. There is otherwise a scarcity of recent work exploring the presence of retinopathy with the development of dementia.

In summary, there is clear evidence that retinopathy is a prognostic factor for incident cardiovascular events, especially ischaemic stroke. However, the low prevalence of such features (i.e. Grade 3 retinopathy and above) in the general population limits its utility in a population-based screening scenario.

2.3.1.2 Retinal vascular morphometry

Retinal vascular morphometry refers to the quantitative (both Euclidean and non-Euclidean) characteristics that can be derived from the retinal vasculature. For the purposes of this report, calibre, tortuosity and fractal dimension will be discussed however others, including bifurcation indices, have been described[68]. While the early work of Keith, Wagener and Barker highlighted the qualitative features indicative of hypertensive retinopathy[56], some of which have been expounded in Section 2.3.1.1 Retinopathy, digitised retinal images in the 1990s also allowed derivation of quantitative measurements of retinal vessels[69]. Initially manual segmentation (outlining, by hand, retinal vessels and disease features) was performed, which had

moderate intergrader variability, however the last few years has seen the emergence of semi-automated and a few fully automated systems[70].

Calibre

Research into the association of retinal vascular calibre must be interpreted in the context of its limitations. Calibre is sensitive to certain device-specific features, such as magnification, and therefore many systems have developed tools of extracting reproducible measurements through statistical methods. For example, the software used in the Atherosclerosis Risk in Communities (ARIC) studies which later formed the foundation of the Singapore Vessel Assessment System (SIVA), constructs the variable Central Retinal Artery Equivalent (CRAE), which result from fitting a linear regression model from the arteriolar width and taking the residual (the counterpart, Central Retinal Vein Equivalent (CRVE) similarly models the venular width)[70]. A resulting Arteriolar-to-Venule ratio (AVR) has often been reported in the literature as the CRAE divided by the CRVE and is thought to be robust to alterations in magnification[71]. Other programmes, such as that found in the Quantitative Analysis of Retinal Vessel Topology and Size (QUARTZ) system, take many measures and summarise using means[72]. The heterogeneity of outputs limits aggregation and performance of meta-analysis. To what extent different image analysis systems agree has been challenged – for example, SIVA has been shown to generate larger measurements on average compared to another major image analysis system, Interactive Vessel Analysis (IVAN)[73]. When comparing SIVA with another system, the Retinal Analysis (RA) software from the University of Wisconsin, SIVA generated larger absolute values and limits of agreement showed proportional bias (r = -0.240, p=0.008) however correlations between systemic variables (age, height body-mass

index [BMI], blood pressure) and retinal vascular calibre was similar for SIVA and RA[74]. The agreement between SIVA and Vessel Assessment and Measurement Platform for Images of the Retina (VAMPIRE), another system developed by the University of Dundee and the analysis system used in this project, was poor (intraclass correlation coefficient: 0.159-0.410)[75]. Such findings suggest challenges in the future in standardising retinal vascular morphometry from differing algorithms and highlight the importance of calibration for any prognostic model where such outputs act as predictor variables.

Renewed interest in the changes in retinal vascular calibre (specifically arteriolar narrowing) as a feature of hypertension were espoused by Scheie in 1953[76] but were not quantitatively evaluated until 1999 when Sharrett et al reported results from the retinal photography of 9300 non-diabetic participants between 50 and 71 years of age in the ARIC study[77]. Manually segmenting arterioles and venules at a specified area between ½ and 1 optic disc diameter from the optic disc margin and calculating the AVR, they found a significant association between decreasing AVR and both current and previous mean arterial blood pressure. Subsequent work also derived from the ARIC study showed that compared to the fifth (largest AVR ratio), the first quintile was associated with 1.98 times (1.09, 3.60) the risk of ischaemic stroke when adjusting for age, sex, ethnicity and centre of data collection but was no different (1.24, 95% CI: 0.66, 2.31) after adjustment for all recorded vascular risk factors[69]. Similar work, again from ARIC, did shown an association between AVR and incident coronary event (defined as myocardial infarct, fatal coronary heart disease or coronary revascularization therapy) but only among women (adjusted risk ratio 1.37 per standard deviation decrease in AVR, 95% CI: 1.08, 1.72)[65].

However, noting that AVR was a relatively crude measure of vascular morphometry, discrimination of arteriolar versus venular calibre has subsequently become possible. While arteriolar calibre does indeed associate strongly with older age, it is retinal venular width which has greater prognostic value in CVD events. An individual participant meta-analysis of 20,798 participants with 945 incident strokes over 12 years of follow up across six prospective cohort studies showed no association between arteriolar calibre and risk of stroke however wider retinal venular calibre did predict stroke with a pooled hazard ratio of 1.15 (95% CI: 1.05, 1.25 per 20 micron increase in calibre)[78]. A similar analysis instead exploring incident CHD events showed elevated risk with rising retinal venular calibre (1.16, 95% CI: 1.06, 1.26, per 20 micron increase) and decreasing arteriolar calibre (1.17, 95% CI: 1.07, 1.28, per 20 micron decrease) but only in women[79]. More recently, similar findings regarding the risk of elevated venular width and diminished arteriolar calibre have been found in longer-term (16 years) follow up in ARIC as well as in incident heart failure[80,81]. A systematic review and meta-analysis in 2020 assessing the association between calibre and CVD concluded that both reduced arteriolar calibre (1.14, 95% CI: 1.05, 1.23 per standard deviation change) and increased venular calibre (1.20, 95% CI: 1.12, 1.28) were associated with incident stroke but that the evidence for coronary heart disease was inconsistent[82].

The association of retinal vascular calibre with all-cause dementia is less well-described than in CVD. Cross-sectional analyses have highlighted conflicting results, particularly with retinal venular calibre. Early reports highlighted reduced retinal venular calibre among individuals with AD or cognitive decline compared to healthy

controls[83,84], while others have suggested retinal venular dilatation[85]. The prospective Rotterdam study found larger venular calibre is associated with an increased risk of dementia (HR: 1.31, 95% CI: 1.06, 1.64 per SD increase)[86]. However, this was not reproduced in the ARIC study, although they did note an association between retinal arteriolar calibre and word fluency[87]. More recently, Cheung et al extracted retinal vascular calibre using a deep learning-based segmentation tool finding an association between both narrower retinal arteriolar calibre (HR 1.26, 95% CI: 1.06, 1.49 per SD decrease) and larger retinal venular calibre (HR: 1.20, 95% CI: 1.01, 1.43 per SD increase) with the development of cognitive decline and incident dementia. Between all these studies, there is heterogeneity in the case definition of dementia, cognitive assessment techniques and cohort profile.

In summary, retinal vascular calibre is an inconsistent predictor variable for incident CVD events and all-cause dementia. Most studies have been restricted to prospective epidemiological cohorts. Calibre has also not been combined with other imaging modalities (e.g. optical coherence tomography) metrics for prediction. In a few exceptions, calibre has been combined with other CFP-derived metrics, such as tortuosity or fractal dimension. Finally, there are concerns with measurement error and standardisation among different semi-automatic tools for extracting retinal vascular indices.

Fractal dimension

Although an ancient concept, the quantitative value of fractal dimension (FD) was limited until the emergence of computer systems in the 1960s when Benoit

Mandelbrot published his landmark paper on the superficially simple question of the length of the British coastline[88]. Mandelbrot noted that coastlines, like other so-called fractals, are geometric structures with a repeating motif on an ever-reducing scale. This feature, termed self-similarity, is highly prevalent throughout nature and was defined in the 1990s as a potential proxy for the nonlinear dynamics of physiological ageing[89]. For example, Lipsitz and Goldberger proposed that ageing was defined by a progressive loss of complexity with manifestations from declining heart rate variability to the decreasing waveforms evident on electroencephalography. Anatomic structures, from neuronal dendrites to retinal vasculature, also exhibit a form of complexity through their branching indices[90]. However, these geometric structures cannot be measured using traditional Euclidean metrics, such as length, and instead rely on other means, such as FD. FD therefore provides a global measure of the complexity of branching patterns (Figure *7*). Measurement of FD can be undertaken through different procedures, which are beyond the scope of this report and have been reviewed elsewhere; in vascular systems, FD is commonly estimated using the box-counting method[91,92]. In brief, a retinal photograph is i) segmented to provide a skeletonised representation of the vascular tree, ii) captured using a series of circles or rectangles of varying radii or length and iii) the number of pixels occupied within each circle/rectangle counted (Figure *8*). The logarithm of the number of pixels occupied is then plotted against the logarithm of the geometric variable (e.g. radius) with the slope representing the FD.

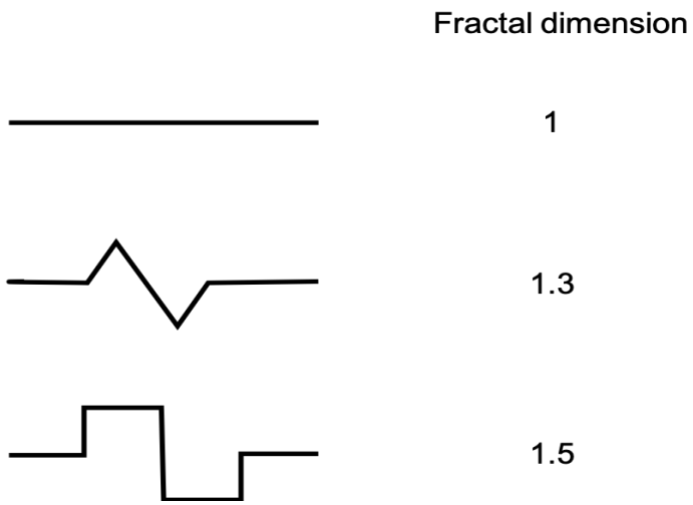

Figure 7: Examples of differing fractal dimensions (FD).

With greater FD, greater complexity and non-linearity is seen.

There are many potential advantages of studying retinal FD over more traditional vascular metrics, such as calibre and tortuosity. Firstly, FD provides a global metric of the vascular snapshot as opposed to the highly localised nature of calibre which, for example, may be heterogenous in its capture (e.g. 2 disc diameters from the optic nerve in some studies, 3 disc diameters in another). Secondly, FD is not as vulnerable to alterations in camera magnification; this is of growing significance given the range of imaging vendors available and the rapid evolution of device generations even among the same vendor. Finally, FD is not as sensitive to the retinal pulse cycle as other metrics might be[93–95]. Retinal vascular calibre is known to vary throughout the pulse cycle with changes of 4.82% and 3.46% in venular and arteriolar diameters respectively from systole to diastole[96] whereas previous work has shown that FD estimated using the box-counting method does not vary significantly throughout the pulse cycle[97]. However, notwithstanding these strengths, FD is exquisitely sensitive to the segmentation quality (and therefore the image quality). Reductions in brightness and contrast or alterations in focus and colour can

significantly affect FD [98] making spurious associations with age/dementia conceivable simply through confounding by cataract and small pupils. Some have exploited this characteristic of FD to generate separate metrics for assessing image quality [99]. Thus, image quality should be taken into consideration when analysing retinal FD.

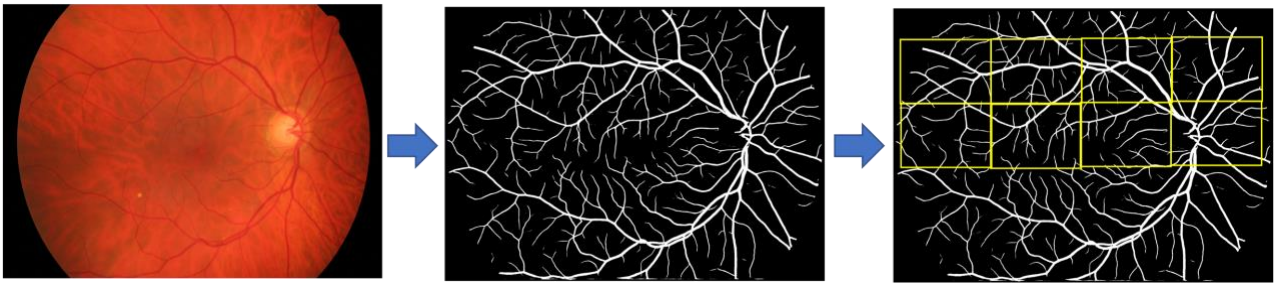

Figure 8: Evaluation of retinal fractal dimension.

Following cropping of the retinal photograph, the image is then segmented to provide a grey-scale representation of the vasculature followed by calculation of fractal dimensions using the box-counting method.

The application of FD analysis to retinal morphology was first published by Family et al and then Mainster et al, who highlighted the self-similarity of the retinal vasculature[100,101]. Relying on fluorescein angiography, Mainster et al noted progressive reduction in FD from the central to peripheral retina and a difference in the FD of the arteriole and venous systems. Since the report of Mainster et al, FD analysis has been limited due to the challenge of manual segmentation however the emergence of semi-automated FD analyses tools from 2008 onwards paved the way for descriptions of its underlying determinants. Liew et al demonstrated high intragrader and intergrader reliability in their semi-automated program for calculating FD (intraclass correlation coefficient range 0.93-0.95) among two readers with two-

week grading intervals. They also showed, among 300 participants from the Blue Mountains Eye Study, that FD was inversely associated with age with a correlation coefficient of -0.42 supporting the hypotheses of Lipsitz and Goldberger that natural ageing is characterised by a loss of complexity. Adjusting for age and sex, Liew et al also found a significant difference in FD between those with hypertension (defined using an adaptation of the 2003 World Health Organization guideline) versus those without (1.441 vs 1.431, p=0.02)[102]. These findings were supported by a subsequent population-based study of Chinese, Malay and Indian participants in Singapore. Elaborating on the case definition of elevated blood pressure, Sng et al found that FD was indeed reduced among those with hypertension after adjustment for relevant confounders but interestingly those with the lowest FD had increased odds of having uncontrolled treated or untreated hypertension versus controlled treated hypertension which may suggest a dynamic role for FD[103]. FD may not just be indicative of pathological hypertension; retinal FD among healthy children can also be modelled using mean arterial blood pressure (β= -0.083, 95% CI -0.145,-0.021, p=0.009, adjusted for age, sex and height)[104].

The relationship between FD and CVD events requires further characterisation. Using data again from the Blue Mountains Eye Study linked with the Australian National Death Index, Liew et al evaluated the association between FD and 14-year risk of death secondary to coronary heart disease. Rather than finding a linear relationship, they instead defined a “suboptimal FD” category to fit a U-shaped association model where people in the lowest and highest quartiles of FD measurements had the highest risk of mortality. Among this group, hazard ratios were 1.39 (95% CI: 1.12, 1.72, p=0.003) for the lowest and 1.55 (95% CI: 1.21, 1.99,

p=0.0005) for the highest FD quartiles, compared with the middle two quartiles[105]. In a recent systematic review of retinal FD in ischaemic stroke, retinal FD was found to be decreased in those with prevalent and incident ischaemic stroke[106]; one report also adjusted for calibre and tortuosity showing the added value of incorporating FD over calibre and tortuosity for discriminating between those who develop stroke[107,108]. There has been inconsistent evidence on whether FD can distinguish between lacunar and other types of ischaemic stroke[109–111].

Given the shared pathophysiology with CVD, FD has also been assessed in participants with neurodegenerative disease. The systematic review of Lemmens et al also assessed the role of FD in cognitive impairment and dementia. Retinal FD does not appear to associate with cognition among healthy older adults however there is consistent evidence that, compared to cognitively normal controls, patients with AD and vascular cognitive impairment have decreased FD though studies in this domain remain relatively small with only one study having >100 cases[112,113].

Tortuosity

Describing the deviation of a given entity from a straight line (Figure *9*), tortuosity can be mathematically expressed, in its most basic form, as:

$$\frac{Arc\ length}{Chord\ length}$$

For a straight line, this would equate to 1. While this formula has been used in several ophthalmic investigations of tortuosity[114–117], another popular variation incorporates the total squared curvature[22,118–120]:

$$\frac{Total\ squared\ curvature}{Arc\ length}$$

Strengths of tortuosity include its independence from short-term fluctuations in systemic circulation and the pulse cycle (unlike calibre)[93,96] however a shortcoming is the heterogeneity in tortuosity indices. In a systematic review in 2013, fourteen separate methods for estimating tortuosity had been used in retinal imaging research[121] rendering inter-study comparison challenging. This likely explains the scarcity of meta-analyses on this metric in retinal vascular research.

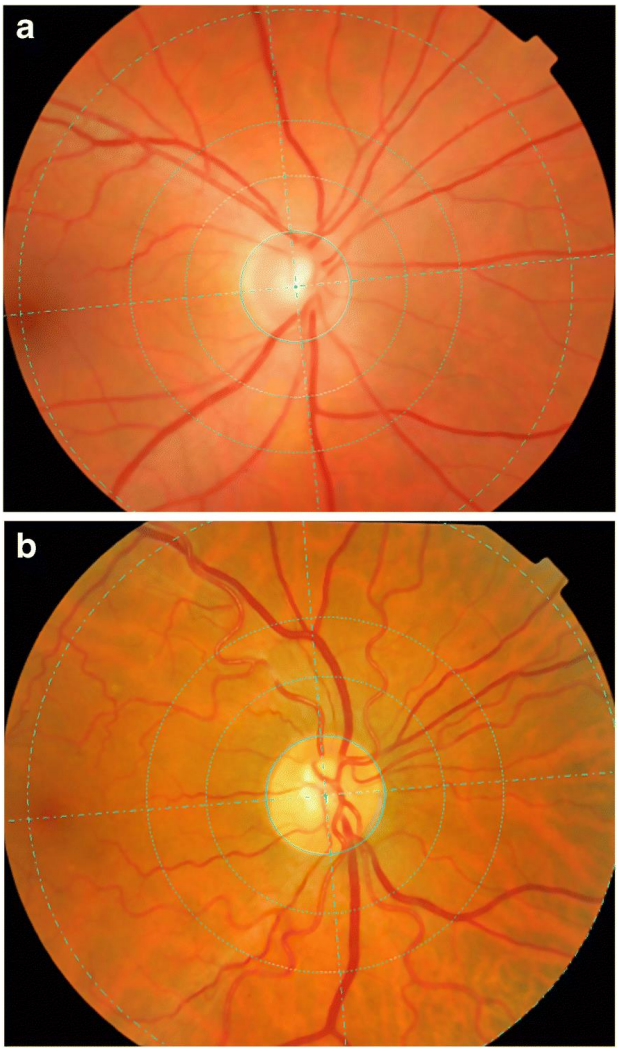

Figure 9: Example retinal images showing lower relative (a) versus higher relative arteriolar tortuosity (b).

Note that retinal arteriolar generally have lower calibre and have less of a deep red colour. From Sandoval-Garcia E, McLachlan S, Price AH, MacGillivray TJ, Strachan MWJ, Wilson JF, Price JF. Retinal arteriolar tortuosity and fractal dimension are associated with long-term cardiovascular outcomes in people with type 2 diabetes. Diabetologia. 2021 Oct;64(10):2215-2227. Figure available under CC license, no changes made.

Retinovascular tortuosity is associated with cardiometabolic risk factors. Findings from two separate retinal image analysis systems (SIVA and QUARTZ) in three different population-based cohorts (Singapore Malay Eye Study [SMES] and

European Prospective Investigation into Cancer—Norfolk Eye Study [EPIC-Norfolk] and UK Biobank) have shown similar findings for venular tortuosity, reporting an association between increased tortuosity and higher blood pressure and prevalent type 2 diabetes mellitus[16,22,23]. In EPIC-Norfolk, venular tortuosity was associated with several features of metabolic syndrome, including glycated haemoglobin (HbA1c) and BMI even when excluding those with diabetes mellitus leading the authors to posit that tortuosity may be altered early in the disease process[16]. However, directions of effect for arteriolar tortuosity have differed – while reduced tortuosity was associated with older age and higher blood pressure in SMES, increased tortuosity was seen with higher systolic blood pressure in EPIC-Norfolk and UKBB and older age in EPIC-Norfolk. Retinal vascular tortuosity is also associated with previous ischaemic stroke - in a nested case-control study of the Singapore Epidemiology of Eye Disease study, Ong et al found both arteriolar tortuosity (OR: 1.56, 95% CI: 1.25, 1.95 per SD increase) and venular tortuosity (OR: 1.49, 95% CI: 1.27, 1.76, per SD increase) were associated with greater odds of stroke[122]. In their 2022 systematic review, Biffi et al only identified one relevant study examining tortuosity in cerebral small vessel disease – Hilal et al investigated participants in the Epidemiology of Dementia in Singapore Study observing an association between arteriolar tortuosity and multiple cerebral microbleeds (RR: 1.25, 95% CI: 1.03, 1.61)[123,124].

Whether retinal vascular tortuosity provides prognostic utility for incident cardiovascular events has been investigated in diabetic populations. Among diabetic participants in the Edinburgh Type 2 Diabetes study, arteriolar tortuosity was associated with incident stroke and transient ischaemic attacks (TIA) (HR 1.27, 95%

CI: 1.02, 1.58) although adjustment for diabetic retinopathy status led to significant dampening of the estimate[125]. Mordi et al examined retinal imaging and genetic data of participants in the Patients in the Genetics of Diabetes Audit and Research Tayside Scotland (GoDARTS) study finding that venous tortuosity independently predicted major adverse cardiovascular event (MACE) occurrence and improved discrimination performance beyond a polygenic risk score[126]. However, overall performance was still modest (AUC 0.69) and this was a relatively homogenous diabetic population.

The evidence for an association between retinal vascular tortuosity and cognitive decline is limited and conflicting. While an analysis of the SEED study showed an association between AD and increased arteriolar and venular tortuosity[112], an opposite direction of effect has been found in other studies[127,128]. Venular tortuosity was also significantly reduced in individuals with AD in a small cohort of 103 participants undergoing ultra-widefield imaging[129]. Samples have generally been of small size.

In summary, heterogeneity in tortuosity estimation methods limit meta-analytical reports in retinal imaging research. While there is evidence of an association between venular tortuosity, blood pressure and metabolic dysfunction, relationships among other estimates have been inconsistent. Retinal vascular tortuosity is less frequently reported in the literature compared with other morphometric features, such as calibre or fractal dimension. Especially in the context of cognitive decline and incident cardiovascular events, the findings have often conflicted.

2.3.2 Optical coherence tomography

Nomenclature regarding OCT sublayers in this thesis will be in line with the agreed lexicon of the International Nomenclature for Optical Coherence Tomography Panel[130]. OCT is a rapid minimally-invasive modality providing high-resolution cross-sectional imaging based on the measurement of back reflected infrared light (Figure *10*). Since its inception in 1991, OCT has progressed from naive technology to primary clinical trial outcome measure and provides outputs for nationally-recommended thresholds for treatment of many macular diseases [131,132]. Moreover, its role is no longer confined to retinal disease, where it was first promulgated, but rather use of OCT has redefined the management of other ophthalmic subspecialties, such as glaucoma, and systemic diseases. Thickness of the retinal nerve fibre layer (RNFL) as measured by OCT is now a recognised outcome measure in clinical trials of potential therapies for multiple sclerosis[133].

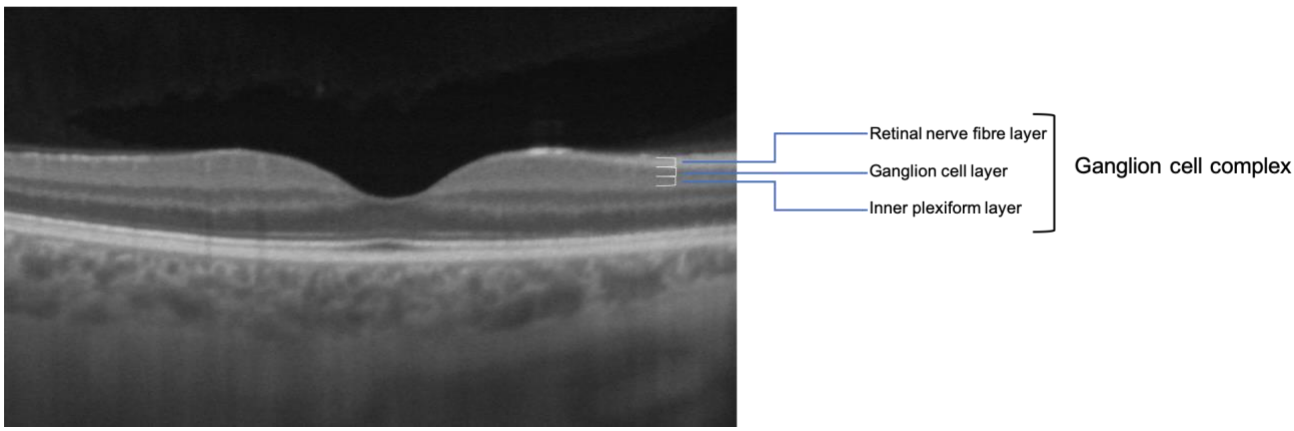

Figure 10: Optical coherence tomography (OCT) of the macula.

Most research into OCT for neurodegenerative disease has focused on the inner retinal layers of RNFL, ganglion cell layer (GCL) and inner plexiform layer (IPL). Due to challenges in segmenting the layers individually, the GCL and IPL thicknesses are

often combined to form a GC-IPL. When GC-IPL is additionally combined with RNFL, this is known as the ganglion cell complex (Figure *10*).

The ophthalmic hallmarks of neurodegenerative disease are changes within the inner retinal sublayers, in particular those of the ganglion cell-inner plexiform (GC-IPL) layer and RNFL[41]. Regarding nomenclature, the peripapillary RNFL represent the convergence of retinal ganglion cells from across the entire retina to the circumference of the optic nerve. The ganglion cell and inner plexiform layers are challenging to distinguish independently with modern segmentation systems and are therefore often evaluated in tandem as the GC-IPL. The ganglion cell complex (GCC) incorporates the macular RNFL in addition to GC-IPL (Figure *10*). Posterior to the inner plexiform layer lies the inner nuclear layer (INL, Figure *11*), where the cell bodies of the horizontal, bipolar, amacrine and Muller cells reside. Importantly, dopamine content within the retina centres on the dopaminergic amacrine cells, which are in the INL[134–136] (Figure *11*).

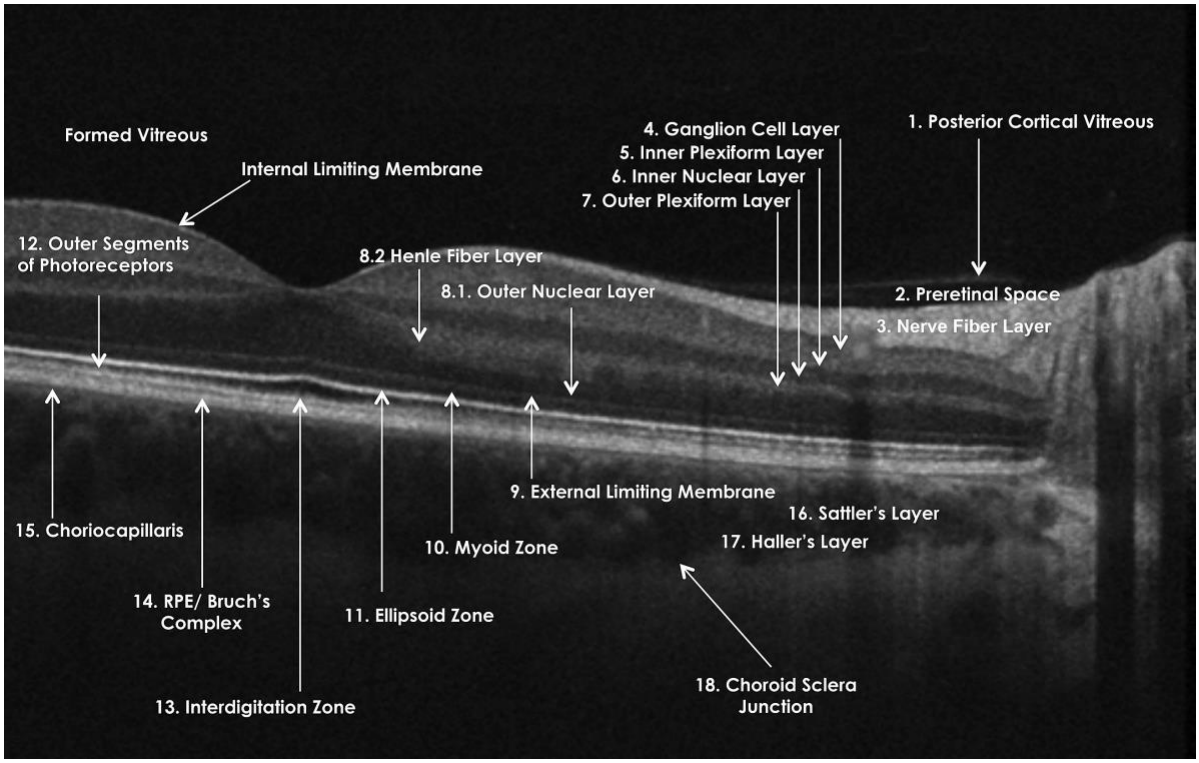

Figure 11: Annotated retinal optical coherence tomography scan annotated according to the agreed lexicon from the International Nomenclature for Optical Coherence Tomography [IN • OCT] Panel.

Reused with permission from. Staurenghi G, Sadda S, Chakravarthy U, Spaide RF; Ophthalmology. 2014 Aug;121(8):1572-8.

While earlier imaging modalities, such as scanning laser polarimetry, allowed measurement of some of these layers (such as the RNFL), most research understanding the association between neurodegenerative disease and the retina has used OCT[137]. There is now sizeable evidence across several landmark prospective cohort studies and three systematic reviews since 2019 that prevalent mild cognitive impairment (MCI) and dementia, in particular AD, are associated with reduced thickness of the peripapillary RNFL and macular GC-IPL on OCT[41,138–140]. Chan et al performed a meta-analysis across 30 studies including 1257 patients with

AD and 1460 controls. They found convincing evidence of reduced thickness in GC-IPL (standardised mean difference of -0.46 microns, 95% CI: -0.80, -0.11), RNFL (-0.67, 95% CI: -0.95, -0.38) and GCC thickness (-0.84 microns, 95% CI: -1.10, -0.57)[139]. A recent umbrella systematic review, which included fourteen systematic reviews examining ocular biomarkers in AD, estimated an area under the curve (AUC) range of 0.63 to 0.69 for discriminating between AD and healthy controls using GC-IPL[140]. Few groups have also leveraged deep learning for modelling dementia with retinal OCT. Wisely et al sequentially investigated individual and collective image modalities (OCT, wide-field colour photography and fundus autofluorescence photography) for discriminating symptomatic AD from healthy controls finding that the single most useful input were spatial thickness maps of the macular GC-IPL[141]. However, it should be noted that the numbers were relatively small (*n* cases = 36). These studies also importantly all pertain to prevalent disease.

Two studies have elucidated the potential predictive value of OCT in MCI and dementia. Studying participants within UK Biobank (UKBB) who had OCT imaging, Ko et al found that reduced macular RNFL thickness was not only associated with worse cognitive performance across 32,038 participants cross-sectionally but those with follow up data within the lowest quintiles with follow up data (*n*=1251 participants) had nearly twice times the odds of performing worse on cognitive testing 2-4 years later[142]. Similarly, results from the Rotterdam study published the same month showed prevalent dementia to be associated with thinner GC-IPL but not RNFL. However, when considering 86 participants with incident dementia, thinner RNFL was associated with greater hazards (HR 1.43, 95% CI: 1.15, 1.78) while GC-IPL was not[143]. It is therefore difficult to rationalise the different

contributions of RNFL versus GC-IPL, and a further challenge comes from the design in several studies. For example, the issues identified across the reports include heterogenous criteria for dementia/MCI diagnosis, selective location reporting of the OCT-derived metrics (e.g. some reports may report the RNFL inferior quadrant only), small sample sizes, residual confounding, and incorrect identification of controls[41]. In general, there is a scarcity of literature examining the role of retinal imaging in incident AD and other forms of dementia.

2.4 Hospital Episode Statistics

Healthcare in the United Kingdom (UK) adopts a universal health care model with the majority of the population (>97%) receiving their hospital-based care within the National Health Service (NHS)[144]. Following discharge, routinely collected data during a patient's admission are subsequently translated into corresponding International Classification of Diseases (ICD) codes by clinical coders within the respective institution and submitted to the Secondary Uses Service overseen by NHS Digital (previously the Health and Social Care Information Centre) providing a unified record-level national repository of Hospital Episode Statistics (HES) admitted patient care for the majority of the population residing within England[145,146]. While clinical coders have reasonable accuracy in converting clinical notes into codes[147], concerns remain over the lack of clinical validation of HES (for example, >50% of hospital consultants have never had contact with clinical coders in a 2012 survey[148]). The original purpose of HES was the monitoring of service activity and negotiation of financial reimbursement but it is increasingly used for epidemiological research. HES data are amenable to research as a sole resource but can also be deterministically linked to other datasets, as in the case of UK Biobank, the Avon Longitudinal Study of Parents and Children or the European Prospective Investigation into Cancer in Norfolk[149,150].

HES Admitted Patient Care data consists of discrete episodes coded with a maximum of twenty diagnostic codes with admission and discharge date. Each episode pertains to care under a given consultant such that a single admission may incorporate several episodes related to the same event. More concretely, a patient suffering from acute renal failure may initially be admitted under a general medical

consultant before transfer to a specialist nephrologist followed by transfer to a separate consultant overseeing emergency haemodialysis - this would result in three distinct HES episodes despite being a sole admission. Diagnostic codes in HES are recorded using the International Classification of Diseases (ICD) 10th revision.

Previous work has suggested that HES is a reliable resource for epidemiological research in dementia. Using data from the Million Women Study, Brown et al. compared completion of dementia diagnoses in HES against two reference standards – the primary care database, Clinical Practice Research Datalink (CPRD), and a survey of 244 general practitioners. HES-derived dementia labels agreed fully with both primary care sources in 85% of participants and this increased to 95% and 88% for those with a HES diagnosis specifically of Alzheimer's disease or vascular dementia respectively[151]. However, HES diagnoses were generally recorded later, being on average first mentioned 1.5 years later than in CPRD. Therefore, patients with HES-coded dementia may have more advanced disease and the identification of incident dementia is limited.

Herret et al conducted a comprehensive assessment of coding of myocardial infarction across primary care, secondary case and disease registry databases[152]. Pertinent findings include that the prevalence of CVD risk factors and comorbidities was similar across all databases, fatal myocardial infarctions were unlikely to be recorded in hospital sources (36.7% of those from death registry data were recorded in HES) and the positive predictive value of an acute myocardial infarction diagnosis in HES was 91.5% (90.8, 92.1). Linkage of HES with primary care and death certificate data through the British Heart Foundation initiative on COVID-19 for more

than 54 million patients in the UK revealed that for incident myocardial infarction, when considering all three sources, HES records included ~80% of cases. For ischaemic stroke, this figure was 65%[153]. For CVD therefore, greater trust can be placed in HES diagnoses of acute myocardial infarction than ischaemic stroke, and the study design of nested case-controls may reduce some of the information bias if data is missing at random. A number of techniques correcting for misclassification bias using diagnostic accuracy measures, such as positive predictive value have been described[154–157].

2.5 Summary of the literature as a rationale for this project

This review of the literature highlights the association of retinal biomarkers (captured either through CFP or OCT) with cardiovascular and neurodegenerative disease however there remain several key gaps and methodological issues.

Firstly, most evidence arises from prospective epidemiological cohorts, such as UK Biobank. While these undoubtedly represent powerful vehicles for discovery science, they are limited by factors of population-based cohort studies, such as a small number of rare diseases and potential recruitment of more health-conscious individuals as volunteers. Participants in UKBB are less likely to be obese, smoke, or drink alcohol and accordingly, mortality rates for participants aged 70-74 in UKBB are 46.2% and 55.5% lower for men and women respectively than the general UK population[158]. Moreover, among participants recruited between 2006-2010, 94.6% were of White ethnicity[158]. Thus, risk factor associations and clinical prediction models established using such cohorts may have limited external validity when considering the general population.

Secondly, while cross-sectional associations between retinal morphology and prevalent dementia are abundant in the literature, there is a scarcity of incident dementia prediction. Modifiable risk factors and emerging pharmacological therapies for dementia are likely to be most effective when implemented early in the disease course yet there remains, to date, no retinal imaging-based prediction model for the development of dementia.

Thirdly, given the role of cardiometabolic and neurodegenerative dysfunction across many non-communicable diseases, retinal morphology likely differs in those with many systemic disorders. Discovery of eye-brain relationships could further our understanding of biological mechanisms into disease and highlight potential outcome measures for disease progression and treatment response.

Fourthly, the use of multimodal ophthalmic imaging as variables for prognostic factor and individual risk prediction is limited. UK Biobank participants did undergo both retinal CFP and OCT yet there are few published reports which analyses both in conjunction for risk prediction of systemic disease. Given that a) CFP-derived metrics, such as fractal dimension, have strong associations with cerebrovascular disease, b) OCT-derived metrics associate strongly with prevalent dementia, and that c) there is a clear interplay between these two chronic complex disorders of ageing[159,160], I would hypothesise that the combination of both modalities provide incremental prognostic performance.

3. Aims

The overarching aim of this doctoral research is to explore to what extent ocular phenotypes can be used to further our understanding of non-communicable systemic diseases, particularly those with neurodegenerative and cardiovascular underpinnings. The specific research objectives are:

Objective 1 – Creation of AlzEye

- To establish a real-world health dataset linking retinal imaging and systemic disease data from Hospital Episode Statistics
- To extract clinically relevant retinal features from imaging using fully automated segmentation tools

Objective 2 – Description and overall prognosis

- To evaluate the mortality rate and incidence rates of CVD events in patients with a new diagnosis of cataract, glaucoma, age-related macular degeneration and proliferative diabetic retinopathy
- To evaluate the mortality rate and incident rates of CVD events in patients with a new acute neurophthalmic event (non-arteritic ischaemic optic neuropathy, ocular cranial neuropathy, and retinal artery occlusion)

Objective 3 – Discovery

Exemplar conditions were chosen based on public health importance, strong pathophysiological basis with cardiometabolic and neurodegenerative dysfunction. Further details are given in section 6.1 Oculomic exemplars.

- To investigate the association between multimodal retinal imaging and schizophrenia
- To investigate the association between inner retinal morphology and Parkinson's disease
- To investigate the association between multimodal retinal imaging and periodontitis
- To investigate the association between multimodal retinal imaging and amblyopia

Objective 4 – Prediction

- To develop, internally validate and externally validate static clinical prediction models for all-cause dementia using retinal imaging and sociodemographic data

4. Methods

Two datasets were leveraged for conducting this project – i) AlzEye, a record-level linkage dataset of NHS hospital attendances of Moorfields Eye Hospital (MEH) patients and ii) UK Biobank, a prospective community-based prospective cohort study. In this section, the creation of AlzEye is first described including the source of the relevant variables and the linkage process. The design and relevant ophthalmic examination and investigations within UK Biobank are then discussed. Extraction of clinically relevant retinal features for both then follows finishing with a description of the overall statistical analysis plans. Further Methods tailored to each objective are provided in subsequent chapters.

4.1 The AlzEye project

The AlzEye project dataset comprises a retrospective cohort dataset of patients who have attended Moorfields Eye Hospital NHS Foundation Trust (MEH) between 1 January 2008 and 1 April 2018. Patients were included if they were aged 40 years and over, had valid NHS numbers and had attended any department where retinal imaging may have been conducted (e.g. glaucoma, retina, neuro-ophthalmology or emergency ophthalmic services). Those with invalid NHS numbers, dates of birth or who had previously opted out of their health data being used for purposes of research (described in the NHS as a 'Type 2 opt-out') were excluded. Ethnicity group was self-reported by the patient according to categories outlined in the UK Census[161]. To preserve anonymity, individual ethnic groups were then grouped as (1) Asian or Asian British, (2) Black or Black British, (3) Mixed, (4) Other Ethnic Group, (5) White or (6) Unknown. Relative socioeconomic deprivation was estimated using the Index of Multiple Deprivation (IMD) decile. IMD is the standard UK measure of relative deprivation and socio-economic status (SES) across seven domains of income, employment, education, health, and barriers to housing and services, crime and living environment[162]. IMD was estimated by permuting the IMD 2015 rank from the patient's postcode through Lower Super Output Areas followed by aggregation into deciles. Mortality data were derived from the MEH database, which is updated on fortnightly using reports extracted from the NHS National Spine and is completed on an individual basis by the MEH data quality team to ensure accuracy. Data are completed on any patients who have ever attended MEH. Mortality data up to the end of the study period, 1 April 2018, were included.

4.1.1 Public engagement

Patient and public involvement and engagement (PPIE) has been embedded within AlzEye since its inception. Priority setting was explored through presentations at public engagement events and charity and other public forums. In addition, a survey sent to 483 people was carried out in late 2017 to gauge the acceptability of using anonymised MEH patient data without consent. With a response rate of 21%, >90% of respondents thought it was acceptable for eye scans, acquired as part of their routine care, to be used for the purposes of research (Appendix 6: PPIE survey). Additional comments included concerns of data being passed to third parties and the risk of data breaches/leaks.

Three members of the public have also been recruited as part of the AlzEye Working Group. This group meets quarterly to discuss the ongoing management of the study, review any information governance concerns and exchange ideas on data presentation. Layperson members will be actively involved in disseminating the study results in public forums.

4.1.2 Approvals

The AlzEye study and data governance were firstly approved by MEH Research and Development (internal reference: KEAP1004) for sponsorship confirmation. I then applied to and received approval from the National Research Ethics Service (18/LO/1163) and subsequently the Confidential Advisory Group for Section 251 support (18/CAG/0111), which grants temporary lifting of the common law duty of confidentiality around confidential patient information ‘in the public interest’ or ‘in the interests of improving patient care’ (National Health Service Act 2006). The National

Health Service Health Research Authority granted final approval shortly thereafter providing the legal basis for an application to the NHS Digital Data Access and Request Service[163] (*Figure 12*). Following internal NHS Digital review and prior to data release, the DARS application was scrutinised by the Independent Group Advising on the Release of Data (IGARD) in line with Section 263(2) of the Health and Social Care Act 2012, the Code of Practice on confidential information. IGARD is an independent panel with a broad range of expertise, from legal to information governance to epidemiology. Support for AlzEye was given by IGARD in January and August 2019 citing that 'aspects of the application could be used as an exemplar by NHS Digital to help other researchers with their applications to the Data Access Request Service (DARS)'[164] (*Figure 12*).

The dataset was finalised upon completion of engineering work parsing manufacturer-specific file formats to non-proprietary data structures amenable to image analysis with appropriate deidentification. A secure cloud-based informatics pipeline was used for transfer of images to UCL from MEH, the establishment of which was delayed by the COVID-19 pandemic. Imaging data was stored (with backup) across dedicated network-attached storage device within the UCL School of Life and Medical Sciences (SLMS) and only accessible to members of the AlzEye research team. All data entities were listed within the UCL SLMS Information Asset Register.

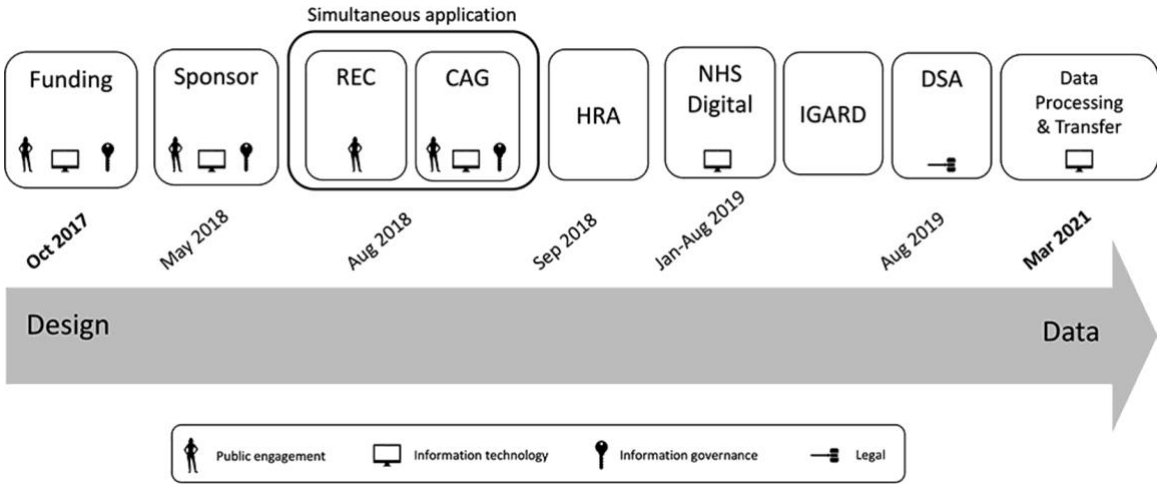

Figure 12: The approvals process for AlzEye.

CAG, Confidential Advisory Group; DSA, data sharing agreement; HRA, Health Research Authority; IGARD, Independent Group Advising on the Release of Data; NHS, National Health Service; REC, research ethics committee. *From Wagner SK, Hughes F, Cortina-Borja M et al. AlzEye: longitudinal record-level linkage of ophthalmic imaging and hospital admissions of 353 157 patients in London, UK. BMJ Open. 2022 Mar 16;12(3):e058552*[165]*. Figure available under CC license, no changes made).*

4.1.3 Linkage strategy

The linkage strategy was designed through collaboration between information governance, information technology, computer scientists and clinicians based at MEH, University College London (UCL) and NHS Digital. The data originator (MEH) never received HES admissions data and the third party (UCL) did not receive personally identifiable information. Patient link identifiers consisting of a unique NHS identification number, sex and date of birth originating from MEH were transferred to NHS Digital in conjunction with a unique study ID generated using a cryptographic hash function. Ophthalmic covariates, mortality data, and patient's sociodemographics with study ID were transferred to UCL. Ophthalmic imaging data

pertaining to the patients within the study were extracted and de-identified during conversion from their proprietary format to Digital Imaging and Communications in Medicine (DICOM) format before transfer to UCL. Following linkage with HES, NHS Digital returned HES data to UCL where it was linked with MEH-based ophthalmic data in the UCL using the study ID (Figure *13*). AlzEye HES data is stored within the UCL Data Safe Haven, a “walled garden” trusted research environment certified to ISO27001 information security standards. For analyses, targeted extracts of the HES data may be exported from the Data Safe Haven.

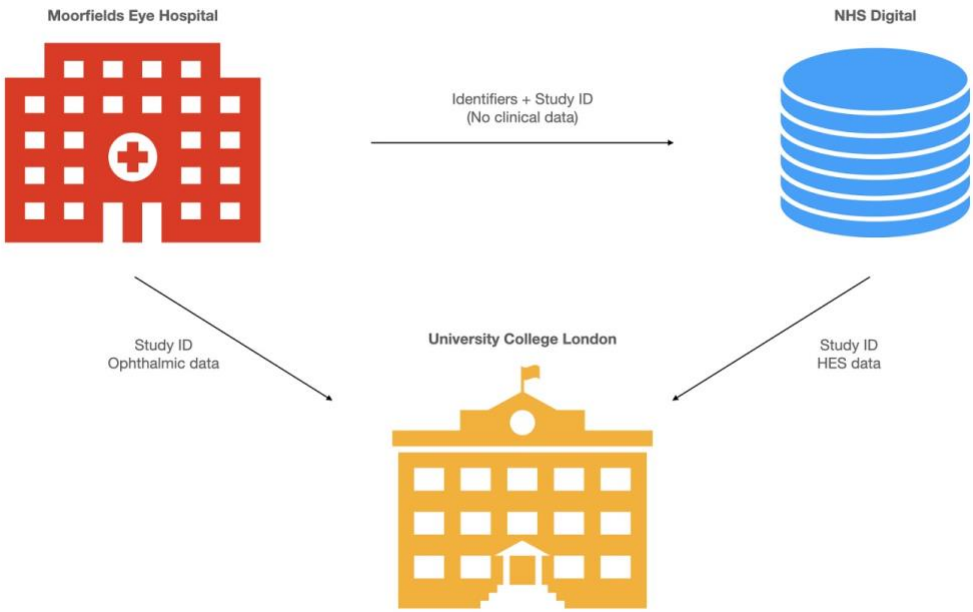

Figure 13: Linkage approach of AlzEye.

Moorfields Eye Hospital firstly securely transfers a spreadsheet of identifiers with a study ID to NHS Digital and secondly the study ID with ophthalmic data, including diagnoses and retinal imaging, to University College London. NHS Digital links the identifiers with the Hospital Episode Statistics database and returns the admissions data just with the study ID to UCL. UCL links the ophthalmic data from Moorfields Eye Hospital with HES data from NHS Digital using the study ID. HES: Hospital Episode Statistics, NHS: National Health Service

4.1.4 Ophthalmic variables

Patient-level ophthalmic variables were extracted from the MEH data warehouse, which aggregates information from the patient administration system (PAS), electronic health record (EHR) and imaging database, all linked through a unique MEH hospital identification number. Sociodemographic data, including date of birth, sex, ethnicity and postcode as well as patient clinic and operation appointment patterns are housed within PAS. As a tertiary ophthalmic unit, MEH adopts referral

pathways such that patients are seen in their relevant subspecialist clinic rather than general ophthalmic services. Accordingly, a patient with multiple ophthalmic conditions will be under the care of several ophthalmic subspecialists. For example, a patient with a diagnosis of uveitis will begin under the review of a specialist retinal clinic following referral from primary care or an eye emergency department. Should the patient develop glaucoma after two years of care under the retina team, they would then typically be referred to a specialist glaucoma clinic within MEH and thus remain under the care of two separate teams. Surgical procedures were recorded in the electronic health record at MEH from September 4th, 2012. Operation details, including procedure name, laterality and indication for surgery are contained within the MEH EHR and uploaded to the MEH data warehouse. For example, a patient undergoing the most common operation in the UK, cataract extraction, would therefore have an entry for the typical procedure, phacoemulsification and intraocular lens implant, with the indication of cataract and the sequence of eye displayed.

For describing the ophthalmic burden of the cohort, four common diseases were studied - cataract, glaucoma, wet age-related macular degeneration (AMD) and proliferative diabetic retinopathy (PDR) as they collectively account for more than 65% of sight loss in the UK and worldwide (Section 5.1.1 Common ophthalmic diseases) [166–168]. Moreover, all four conditions have been previously associated with increased incidence of cardiovascular disease[169–172]. Cataract was defined as any operation codes denoting phacoemulsification surgery and the indication of cataract and only first eye cataract surgery was included as the commencing event of interest in this report. This is because I was interested in the earliest potential sign of systemic disease as represented by ocular disease and second eye surgery is more

frequently associated with certain demographic characteristics, is often considered a lifestyle choice and has had mixed support in public policy in the last two decades[173–175]. Glaucoma was defined as any patient attending the glaucoma clinic three or more times with ongoing follow up from 1st January 2010. The first two years of the study period were excluded as this may have incorporated patients with previous diagnoses of glaucoma where the maximum follow up interval can approach two years. Diabetic eye disease provides a special case due to audit procedures mandated by the NHS Diabetic Eye Screening Programme. Coding of eye disease secondary to diabetes mellitus is rigorously validated by a dedicated team within MEH databases with a separate database consisting of all cases of diabetic eye disease in conjunction with retinopathy and maculopathy grades according to the NHS Diabetic Eye Screening Programme criteria at hospital appointment from 12th September 2013. Proliferative diabetic retinopathy dates were recorded as the first appointment for each patient where the corresponding diagnosis was first made at the hospital appointment. Age-related macular degeneration can be categorised into two major variants - dry and wet. Dry AMD is slowly progressive and no active hospital intervention currently exists and it is thus MEH standard practice for patients with typical features to be discharged with lifestyle and monitoring advice. In contrast, wet AMD requires treatment through intravitreal injections. Leveraging previous work evaluating all patients with wet AMD at MEH from 2008 onwards with manual clinician-led validation of the dataset provided the diagnostic codes for this disease group[176,177].

Extraction of ophthalmic variable data for other conditions is described in the subsequent chapters. In general, conditions presenting acutely and thus presenting

through the MEH emergency eye service, were identified through structured diagnostic codes in PAS.

4.1.5 Systemic disease variables

Data from MEH was linked with the NHS Digital hospital episode statistics (HES) admitted patient care database from 2007/2008 to 2017/2018, a centralised national data warehouse of all admissions at NHS hospitals in England coded using ICD. In line with previous reports, myocardial infarction was defined as code I21 or I22[178–180]. Similarly, stroke was defined as code I61-I64. Dementia was defined as ICD codes E512, F00, F01, F02, F03, F10.6, F10.7, G30, or G31.0, derived from previous work evaluating the agreement between HES admitted patient care data and primary care data, through general practitioner surveys and the Clinical Practice Research Datalink (CPRD)[151]. Numbers specifically for Alzheimer's disease (F00, G30) and vascular dementia (F01) are also described. Important confounders of the relationship between retinal morphology and cardiovascular or neurodegenerative disease are hypertension and diabetes mellitus (Table *1*). These were also identified through coding within HES.

Group	Disease	ICD code(s)
Cardiovascular	Acute coronary syndrome	I21, I22[152]
	Heart failure	I50
	Atrial Fibrillation	I48
	Hypertension	I10, I15
	Subarachnoid haemorrhage	I60
	Intracerebral haemorrhage	I61[181]
	Ischaemic stroke	I63-I64[181]
	All stroke	I60, I61, I63, I64[181]
Neurodegenerative	Alzheimer's disease	F00, G30
	Vascular dementia	F01
	Parkinson's disease	G20[182,183]
	All-cause dementia	E512, F00, F01, F02, F03, F106, F107, G30, G310[151]
Other	Diabetes mellitus (Type 1 and 2)	E10, E11
	Schizophrenia	F20[182]

Table 1: Codes from the 10th revision of International Classification of Diseases (ICD) relating to diabetes mellitus, cardiovascular and neurodegenerative diseases. Note that previous work investigating the validity of ICD code definitions for different phenotypes are referenced, further details on their accuracy are given in subsequent chapters.

4.2 UK Biobank

Data from the United Kingdom Biobank (UKBB) study was used in this project for two main purposes – i) discovery of eye-body associations where systemic disease case definitions were too vague or absent within AlzEye and ii) to replicate and/or externally validate associations and prediction models estimated within AlzEye in a group more typical of the general UK population.

4.2.1 Cohort profile

United Kingdom Biobank (UKBB) is a prospective epidemiological cohort study of 502,656 UK residents aged between 37 and 73 years. Participants were initially recruited between 2006 and 2010 and gave informed consent to undergo deep phenotyping for the investigation of health and disease (more information available at: https://www.ukbiobank.ac.uk/). This included extensive touchscreen questionnaires, physical measurements, and several investigations. From the full cohort, a subset of 117,175 participants (eye subset) additionally underwent enhanced ophthalmic testing including visual acuity, intraocular pressure, refraction and keratometry across six centres within the UK (Liverpool, Sheffield, Birmingham, Swansea, Croydon and Hounslow)[183]. From the eye subset, 67,321 UKBB participants received retinal imaging with both colour fundus photography (CFP) and optical coherence tomography (OCT) at the initial visit[184,185]. As detailed in Section 2.4 Hospital Episode Statistics, UKBB has also been linked with HES admitted patient care data.

Similar to AlzEye, participants self-reported ethnicity as per categories defined by the UK Census. Socioeconomic status, however, was defined through two separate

tools: as with AlzEye, the IMD score was quantified through the participant's postcode. However, the UKBB eye cohort included participants across England and Wales and IMD scores are not comparable across constituent nations of the UK unless adjustments are made[186]. Therefore, in some cases, the Townsend deprivation index was used. The Townsend deprivation index is similarly derived from the participant's postcode and based on four main areas – unemployment, non-car ownership, non-home ownership and household overcrowding[187]. Advantages of the Townsend index include that its estimation is based on output area, which covers 100-625 people (in contrast to IMD which relates to Lower-layer Super Output area covering 1000-3000 people) and that it can be used across the UK. However, some consider the domains of Townsend index, such as car ownership, not to represent poverty/deprivation well. For example, car ownership may be much lower in super urban environments, such as London[188].

4.2.1 Ophthalmic variables

UKBB participants within the eye subset completed an additional set of touchscreen questionnaires asking about whether they had previously diagnosed with specific eye diseases (Field ID: 6148, *Figure 14*) or previously had eye surgery (Field ID: 5181).

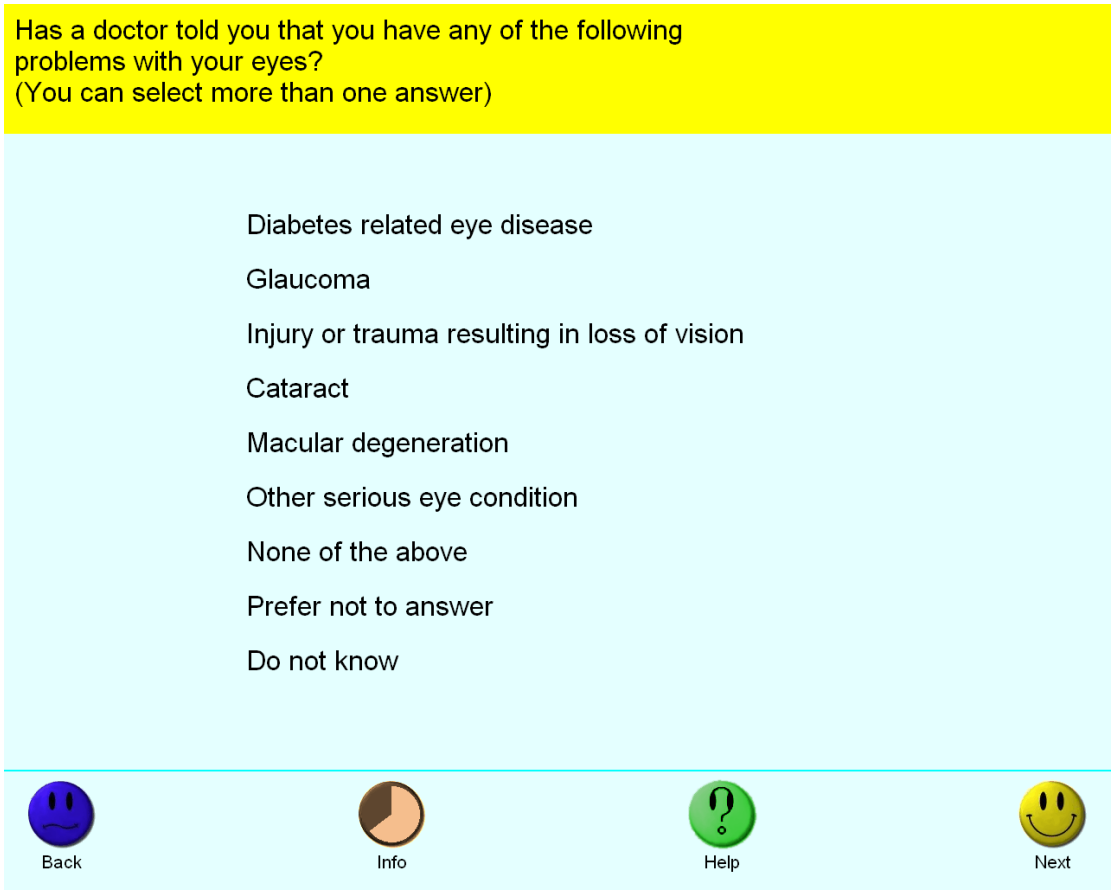

Figure 14: Example touchscreen questionnaire image within UK Biobank asking participants within the eye cohort about previous eye diseases (Field ID 6148).

Ophthalmic measurements, including visual acuity, intraocular pressure, refraction, and corneal hysteresis were acquired on participants within the eye cohort. Visual acuity was measured using logarithm of the minimum angle of resolution (LogMAR) chart using a computer screen with standard illumination with the right eye measured first. Testing was done at 4 metres with the participant's distance refraction (e.g. spectacles) where applicable. Non-cycloplegic refraction was acquired using an automated refractometer (Tomey RC-5000 Auto Refkeratometer [Tomey, Nagoya, Japan]). A maximum of 10 measurements per eye were taken and the reliability recorded. Details on intraocular pressure and corneal hysteresis measurement can

be found in the UKBB Eye and Vision Consortium cohort profile paper however they were not used for this project[183].

Macula-centred CFP and OCT were acquired using the Topcon 3D-OCT 1000 Mark II device (Topcon Corporation, Tokyo, Japan) in a darkened room without pupillary dilation. CFPs were 45 degree and had a scanning speed of 18,000 A-scans per second. OCTs covered a 6.0 mm × 6.0 mm area and had 128 horizontal B scans and 512 A-scans per B-scan. Images from both eyes, where available, were used. UK Biobank technicians were certified to acquire retinal images following completion of a structured training programme and competency examination[185]. Approximately 10% of OCT images acquired were quality assessed by the MEH Reading Centre. For this project, only participants who had completed the touchscreen questionnaire and undergone retinal imaging were included[184,185].

4.2.3 Systemic disease variables

Participants within UKBB underwent multimodal deep phenotyping to characterise health and disease. For this project, data on systemic health was derived from four major sources – touchscreen questionnaire and interview, physical examination, biomarker measurement and linkage with other national datasets.

Touchscreen questionnaire and interview

Participants were asked about past and current medical conditions as well as medications and previous procedures through a verbal interview with a trained nurse (Field ID 20002). These were recorded using a hierarchical tree format.

Physical examination

As part of the baseline visit, participants had several physical measurements done at the Assessment centre. This included automated blood pressure and ancillary measurements in specific groups (e.g. carotid ultrasound, hearing tests). Further information can be found under Category 100006 on the UKBB showcase[189].

Biomarker measurement

Several biological samples were taken from UKBB participants. An exhaustive list can be found on the UKBB website[190] but this project will mainly focus on diabetic biomarkers, including glucose and glycated haemoglobin.

Linkage with other datasets

Data from UK participants has been linked with several national resources, including primary care data and national cancer registries[191]. Relevant to this project are linkage with:

- National death registries which contain data on date and cause of death coded using the ICD-10 ontology
- Hospital Episode Statistics Admitted Patient Care, as per AlzEye, which is coded using ICD-9 and ICD-10.

Differences in case definition between UKBB and AlzEye

While case definitions of systemic disease outcomes in UKBB generally reflected those used in AlzEye, there are some differences. Firstly, UKBB has lifetime HES data in contrast to AlzEye, which has HES data dating back to 2008. Thus, AlzEye may miss some cases of preceding disease (e.g. myocardial infarction occurring in

2005) leading to misclassification of cases and controls. The bias is likely to be towards the null as differences between arms will be artificially reduced. Secondly, UKBB additionally has self-reported disease diagnosis derived from the verbal interview. If a participant reported a previous heart attack, then they would be excluded as controls.

4.3 Retinal image analysis

The research reported in this thesis focussed on two retinal imaging modalities - colour fundus photography (CFP) and optical coherence tomography (OCT). Retinal imaging data from both AlzEye and UKBB were acquired using Topcon devices. For UKBB, all images were captured on the 3D-OCT 1000 Mark II device while AlzEye contained data acquired on five separate Topcon devices. Raw proprietary format data was converted to DICOM format using the *private-eye* library developed in-house at Moorfields Eye Hospital. As part of the conversion process, an accompanying comma separated value file was generated with image metadata alongside the file path. All images analysed in this project were macula-centred.

4.3.1 Colour fundus photography

CFPs in both AlzEye and UKBB were analysed using two separate retinal image analysis software – the Vessel Assessment and Measurement Platform for Images of the REtina (VAMPIRE)[192] and AutoMorph[193].

VAMPIRE is an automated segmentation software developed and licensed by the University of Dundee[194]. Access to VAMPIRE was provided through collaborators Professor Emanuele Trucco and Dr Muthu Mookiah, University of Dundee. DICOM CFPs, converted into portable network graphics (png) format, were input to the VAMPIRE executable. Images were firstly cropped and resized. The retinal vasculature is then segmented using a deep learning U-net architecture, a recognised convolutional neural network designed specifically for medical image segmentation[195]. The software automatically then assigns a categorical outcome of

image quality as ‘good’, ‘okay’ or ‘poor’ based on the segmentation. Scripts to extract vessel indices of fractal dimensions were then run on the segmentations.

AutoMorph is an openly available automated deep learning pipeline providing retinal vascular and optic nerve segmentation of CFP[193] (*Figure 15*). AutoMorph was developed at UCL by colleague and PhD student, Yukun Zhou, during this PhD. AutoMorph also provides a modular framework consisting of pre-processing of the image, quantification of image quality, retinal vascular and optic nerve segmentation (both optic cup and disc), and extraction of quantifiable features in tabular format (*Figure 16*). These consist of previously published packages as individual components of the pipeline – *BF*-Net for vascular segmentation[196], *EyeQ* for image pre-processing[197], *lwnet* for optic nerve segmentation[198] and *retipy* for feature measurement and extraction[199]. Of note, AutoMorph provides a continuous score in addition to categorical (good, ok, poor) gradings for image quality allowing adjustment in multivariable models. As highlighted in section 2.3.1.2 Retinal vascular morphometry, certain features (e.g. retinal fractal dimension) may be associated with both image quality as well as risk factors of non-communicable disease (e.g. age), underlining the importance of considering quality as a potential confounder. As a result of analyses conducted on UKBB for this PhD, AutoMorph outputs will be made available on the UKBB Data Showcase.

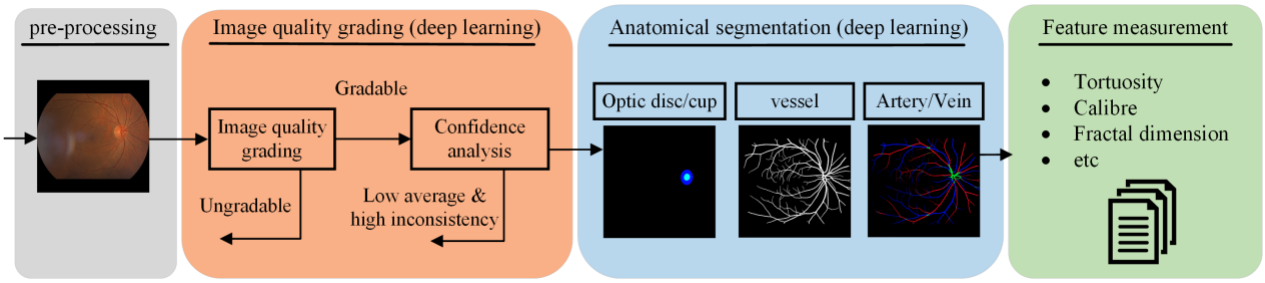

Figure 15: AutoMorph pipeline denoting, image quality, segmentation, and feature extraction steps.

Image courtesy of Y Zhou (https://rmaphoh.github.io/projects/automorph.html).

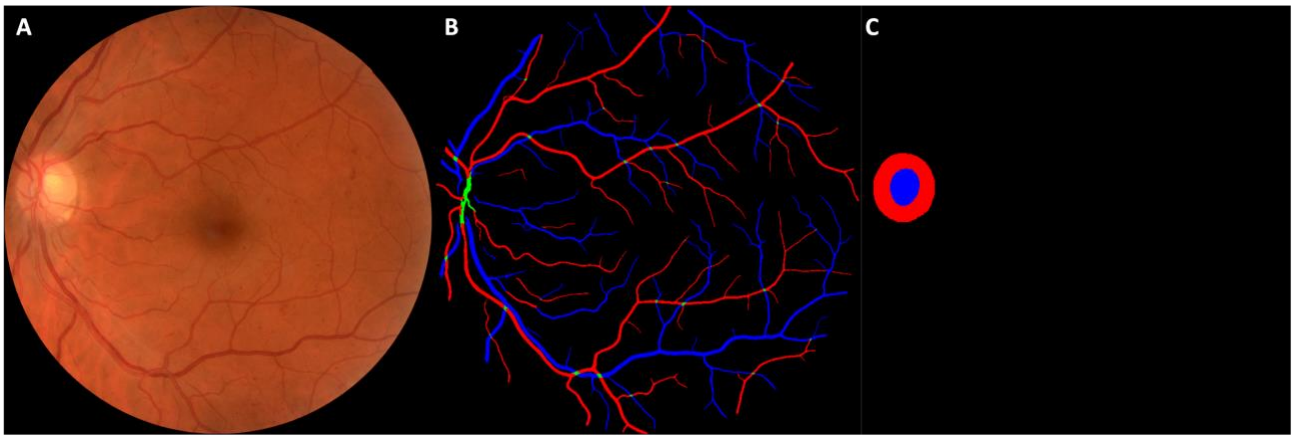

Figure 16: Example left colour fundus photograph (A) with artery-vein (B) and optic nerve segmentation (C) generated by AutoMorph.

Red pixels indicate arterioles and optic disc neuroretinal rim while blue pixels indicate venules and optic cup.

4.3.2 Optical coherence tomography

OCT images were segmented and retinal sublayer thicknesses extracted using the Topcon Advanced Boundary Segmentation Tool (TABS) version 1.6.2.6 (*Figure 17*).

The TABS software was provided by Mr Tony Ko and Dr Christopher Mody from Topcon Ltd through a license agreement between myself and Topcon.

TABS uses dual-scale gradient information to automatically segment eleven retinal layer boundaries in a rapid fashion (*Figure 17*). Foveal position is also automatically determined for central grid placement and derivation of spatial regions equivalent to those outlined by the Early Treatment of Diabetic Retinopathy (EDTRS) study[200]. Associations of outputs from TABS with systemic disease and risk factors in UKBB have been extensively published previously [15,184,185].

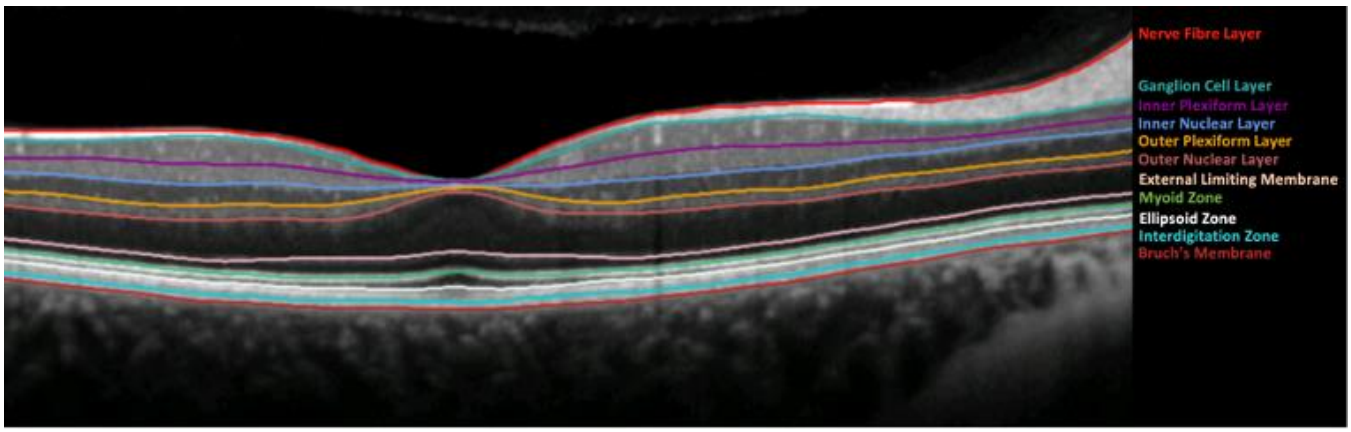

Figure 17: Example segmentation of the eleven boundaries segmented by the Topcon Advanced Boundary Segmentation software.

For both AlzEye and UKBB, macula-centred OCTs in their proprietary format (.fds, .fda) were input to TABS. Output pixel-level data was then converted into mean retinal sublayer thicknesses according to location (relative to the fovea). These scripts were written by collaborator, Mr David Romero-Bascones, Mondragon Unibertsitatea. Sublayers were defined according to the nomenclature from the

International Nomenclature for Optical Coherence Tomography[130]. For inner retinal layers, such as the GC-IPL and RNFL, sublayer thicknesses from the parafoveal ETDRS sectors were averaged to give a mean value (*Figure 18*). The fovea was not included as retinal ganglion and bipolar cells are typically absent[201].

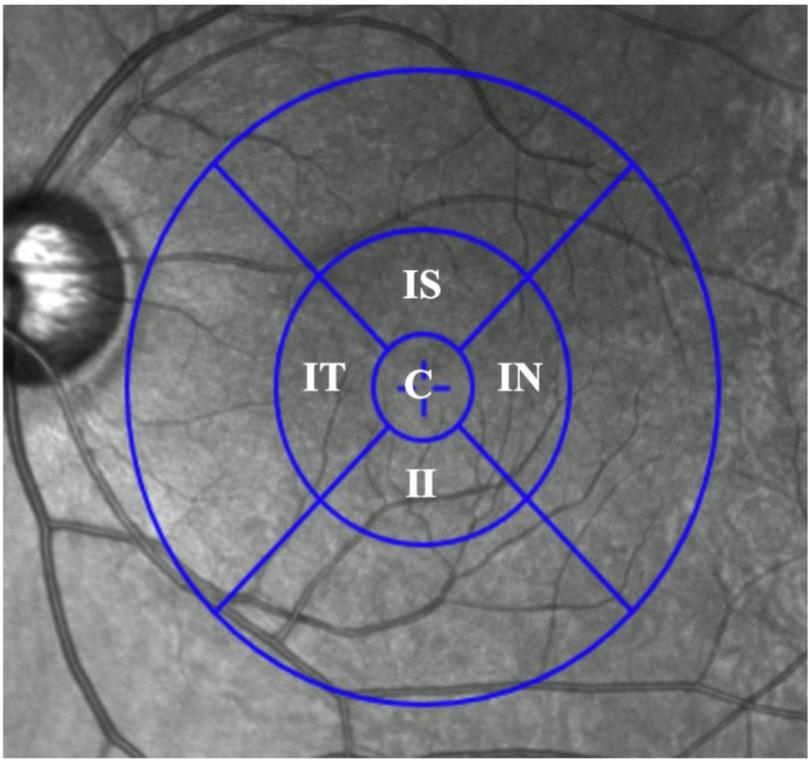

Figure 18: Anatomical localisation for estimation of retinal sublayer thicknesses.

Retinal sublayer thicknesses were averaged according to their position, relative to the fovea. In most cases, this was the parafoveal region. As the fovea is void of the inner retinal layers in the normal eye, this was not included in averaging. C: centre, II: inner inferior, IN: inner nasal, IS: inner superior, IT: inner temporal.

TABS provides additional metadata for each image to establish scan quality based on segmentation error, movement artifact and poor quality. In general, I adhered to previously published literature using a quantile-based approach for image quality control[15,184]. This excluded the poorest 20% of images based on the following

metadata variables: quality, the minimum motion correlation, maximum motion delta, maximum motion factor and inner limiting membrane indicator. The motion indicators are based on the Pearson correlations and absolute differences between the thickness data of the entire retina and retinal nerve fibre layer from each set of consecutive B-scans. The lowest correlation and the highest absolute difference in a scan serve as the resulting indicator scores and identify blinks, eye motion artifacts, and segmentation failures. The inner limiting membrane indicator is a measure of the minimum localised edge strength around the inner limiting membrane boundary across the entire scan; this is useful for identifying blinks, scans that contain regions of severe signal fading, and segmentation errors.

4.4 Statistical analysis

The three main strands of this project align with the initial three stages of the PROGnosis RESearch Strategy (PROGRESS) framework – namely fundamental prognosis research, prognostic factor research, and prognostic model research[202–204].

In the first strand of this doctoral research, *Description*, I summarised the cohort profile of AlzEye and overall prognosis of cardiovascular events and death following diagnosis of specific ophthalmic diseases. Theme 1 of the PROGRESS framework focuses on "the course of health related conditions in the context of the nature and quality of current care"[202]. As AlzEye represents real-world data from >350,000 NHS users in a diverse urban environment, it provides a snapshot of current care within the UK.

In the second strand, *Discovery,* I investigated the association between retinal morphology and specific systemic diseases in both cross-sectional and longitudinal analyses. For the latter, association between retinal features and a subsequent clinical outcome will be explored. Theme 2 of the PROGRESS framework "aims to discover and evaluate factors that might be useful as modifiable targets for interventions to improve outcomes, building blocks for prognostic models, or predictors of differential treatment response"[203].

For the final strand, *Prediction*, I assessed the utility of retinal features from multimodal imaging as predictor variables in clinical prediction models. Although several imaging-based indices (e.g. ganglion cell layer) are associated with the

development of all-cause dementia at a population level, it is unclear whether this can translate to effective individual level prediction. Theme 3 of the PROGRESS framework aims to “review how such models are developed and validated, and then address how prognostic models are assessed for their impact on practice and patient outcomes”[204].

In this section, broad statistical analyses principles are outlined. More specific details to each theme are given in the subsequent chapters.

4.4.1 Description - Overall prognosis and prognostic factors

Descriptive analysis of systemic disease and events among ophthalmic populations was through incidence rates, calculated as the number of new events in the study period per 100,000 person-years at risk (PYAR) with 95% Poisson confidence intervals with the logarithm of the total PYAR as the model’s offset. The at-risk period was defined from the time of ophthalmic diagnosis/event until the earliest of i) death, ii) first event (such as myocardial infarction) or iii) conclusion of the data period on 1st of April 2018.

Time to event between groups was compared using the non-parametric log rank test and event trajectories illustrated visually with Kaplan-Meier curves. Adjusted survival analysis is through cause-specific hazard ratios estimated by Cox proportional hazards modelling[205]. In most instances, fixed baseline covariates of age (at time of ophthalmic event/diagnosis as a continuous variable), sex, ethnicity and socioeconomic deprivation were used. In cases where the competing risk of death is prominent, such as individuals with ophthalmic diseases typical of older populations,

like age-related macular degeneration, subdistribution hazard ratios (sHR) with 95% confidence intervals (CI) were estimated as a sensitivity analysis using the semiparametric competing risks regression model approach described by Fine and Gray[206].

Given the risk of residual confounding with acute neurophthalmic conditions (especially for hypertension and diabetes mellitus), I used propensity score matching (PSM) to estimate the average marginal effect of the ophthalmic disease on time to event (MI, ischaemic stroke or death)[207]. I matched on age, sex, hypertension, and diabetes using a 8:1 greedy nearest neighbour without replacement approach, where PSM is estimated using logistic regression. Balance between controls and cases was assessed using standardised mean differences, variance ratios and empirical cumulative density function[208–211]. No exposed units were discarded.

It is noted that recently, some have advocated for foregoing the traditional approach of testing the proportional hazards assumption however violation was formally assessed in this project[212]. The assumption of proportional hazards was assessed using global and covariate-specific χ^2 testing and visualisation of graphs of scaled Schoenfeld residuals against transformed time as proposed by Grambsch and Therneau[213]. Stratification is implemented for any parameters violating the assumption (for χ^2 testing, a *p*-value <0.05 was considered significant). Nonlinearity between age and log hazard was assessed by plotting Martingale residuals of the null Cox proportional hazards model. Statistical analyses are conducted in R version 4.1.0 (R Core Team, 2021).

4.4.2 Discovery – Prognostic and risk factor associations

Initial data distributions were analysed visually and statistically. Continuous variables were compared between groups using either the Student's t test or Mann-Whitney-Wilcoxon test and categorical variables through either the Chi-squared or *U*-Statistic permutation test of independence[214]. To examine the association between prevalent diseases and retinal morphology, I generally fitted linear mixed effects models with a random intercept at the individual level to account for the multilevel structure of eyes nested in participants. Models were fitted through maximum likelihood estimation and were adjusted for age, sex, ethnicity group, diabetes mellitus and hypertension. To assess the risk of residual confounding by diabetic status in some cases (i.e. comparing individuals with more severe diabetic eye diseases versus less severe and only adjusting for diabetes mellitus overall), sensitivity analyses were performed in some cases excluding all individuals with diabetes mellitus. Degrees of freedom were estimated using Satterthwaite's approximation[215]. Where variables with missing data were used and when appropriate, I used conditional multiple imputation with chained equations using multinomial logistic regression models on all exposure and outcome variables, in their raw form, and report pooled adjusted regression coefficients[216].

To examine the association between retinal morphology and incident disease, I estimated cause-specific adjusted hazard ratios (HR) using either Cox proportional hazards or, for hierarchical data, frailty models including a gamma-distributed random effect on the intercept at the individual level[217,218]. The at-risk period was defined from the time of retinal imaging acquisition until the earliest of death, hospital admission with a relevant diagnostic code or conclusion of the data refresh date for

our UKBB application (1st December 2020). Given that previous evidence has shown HES-based codes for neurodegenerative diseases can be recorded for the first time after already being recorded much earlier in primary care records, I additionally performed sensitivity analyses excluding all incident cases within 24 months of retinal imaging[151]. All analyses are conducted in R version 4.1.0 (R Core Team, 2021. R Foundation for Statistical Computing, Vienna, Austria) and the relevant packages for this theme include the `mice`, `survival` and `lmer` packages [219–221].

4.4.3 Prediction - Clinical prediction models

Several modelling strategies were employed within this project and guided by the data distribution, underlying assumptions, and overall objectives. It is acknowledged that there may be no one 'perfect' model and rather that, collectively, the different approaches improved understanding towards the overall research aims. Of note, for a patient to be labelled as not having dementia (i.e. control), they must have a HES episode but without dementia as one of the diagnostic codes. As mentioned earlier, although HES admitted patient care data may have reasonable agreement with primary care records, it is well-known that dementia underdiagnoses are frequent[151]. Further statistical methods for clinical prediction model development and validation are in section 7.1.2 Methods.

4.7.3 Sample size

Prior to receipt of HES data from NHS Digital, sample size calculations were estimated for prognostic factor research modelling the outcome of dementia and

cardiovascular events based on retinal imaging-based biomarkers. For quantitative variables such as arteriole-to-venule ratio (AVR), scans were divided into quintiles for analysis. With 90% power, an alpha of 5% and a 1:1 ratio, a total sample size of 464 is required to detect an odds ratio of two (previous ratios derived from the ARIC study)[69]. For the association between optical coherence tomography-derived retinal nerve fibre layer and ganglion cell-inner plexiform layer thicknesses and neurodegenerative disease, given an odds ratio of 1.4 with a significance level of 5% and a statistical power of 90% on a 1:1 matched study design, a total sample size of 2106 would be required[143].

Although previous work has suggested a requirement of approximately ten events per variable when developing a multivariable risk prediction model, this has remained a controversial area in estimating sample size for model development[222–225]. I therefore used the work of Riley et al on minimum sample size calculation for time-to-event data and estimating required events per variable, which is underpinned by i) the need for small optimism in measured effects, ii) a low absolute difference ≤0.05 in the apparent performance of the model and adjusted Nagelkerke's R^2 value and iii) precise estimation of population overall risk[226]. The maximum sample size of the three steps above is chosen.

In summary, the number of participants (n) can be estimated for step i) as thus:

$$n = \frac{p}{(S-1)\ln\left(1 - \frac{R^2_{CS\_adj}}{S}\right)}$$

Where:

n = number of participants

p = number of predictor variables

S = Expected shrinkage factor

$R^2_{CS\_adj}$ = Apparent estimate of model Cox-Snell R^2

Given variables of sociodemographic characteristics (e.g. age, sex, ethnicity), medical comorbidity (e.g. diabetes mellitus, hypertension) and retinal biomarkers (e.g. calibre, retinal nerve fibre layer thickness), predictor variables were estimated at 110. Estimation of the global shrinkage factor is 0.9. Calculation of the $R^2_{CS\_adj}$ is convoluted and full details are given in Appendix 2: Sample size calculation. This is due to the absence of previous Cox-Snell's R^2 in the literature with a heavy focus on the concordance (*c,* analogous to the area under the curve [AUC] in logistic regression) statistic as a performance measure.

The work of Wisely et al achieved an AUC of 0.809 for maps of the GC-IPL alone[141]. Using this as an estimate of model performance and an outcome proportion of 0.05, (step i) gives an estimated sample size for dementia risk prediction using 110 predictor variables of 4,377 participants. Step ii), where we seek to ensure a small absolute difference of ≤ 0.05 in the model's apparent and adjusted Nagelkerke's R^2 results in 5,958 participants. Finally, step iii) ensuring a precise estimate of overall risk in the population with an absolute margin of error ≤ 0.05 gives values of participants. The maximum value of these sample size estimations, 5958 participants, with 298 events, are therefore required. As seen in *Table 46*, the AlzEye development cohort 1,419 patients with incident all-cause dementia, suggesting sufficient statistical power.

5. Description

This chapter focuses on the theme of ocular phenotypes as sentinel events for emerging systemic disease. It has the purpose of a) familiarising the reader with the AlzEye cohort, b) reproducing consistent epidemiological patterns regarding common ophthalmic diseases, and c) providing some novel insights on the non-communicable disease burden in those newly diagnosed with an ophthalmic disease. The chapter will consist of three main sections. In section 5.1 AlzEye: cohort profile, the basic sociodemographic, ophthalmic, and systemic disease profile of the AlzEye cohort is described providing context for the interpretation of subsequent results. Importantly, AlzEye is a real-world dataset of NHS users and is not representative of the general UK population – it is markedly diverse and skewed towards greater levels of socioeconomic deprivation. In section 5.2 Common chronic ophthalmic disease, the mortality and incidence of major cardiovascular events (myocardial infarction and ischaemic stroke) by the leading causes of sight impairment in the UK are described. Finally, in section 5.3 Acute neurophthalmic diseases, a more analytic approach is taken with a matched analysis of several acute neurophthalmic conditions presenting to the Moorfields Eye Hospital emergency department.

5.1 AlzEye: cohort profile

Extraction of unique patients attending the relevant MEH outpatient clinics between January 1st 2008 and April 1st 2018 generated a cohort of 353,191 individuals. Thirty-four patients with undetermined/unknown sex were excluded leaving a total of 353,157. Of these, 187,811 patients had a total of 1.37 million HES episodes in the study period.

A breakdown of sociodemographic details by category of the cohort are provided in Table *2*. It is noted that the AlzEye cohort has more women than men and is skewed towards older age groups. Ethnicity data was missing or other in 39% of the cohort. The cohort was also skewed towards greater levels of deprivation.

	Characteristic	N (%)
	All	353,157
Sex	**Female**	190,494 (53.9)
	Male	162,663 (46.1)
Age group[a]	**40-49 years**	35,262 (10.0)
	50-59 years	66,101 (18.7)
	60-69 years	79,018 (22.4)
	70-79 years	84,942 (24.1)
	80+ years	87,834 (24.9)
Ethnicity	**Black**	31,614 (9.0)
	South Asian	48,119 (13.6)
	White	135,743 (38.4)
	Other/Unknown	137,681 (39.0)
IMD decile[b, c]	**1 (most deprived)**	18,194 (5.2)
	2	50,443 (14.3)
	3	50,869 (14.4)
	4	42,603 (12.1)
	5	38,964 (11.0)
	6	36,906 (10.5)
	7	31,317 (8.9)
	8	28,180 (8.0)
	9	29,906 (8.5)
	10 (least deprived)	24,610 (7.0)
	Unknown	1165 (0.3)

Table 2: Baseline sociodemographic characteristics of the AlzEye cohort.

[a]Age is taken as that of April 1st, 2018. [b]Missing values for 1165. [c]Decile one indicates the most deprived decile. *From Wagner SK, Hughes F, Cortina-Borja M et al. AlzEye: longitudinal record-level linkage of ophthalmic imaging and hospital admissions of 353 157 patients in London, UK. BMJ Open. 2022 Mar 16;12(3):e058552. doi: 10.1136/bmjopen-2021-058552*[165]*, table available under CC license, no changes made.*

5.1.1 Common ophthalmic diseases

An illustration of the major common ophthalmic diseases within the cohort is shown in a CONSORT-style diagram in *Figure 19*. Following the case definition (see Section 4.1.4 Ophthalmic variables) and exclusion of invalid dates, a total of 59,102 patients had first eye cataract, 31,060 glaucoma, 7214 neovascular AMD and 2494 PDR.

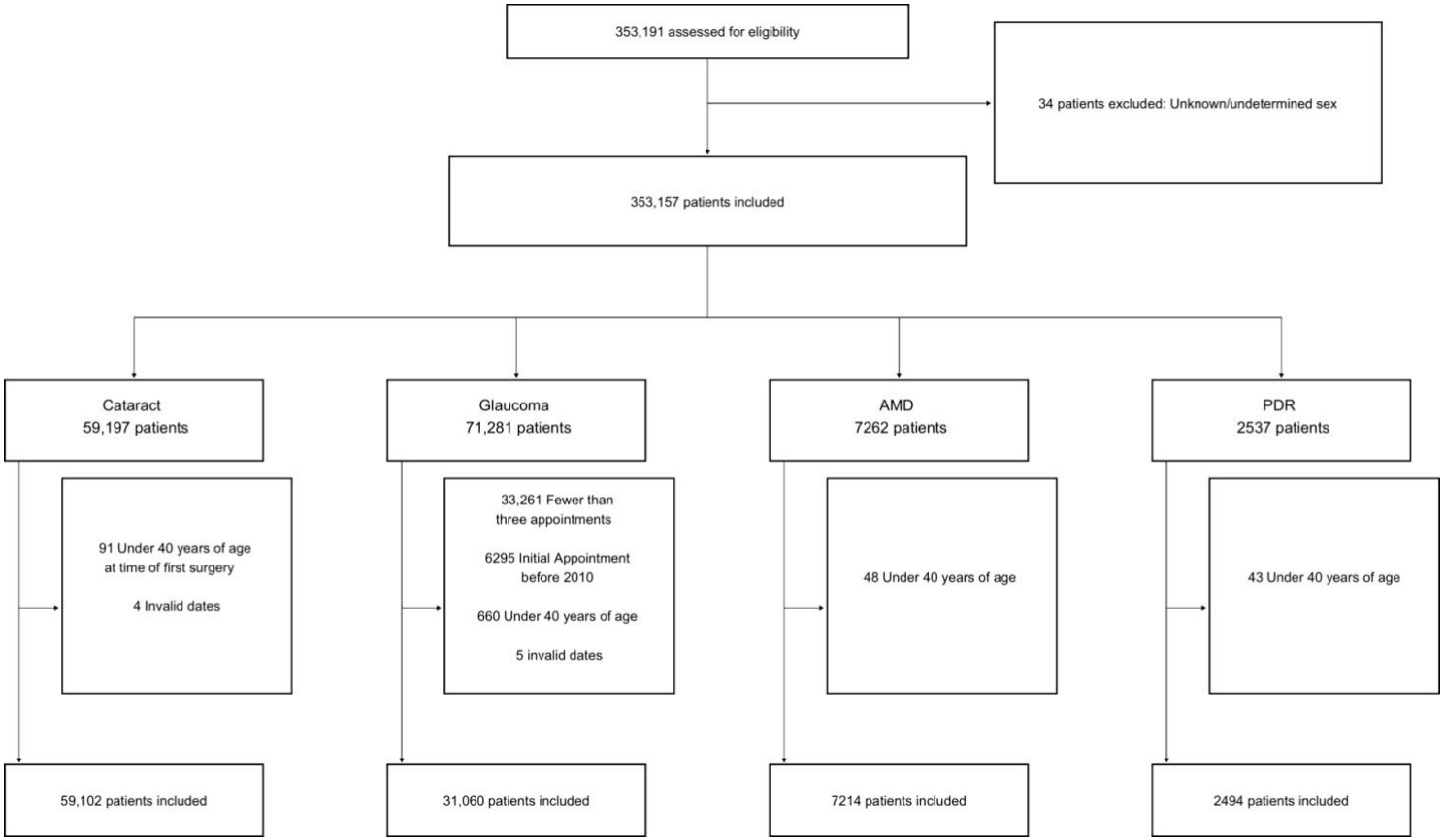

Figure 19 : Flow diagram from the raw AlzEye cohort into four major ophthalmic diseases of cataract, glaucoma, neovascular age-related macular degeneration and proliferative diabetic retinopathy.

AMD: age-related macular degeneration, PDR: proliferative diabetic retinopathy. *From Wagner SK, Hughes F, Cortina-Borja M et al. AlzEye: longitudinal record-level linkage of ophthalmic imaging and hospital admissions of 353 157 patients in London, UK. BMJ Open. 2022 Mar 16;12(3):e058552. doi: 10.1136/bmjopen-2021-058552*[165]*, figure available under CC license, no changes made.*

Mean age (+/- standard deviation) of those undergoing first eye cataract surgery (71.5 +/- 10.8 years) and newly diagnosed with AMD (78.0 +/- 10.0 years) was higher than of patients with glaucoma (64.8 +/- 12.3 years) or proliferative diabetic retinopathy (60.5 +/- 10.6 years, *Table 3*). While those of White ethnicity accounted for most cases (41.7% cataract, 39.5% glaucoma, 65.4% AMD) this was not reflected in PDR where South Asians were the largest group (33.7%). Socioeconomic deprivation of the cohort was skewed towards the more deprived across all diseases.

	Characteristic	Age of cataract surgery mean (SD) years	Age of Glaucoma diagnosis mean (SD)	Age of AMD diagnosis mean (SD)	Age of PDR diagnosis Mean (SD)
	All	71.5 (10.8)	64.8 (12.3)	78.0 (10.0)	60.5 (10.6)
Sex	**Female**	72.1 (10.5)	65.4 (12.1)	78.7 (9.9)	62.0 (10.5)
	Male	70.7 (11.1)	64.2 (12.4)	77.0 (10.2)	59.6 (10.6)
Ethnicity	**Asian**	68.7 (9.6)	63.9 (11.5)	74.6 (10.0)	61.6 (9.7)
	Black	68.9 (10.9)	62.3 (12.1)	72.9 (9.6)	62.1 (10.8)
	White	73.6 (10.8)	67.3 (12.1)	78.9 (9.8)	61.0 (11.3)
	Other/Unknown	71.3 (10.7)	63.3 (12.3)	77.5 (10.3)	58.2 (10.5)
IMD decile	**1 (more deprived)**	70.3 (11.1)	62.5 (12.3)	77.0 (10.2)	58.8 (10.6)
	2	70.0 (11.0)	62.8 (12.4)	77.2 (10.3)	60.3 (10.5)
	3	70.5 (10.9)	63.8 (12.5	77.3 (10.2)	60.1 (10.5)
	4	70.9 (10.8)	64.7 (12.2)	77.4 (10.4)	61.0 (10.5)
	5	71.6 (10.6)	65.3 (12.1)	78.3 (10.0)	61.3 (10.2)
	6	72.3 (10.6)	65.6 (12.2)	78.5 (9.8)	60.3 (10.8)
	7	72.6 (10.3)	66.0 (12.1)	78.4 (9.8)	60.6 (10.1)
	8	72.8 (10.3)	66.2 (12.1)	78.9 (9.7)	60.8 (11.0)
	9	73.0 (10.4)	66.3 (11.8)	78.2 (10.0)	61.6 (11.3)
	10 (less deprived)	73.1 (10.5)	66.3 (11.9)	78.8 (9.9)	62.2 (11.8)

Table 3: Age of ophthalmic event or diagnosis within the AlzEye cohort by sociodemographic variables.

SD: standard deviation, AMD: Age-related macular degeneration, PDR: proliferative diabetic retinopathy

5.1.2 Systemic diseases

Among the 187,811 patients with recorded HES episodes, 12,463 patients had episodes with coded myocardial infarction, 12,557 patients with ischaemic stroke and 13,392 with dementia. Within the dementia group, 4,500 patients had codes that were specific for Alzheimer's dementia and 3,392 for vascular dementia (Table *4*).

Group	Disease	ICD code(s)	Number of patients
Cardiovascular	Acute coronary syndrome[178–180]	I21, I22	12,463
	Heart failure	I50	24,205
	Atrial Fibrillation	I48	33,006
	Hypertension	I10, I15	152,885
	Ischaemic stroke	I61-I64	12,557
Neurodegenerative	Alzheimer's disease	F00, G30	4,500
	Vascular dementia	F01	3,392
	Parkinson's disease[227]	G20	3,224
	All-cause dementia[151]	E512, F00, F01, F02, F03, F106, F107, G30, G310	13,392
Other	Diabetes mellitus (Type 1 and 2)	E10, E11	71,977

Table 4: Number of patients by selected examples of specified 10th revision of International Classification of Diseases (ICD) codes relating to diabetes mellitus, cardiovascular and neurodegenerative diseases[145].

From Wagner SK, Hughes F, Cortina-Borja M et al. AlzEye: longitudinal record-level linkage of ophthalmic imaging and hospital admissions of 353 157 patients in London, UK. BMJ Open. 2022 Mar 16;12(3):e058552. doi: 10.1136/bmjopen-2021-058552[165]*, table available under CC license, no changes made.*

5.1.3 Retinal imaging

During the study period, a total of 6,261,931 images were acquired on 154,830 patients. The three leading image modalities were colour retinal photographs (n=1,874,175), OCT (n=1,567,358) and red-free photographs (n=1,147,487). The distribution of imaging modalities across the three vendors used for retinal imaging at MEH - Topcon (Topcon corp, Tokyo, Japan), Heidelberg (Heidelberg Engineering, Heidelberg, Germany) , and Optos (Optos, Dunfermline, UK) - are shown in Table 5.

Most images were acquired on the Topcon system (n=5,553,826, 88.7%). Number of images by year is shown in *Figure 20*. During the study period, annual imaging acquisition increased from 229,868 scans in 2008 to 1,021,904 in 2017.

Vendor	Modality	Number of images	Number of patients
Topcon	Angiography	1,128,723	21,225
	Autofluorescence	11,761	2078
	Colour photography	1,874,175	139,307
	Red-free	1,146,854	122,453
	OCT	1,391,826	138,911
	Other	487	48
Heidelberg	Angiography	89,264	4061
	Autofluorescence	94,533	16,863
	Infrared	192,634	21,676
	OCT	175,532	21,191
	Other	19,781	2439
Optos	Angiography	77,813	2215
	Autofluorescence	18,590	5666
	Pseudocolour photography	39,958	6887

Table 5: Retinal imaging within the AlzEye dataset by vendor and imaging modality.

OCT: Optical coherence tomography. Angiography refers to dye-based techniques (fluorescein and indocyanine green). *From Wagner SK, Hughes F, Cortina-Borja M et al. AlzEye: longitudinal record-level linkage of ophthalmic imaging and hospital admissions of 353 157 patients in London, UK. BMJ Open. 2022 Mar 16;12(3):e058552. doi: 10.1136/bmjopen-2021-058552*[165]*, table available under CC license, no changes made.*

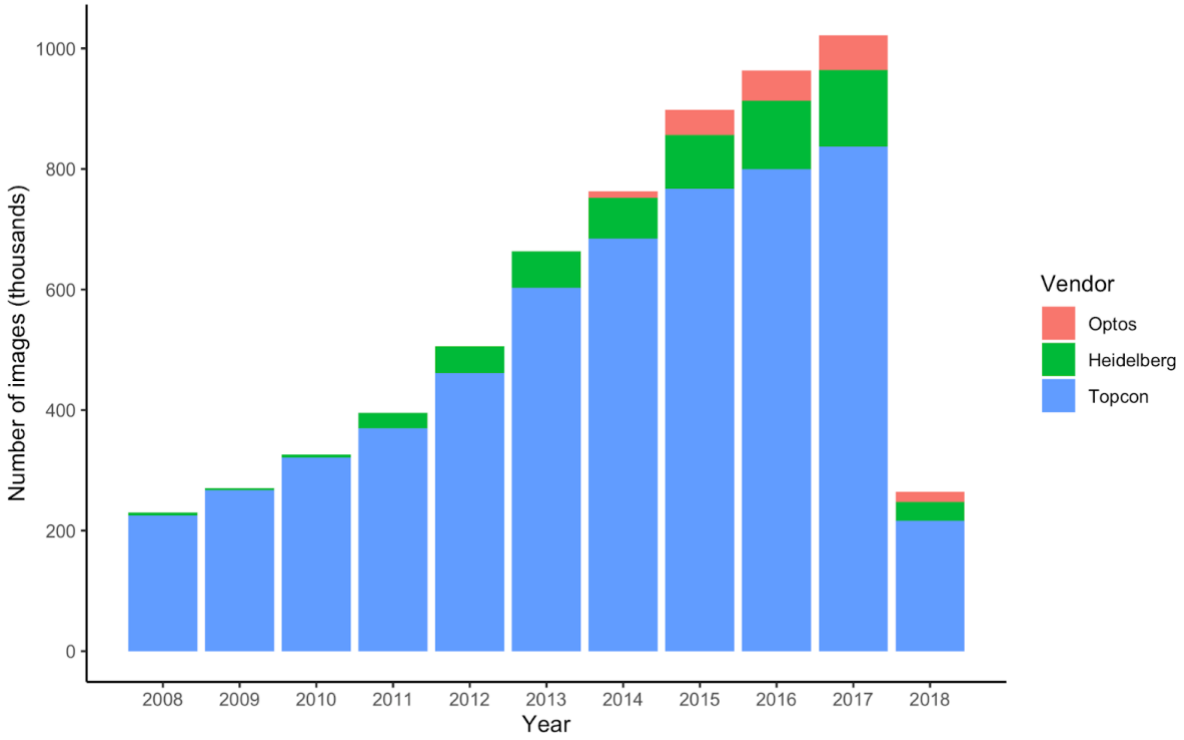

Figure 20: Stacked bar chart showing number of retinal images acquired by year per vendor within the AlzEye dataset.

From Wagner SK, Hughes F, Cortina-Borja M et al. AlzEye: longitudinal record-level linkage of ophthalmic imaging and hospital admissions of 353 157 patients in London, UK. BMJ Open. 2022 Mar 16;12(3):e058552. doi: 10.1136/bmjopen-2021-058552[165]*, figure available under CC license, no changes made.*

5.1.4 Discussion

To my knowledge, AlzEye represents the world's largest retinal imaging research dataset available presently, linking secondary healthcare ophthalmic data from 353,157 patients seen over a 10-year period with information on general health and key systemic diseases, as captured through admissions to any hospital within the NHS of England. This comprises 6,261,931 images, obtained using seven different modalities from three different manufacturers, in 154,830 patients who received

retinal imaging. The current large-scale UK cohort, UKBB, provides useful context for AlzEye. Cross-sectional data are available in UKBB with two retinal imaging modalities (colour retinal photography and OCT) obtained using technology from one manufacturer (Topcon) and at a single time point in 67,321 people. Notwithstanding the recognised limitations of real-world datasets and the coding within the HES database, AlzEye provides some distinct advantages beyond purely scale. Imaging data are longitudinal, highly multimodal and pertain to an ethnically and socioeconomically diverse cohort representative of the adult population with eye disease.

UKBB is the major comparator for AlzEye, being the largest of the prospective epidemiological cohort datasets which provides cross-sectional retinal imaging in association with systemic disease variables[183]. One of the limitations of UKBB is that, unlike AlzEye, it provides minimal longitudinal retinal images. Another prospective cohort study, the Rotterdam Study, does collect longitudinal retinal imaging data from approximately 15,000 participants, of which 5065 participants were eligible for OCT scanning in 2017[228]. The Rotterdam Study has uncovered several landmark findings, particularly in regard to causal determinants, but its cohort remains relatively small in comparison to UKBB and AlzEye with the majority of participants recruited from one district within Rotterdam, the Netherlands[229,230]. The Singapore Epidemiology of Eye Disease is one longitudinal multimodal retinal imaging initiative which is underway, in which 10,033 participants of Chinese, Indian and Malay ethnicity have been recruited to undergo six-yearly retinal imaging[231]. A recent review of ophthalmic imaging datasets did not reveal any additional relevant publicly available datasets that included linked systemic health data[232]. Additionally,

my own review of the literature has not identified any examples of large-scale linked real-world datasets (including those with restricted access) which include linked systemic health data. The scarcity of such resources suggests that the construction of such datasets is challenging to undertake, presumably due to factors such as cost, required duration and delayed output, retention of participants and concerns over technological redundancy. The AlzEye approach is an important alternative model in this context.

Several epidemiological opportunities arise with AlzEye. First, it provides a real-world snapshot of ophthalmic secondary care use, representing approximately 1.2% of the UK population aged 40 years and above (2,7858,459 in 2011[233]). This is a powerful tool for informing public health and policymaking in eye services and is exceptional in characterising the potential impact that may arise from the intersect between disabling diseases such as stroke and PDR. Second, it allows the identification and exploration of relationships between newly diagnosed ophthalmic disease (or newly referred to hospital eye services) and emerging systemic events and accruing multimorbidity. Patients tend to respond early to issues with their sight and an understanding of how an ophthalmic presentation is linked to an increased likelihood of serious systemic disease may provide an opportunity for earlier intervention in those diseases[234]. Third, nested case–control studies evaluating retinal-based oculomic biomarkers in those with systemic diseases (e.g. dementia) can provide insight into their value in either static or dynamic risk prediction. Newer modelling approaches have highlighted the potential utility of the retina in screening for and risk stratification of cardiovascular, neurodegenerative, renal, hepatic and haematological diseases[141,235–239]. Finally, by its magnitude and wealth of high-quality labels, both

ophthalmic and systemic, AlzEye provides a powerful catalyst for high-dimensional model development, echoing that of ImageNet, a database currently exceeding 14 million images, which propelled deep learning and computer vision research forward a decade ago[240].

Despite the opportunities afforded by AlzEye, there are several limitations to this kind of approach and potential sources of bias. First, caution must be paid to the validity of HES diagnostic coding[241]. Although previous validation studies have concluded that discharge coding within HES is sufficiently robust for research purposes[147,151], sizeable proportions of cases may be missed when using individual sources[152]. For example, recent work linking the EHRs of 54.4 million people in England showed that HES captured 80.5% and 65% of myocardial infarctions and stroke/transient ischaemic attacks, respectively, when compared with linkage additionally incorporating death registry and primary care records[153]. One mitigation strategy for this source of bias for real-world data is therefore linking to multiple sources. Secondly, the risk of selection bias using hospital-attending cohort, as the individuals within the AlzEye cohort are likely to have greater medical comorbidity than the general population, limiting the external validity of any findings. In addition, by the very nature of the dataset, patients within the AlzEye cohort will have definite or suspected ophthalmic disease, particularly among those with repeated retinal imaging. Finally, there is a risk of under-recording of potentially important variables such as smoking may also lead to residual confounding. Readers of any analyses resulting from AlzEye should be cognisant of these issues.

5.1.5 Summary

In summary, the AlzEye study represents a large multimodal dataset from an ethnically and socioeconomically diverse cohort attending Moorfields Eye Hospital NHS Foundation Trust. As a hospital-attending population with an enriched medical comorbidity burden, researchers will need to be cognisant that it may not be representative of the wider UK population. Nonetheless, it provides an exceptional health data foundation for discovery science and further investigation into the retinal associations of common chronic complex diseases.

5.2 Common chronic ophthalmic diseases

5.2.1 Introduction

Diagnosis of certain ophthalmic diseases is associated with a heightened risk of subsequent cardiovascular disease (CVD) and may represent an early harbinger of emerging multimorbidity[242]. In some cases, such as diabetes mellitus, multi-organ impairment results from shared pathophysiological mechanisms such that newly diagnosed proliferative diabetic retinopathy signifies a higher risk of incident chronic renal disease and CVD [243,244]. In other cases, such as that in isolated ophthalmic diseases, similar associations have been described although the mechanisms are less well understood. A higher risk of subsequent ischaemic heart disease has been found in people with cataract [245], rates of myocardial infarction are elevated in those with late age-related macular degeneration [170,172] and greater cardiovascular mortality is seen in persons previously diagnosed with open-angle glaucoma [169,246,247]. As a sentinel event, ophthalmic diagnosis may therefore highlight an opportune event for risk stratification of those with evolving CVD.

Such associations have been predominantly investigated through two approaches. Firstly, large epidemiologic population-based studies incorporating ophthalmic examination have prospectively evaluated the incidence of CVD-related events among cohorts of certain eye diseases. However, the challenges of such approaches include small numbers of cases and potentially limited generalisability to the wider population. An alternative design has been the leveraging of routine clinical records, such as health insurance data and national coding systems. While the broader reach of this approach may result in larger cohorts, the quality of recording of ophthalmic diseases within such systems can be variable. In a recent study in the

United States, coding for glaucoma using the International Classification of Diseases, 9th revision, Clinical Modification (ICD-9) had a positive predictive value of only 66% using a reference standard judged by ophthalmologists[248].

This analysis focuses on glaucoma, neovascular age-related macular degeneration (nAMD), diabetic retinopathy and cataract, which collectively account for more than 65% of sight loss in the UK and worldwide[166–168]. Through an initial fundamental prognosis research strategy[202], the objective was to characterise the risk of incident cardiovascular events in patients attending hospital eye services and consequently highlight whether certain groups, newly receiving a diagnosis of an ophthalmic disease, may benefit from CVD risk assessment.

5.2.2 Methods

This was a substudy using data from the AlzEye project. Ophthalmic variables of cataract, glaucoma, AMD and proliferative diabetic retinopathy have been defined previously (section 4.1.4 Ophthalmic variables). Systemic disease data was described in section 4.1.5 Systemic disease variables. Mortality data was extracted from the MEH data warehouse. Mortality data is updated every two weeks by the MEH Data Quality team. Case definitions for cardiovascular events are as previously described (Table *1*).

Summary statistics comprised mean and +/- standard deviation (SD) for continuous variables and percentages for categorical variables. Frequency of outcomes was measured using incidence rates, calculated as the number of new events (MI or

ischaemic stroke) in the study period per 100,000 person-years at risk (PYAR) with 95% confidence intervals calculated using the Poisson distribution with the offset as the logarithm of the total PYAR. The at-risk period was defined from the time of ophthalmic diagnosis/event until the earliest of i) death, ii) first event (MI or ischaemic stroke) or iii) conclusion of the data period on 1st of April 2018. Both crude rates and those stratified by sociodemographic covariates of age group (ten-year intervals), sex, ethnicity and socioeconomic deprivation were calculated. HES admission data prior to the ophthalmic event or diagnosis was variable depending on the time of presentation leading to potential selection bias. For this reason, patients with cardiovascular or cerebrovascular events prior to their ophthalmic event were not excluded in the calculation of incidence rates.

Cause-specific hazard ratios were estimated from Cox proportional hazards modelling with fixed baseline covariates of age (at time of ophthalmic event/diagnosis as a continuous variable), sex, ethnicity, and socioeconomic deprivation. In consideration of the competing risk of death, subdistribution hazard ratios (sHR) with 95% confidence intervals (CI) were estimated as a sensitivity analysis using the multivariable semiparametric competing risks proportional hazards model approach described by Fine and Gray with the event of interest taken as either MI or stroke with death as a competing risk[206]. The assumption of proportional hazards was assessed using global and covariate-specific χ^2 testing and visualisation of graphs of scaled Schoenfeld residuals against transformed time. Stratification was implemented for any parameters violating the assumption. Nonlinearity between age and log hazard was assessed by plotting Martingale residuals of the null Cox proportional hazards model. All statistical testing was two-

tailed with the level of significance at 0.05. Statistical analyses were conducted in R version (R Core Team, 2012. R Foundation for Statistical Computing, Vienna, Austria) and employed the *cmprsk* and *survival* packages[249,250].

5.2.3 Results

Incidence rates

Incidence rates for MI and stroke for each ophthalmic disease group are shown in Table *6*-Table *9*. Key findings related to systemic disease are given below with ophthalmic disease-specific results discussed in the Table footnotes. All incidence rates are per 100,000 PYAR.

Key findings relating to myocardial infarction

Despite being the youngest group, the crude rate of MI (1449.8, 95% CI: 1173.3, 1766.5) was highest among those with PDR. Among cataract, glaucoma and AMD patients, men had a higher incidence rate of MI, with the highest rate being most notably in glaucoma (Male 398.6 (95% CI: 353.3, 447.6), Female 208.3 (95% CI: 177.8, 242.0). While those of Asian ethnicity had the highest rate of MI across all diseases, this was particularly notable among cataract and glaucoma patients. The MI incidence rate among cataract patients between 50-59 years (368.8, 95% CI: 288.0, 463.6) was much higher than that of cataract patients aged 40-49 years (35.3, 95% CI: 5.9, 108.8). This contrasted with those with neovascular AMD, who had similar rates until the age of 70 and PDR, where incidence rates were high even among the youngest age group.

Key findings relating to ischaemic stroke

As with myocardial infarction, the crude incidence rate for ischaemic stroke (1123.3, 95% CI: 883.4, 1403.1) was highest among those with PDR. Incidence rates were similar among sexes apart from in cataract, where men had a higher incidence of ischaemic stroke (672.2, 95% CI 613.6, 734.4) than women (555.2, 95% CI: 508.4, 604.7). There were no clear differences in incidence rates among ethnic groups though White patients with cataract had higher incidence (674.0, 95% CI: 616.4, 735.2) than Asian patients (529.5, 95%CI 457.5, 608.6). Ischaemic stroke incidence was higher among older age groups.

	Characteristic	Cataract n (%)	MI *n*	Stroke *n*	Incidence rate MI (95% CI)	Incidence rate Stroke (95% CI)
	All	59,102 (100)	806	987	494.6 (461.2-529.5)	606.0 (569.0-644.6)
Sex	**Female**	33,121 (56.0)	342	511	371.0 (333.1-411.7)	555.2 (508.4-604.7)
	Male	25,981 (44.0)	464	476	655.5 (597.7-717.0)	672.2 (613.6-734.4)
Age group at diagnosis	**40-49 years**	1,904 (3.2)	2	8	35.3 (5.9-108.8)	141.4 (64.6-263.1)
	50-59 years	6,522 (11.0)	68	35	368.8 (288.0-463.6)	189.1 (133.2-258.9)
	60-69 years	15,105 (25.6)	148	139	346.2 (293.4-405.0)	324.9 (273.9-382.0)
	70-79 years	21,047 (35.6)	313	373	536.5 (479.3-598.2)	639.5 (576.8-706.6)
	80+ years	14,524 (24.6)	275	432	728.1 (645.4-817.6)	1149.4 (1044.3-1261.2)
Ethnicity	**Asian**	12,107 (20.5)	265	189	746.0 (659.8-839.5)	529.5 (457.5-608.6)
	Black	5,760 (9.7)	52	110	296.2 (222.8-384.1)	629.5 (519.1-754.6)
	White	24,646 (41.7)	330	495	448.3 (401.7-498.5)	674.0 (616.4-735.2)
	Other/Unknown	16,589 (28.1)	159	193	438.3 (373.6-509.9)	532.4 (460.8-611.1)
IMD decile[a]	**1 (most deprived)**	3,307 (5.6)	46	66	502.3 (370.8-661.8)	722.6 (562.0-911.2)
	2	8,521 (14.4)	143	147	609.1 (514.6-714.5)	626.6 (530.7-733.4)
	3	8,923 (15.1)	136	159	552.8 (465.0-651.0)	646.6 (551.2-752.4)
	4	6,883 (11.6)	81	127	425.2 (339.2-524.6)	667.8 (558.3-790.8)
	5	6,720 (11.4)	98	114	528.8 (430.9-640.5)	614.8 (508.7-734.6)
	6	6,518 (11.0)	80	105	447.5 (356.4-552.8)	588.1 (482.6-707.8)
	7	5,461 (9.2)	67	79	436.3 (340.0-549.3)	514.8 (409.5-636.8)
	8	4,430 (7.5)	50	74	408.6 (305.5-532.5)	605.4 (477.8-754.0)
	9	4,506 (7.6)	62	60	511.4 (394.4-649.5)	493.4 (378.9-629.0)
	10 (least deprived)	3,742 (6.3)	42	55	407.4 (296.3-543.4)	534.6 (405.4-688.5)

Table 6: Crude and stratified incidence rates of myocardial infarction and stroke in patients undergoing first eye cataract surgery.

Incidence rates are presented per 100,000 person-years at risk. CI: Confidence interval, MI: Myocardial infarction, SD: Standard deviation. [a]Missing values from 91 patients.

Incidence of both MI and ischaemic stroke was higher for men than women and older age groups. Asian patients had the highest incidence of MI while White patients had the highest incidence of ischaemic stroke. While there did appear to be a trend towards lower incidence of both MI and stroke with less deprivation, this was marginal and point estimates had overlapping confidence intervals.

	Characteristic	Glaucoma *n* (%)	MI *n*	Stroke *n*	Incidence rate MI (95% CI)	Incidence rate Stroke (95% CI)
	All	31,060 (100)	437	512	297.7 (270.7-326.5)	348.9 (319.5-380.0)
Sex	**Female**	16,322 (52.5)	162	242	208.3 (177.8-242.0)	311.6 (273.9-352.5)
	Male	14,738 (47.5)	275	270	398.6 (353.3-447.6)	390.8 (346.0-439.3)
Age group at diagnosis	**40-49 years**	4,049 (13.0)	6	10	29.3 (11.7-59.4)	48.9 (24.5-85.7)
	50-59 years	6,725 (21.7)	61	42	188.1 (144.8-239.3)	129.2 (94.0-172.3)
	60-69 years	8,690 (28.0)	95	92	229.7 (186.6-279.1)	222.4 (180.0-271.0)
	70-79 years	7,625 (24.5)	152	203	426.9 (362.6-498.4)	571.2 (496.2-653.4)
	80+ years	3,971 (12.8)	123	165	726.0 (605.1-861.9)	976.5 (835.0-1133.2)
Ethnicity	**Asian**	4,406 (14.2)	114	78	539.0 (446.0-644.1)	366.9 (291.4-454.4)
	Black	4,321 (13.9)	47	69	207.4 (153.6-272.5)	305.6 (239.0-383.5)
	White	12,284 (39.5)	174	245	283.7 (243.6-328.0)	399.8 (351.8-452.0)
	Other/Unknown	10,049 (32.4)	102	120	244.9 (200.4-295.6)	288.2 (239.7-342.9)
IMD decile[a]	**1 (most deprived)**	1,665 (5.4)	26	32	323.8 (214.8-464.7)	398.1 (275.6-552.4)
	2	4,482 (14.4)	65	67	305.5 (237.1-385.9)	314.6 (245.1-396.0)
	3	4,276 (13.8)	55	62	267.6 (202.9-344.6)	301.5 (232.5-382.9)
	4	3,706 (11.9)	51	63	293.1 (219.9-381.1)	363.0 (280.6-460.2)
	5	3,411 (11.0)	61	67	376.4 (289.7-478.9)	413.2 (322.0-520.2)
	6	3,121 (10.0)	44	56	295.5 (216.6-391.7)	376.3 (286.1-483.6)
	7	2,783 (9.0)	39	41	297.8 (213.9-401.3)	313.2 (226.8-419.0)
	8	2,588 (8.3)	29	41	237.2 (161.0-334.3)	335.8 (243.2-449.3)
	9	2,792 (9.0)	35	43	271.3 (191.1-371.4)	333.3 (243.4-443.1)
	10 (least deprived)	2,135 (6.9)	32	39	329.1 (227.8-456.7)	401.2 (288.1-540.6)

Table 7: Crude and stratified incidence rates of myocardial infarction and stroke in patients with glaucoma.

Incidence rates are presented per 100,000 person-years at risk.

CI: Confidence interval, MI: Myocardial infarction, SD: Standard deviation [a] Missing values of 101 patients were excluded.

Men had higher incidence than women for MI. Incidence of both MI and stroke increased with higher age group at diagnosis. Asian patients had higher incidence of MI but incidence rates of ischaemic stroke were similar among all self-reported ethnic groups. Rates were similar for both MI and stroke among groups of differing IMD decile.

	Characteristic	AMD *n* (%)	MI *n*	Stroke *n*	Incidence rate MI (95% CI)	Incidence rate Stroke (95% CI)
	All	7,214 (100)	163	259	528.5 (451.4-613.8)	843.6 (745.0-950.5)
Sex	**Female**	4,400 (61.0)	90	165	465.5 (375.8-568.4)	857.9 (733.5-995.5)
	Male	2,814 (39.0)	73	94	634.2 (499.6-791.0)	819.6 (664.9-996.6)
Age group at diagnosis	**<60 years**	402 (5.6)	5	4	228.2 (81.8-490.5)	181.8 (56.4-422.4)
	60-69 years	892 (12.4)	8	10	190.9 (87.2-355.3)	238.9 (119.7-419.0)
	70-79 years	2,259 (31.3)	46	65	452.1 (333.7-595.6)	642.1 (498.4-811.2)
	80+ years	3,661 (50.7)	104	180	727.9 (596.8-876.9)	1268.0 (1091.7-1462.4)
Ethnicity	**Asian**	622 (8.6)	20	21	782.0 (487.4-1176.5)	819.0 (516.7-1220.8)
	Black	179 (2.5)	1	10	124.9 (7.1-549.6)	1283.3 (643.0-2250.6)
	White	4,720 (65.4)	110	176	514.3 (424.1-616.5)	826.3 (710.1-954.4)
	Other/Unknown	1,693 (23.5)	32	52	524.6 (363.2-727.9)	858.3 (645.6-1113.1)
IMD decile[a]	**1 (most deprived)**	334 (4.6)	10	4	709.0 (355.3-1243.5)	283.1 (87.9-657.6)
	2	821 (11.4)	18	40	530.4 (321.5-814.4)	1186.9 (856.0-1593.6)
	3	913 (12.7)	31	31	782.5 (538.4-1091.2)	754.2 (539.6-1093.6)
	4	725 (10.0)	19	27	598.6 (368.1-909.4)	848.3 (567.2-1209.7)
	5	787 (10.9)	16	38	481.7 (282.5-757.7)	1154.5 (825.2-1561.4)
	6	856 (11.9)	16	29	455.3 (267.0-716.2)	830.4 (563.6-1170.3)
	7	753 (10.4)	18	31	570.3 (345.8-875.8)	984.0 (677.0-1372.1)
	8	700 (9.7)	16	20	528.2 (309.8-830.8)	660.8 (411.8-994.1)
	9	691 (9.6)	11	16	360.4 (187.1-617.2)	529.4 (310.5-832.7)
	10 (least deprived)	617 (8.6)	8	23	292.6 (133.7-544.5)	850.6 (548.6-1247.1)

Table 8: Crude and stratified incidence rates of myocardial infarction and stroke in patients with neovascular age-related macular degeneration.

Incidence rates are presented per 100,000 person-years at risk. AMD: Age-related macular degeneration, CI: Confidence interval, MI: Myocardial infarction [a]17 values had missing data for IMD decile. Given that AMD is traditionally diagnosed only after 49 years of age, the youngest age group is <60 years.

Men and women had similar incidence of ischaemic stroke; incidence of MI was slightly higher in men with overlapping confidence intervals. Rates of MI and stroke were similar up to age 70 and then increased. In particular, those 80+ years with AMD had much higher incidence of stroke than those 70-79 years. While Black patients had a low incidence of MI, there was only 179 patients and one event. Incidence rates by IMD decile were variable and likely reflect the small number of cases in each group.

	Characteristic	PDR *n* (%)	MI *n*	Stroke *n*	Incidence rate MI (95% CI)	Incidence rate Stroke (95% CI)
	All	2,494 (100)	92	72	1449.8 (1173.3-1766.5)	1123.3 (883.4-1403.1)
Sex	**Female**	950 (38.1)	27	27	1100.3 (735.7-1569.0)	1094.8 (732.0-1561.2)
	Male	1,544 (61.9)	65	45	1670.1 (1296.3-2109.6)	1141.1 (839.4-1507.8)
Age group at diagnosis	**40-49 years**	407 (16.3)	7	3	661.0 (284.0-1278.2)	280.1 (69.6-726.0)
	50-59 years	800 (32.1)	20	17	964.1 (600.9-1450.5)	815.6 (486.7-1266.9)
	60-69 years	770 (30.9)	30	28	1515.8 (1036.0-2124.7)	1398.8 (942.6-1982.8)
	70-79 years	407 (16.3)	28	21	2807.1. (1891.6-3979.1)	2080.7 (1312.8-3101.7)
	80+ years	110 (4.4)	7	3	2967.7 (1275.1-5738.9)	1233.3 (306.7-3196.8)
Ethnicity	**Asian**	840 (33.7)	50	24	2236.0 (1672.1-2914.3)	1048.8 (683.2-1526.1)
	Black	326 (13.1)	6	15	712.7 (283.3-1444.1)	1814.0 (1043.8-2892.7)
	White	601 (24.1)	19	14	1213.0 (746.0-1842.9)	890.0 (501.3-1440.8)
	Other/Unknown	727 (29.1)	17	19	999.1 (596.2-1552.0)	1103.7 (678.8-1676.9)
IMD decile[a]	**1 (most deprived)**	208 (8.3)	10	8	1790.6 (897.2-3140.3)	1415.8 (647.0-2635.1)
	2	464 (18.6)	16	13	1386.1 (813.0-2180.4)	1112.0 (611.7-1830.4)
	3	485 (19.4)	18	17	1493.7 (905.5-2293.7)	1413.9 (843.8-2196.4)
	4	289 (11.6)	10	7	1314.7 (658.7-2305.6)	914.5 (392.9-1768.3)
	5	285 (11.4)	10	10	1372.6 (687.8-2407.2)	1369.5 (686.2-2401.8)
	6	255 (10.2)	11	7	1639.1 (851.1-2807.0)	1022.1 (439.2-1976.5)
	7	178 (7.1)	7	4	1680.8 (722.2-3250.3)	936.8 (290.8-2175.9)
	8	126 (5.1)	2	3	631.5 (105.0-1948.7)	937.8 (233.2-2430.8)
	9	119 (4.8)	5	2	1521.7 (545.6-3270.5)	595.8 (99.0-1838.7)
	10 (least deprived)	78 (3.1)	3	1	1609.9 (400.3-4173.1)	525.2 (30.0-2310.0)

Table 9: Crude and stratified incidence rates of myocardial infarction and stroke in patients with proliferative diabetic retinopathy.

Incidence rates are presented per 100,000 person-years at risk. CI: Confidence interval, MI: Myocardial infarction, PDR: Proliferative diabetic retinopathy, SD: Standard deviation [a]7 patients had missing data.

The PDR group was the smallest ophthalmic cohort at 2,494 patients and CI were wider. MI and stroke incidence increased by older age group. Asian patients had higher incidence of MI than Black patients. Although CI were wide, there did appear to be a clear trend of reduced incidence of stroke among those less deprived.

Unadjusted survival analyses

Unadjusted survival analysis via Kaplan-Meier curves for the incidence of MI and stroke are shown in *Figure 21-Figure 24* for cataract, glaucoma, AMD and PDR respectively.

Key findings from unadjusted survival analysis

There was strong statistical evidence for a univariable difference in time-to-MI and time-to-stroke for sex, age and ethnicity among patients with cataract and glaucoma. Among those commencing treatment for AMD, age appeared the only significant variable associated with event-time for both MI and stroke. Among those with PDR (the smallest cohort), there were differences in MI and stroke incidence between age groups and for MI alone, between ethnicity groups.

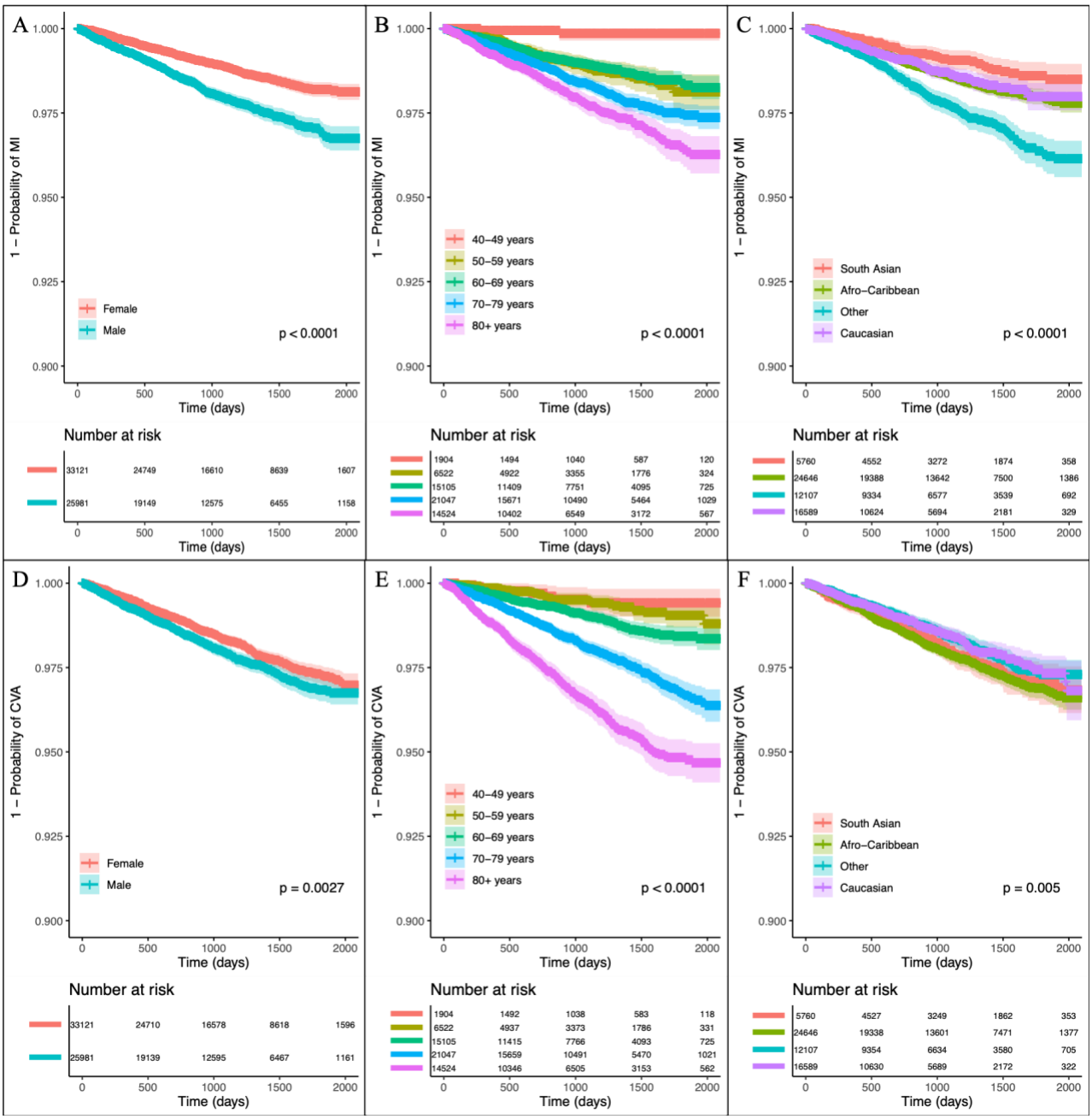

Figure 21: Survival curves for cataract.

Unadjusted Kaplan-Meier curves for the incidence of myocardial infarction (A-C) and ischaemic stroke (D-F) by groups of sex (A, D), age deciles (B, E) and ethnicity group (C, E) following first eye cataract surgery. Line shading represent confidence intervals. *p*-value is for the log-rank test. Designed using the survminer package. There was a significant difference between all groups in the probability of MI or stroke among cataract patients. MI: myocardial infarction, CVA: ischaemic stroke.

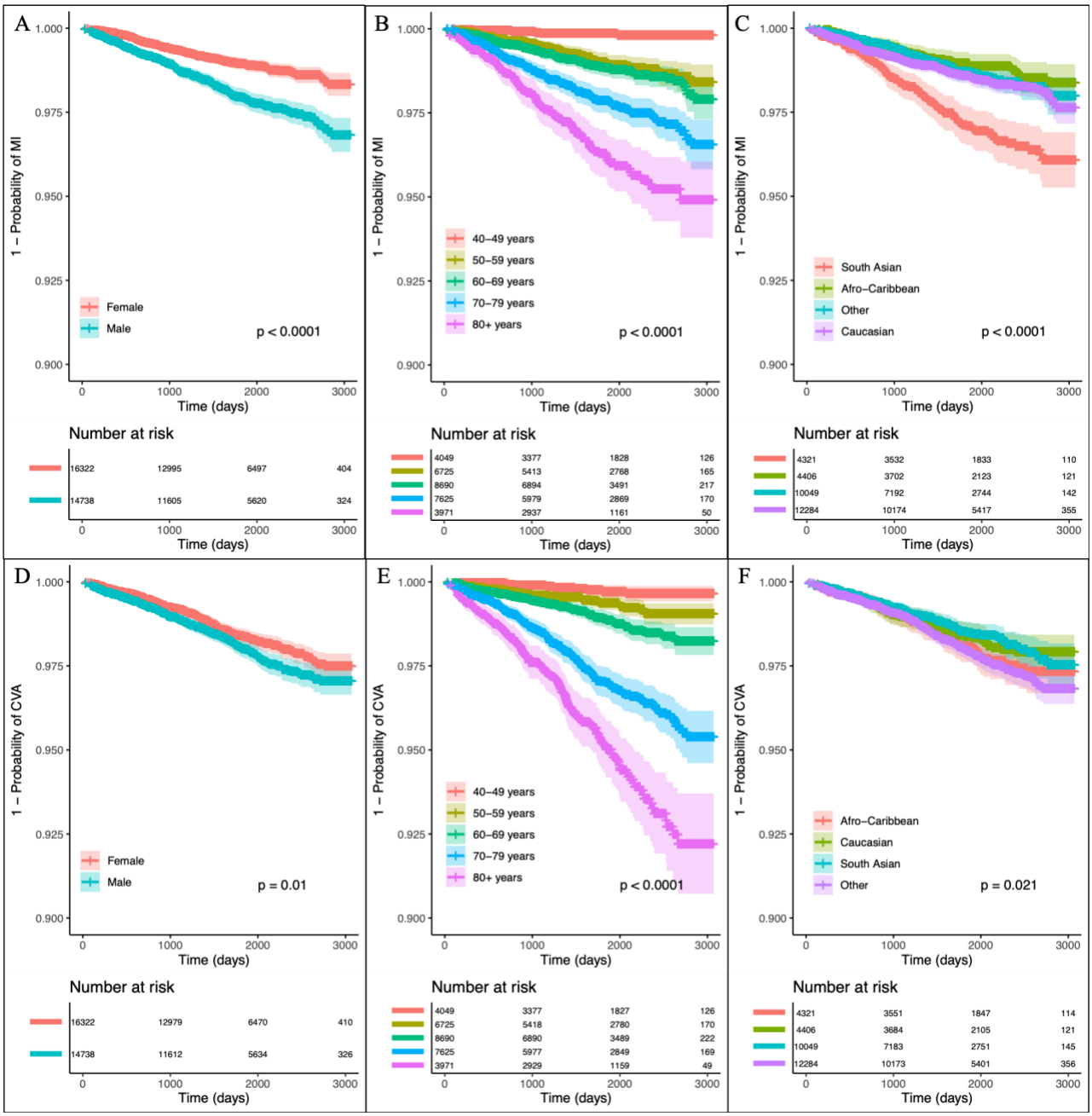

Figure 22: Survival curves for glaucoma.

Unadjusted Kaplan-Meier curves for the incidence of myocardial infarction (A-C) and ischaemic stroke (D-F) by groups of sex (A, D), age deciles (B, E) and ethnicity group (C, E) following glaucoma diagnosis. Line shading represent confidence intervals. *p*-value is for the log-rank test. Designed using the survminer package. There was a significant difference between all groups in the probability of MI or stroke among glaucoma patients. MI: myocardial infarction, CVA: ischaemic stroke.

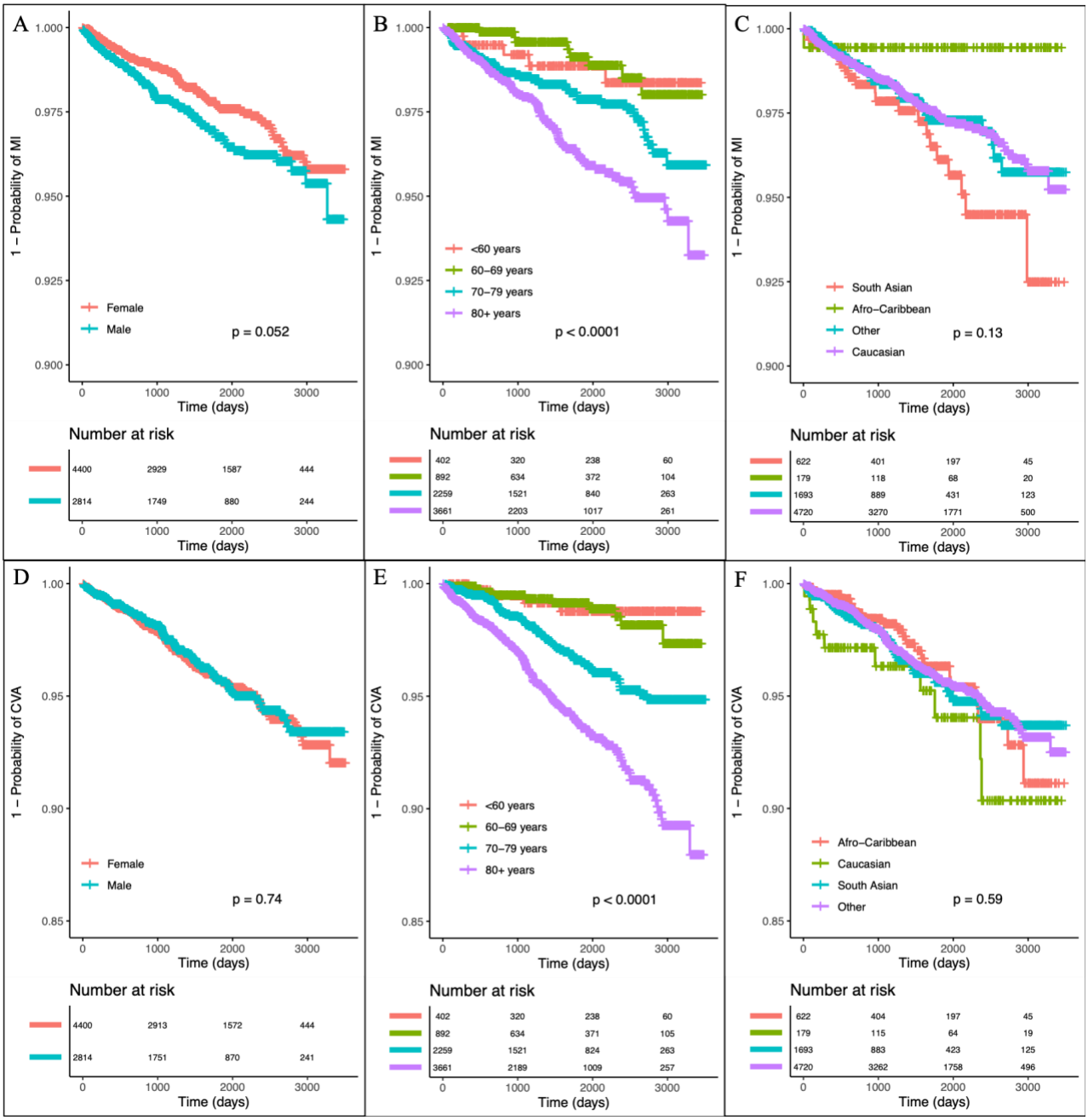

Figure 23: Survival curves for neovascular age-related macular degeneration.

Unadjusted Kaplan-Meier curves for the incidence of myocardial infarction (A-C) and ischaemic stroke (D-F) by groups of sex (A, D), age deciles (B, E) and ethnicity group (C, E) following 1st injection for neovascular age-related macular degeneration. *p*-value is for the log-rank test. Designed using the survminer package. The probability of MI and stroke were significantly different between age groups/ There was a trend for men to have a greater probability of MI than women but this was not statistically significant. MI: myocardial infarction, CVA: ischaemic stroke.

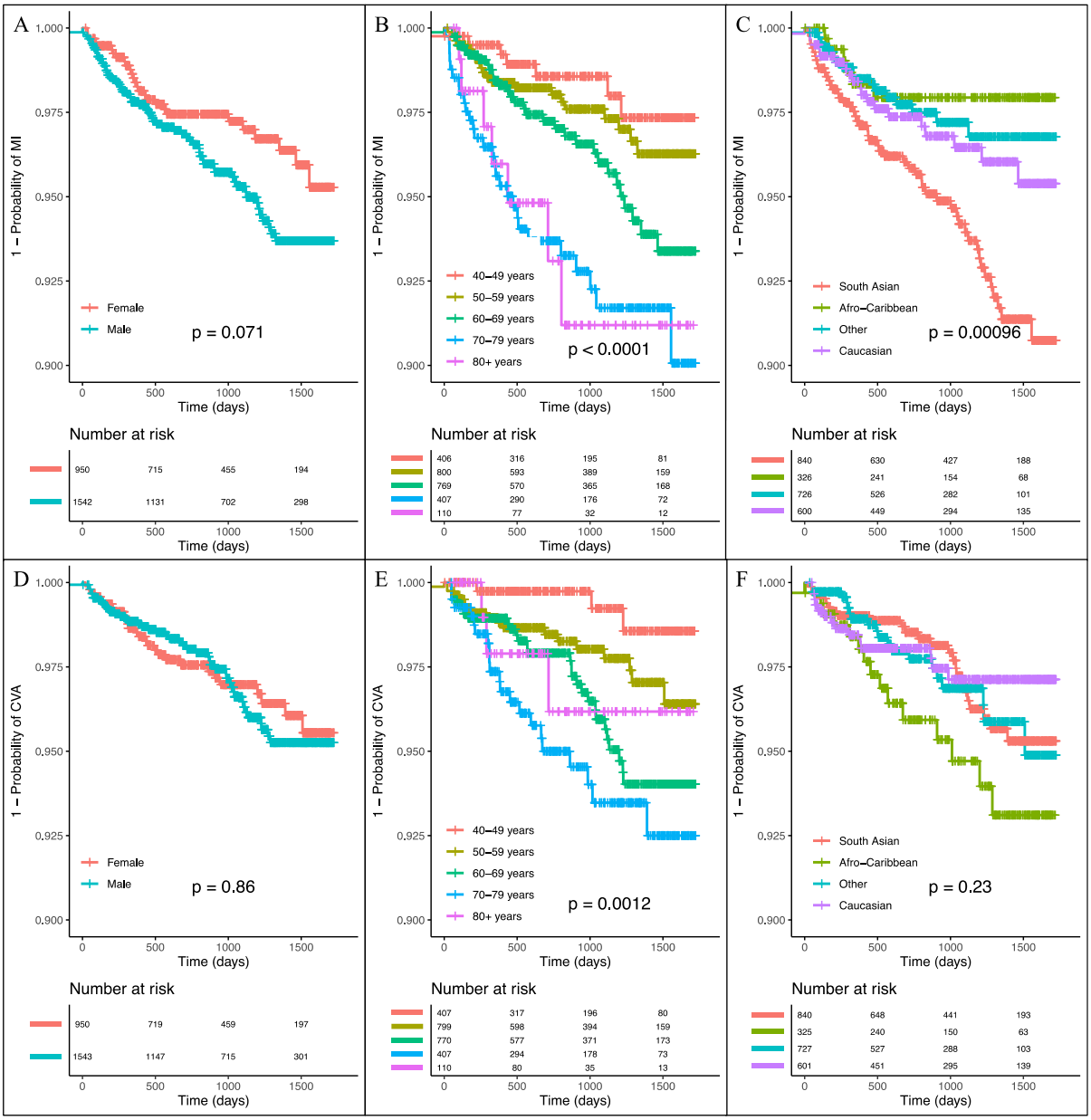

Figure 24: Survival curves for proliferative diabetic retinopathy.

Unadjusted Kaplan-Meier curves for the incidence of myocardial infarction (A-C) and ischaemic stroke (D-F) by groups of sex (A, D), age deciles (B, E) and ethnicity group (C, E) following new diagnosis of proliferative diabetic retinopathy. *p*-value is for the log-rank test. Designed using the survminer package. Probability of MI and stroke differed between age groups. Probabilty of MI also differed between ethnic groups. MI: myocardial infarction, CVA: ischaemic stroke.

Adjusted survival analyses

Subdistribution (sHR) and cause-specific hazard ratios (cHR) are shown in Table *10* - Table *13*. Cataract was associated with a particularly elevated hazard of MI per decade of age (cHR 1.54, 95% CI: 1.43, 1.66) compared to glaucoma (1.06, 95% CI: 1.05, 1.07), AMD (1.05, 95% CI: 1.03, 1.07) and PDR (1.05, 95% CI: 1.03, 1.07). Similar results were seen for stroke incidence in those with cataract (cHR 1.90, 95% CI: 1.77, 2.04) versus other ophthalmic diseases. Asian ethnicity was associated with increased hazards for MI among those with cataract (cHR 2.67, 95% CI: 1.98, 3.61), glaucoma (cHR 2.40, 95% CI: 1.69, 3.40) and PDR (cHR 3.32, 95% CI: 1.41, 7.84). Less deprivation, as measured through IMD decile, was associated with reduced hazards for MI in those with cataract (0.95, 95% CI: 0.92, 0.97) and AMD (0.92, 95% CI: 0.87, 0.97). In the sensitivity analysis across all covariates and diseases, cause-specific hazard ratios were similar to those estimated through subdistribution hazard ratios generated through Fine-Gray competing risks regression (Table *10* - Table *13*).

		Cataract							
		Subdistribution hazard model		Cause-specific hazard model		Subdistribution hazard model		Cause-specific hazard model	
		MI	Death	MI	Death	Stroke	Death	Stroke	Death
Increasing Age	**(per decade)**	1.48 (1.38-1.58)	2.33 (2.25-2.42)	1.54 (1.43-1.66)	2.30 (2.22-2.38)	1.79 (1.68-1.92)	2.29 (2.21-2.38)	1.90 (1.77-2.04)	2.31 (2.23-2.39)
Sex	**Female**	Reference		Reference		Reference		Reference	
	Male	1.77 (1.53-2.03)	*	1.81 (1.57-2.09)	*	*	*	*	*
Ethnicity	**Black**	Reference		Reference				Reference	
	Asian	2.65 (1.97-3.58)	*	2.67 (1.98-3.61)	*	0.93 (0.73-1.17)	*	0.92 (0.73-1.17)	*
	White	1.36 (1.01-1.83)	*	1.39 (1.03-1.88)	*	0.88 (0.71-1.09)	*	0.90 (0.72-1.12)	*
	Other	1.37 (1.00-1.87)	*	1.41 (1.03-1.94)	*	0.76 (0.60-0.96)	*	0.79 (0.62-1.00)	*
IMD	**(per increase in decile)**	0.95 (0.92-0.98)	0.96 (0.95-0.97)	0.95 (0.92-0.97)	0.94 (0.93-0.95)	0.95 (0.93-0.98)	0.96 (0.95-0.97)	0.95 (0.93-0.97)	0.94 (0.93-0.95)

Table 10: Adjusted hazard ratios with 95% confidence intervals from subdistribution and cause-specific hazard models for myocardial infarction, stroke and death among patients undergoing first eye cataract surgery.

MI: Myocardial infarct, IMD: Index of multiple deprivation. * Modelling was stratified on this variable due to violation of the proportional hazards assumption. Subdistribution hazard ratios are derived from the Fine-Gray competing risks regression model and cause-specific hazard ratios from Cox proportional hazards modelling

Patients with cataract were 54% more likely to have an MI with each decade increase in age at time of first eye surgery. Men and those of Asian ethnicity also had increased hazards of MI. For each decile increase in IMD (i.e. less deprivation), patients were 5% less likely to have an MI. Patients with cataract were 90% more likely to have an ischaemic stroke with each decade increase in age. There was no evidence of an association between ethnicity and stroke incidence on adjusted survival analysis. Similarly to MI, reduced deprivation was associated with reduced likelihood of ischaemic stroke.

		Glaucoma							
		Subdistribution hazard model		Cause-specific hazard model		Subdistribution hazard model		Cause-specific hazard model	
		MI	Death	MI	Death	Stroke	Death	Stroke	Death
Increasing Age	**(per decade)**	1.06 (1.05-1.07)	1.11 (1.10-1.12)	1.06 (1.05-1.07)	1.11 (1.11-1.12)	1.07 (1.03-1.08)	1.11 (1.10-1.11)	1.08 (1.07-1.08)	1.11 (1.11-1.12)
Sex	**Female**	Reference		Reference		Reference		Reference	
	Male	2.00 (1.64-2.44)	1.51 (1.38-1.66)	2.04 (1.67-2.48)	1.59 (1.45-1.74)	1.33 (1.12-1.59)	1.55 (1.41-1.70)	1.36 (1.14-1.62)	1.58 (1.44-1.73)
Ethnicity	**Black**	Reference		Reference				Reference	
	Asian	2.39 (1.69-3.39)	*	2.40 (1.69-3.40)	*	1.15 (0.83-1.60)	*	1.16 (0.83-1.61)	*
	White	1.13 (0.81-1.58)	*	1.15 (0.82-1.61)	*	1.00 (0.76-1.32)	*	1.02 (0.77-1.35)	*
	Other	1.14 (0.80-1.63)	*	1.19 (0.93-1.69)	*	0.91 (0.67-1.23)	*	0.95 (0.70-1.29)	*
IMD	**(per increase in decile)**	0.97 (0.93-1.01)	*	0.97 (0.93-1.01)	*	0.98 (0.95-1.02)	*	0.98 (0.95-1.02)	*

Table 11: Adjusted hazard ratios with 95% confidence intervals from subdistribution and cause-specific hazard models for myocardial infarction, stroke and death among patients with glaucoma.

MI: Myocardial infarct, IMD: Index of multiple deprivation. * Modelling was stratified on these variables due to violation of the proportional hazards assumption. Subdistribution hazard ratios are derived from the Fine-Gray competing risks regression model and cause-specific hazard ratios from Cox proportional hazards modelling.

Patients with glaucoma had a 6% and 8% increased probability of MI and stroke respectively per decade increase in age. Men had increased hazards of both MI and stroke. Asian patients had 139% increased probability of MI compared to Black patients. There was no association of socioeconomic deprivation with probability of MI or stroke among glaucoma patients.

		Age-related macular degeneration							
		Subdistribution hazard model		Cause-specific hazard model		Subdistribution hazard model		Cause-specific hazard model	
		MI	Death	MI	Death	Stroke	Death	Stroke	Death
Increasing Age	**(per decade)**	1.04 (1.02-1.06)	1.10 (1.09-1.10)	1.05 (1.03-1.07)	1.10 (1.09-1.11)	1.06 (1.05-1.08)	1.09 (1.08-1.10)	1.08 (1.06-1.09)	1.10 (1.09-1.11)
Sex	**Female**	Reference		Reference		Reference		Reference	
	Male	1.33 (0.98-1.82)	1.41 (1.27-1.58)	1.41 (1.03-1.93)	1.42 (1.28-1.58)	0.99 (0.77-1.27)	1.46 (1.31-1.63)	1.06 (0.82-1.37)	1.43 (1.29-1.59)
Ethnicity	**Black**	Reference		Reference				Reference	
	Asian	5.78 (0.76-43.78)	1.12 (0.65-1.93)	5.86 (0.78-43.87)	1.16 (0.69-1.97)	0.56 (0.26-1.19)	1.21 (0.67-2.19)	0.56 (0.26-1.20)	1.10 (0.65-1.86)
	White	3.33 (0.46-24.17)	1.45 (0.88-2.38)	3.43 (0.48-24.77)	1.46 (0.90-2.37)	0.41 (0.21-0.79)	1.67 (0.98-2.87)	0.42 (0.22-0.81)	1.37 (0.84-2.22)
	Other	3.46 (0.47-25.74)	1.42 (0.85-2.36)	3.62 (0.49-26.64)	1.44 (0.88-2.36)	0.43 (0.22-0.87)	1.65 (0.95-2.85)	0.45 (0.23-0.90)	1.36 (0.83-2.22)
IMD	**(per increase in decile)**	0.93 (0.87-0.98)	0.94 (0.93-0.96)	0.92 (0.87-0.97)	0.94 (0.92-0.96)	0.98 (0.93-1.02)	0.94 (0.92-0.96)	0.97 (0.93-1.02)	0.94 (0.92-0.96)

Table 12: Adjusted hazard ratios with 95% confidence intervals from subdistribution and cause-specific hazard models for myocardial infarction, stroke and death among patients with age-related macular degeneration.

MI: Myocardial infarct, IMD: Index of multiple deprivation. Subdistribution hazard ratios are derived from the Fine-Gray competing risks regression model and cause-specific hazard ratios from Cox proportional hazards modelling.

Patients with neovascular AMD had a 5% and 8% increased probability of MI per decade of age for MI and ischaemic stroke respectively. Less deprivation (increase in IMD decile) was associated with a 7% and 3% reduced probability of MI and ischaemic stroke respectively.

		Proliferative diabetic retinopathy							
		Subdistribution hazard model		Cause-specific hazard model		Subdistribution hazard model		Cause-specific hazard model	
		MI	Death	MI	Death	Stroke	Death	Stroke	Death
Increasing Age	**(per decade)**	1.04 (1.02-1.06)	1.06 (1.04-1.07)	1.05 (1.03-1.07)	1.06 (1.05-1.08)	1.05 (1.03-1.07)	1.06 (1.05-1.08)	1.05 (1.03-1.08)	1.05 (1.03-1.07)
Sex	**Female**	Reference		Reference		Reference		Reference	
	Male	1.53 (0.97-2.39)	1.31 (0.97-1.77)	1.55 (0.99-2.44)	1.35 (1.02-1.79)	1.20 (0.74-1.95)	1.39 (1.03-1.88)	1.25 (0.77-2.03)	1.20 (0.74-1.95)
Ethnicity	**Black**	Reference		Reference		Reference		Reference	
	Asian	3.32 (1.41-7.83)	1.10 (0.68-1.78)	3.32 (1.41-7.84)	1.40 (0.89-2.20)	0.63 (0.32-1.24)	1.35 (0.83-2.19)	0.63 (0.35-1.24)	0.63 (0.32-1.24)
	White	1.89 (0.75-4.67)	1.62 (0.99-2.66)	1.91 (0.95-4.86)	1.69 (1.06-2.70)	0.57 (0.26-1.24)	1.72 (1.04-2.83)	0.89 (0.28-1.26)	0.57 (0.26-1.24)
	Other	1.55 (0.60-4.01)	1.05 (0.62-1.78)	1.57 (0.61-4.04)	1.11 (0.68-1.83)	0.78 (0.38-1.63)	1.10 (0.65-1.88)	0.81 (0.40-1.62)	0.78 (0.38-1.63)
IMD	**(per increase in decile)**	0.96 (0.88-1.05)	0.94 (0.89-1.01)	0.96 (0.88-1.05)	0.93 (0.88-0.99)	0.95 (0.86-1.05)	0.94 (0.89-1.00)	0.95 (0.85-1.05)	0.95 (0.86-1.05)

Table 13: Adjusted hazard ratios with 95% confidence intervals from subdistribution and cause-specific hazard models for myocardial infarction, stroke and death among patients with proliferative diabetic retinopathy.

MI: Myocardial infarct, IMD: Index of multiple deprivation.

Subdistribution hazard ratios are derived from the Fine-Gray competing risks regression model and cause-specific hazard ratios from Cox proportional hazards modelling.

Patients with PDR had a slightly increased probability of MI and stroke with increasing age. Asian ethnicity was associated with 3.32 times the probability of MI compared to those of Black ethnicity.

5.2.4 Discussion

In these analyses of specific ophthalmic disease groups in AlzEye, a sharp increase in the incidence rate of MI was seen in patients newly undergoing cataract surgery from 35.3 (5.9-108.8) for 40–49-year-olds and 368.8 (299.0-463.6) per 100,000 for 50-59-year-olds PYAR. Cox proportional hazards modelling showed that for each decade increase in age, patients newly undergoing first eye cataract surgery had a 54% increase in MI probability after adjusting for sex, ethnicity, and level of socioeconomic deprivation. Rates of MI and stroke among those with PDR were higher than all other ophthalmic disease cohorts, even in the youngest age group. Within the cataract and glaucoma groups, Asian ethnicity was associated with higher rates of MI. The findings suggest that the incidence of MI in patients with an early diagnosis (under the age of 60) of cataract increases sharply; this group may benefit from appropriate risk stratification, for example, through encouraging cardiovascular health screening and highlighting them to primary care.

The results should be interpreted in the context of the limitations recognised with using hospital admissions data, which is foremost collected for reimbursement purposes. Firstly, I report on a select population, which is attending secondary hospital-based ophthalmic services, with possibly disparate levels of morbidity. Although the UK NHS recommends that all individuals should undergo regular

community eye surveillance throughout their lifetime[251], the level of population adherence to such guidance is unclear. Similarly, all those with diagnosed diabetes mellitus are recruited into the national diabetic retinopathy screening programme; attendance of this was estimated at 81% in 2011-2012[252]. The characteristics of this population might therefore be disproportionately represented by two polarising patient groups - health-conscious individuals and those with significant comorbidity associated with ophthalmic disease and increasing age. Indeed, summary figures of the AlzEye cohort shown an ethnically and socioeconomically diverse population skewed towards greater levels of deprivation (Table *2*). Thus, they are likely to be at higher risk of the chronic diseases of ageing, namely cardiovascular diseases, and dementia, which will be of focus in this project. Secondly, while I assessed the influence of some sociodemographic features on the incidence rates of MI and stroke, I did not exhaustively analyse, in the absence of relevant data, all potential confounders, such as pre-existing hypertension or smoking status, which would typically be measured in prospective epidemiological cohorts. For example, my finding of steeply rising rates of MI in younger patients may reflect the strong known association between cataract and smoking, a well-known risk factor for CVD. Nonetheless, the implication of my finding that such patients should be considered for CVD risk-stratification would still stand despite unmeasured confounding. Thirdly, I deliberately did not exclude patients with preceding CVD events due to the potential resulting selection bias. Instead, I hypothesised that older patients would have been more likely to have had a preceding event and therefore be differentially excluded in my analysis shifting the measure of effect for older groups towards neutrality.

The association between cataract and elevated levels of incident ischaemic heart disease has been noted previously[171,253,254]. Hu et al identified an increased risk of mortality among women aged 45-63 years primarily attributable to coronary heart disease hypothesising that the crystalline lens was a possible surrogate for oxidative stress[253]. However, this data was based on a prospective epidemiological cohort in a specified population of the US, the Nurses' Health Study Cohort, limiting their generalisability to whole populations in contrast to my study, which accounts for a large diverse population attending a publicly funded healthcare service in the UK. Using a record-linkage approach of a national insurance program in Taiwan, another report showed an elevated incidence of ischaemic heart disease in 32,456 patients with cataract[171]. Adjusted HR for those with cataract versus matched controls was greatest for those under the age of 50 (1.75, 95% CI: 1.32, 2.30) supporting my findings. As noted by the authors however, limitations included reliance on ICD coding for cataract presence and the data originating from an ethnically homogenous population in Taiwan. Ophthalmic diagnostic codes, in this report, however come from actual hospital operation records. The agreement of secondary care hospital records (as in this report) with national coding systems, such as HES, will be explored in this project. In a recent study in the United States, coding for glaucoma using the International Classification of Diseases, 9th revision, Clinical Modification (ICD-9) had a positive predictive value of only 66% of individuals using a reference standard judged by ophthalmologists[248].

Since 2018, ophthalmology has been the busiest outpatient specialty in the United Kingdom NHS accounting for nearly eight million appointments annually [255] and cataract surgery is currently the most frequently performed operation. Of additional

relevance to this issue is the importance the public places on vision. Sight is consistently ranked the most highly valued sense and a recent survey revealed that individuals would rather relinquish five years of perfect health than suffer complete sight loss [234]. Such sentiment also manifests itself in health seeking behaviour. In 2012, while only 9.0% of the UK population aged 40-59 years consulted their primary care physician for the *NHS Health Check*, a national programme of structured clinical assessment and management of CVD risk for those over 40 [256], a YouGov survey in 2011 showed that 80% of those 45-54 years of age reported attending their local eye professional for a routine vision check at least every four years [257]. Given the vast net cast by national ophthalmic services and the public motivation in maintaining their eye health, diagnosis of cataract in young patients may represent an opportune event for the early detection of evolving CVD. Communication between eye specialists, either ophthalmologists or optometrists in the community setting, and general practitioners could highlight the heightened risk of CVD in patients upon diagnosis.

5.2.5 Summary

In this section, I describe the incidence of myocardial infarction and ischaemic stroke in patients following diagnosis with four leading causes of visual impairment and then assess the association of cardiovascular event risk with sociodemographic profile. I observed epidemiological patterns consistent with previously published literature, such as an increased risk of MI in men and South Asian patients (compared to Black patients). However, there were also some new findings – for example, the incidence rate of myocardial infarction in patients with cataract increased sharply from those aged 40-49 years to those aged 50-59 years.

5.3 Acute neurophthalmic diseases

5.3.1 Introduction

The general ophthalmologist staffing the emergency eye department may be presented with several acute neurophthalmic eye conditions with potentially devastating systemic sequelae. Prompt recognition and subsequent liaison with appropriate specialties (e.g. stroke physicians) is crucial in minimising patient morbidity and mortality. In this section, I investigate the incidence of myocardial infarction, ischaemic stroke and death following several acute neurophthalmic conditions, namely i) retinal arteriolar occlusion (RAO), ii) ocular cranial nerve palsies (OCP) and, iii) non-arteritic anterior ischaemic optic neuropathy (NAION). In some cases, there has been convincing evidence of an elevated risk of cardiovascular events following an acute neurophthalmic disease (e.g. ischaemic stroke following central retinal artery occlusion) while in others, the evidence remains unclear (e.g. NAION). The AlzEye cohort provides an opportunity to investigate the incident risk using ophthalmologist-labeled ocular diagnoses in a diverse real-world patient group.

Retinal artery occlusion

Ischemic events of the retinal arterial vasculature are a cause of acute painless monocular vision field loss. Central retinal artery occlusion (CRAO) and branch retinal artery occlusion (BRAO) lead to irreversible retinal infarction, whereas the ischemic event in transient monocular vision loss (TMVL), also called amaurosis fugax, is reversible[258]. The underlying causes and mechanisms of action are comparable to a stroke in the internal carotid artery territory[259]. Therefore, CRAO and BRAO are considered part of the stroke spectrum and TMVL that of transient

ischemic attacks (TIA)[260,261]. The risk of suffering a recurrent stroke after TIA is reported to be 10% in the first week following the event with about half of events occurring within 24 hours[262,263]. A recent meta-analysis of asymptomatic and symptomatic patients with retinal artery occlusions found signs of acute cerebral ischemia on MRI in 30% of patients with CRAO and 25% of patients with BRAO; another MRI-based study assessing patients with CRAO, BRAO and TMVL however found that in up to 90% of patients, no additional neurological symptoms were reported, and the infarction was labelled as silent[264]. Urgent assessment and treatment of these patients can reduce the risk of further strokes by up to 80%[261,265]. The list of differential diagnoses for TMVL is long and consists of many non-urgent entities, however scenarios such as embolic TMVL require urgent evaluation, underlining the importance of prompt clinical evaluation[262].

Ocular cranial palsies (OCP)

Palsies affecting the III (CN3), IV (CN4) and VI (CN6) cranial nerves, are a common presentation to ophthalmic emergency centres. The aetiology is typically attributed to microvascular ischaemia, with most patients exhibiting vasculopathic risk factors, such as diabetes, hypertension or hypercholesterolemia[266]. Whilst the majority of cranial nerve palsies are associated with spontaneous resolution and a favourable prognosis, the incident risk of extra-ocular outcomes remains poorly understood[267,268]. As the risk factors that predispose to microvascular OCP dysfunction correspond with macrovascular risk factors for cardiovascular disease, stroke and myocardial infarction (MI), an association between nerve palsies and incident cardiovascular events is mechanistically feasible[269–271].

Non-arteritic ischaemic optic neuropathy (NAION)

Non-arteritic ischaemic optic neuropathy (NAION) is a leading cause of acute optic neuropathy in adults over 50 years of age[272,273]. It is typically a unilateral disease, presenting with sudden painless vision loss, The specific pathophysiology behind NAION is complex[274] but widely believed to be caused by inadequate blood supply to the optic nerve head as a result of hypoperfusion or non-perfusion of the short posterior ciliary arteries[275]. This is supported by its documented association with systemic vascular comorbidities including hypertension, hypercholesterolaemia, diabetes mellitus, and ischaemic heart disease[276–278]. Tobacco use has also been described as a risk factor[279]. Nonetheless, the description of non-vascular risk factors, such as small and crowded optic discs or genetic polymorphisms, indicate that the pathogenesis is likely multifactorial in nature[274,280].

5.3.2 Methods

These analyses were undertaken using a propensity-matched cohort substudy using data from AlzEye. Relevant to this section, I collected ophthalmic diagnoses of all attendances to the emergency ophthalmology department of adults aged 40 years and over between August 1st 2014 and April 1st 2018 inclusive at the principal site of Moorfields Eye Hospital NHS Foundation Trust (MEH). Individual-level ophthalmic records were linked with hospital admissions data using the Hospital Episode Statistics (HES) database overseen by NHS Digital.

The following exposures were investigated in this report:

- Retinal artery occlusions

    - CRAO, BRAO and TMVL
- Ocular cranial palsies
    - CN3, CN4 and CN6
- Non-arteritic anterior ischaemic optic neuropathy

Diagnoses for the exposures were derived from structured diagnostic codes in the MEH electronic health record system, the Patient Administration System, entered by ophthalmologists servicing the MEH emergency department. The event outcomes of myocardial infarction (MI) and ischaemic stroke as well as medical comorbidity data were extracted from Hospital Episode Statistics (HES). As mentioned previously, MI was defined as code I21 or I22, ischaemic stroke as code I63-I64. Other relevant ICD codes were chosen based on literature review and are listed in the appropriate Results tables. Carotid endarterectomy (CEA) surgery was coded as L29 through the Operating Procedure Code Supplement (OPCS), a clinical classification system for operative procedures and interventions[281]. Mortality data were derived from the MEH database (Section 4.1.5). Mortality data up to the end of the study period, 1st April 2018, was included.

Statistical analysis

Summary statistics were median +/- interquartile range (IQR) for continuous variables and percentages for categorical variables. Categorical variables were compared using the U-statistic Permutation test of independence (an iteration of the Pearson's chi-squared test with exact non-asymptotic Type 1 error control at the nominal level) and continuous variables through the Wilcoxon-Mann-Whitney U test[282]. Incidence rates were estimated as the number of new events in the study

period per 1,000 person-years at risk (PYAR) with 95% confidence intervals calculated using the Poisson distribution (offset as the logarithm of the total PYAR). The at-risk period was defined from the time of ophthalmic event until the earliest of i) death, ii) first event (MI or ischaemic stroke) or iii) conclusion of the data period on April 1st 2018. Those with a previous cardiovascular event were not excluded for the calculation of incidence rates however prior events are described. I used propensity score matching (PSM) to estimate the average marginal effect of the acute neurophthalmic event on time to event (MI, ischaemic stroke or death)[283]. I matched on age, sex, hypertension and diabetes using an 8:1 greedy nearest neighbour without replacement approach, where PSM was estimated using logistic regression. I assessed balance between controls and cases using standardised mean differences, variance ratios and empirical cumulative density function[208–211]. No exposed units were discarded. Time to event between groups was compared using the non-parametric log rank test and event trajectories illustrated visually with Kaplan-Meier curves. For comparing the incidence of having a CEA between groups with RAO, I estimated the incidence rate ratio (IRR) and tested against the null hypothesis that the IRR was 1. Statistical analyses were conducted in R version 3.6.4 (R Core Team, 2012. R Foundation for Statistical Computing, Vienna, Austria) using the matchit and survival packages.

5.3.3 Results

Retinal artery occlusion

Between August 1st 2014 and March 31st 2018, a total of 566 patients received a diagnosis of RAO and/or TMVL - 190 patients experienced a CRAO, 178 a BRAO and 205 TMVL (i.e. some had more than one event). Summary characteristics

stratified by each ophthalmic event are shown in Table *14*. Good matching between cases and propensity-matched controls was achieved (Appendix 7: Propensity-matching quality for retinal artery occlusion). Time-to-event analysis with Kaplan-Meier curves for MI, ischemic stroke and death for all three entities are displayed in *Figure 25*.

		CRAO n=190	BRAO n=178	TMVL N=205
Sex n (%)	Female	68 (35.6)	61 (34.3)	109 (53.2)
	Male	122 (64.4)	117 (65.7)	96 (46.8)
Age median (IQR)	Years	70.1 (61.6.1-78.6)	69.9 (59.0-80.8)	68.1 (58.5-77.7)
Ethnicity n (%)	Asian (South)	22 (11.6)	19 (10.7)	35 (17.1)
	Black	20 (10.5)	13 (7.3)	16 (7.8)
	White	108 (56.8)	109 (61.2)	115 (56.1)
	Other/Unknown	40 (21.1)	37 (20.8)	39 (19.0)
SES median (IQR)	Decile	5 (3-7)	6 (3-8)	5 (1.5-6.5)
Preceding MI	N (%)	5 (2.6)	9 (5.1)	8 (3.9)
Preceding CVA	N (%)	4 (2.1)	3 (1.7)	3 (1.4)
Mortality rate	Per 1,000 PYAR	29.9 (17.6-47.1)	12.7 (5.0-25.7)	12.4 (5.3-24.1)
Incidence rate - Myocardial infarct	Per 1,000 PYAR	9.6 (3.4-20.5)	4.3 (0.7-13.1)	7.2 (2.2-16.8)
Incidence rate - Ischaemic stroke	Per 1,000 PYAR	13.5 (5.8-26.1)	6.4 (1.6-16.7)	7.1 (2.2-16.6)

Table 14: Baseline sociodemographic data of the cohort stratified by ophthalmic event.

CRAO = central retinal artery occlusion, BRAO = branch retinal artery occlusion, CVA = ischaemic stroke, TMVL = transient monocular visual loss, IQR = interquartile range, SES = socioeconomic status through index of multiple deprivation where 1 is the most deprived and 10 the least deprived decile.

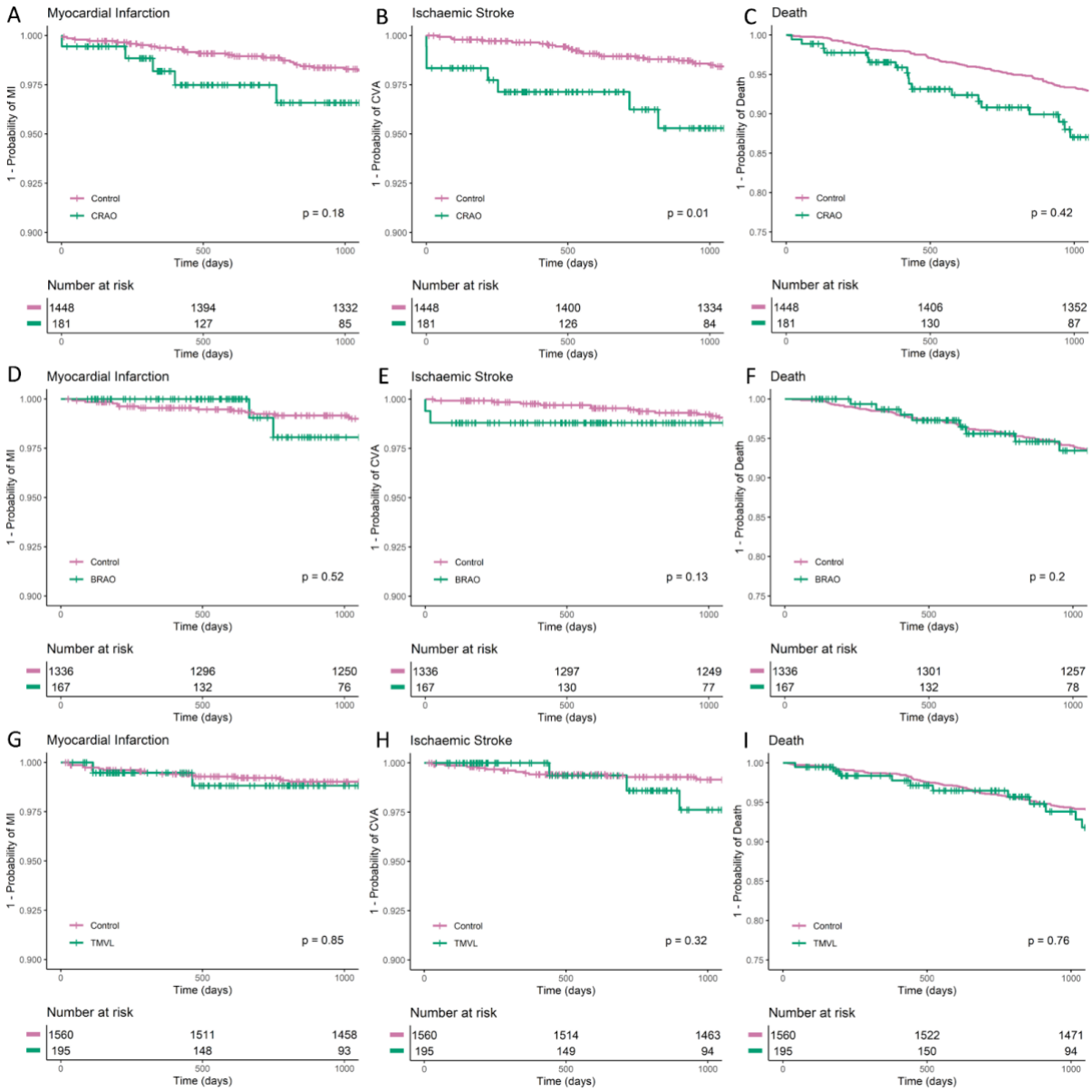

Figure 25: Collage of Kaplan-Meier curves by ophthalmic and systemic event for cases (green) and propensity-matched controls (magenta).

A-C depict 1-probability for MI, CVA and death respectively for individuals who have experienced a CRAO, D-F for those with a BRAO and G-I for those with TMVL. The p value is derived using the log-rank test.

BRAO: branch retinal artery occlusion, CRAO: central retinal artery occlusion, CVA: ischaemic stroke, MI: myocardial infarction, TMVL: transient monocular vision loss.

A total of 190 patients (64.4% male) with a median age of 70.1 (53.1-87.1) years were diagnosed with a CRAO during the study period (Table *14*). During the study period, 34 patients died. Five patients had an incident MI at a median of 322 (234.5-409.5) days including one patient who had an MI one day after CRAO diagnosis. Seven patients had an ischaemic stroke following CRAO with three patients diagnosed within one day after the CRAO diagnosis. Individuals with a CRAO were no more likely to experience an MI (HR: 1.61, 95% CI: 0.64, 4.03, *p*=0.31) or death (HR: 1.16, 95% CI: 0.72, 1.85, *p*=0.55) however they had 191% greater hazards of developing an ischaemic stroke (HR: 2.91, 95% CI: 1.25, 6.76, *p*=0.013, *Table 15*). One patient had had a CEA prior to their CRAO. Of the five patients, who had a CEA following a CRAO, three were within 14 days. Of the 190 patients with a CRAO, 136 had a hospital admission during the study period.

Of 178 patients who experienced a BRAO during the study period, 117 were male (65.7%) and the median age at presentation was 69.9 (59.0-80.8) years. Only two patients had incident MI following a diagnosis of BRAO with a median time of 707 (685.5-728.5). Only two patients had an incident ischaemic stroke, one of which was within 4 weeks following the BRAO. Hazards of MI, ischaemic stroke and death were no different between individuals with a BRAO and propensity-matched controls. Two patients had a previous CEA and 11 patients (6.2%) had one following their BRAO at a median of 12.5 (8.75-16.5) days. Those with a BRAO were significantly more likely to have a subsequent CEA compared to those with CRAO (IRR 2.84, 95% CI 1.00-8.07, *p*=0.04, *Figure 26*).

Among 205 patients who were diagnosed with TMVL in the study period, the median age was 68.1 (58.5-77.7) years of age and, in contrast to CRAO or BRAO, most patients were female (n=109, 53.2%). Eight individuals had a preceding MI and three had a preceding CVA. There were four cases of incident MI (median 702 +/- 733 days) and four cases of incident ischaemic stroke however for neither were the events within 1 year. There was no different in time to MI, ischaemic stroke or death between those with TMVL and propensity-matched controls. Eleven patients had a CEA following an episode of TMVL at a median of 7 (5-10.75) days (10/12 within 14 days).

Hypertension (prevalence: CRAO 53.7%, BRAO 75%, TMVL: 63.4%) and diabetes mellitus (prevalence: CRAO 18.4%, BRAO 19.8%, TMVL: 19.1%) were common at presentation (Table *16*). Six percent of patients with a CRAO were newly diagnosed with atrial fibrillation within 1 year (incidence rate 0.06 per PYAR, 95% CI: 0.04, 0.09) while 3.7% (n=5) ultimately received a diagnosis of giant cell arteritis (Table *16*).

Diagnosis	Myocardial infarction		Ischaemic stroke		Death	
	HR (95% CI)	***p*-value**	**HR (95% CI)**	***p*-value**	**HR (95% CI)**	***p*-value**
Central retinal artery occlusion	1.61 (0.64, 4.03)	0.31	**2.91 (1.25, 6.76)**	**0.013**	1.16 (0.72, 1.85)	0.55
Branch retinal artery occlusion	1.91 (0.42, 8.69)	0.41	2.10 (0.59, 7.43)	0.25	0.51 (0.22, 1.18)	0.12
Transient monocular vision loss	1.19 (0.27, 5.15)	0.82	1.23 (0.37, 4.10)	0.73	0.87 (0.51, 1.49)	0.61

Table 15: Association between retinal ischaemic event and incident myocardial infarction, ischaemic stroke and death.

Adjusted hazard ratios were estimated through 8:1 propensity-matched Cox proportional hazards models. All models were adjusted for age, sex, hypertension and diabetes mellitus. CI: confidence interval, HR: hazard ratio

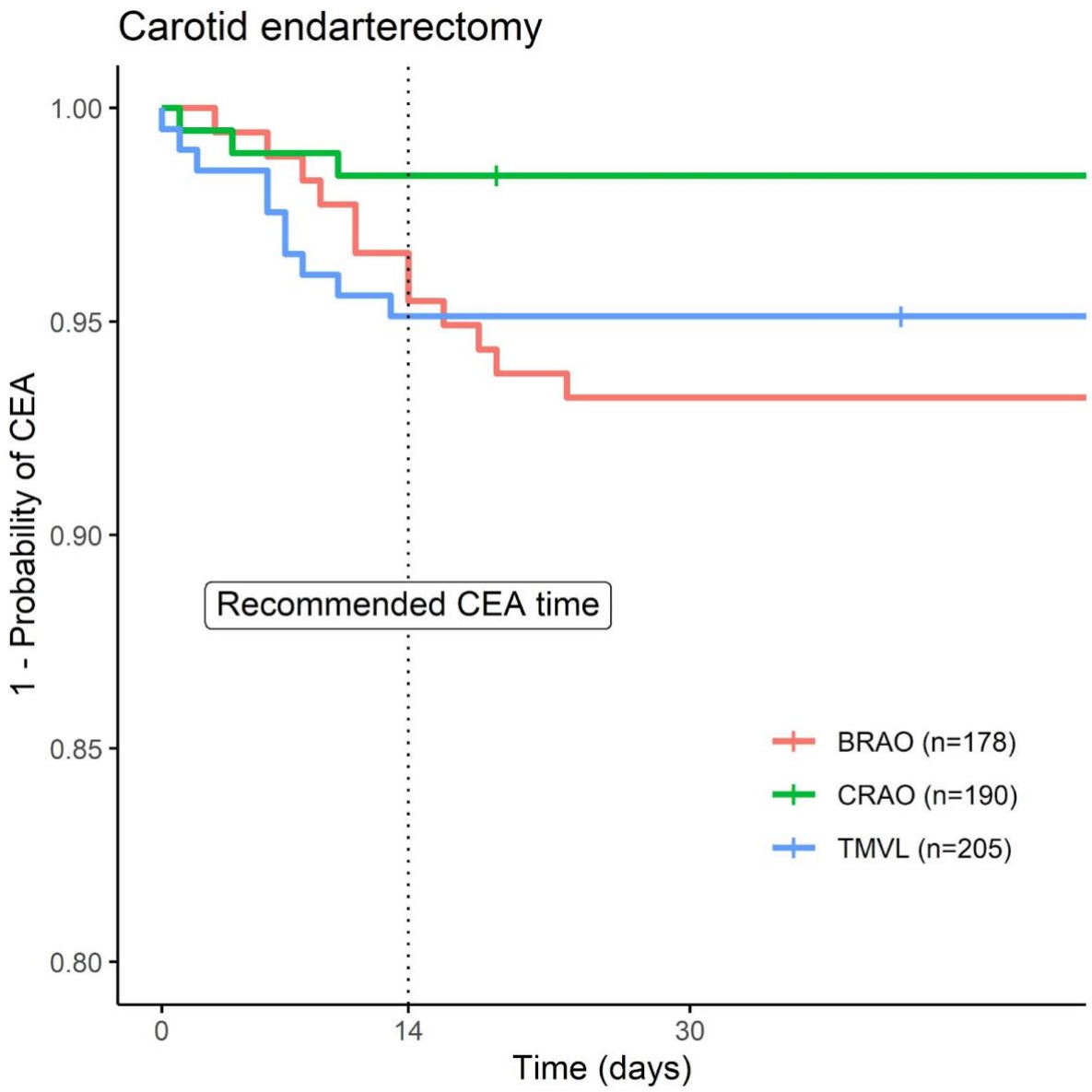

Figure 26: Kaplan-Meier curves for time to carotid endarterectomy among those with central retinal artery occlusion, branch retinal artery occlusion and transient monocular visual loss.

The dotted vertical line at 14 days indicates the recommended maximum duration between retinal ischaemic event and undergoing carotid endarterectomy. BRAO: branch retinal artery occlusion, CEA: carotid endarterectomy, CRAO: central retinal artery occlusion, TMVL: transient monocular visual loss.

Comorbidity	CRAO (n=136)			BRAO (n=96)			TMVL (n=131)		
	Prevalent n (%)	Incident n (%)	Incidence rate PYAR (95% CI)	Prevalent n (%)	Incident n (%)	Incidence rate PYAR (95% CI)	Prevalent n (%)	Incident n (%)	Incidence rate PYAR (95% CI)
Hypertension	73 (53.7)	40 (29.4)	0.44 (0.32, 0.59)	72 (75.0)	22 (22.9)	0.43 (0.27, 0.63)	83 (63.3)	23 (17.6)	0.24 (0.15, 0.36)
Diabetes Mellitus	25 (18.4)	17 (12.5)	0.06 (0.03, 0.09)	19 (19.8)	5 (5.2)	0.02 (0.01, 0.04)	25 (19.1)	7 (5.3)	0.02 (0.01, 0.05)
Hypercholesterolemia	36 (26.5)	38 (27.9)	0.19 (0.14, 0.26)	37 (38.5)	25 (26.0)	0.17 (0.11, 0.25)	43 (32.8)	21 (16.0)	0.10 (0.06, 0.15)
Atrial Fibrillation	17 (12.5)	19 (14.0)	0.06 (0.04, 0.09)	15 (15.6)	7 (7.3)	0.03 (0.01, 0.06)	22 (16.8)	5 (3.8)	0.02 (0.01, 0.04)
Asthma	11 (8.1)	6 (4.4)	0.02 (0.01, 0.04)	*	*	0.01 (0.00, 0.03)	13 (9.9)	4 (3.1)	0.01 (0.00, 0.03)
COPD	13 (9.6)	10 (7.4)	0.03 (0.01, 0.05)	7 (7.3)	*	0.03 (0.01, 0.05)	*	*	0.01 (0.00, 0.02)
Angina	20 (14.7)	8 (5.9)	0.02 (0.01, 0.05)	12 (12.5)	11 (11.5)	0.04 (0.02, 0.08)	15 (11.5)	7 (5.3)	0.02 (0.01, 0.04)
CKD	13 (9.6)	18 (13.2)	0.05 (0.03, 0.08)	7 (7.3)	9 (9.4)	0.03 (0.02, 0.06)	10 (9.9)	13 (9.9)	0.04 (0.02, 0.07)
Heart Failure	9 (6.6)	16 (11.8)	0.05 (0.03, 0.07)	8 (8.3)	10 (10.4)	0.04 (0.02, 0.07)	11 (8.4)	7 (5.3)	0.02 (0.01, 0.04)
Hypothyroidism	8 (5.9)	7 (5.1)	0.02 (0.01, 0.04)	5 (5.2)	*	0.01 (0.00, 0.03)	11 (8.4)	5 (3.8)	0.01 (0.01, 0.03)
Giant cell arteritis	0	5 (3.7)	0.01 (0.00, 0.03)	0	0	-	0	*	0.01 (0.00, 0.02)

Table 16: Medical comorbidities among those with a hospital admission.

*Suppressed due to small numbers CI: confidence interval, CKD: chronic kidney disease, COPD: chronic obstructive pulmonary disease, PYAR: person-year at risk. COPD: Chronic obstructive pulmonary disease, CRAO: central retinal artery occlusion, BRAO: branch retinal artery occlusion, TMVL: transient monocular visual loss, CKD: chronic kidney disease, CEA: carotid endarterectomy. *fewer than 5 case

Ocular cranial palsies (OCP)

During the study period, a total of 506 individuals were newly diagnosed with CN3 (n=100), CN4 (n=146) and CN6 (n=270) palsies. Median age at presentation ranged from 63.2 (54.4-71.9) for CN4 palsy to 65.5 (56.5-74.5) for CN3 palsy and affected individuals were more likely male (range 60.7-73%, Table *17*). Individuals with an OCP had a higher risk of ischaemic stroke (HR 2.33, 95% CI: 1.10, 4.92, p=0.027) and death (HR 3.07, 95% CI: 2.08, 4.54, p<0.001) but not MI compared to propensity-matched controls (*Figure 27*, Table *18*).

		CN3 N = 100	CN4 N = 136	CN6 N = 270
Sex **n (%)**	**Female**	27 (27)	45 (33.1)	106 (39.3)
	Male	73 (73)	91 (66.9)	164 (60.7)
Age **median (IQR)**	**Years**	65.5 (56.5-74.5)	63.2 (54.4-71.9)	65.0 (56.3-73.6)
Ethnicity **n (%)**	**Asian**	24 (24)	17 (12.5)	64 (23.7)
	Black	8 (8)	9 (6.6)	26 (9.6)
	Other	15 (15)	32 (23.5)	56 (20.7)
	White	46 (46)	67 (49.3)	107 (39.6)
	Unknown	7 (7)	11 (8.1)	17 (6.3)
Preceding MI N (%)		5 (5)	3 (2.2)	5 (1.9)
Preceding CVA N (%)		5 (5)	2 (1.5)	5 (1.9)
Mortality rate Per 1,000 PYAR (95% CI)		21.0 (6.5, 48.9)	4.0 (0.2, 17.6)	13.6 (5.9, 26.3)
Myocardial infarct - Incidence rate **Per 1,000 PYAR (95% CI)**		5.3 (0.3, 23.1)	4.0 (0.2, 17.8)	9.8 (3.5, 21.1)
Ischaemic stroke - Incidence rate - **Per 1,000 PYAR (95% CI)**		27.1 (9.7, 58.1)	12.3 (3.0, 31.8)	9.8 (3.5, 21.1)

Table 17: Baseline sociodemographic data of the cohort stratified by ophthalmic event.

CN3: 3rd cranial nerve palsy, CN4: 4th cranial nerve palsy, CN6: 6th cranial nerve palsy, CVA: ischaemic stroke, IQR = interquartile range, MI: myocardial infarction, PYAR: person-years at risk

Among 100 patients diagnosed with CN3, eleven patients died during the study period at a median of 858 (568-1,148) days following their event. Only one patient had an incident MI two years after the CN3 palsy (incidence rate 5.4, 95% CI: 0.3-23.6, per 1,000 PYAR). There were five cases of incident ischaemic stroke (incidence rate 27.1, 95% CI: 9.7-58.1 per 1,000 PYAR). Of the 100 patients, 76 had a hospital admission during the study period. There was no evidence that individuals diagnosed with CN3 palsy had an increased risk of ischaemic stroke compared to propensity-matched controls (Table *18*) and only weak evidence for increased mortality (HR: 2.89, 95% CI: 1.00, 8.33, p=0.049). Seven (9.2%) patients with CN3 palsies were ultimately diagnosed with myasthenia gravis and four (5.3%) were diagnosed with a cerebral aneurysm (Table *19*).

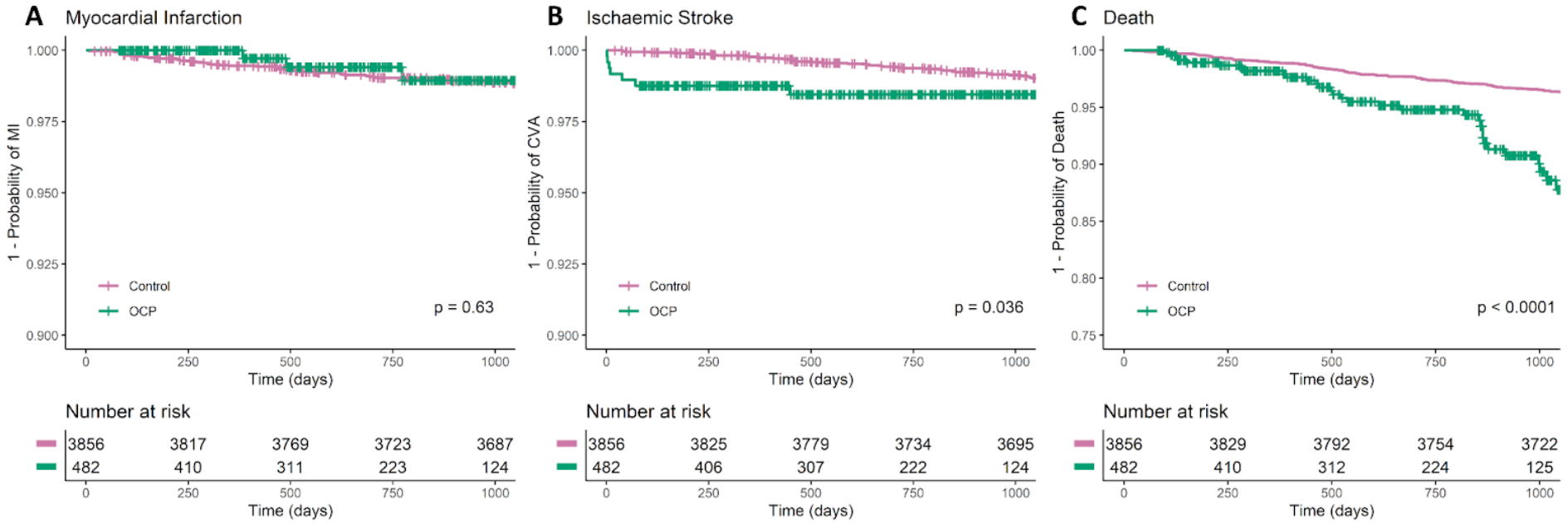

Figure 27: Kaplan-Meier curves for probability of myocardial infarction (A), ischaemic stroke (B) and death (C) for all ocular cranial nerve palsies.

P-values are derived from the log-rank test. OCP: ocular cranial nerve palsies.

Of 136 patients diagnosed with CN4, six died during the study period. One patient had an incident MI and three an incident ischaemic stroke. Individuals with a CN4 had increased risk of mortality (HR: 2.54, 95% CI: 1.03, 6.25, *p*=0.042) but not MI or ischaemic stroke compared to propensity-matched controls. After diagnosis with a CN4 palsy, eight individuals were newly diagnosed with atrial fibrillation during the study period equating to an incidence rate of 0.08 (95% CI: 0.04, 0.16) per person-year at risk (Table *19*).

Outcome	Myocardial infarct		Ischaemic stroke		Death	
	HR (95% CI)	***p*-value**	**HR (95% CI)**	***p*-value**	**HR (95% CI)**	***p*-value**
All OCP	0.75 (0.23, 2.47)	0.64	**2.33 (1.10, 4.92)**	**0.027**	**3.07 (2.08, 4.54)**	**<0.001**
CN3 palsy	*	*	1.93 (0.48, 7.78)	0.35	**2.52 (1.09, 5.80)**	**0.030**
CN4 palsy	*	*	2.56 (0.67, 9.69)	0.17	**2.54 (1.03, 6.25)**	**0.042**
CN6 palsy	1.26 (0.36, 4.36)	0.72	2.51 (0.76, 8.34)	0.13	**4.58 (2.77, 7.57)**	**<0.001**

Table 18: Adjusted hazard ratios estimated through Cox proportional hazards modelling for myocardial infarct, ischaemic stroke and death for CN3, CN4 and CN6 palsy.

*unstable model estimates due to small numbers of cases

CI: confidence interval, HR: hazard ratio

Among 270 patients who had CN6 palsy, five patients had an incident MI (median 468 [415-521] days) with an incidence rate of 9.8 (3.5, 21.1) per 1,000 PYAR. Similarly, five experienced an ischaemic stroke (386 [197.5-574.5] days). All MIs were greater than six months after the CN palsy whereas two strokes occurred within three months. Patients diagnosed with CN6 palsy had similar hazards of MI and incident stroke but significantly greater mortality risk (HR: 5.32, 95% CI: 2.93, 9.68, $p<0.001$). Patients with CN6 palsy had an incidence rate of 0.05 (95% CI: 0.03, 0.08) per PYAR of chronic kidney disease (CKD).

Comorbidity	CN3 (n=76)			CN4 (n=59)			CN6 (n=143)		
	Prevalent n (%)	Incident n (%)	Incidence rate PYAR (95% CI)	Prevalent n (%)	Incident n (%)	Incidence rate PYAR (95% CI)	Prevalent n (%)	Incident n (%)	Incidence rate PYAR (95% CI)
Hypertension	48 (63.2)	14 (18.4)	0.54 (0.30, 0.87)	31 (52.5)	11 (18.6)	0.23 (0.12, 0.39)	82 (57.3)	33 (23.1)	0.37 (0.26, 0.51)
Diabetes Mellitus	31 (40.8)	6 (7.9)	0.09 (0.03, 0.17)	17 (28.8)	6 (10.2)	0.09 (0.04, 0.18)	63 (44.1)	13 (9.1)	0.09 (0.05, 0.15)
Hypercholesterolemia	30 (39.5)	9 (11.8)	0.13 (0.06, 0.23)	23 (39.0)	4 (6.8)	0.07 (0.02, 0.15)	56 (39.2)	20 (14.0)	0.13 (0.08, 0.19)
Atrial Fibrillation	8 (10.5)	4 (5.3)	0.03 (0.01, 0.08)	*	8 (13.6)	0.08 (0.04, 0.16)	7 (4.9)	6 (4.2)	0.02 (0.01, 0.05)
Asthma	9 (11.8)	0	-	5 (8.5)	*	*	11 (7.7)	12 (8.4)	0.05 (0.03, 0.08)
COPD	5 (6.6)	0	-	4 (6.8)	*	*	*	4 (2.8)	0.01 (0.00, 0.03)
Angina	10 (13.2)	3 (3.9)	0.03 (0.01, 0.07)	8 (13.6)	0	*	16 (11.2)	*	*
CKD	10 (13.2)	4 (5.3)	0.03 (0.01, 0.08)	*	3 (5.1)	0.03 (0.01, 0.08)	13 (9.1)	13 (9.1)	0.05 (0.03, 0.08)
Heart Failure	5 (6.6)	3 (3.9)	0.02 (0.01, 0.06)	*	*	*	*	9 (6.3)	0.03 (0.02, 0.06)
Hypothyroidism	4 (5.3)	*	*	3 (5.1)	*	*	13 (9.1)	3 (2.1)	0.01 (0.00, 0.03)
Myasthenia Gravis	0	7 (9.2)	0.05 (0.02, 0.10)	*	*	*	0	4 (2.8)	0.01 (0.00, 0.03)
Giant cell arteritis	0	0	-	0	0	0	0	0	-
Cerebral aneurysm	0	4 (5.3)	0.03 (0.01, 0.07)	0	0	0	0	0	-

Table 19: Medical comorbidities among those with a hospital admission

*Suppressed due to small numbers. CI: confidence interval, CKD: chronic kidney disease, CN3: cranial nerve III palsy, CN4: cranial nerve IV palsy, CN6: cranial nerve VI palsy, COPD: chronic obstructive pulmonary disease, PYAR: person-year at risk.

Non-arteritic anterior ischaemic optic neuropathy

Between August 1st 2014 and March 31st 2018, a total of 231 patients received a diagnosis of NAION. The median age of 63.1 (54.6-71.7) years and 149 (64.5%) were male. Summary sociodemographic characteristics are shown in Table *20*.

Among the cohort, sixteen died during the study period at a median of 681 (352-1,010) days following their episode of NAION with a mortality rate of 37.2 (95% CI: 21.8-58.5) per 1,000 PYAR. The mortality rate was 37.2 (95% CI: 21.8-58.6) per 1,000 PYAR. Five patients had had an MI prior to the episode of NAION at a median of 1,455 (1,209-1,701) days prior. There was one incident case of myocardial infarction four months following NAION giving an incidence rate of 2.4 (95% CI: 0.1-10.3) per 1,000 PYAR. Four patients had a preceding ischaemic stroke prior to NAION with a median of 802 (136.7-1467.3) days while two patients had an incident ischaemic stroke at 468 (265-671) days following the NAION. The incidence rate for ischaemic stroke following an episode of NAION was 4.7 (95% CI: 0.8-14.6) per 1,000 PYAR. We examined the medical comorbidities among the 122 patients, who had a hospital admission during the study period. Over half of patients had a background of hypertension (77.0%) and hypercholesterolemia (51.6%) while 8.2% of patients had sleep apnoea and 11.5% gastro-oesophageal reflux disease. A breakdown of medical comorbidity can be seen in Table *21*.

Propensity score was used to match 888 controls from a potential cohort of 337,759 individuals to the 222 individuals with NAION (4:1 ratio, 9 excluded due to previous events). Adequate balance was achieved following matching with SMD of <=0.1. There was no difference in risk of MI (p=0.33) or ischaemic stroke (p=0.95) between

the control and NAION arms. However, mortality risk was significantly higher in those who experienced a NAION compared to controls (*Figure 28*, Log rank *p*=0.004) and, on Cox proportional modelling, hazards of death were 134% higher in those with NAION (adjusted HR 2.34, 95% CI 1.38, 3.97, *p*=0.002).

		NAION n=231	No admission n=109	Admission n=122
Sex n (%)	**Male**	149 (64.5%)	69	80 (65.6%)
Age median (IQR)	**Years**	63.1 (54.6-71.7)	58.0 (50.1-66.0)	66.0 (57.1-75.0)
Ethnicity n (%)	**Asian**	20	4	16
	Black	12	4	8
	Other	51	28	23
	White	138	67	71
	Unknown	10	6	4
SES median (IQR)	**Decile**	4.5 (5)	5(5)	5(5)

Table 20: Baseline sociodemographic data of the cohort of patients with NAION.

Patients were dichotomised into those who did not require a hospital admission and those in whom a subsequent hospital admission for comorbidity and adverse events was captured. NAION = non-arteritic ischaemic optic neuropathy, IQR = interquartile range, SES = socioeconomic status

		NAION (n=122)		
Comorbidity	**ICD-10 code**	**Prevalent n (%)**	**Incident n (%)**	**Incidence rate PYAR (95% CI)**
Hypertension	I10	75 (61.5)	19 (15.6)	0.28 (0.17, 0.42)
Diabetes Mellitus	E08, E09, E10, E11, E13	41 (33.6)	7 (5.7)	0.04 (0.02, 0.09)
Hypercholesterolemia	E78	53 (43.4)	10 (8.2)	0.08 (0.04, 0.14)
Atrial Fibrillation	I48	7 (5.7)	8 (6.6)	0.04 (0.02, 0.07)
Asthma	J45	10 (8.2)	*	0.01 (0.00, 0.03)
COPD	J44	7 (5.7)	5 (4.1)	0.02 (0.01, 0.05)
Angina	I20	15 (12.3)	*	0.00 (0.00, 0.02)
CKD	N18	11 (9.0)	8 (6.6)	0.04 (0.02, 0.07)
Heart Failure	I50	6 (4.9)	*	0.01 (0.00, 0.03)
Obstructive sleep apnea	G473	6 (4.9)	*	0.02 (0.01, 0.04)

Table 21: Medical comorbidities among those with a hospital admission.

*Suppressed due to small numbers CI: confidence interval, CKD: chronic kidney disease, COPD: chronic obstructive pulmonary disease, ICD: International Classification of Diseases, 10th revision, PYAR: person-year at risk. NAION: non-arteritic anterior ischaemic optic neuropathy. *fewer than 5 case

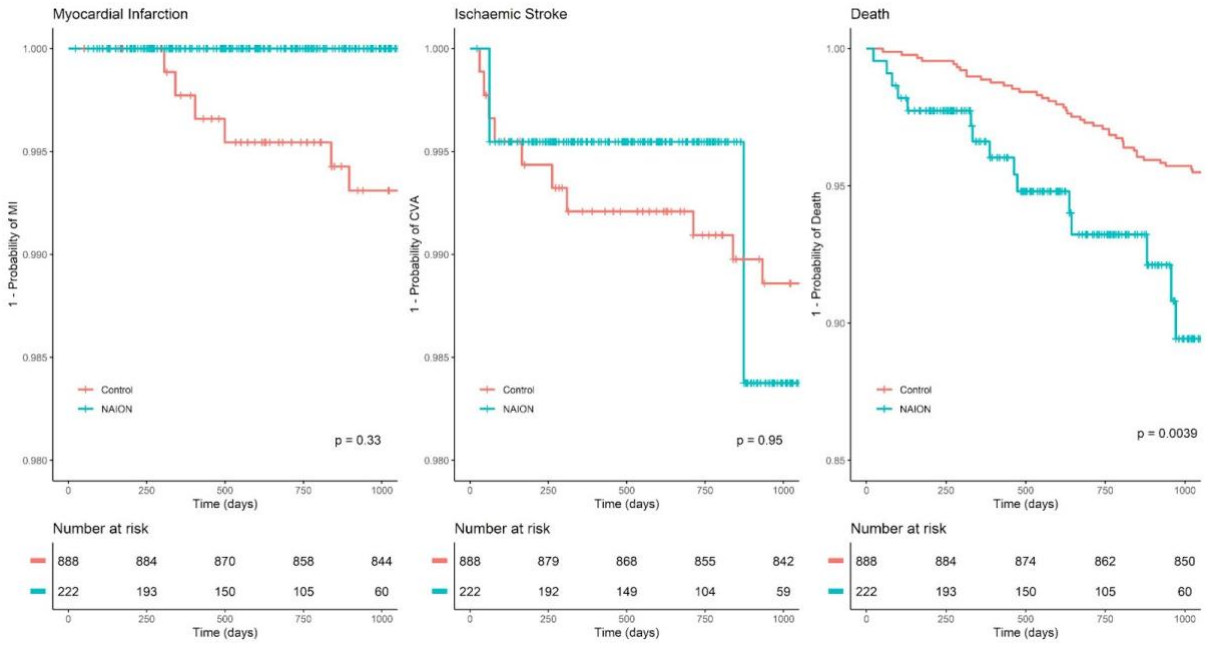

Figure 28: Kaplan-Meier curves for cardiovascular events and death between propensity-matched control and NAION arms.

P-values refer to the Log Rank test.

5.3.4 Discussion

In these propensity-matched cohort studies nested within AlzEye, I observed an increased risk of death in patients affected by OCP and NAION. Those with CRAO had an immediate escalation in stroke risk consistent with previous literature with nearly 4% of CRAOs ultimately receiving a diagnosis of giant cell arteritis. Those with OCP also had an increased risk of ischemic stroke compared to matched controls and 9% of patients with a CN3 were diagnosed with myasthenia gravis. Patients with NAION had similar cardiovascular event risk to controls but there was a demonstrable increase in all-cause mortality warranting further investigation.

Retinal artery occlusion

In this study, I found that individuals with a CRAO had 2.9 times the risk of ischaemic stroke compared to propensity-matched controls. An analysis of US Medicare beneficiaries showed that in the first and second weeks after CRAO, ischemic stroke incidence increased 28-fold and 33-fold, respectively, compared to a control group with hip fractures[284]. This is in line with a population based study from South Korea, where the authors discovered a nearly 22-fold increase in ischemic stroke after three days and a 70-fold rise during the first week following CRAO[285]. Importantly, in both these reports, comparison was made to a general control cohort, whereas my approach leveraged a propensity-matched design as I sought to estimate the marginal risk on cardiovascular event incidence beyond that conferred by sociodemographic (age, sex, ethnicity) and clinical (hypertension and diabetes mellitus) risk factors.

Of interest, those with BRAO were significantly more likely to have a CEA compared to those with CRAO. According to the NASCET study, patients with hemodynamically significant carotid stenosis that results in ipsilateral TMVL, cerebral hemisphere TIA, or mild stroke have a 25% 3-year risk of stroke[286]. Timing of surgery for CEA is paramount with both US and UK guidelines recommending CEA for at-risk patients within 14 days[287,288]. This explains the timely fashion of the surgery but does not explain why patients in our cohort with CRAO were less likely to be undergo the procedure than those with BRAO. While we cannot be certain as to the reason, it may be that patients with CRAO in our study had levels of stenosis exceeding recommended thresholds for CEA. It may as well be related to differential

etiologies such as giant cell arteries contributing to the overall number of patients with CRAO.

Both prevalent and incident AF were common among those with RAO and TMVL in my report – for example nearly 1 in 6 patients with BRAO had AF, and the AF incidence rate post CRAO was 0.06 per person-year at risk (i.e., equivalent to 6% of patients with a CRAO developing AF in the subsequent year). AF, as a source of cardioembolism, is an established risk factor for stroke. The Framingham Study showed a five-fold increase of stroke in patients with AF more than 30 years ago[289] however, uncertainty exists regarding the relationship between episodes of AF and acute stroke. While many consider AF a risk factor for stroke, others advocate that it merely represents left atrial dysfunction that raises the risk of stroke[290]. Moreover, individuals with paroxysmal AF also have higher rates of atherosclerosis. Variable AF prevalence was observed in recent investigations examining retinal ischemia, ranging from 4% to 16%[291–293]. Another study investigating patients suffering from CRAO with pre-existing implantable cardiac device found an incidence of AF in 33.4% of patients at one year following the CRAO and 49.6% at two years post CRAO, compared with 33.6% and 43.2% in patients with ischaemic stroke and 22.3% and 31.9% at two years in a control group with vascular comorbidities[294]. Atrial fibrillation should therefore be considered as risk factor of CRAO and indeed, in cases of cryptogenic CRAO, long-term cardiac monitoring over two to three years may be a prudent addition to the diagnostic process.

Ocular cranial palsies

Individuals with an OCP had 2.3 times the risk of ischaemic stroke compared to matched controls and significantly increased mortality. Examination of the Kaplan-Meier curves showed an immediate escalation in stroke incidence following the OCP diagnosis while the increase in mortality risk was more insidious. A recent meta-analysis of three studies, including 2,756 individuals with OCP and 21,239 matched controls, estimated a pooled HR of 5.96 of ischaemic stroke following the event. Why the estimated risk exceeds that in my report substantially is likely due to several reasons. Firstly, the three reports included within the meta-analysis all came from Taiwan and South Korea[295–297]. The epidemiology of ischaemic stroke and coronary heart disease is known to differ between European and East Asian countries owing to dietary habits, smoking rates, obesity epidemiology and other factors[298]. Secondly, affected patients in all three reports were generally much younger than in my report – for example, cases in the report by Hoi et al had an average age of 54.8 years, in contrast to my results where OCP patients were generally 10 years older. Sex distribution and hypertension and diabetes mellitus rates were generally similar to my report but it is likely that AlzEye is significantly more ethnically diverse. Thirdly, our control groups differ significantly. Controls in AlzEye are likely to have greater level of medical comorbidity as they represent a hospital-attending population while the other three reports use a national cohort design, some with a stratified random sampling approach. Nonetheless, our individual reports agree that there is an increased risk of ischaemic stroke following OCP.

My findings that 5.3% and 9.2% of patients presenting with a CN3 palsy ultimately received a diagnosis of intracerebral aneurysm and myasthenia gravis respectively

echoes previous work highlighting the incidence of non-microvascular causes for these palsies. Chou et al found 13.8% of neurologically isolated CN3 palsies to have non-microvascular causes[299]. Similarly, Tamhankar et al found 13.6% of CN3 palsies (n=22) in their prospective case series to have non-microvascular causes, such as giant cell arteritis and ischaemic stroke[266]. Other reports, however, have concluded that the prevalence of alternative causes is small, though this has usually been defined by those conditions requiring neurological imaging or restricted to CN4 palsies[300,301]. While my results align more with the former, note should be made of the differing inclusion and exclusion criteria. In the aforementioned reports, neurologically isolated CN palsy was usually defined through expert neurophthalmology grading, sometimes with ancillary investigations in a specialist service, while our case definition was based on the assessment of a general ophthalmologist in an emergency ophthalmic unit. Thus, my results are likely to be more representative of the acute presentation to an eye emergency service where the assessing clinician must resolve whether to undergo further investigations, such as imaging. This is the likely explanation for the prevalence of myasthenia gravis in my report. Given the well-known clinical presentation of myasthenia gravis with variable ptosis and diplopia and the complex presentation of a partial CN3 palsy, it is unsurprising that several reports have chronicled delayed diagnosis due to the masquerading of one condition by another[302–305]. My report highlights that for the general ophthalmologist faced with a suspected CN3 palsy, the probability of a non-microvascular origin is considerable. Myasthenia gravis does commonly involve ocular signs and symptoms, but third nerve palsy is not recognised as a common manifestation. It has been documented in case reports and increased awareness

may help to improve currently low diagnostic rates of myasthenia gravis, which can exhibit excellent prognosis when diagnosed early[303].

Non-arteritic anterior ischaemic optic neuropathy

Individuals with NAION had a 2.3 times greater risk of death than matched controls. There is limited evidence in the clinical literature to which I can compare my findings. Guyer et al described 22 deaths in their study of 200 patients with NAION reporting no significant increase in mortality risk compared to the general population[306]. Similarly, Hayreh et al. concluded that there was no evidence to support the fact that NAION patients were at greater risk of death compared to matched controls[278] in their series of 406 patients. It should be noted that these papers were all published over two decades ago making comparison challenging. Moreover, the sociodemographic profile of these cohorts and healthcare setting (both based in the US with no universal healthcare system) differ markedly to that of AlzEye.

Despite the widespread prevalence of vascular risk factors among NAION patients, I did not find an increased risk of MI or ischaemic stroke compared to propensity-matched controls in our study. Findings on the risk of cardiovascular events following NAION has thus far been conflicted – my findings align with Biousse et al who found that two-thirds of patients with NAION had at least one cardiovascular risk factor but no increased risk of cerebrovascular disease[307]. Similarly, no increased risk of cardiovascular or cerebrovascular events in NAION was found in a study published by Hasanreisoglu et al. in 2013[308]. In contrast, Guyer et al found an increased incidence of non-fatal MI and cerebrovascular events in NAION patients both without any identified prior risk factors and in those with systemic hypertension[306]. While

Hayreh et al. found that patients with arterial hypertension and diabetes, who had NAION, had a higher incidence of cerebrovascular events in their cohort compared to matched controls (age, sex and race), there was no significant increase in cerebrovascular events in the idiopathic, hypertensive or diabetic subgroups alone[278]. However, the numbers in the arterial hypertension and diabetes group were small (*n*=43) and one explanation could be residual confounding by diabetes severity.

5.3.5 Summary

In conclusion, my findings support prompt stroke assessment for those presenting with acute CRAO and OCP. For those with arterial occlusion, time to surgical intervention, in the form of carotid endarterectomy, is exceeding that recommended by national guidelines. Results for CN3 highlight that clinicians must be cognisant to masquerade conditions – one in 20 had an intracerebal aneurysm and 9% ultimately received a diagnosis of myasthenia gravis. Finally, in NAION, I did not observe an increased risk of MI or stroke compared to propensity-matched controls however affected patients have a clear increased risk of death which requires further investigation.

6. Discovery

In this chapter, I first discuss my choice of systemic conditions as exemplars for investigating ophthalmic imaging to explore retinal signatures of systemic diseases. I then describe the rationale and findings for each disease. Some of these analyses are intended to confirm previously proposed associations but leverage the generous sample sizes afforded by AlzEye (e.g. schizophrenia). For others (e.g. Parkinson's disease and periodontitis), novel associations with biological plausibility are observed. In the final section, I demonstrate that retinal imaging can also inform our understanding into the biology of disease and its potential mechanisms (amblyopia).

6.1 Oculomic exemplars

The four systemic conditions assessed in this Chapter were chosen based on their public health importance, relationship with cardiometabolic dysfunction and/or neurodegenerative disease, and their representation in AlzEye and UK Biobank.

Attention is first paid to schizophrenia, a neuropsychiatric condition affecting 1 in 300 people worldwide[309]. Increasingly recognised as a multisystemic disorder, individuals with schizophrenia exhibit metabolic dysfunction prior to the first episode of psychosis[310], die fifteen years earlier than the general population owing predominantly to cardiovascular disease[311], and have increased risk of dementia[312]. Several features from retinal imaging have been observed in schizophrenia however findings have been inconsistent and have been limited by small sample sizes and a lack of multimodal imaging.

Parkinson's disease is the fastest growing neurological disorder in the world[313]. Dopaminergic degeneration, the neuropathological hallmark of the disease, has also been identified in the retina in cadaveric studies[314] however this has not been reliably detected with in vivo imaging. Retinal markers that indicate or even anticipate Parkinson's disease would be valuable in advancing care.

Periodontal diseases describe a group of disorders characterised by inflammation of the gums and bones surrounding the teeth. Between 20-50% of the global population is affected[315], and the most advanced form, severe periodontitis, is an independent risk factor for a range of systemic non-communicable diseases, including cardiovascular disease, metabolic syndrome and Alzheimer's dementia[316–319].

Periodontal data is scarce in AlzEye and therefore touchscreen questionnaire responses on oral health from the UK Biobank study were used.

Amblyopia, or lazy eye, is a common neurodevelopmental condition typically affecting one eye. Affecting 1-3% of children globally[320], amblyopia can ‘persist’ into adulthood. Previous work has shown that even the unaffected ‘normal’ eye in children with unilateral amblyopia exhibits differences to healthy eyes suggesting more generalised dysfunction[321,322] however systematic investigations into the retino-neural and retinovascular associations with amblyopia have been limited. Patterns of oculomic differences could inform our understanding of more widespread dysregulation in adults with childhood amblyopia.

6.2 Schizophrenia

6.2.1 Introduction

Schizophrenia is a chronic heterogenous neuropsychiatric disorder with an estimated global prevalence of 23 million people in 2019[323]. It is increasingly recognised as a multisystemic disease[324] with bidirectional dysregulation. Features of endocrine dysfunction, such as impaired glucose tolerance, are present at the first episode of psychosis[310,325] and shared genetic mechanisms have been implicated in diabetes mellitus and psychosis[326]. Treatment with antipsychotics and unhealthy lifestyle practices contribute to a high prevalence of metabolic syndrome among individuals with schizophrenia[327]. Following diagnosis, affected individuals are also more likely to experience cardiovascular disease and premature cognitive decline[312,328,329] with some researchers positing an association between schizophrenia and accelerated senescence[330].

Retinal changes have been observed in individuals with schizophrenia. Two recent meta-analyses concluded that there was evidence for thinner peripapillary retinal nerve fibre layer and macular ganglion cell and inner plexiform layer (mGC-IPL) and enlarged cup-to-disc ratio (CDR) but acknowledged an inconsistency in results and low statistical power[331,332]. For example, across six reports, significant mGC-IPL thinning was found in schizophrenia but only when evaluating right eyes. Optic cup volume is significantly larger in schizophrenia spectrum disorders (SSD), but cup-to-disc area ratio is similar to controls. Preliminary reports also indicate changes in the density of retinal microvasculature in schizophrenia[333–335]. However, most reports exclude participants with other systemic diseases, such as diabetes mellitus and hypertension (both of which impair retinal structure and function), yet these medical

comorbidities are highly prevalent in SSD, challenging the generalisability of any findings.

In this analysis drawing on the AlzEye cohort, I investigated associations between schizophrenia and retinal morphology using cross-sectional multimodal imaging. I hypothesised that individuals with schizophrenia would have enlarged CDR and reduced inner retinal thicknesses, above that which could be explained by the presence of hypertension and diabetes mellitus.

6.2.2 Methods

The primary objective was to assess whether prevalent schizophrenia was associated with a larger CDR and thinner mGC-IPL and RNFL compared to controls. I additionally investigated whether retinal vascular morphology differed in those with schizophrenia.

Variables

The dependent variables were retinal morphological features derived from macula-centred colour fundus photography (CFP) and optical coherence tomography (OCT). Retinal vascular morphometric characteristics, including fractal dimension were extracted from 45-degree CFPs using two deep learning-based tools - the Vessel Assessment and Measurement Platform for Images of the REtina (VAMPIRE) and AutoMorph[75,193]. For retinal sublayers, I only examined mGC-IPL and RNFL, defined according to the International Nomenclature for OCT panel[336]. Thicknesses were estimated using the Topcon Advanced Boundary Segmentation Tool (TABS, version 1.6.2.6), a software leveraging dual-scale gradient information for automated

segmentation of retinal sublayers [185]. All retinal images were acquired using Topcon (Topcon Corporation, Tokyo, Japan) devices. Across the study period, five different Topcon devices were used but approximately 80% were collected on a single device, distribution of devices among cases and controls was similar and the same software version of TABS was used on all images (Table *22*). Images from both eyes, where available, were used.

Imaging device	Schizophrenia (*n*=485)	No schizophrenia (*n*=100, 931)	*p*-value
1000-MK2	12 (2.5)	2,285 (2.3)	0.233
3DOCT-2000	7 (1.4)	867 (0.9)	
3DOCT-2000SA	380 (78.4)	81,676 (80.9)	
FD_OCT	82(16.9)	15,422 (15.3)	
Triton plus	4 (1)	699 (0.7)	

Table 22: Distribution of retinal imaging devices for individuals with and without schizophrenia.

The primary exposure was schizophrenia, defined as an HES episode with ICD code F20. HES-based diagnostic codes for schizophrenia in the UK have previously been validated and demonstrated 90% agreement when compared to a psychiatrist-based hierarchical lifetime diagnosis using longitudinal psychopathology and diagnostic information from individual health records in London, UK[182]. I used the most recent HES admission codes for defining whether an individual had schizophrenia as this demonstrated a positive predictive value of 91%. For image selection, I then chose the earliest “good” or “usable” quality image following a HES episode with a diagnostic code for schizophrenia to reduce the potential bias imparted by ophthalmic treatment (e.g. retinal laser). Further information on how image quality is categorised can be found in AutoMorph’s description[193]. Among those who had multiple images on that same date, I chose the image with the highest image quality score, as outputted by AutoMorph. Controls were individuals in the cohort similarly attending MEH and had received retinal imaging during the study period but who did not have an ICD code of schizophrenia (further details available in our previous report[165]). Secondary exposure variables were age, sex, hypertension (ICD: I10, I15), diabetes mellitus (ICD: E10, E11) and socioeconomic status (SES). SES was

estimated using the index of multiple deprivation (IMD), a composite score linked to postcode covering income, employment, education, health, and barriers to housing and services, crime and living environment[337]. Given some previous evidence of similar retinal findings in mood disorders, I excluded individuals with ICD codes for bipolar affective disorder (F30-F31), SSD (other than schizophrenia, F21-F29) and unipolar depression (F32-F33) [182,338,339] .

Statistical analysis

Continuous variables were compared between groups using the Wilcoxon-Mann-Whitney test and categorical variables through the *U*-Statistic test[214]. I fitted linear mixed effects models using maximum likelihood estimation in line with the Advised Protocol for OCT Study Terminology and Elements (APOSTEL) recommendations[340]. These models included random effects on the intercept to account for the multilevel structure of eyes within individuals, and were adjusted for age, sex, diabetes mellitus, hypertension, socioeconomic status and image quality. Sex, diabetes mellitus and hypertension were coded as categorical variables for modelling. I adjusted for image quality as this has been found previously to be associated with certain retinal vascular features[98]. Degrees of freedom were estimated using Satterthwaite's approximation[215]. I performed two subgroup analyses. Firstly, given the high prevalence of diabetes mellitus among individuals with schizophrenia and its impact on retinal vasculature, and to mitigate the risk of residual confounding conferred by comparing individuals with mild diabetes mellitus to those with more severe disease or those who had received retinal laser treatment, I performed all analyses on a subgroup excluding individuals with diabetes mellitus. Secondly, to examine the association in younger individuals with schizophrenia, I

performed an additional analysis stratifying individuals in the cohort to those <55 and ≥55 years of age. Statistical significance was set at $p<0.05$. All analyses were conducted in R version 4.1.0 (R Core Team, 2021. R Foundation for Statistical Computing, Vienna, Austria) and used the `USP, lmer` and `lmerTest` packages[219,341,342].

6.2.3 Results

Of the initial sample of 154,830, 485 individuals (747 eyes) with schizophrenia and 100,931 individuals (165,400 eyes) without had macula-centred images deemed of sufficient image quality and met my inclusion criteria. Individuals with schizophrenia had a similar distribution of age and sex to those without the condition but were more likely to have hypertension (83.9% versus 48.0%, $p<0.001$), diabetes mellitus (75.1% versus 27.6%, $p<0.001$) and lived in areas of greater deprivation (Table *23*). On unadjusted analysis, individuals with schizophrenia had significantly reduced fractal dimension, vessel density, tortuosity density and increased arteriolar and venular calibre (all $p<0.001$). In addition, they had reduced mGC-IPL and RNFL thickness. The schizophrenia group had slightly larger CDR (0.47 ± 0.09 versus 0.46 ± 0.09, $p<0.001$) but a similar prevalence of glaucoma (Table *23*).

	Characteristic	Schizophrenia (*n*=485)	No schizophrenia (*n*=100, 931)	*p*-value[1]
Demographics	**Age (years)**	64.9 ± 12.2	65.9 ± 13.7	0.08
	Female sex (*n* (%))	258 (53.2)	53,253 (51.2)	0.37
	Socioeconomic status (1=most deprived)	4.1 ± 2.3	5.3 ± 2.6	**<0.001**
Comorbidity	**Hypertension (*n* (%))**	407 (83.9)	49,971 (48.0)	**<0.001**
	Diabetes mellitus (*n* (%))	364 (75.1)	28,762 (27.6)	**<0.001**
	Glaucoma (n (%))	38 (7.8)	7,602 (7.3)	0.71
	Age-related macular degeneration (n (%))	19 (3.9)	5,322 (5.3)	0.18
	Cataract (n (%))	123 (25.4)	20,383 (20.2)	**0.007**
CFP	**Image quality**	0.59 ± 0.34	0.51 ± 0.35	**<0.001**
	Cup-disc ratio[3]	0.47 ± 0.09	0.46 ± 0.09	**<0.001**
	Arteriolar calibre (μm)	65.1 ± 8.4	63.6 ± 8.0	**<0.001**
	Venular calibre (μm)	73.5 ± 10.1	72.0 ± 9.2	**<0.001**
	Fractal dimension	1.46 ± 0.06	1.47 ± 0.05	**<0.001**
	Fractal dimension (VAMPIRE)[4]	1.51 ± 0.03	1.52 ± 0.03	**<0.001**
	Vessel density	0.072 ± 0.013	0.073 ± 0.012	**0.027**
	Distance tortuosity	3.48 ± 1.3	3.41 ± 1.2	0.58
	Tortuosity density	0.71 ± 0.04	0.70 ± 0.04	**<0.001**
OCT	**RNFL (μm)**	26.6 ± 18.5	26.7 ± 13.4	**<0.001**
	mGC-IPL (μm)	77.4 ± 16.8	82.4 ± 16.1	**<0.001**

Table 23: Baseline and summary statistics for the cohort.

Results are shown at the level of the individual - those from retinal imaging represent the means of the two eyes. Except where indicated, all characteristic results are shown as mean ± standard deviation.[1] *p*-values were obtained using the Mann-Whitney-Wilcoxon test for continuous variables and the *U*-Statistic permutation test of independence for categorical variables. [2] Socioeconomic status was missing for no individuals with schizophrenia and 343 individuals without schizophrenia. [3] Optic nerve measurements were available for 450 individuals with schizophrenia and 93,045 without.

Adjusting for age, sex, SES and image quality, schizophrenia was associated with reduced mGC-IPL thickness, reduced fractal dimension, reduced vessel density, greater tortuosity density and enlarged CDR (Table *24*). There was no association between schizophrenia and RNFL. When additionally adjusting for hypertension and diabetes mellitus, there was no association between schizophrenia and retinovascular characteristics except VAMPIRE-based fractal dimension (-0.14, 95% CI: -0.22, -0.05], p=0.001). Individuals with schizophrenia maintained a larger CDR (0.01, [0.00, 0.02], p=0.041) and thinner mGC-IPL (-4.05 microns, 95% CI: -5.40, -2.69, $p=5.4 \times 10^{-9}$).

		Model 1[1]		Model 2[2]		Non-diabetic subgroup[3]	
Modality	**Characteristic**	**Regression coefficient**	***p*-value**	**Regression coefficient**	***p*-value**	**Regression coefficient**	***p*-value**
CFP	CDR (ratio)	0.01 (0.01, 0.02)	**6.0×10^{-4}**	0.01 (0.00, 0.02)	0.041	0.01 (0.00, 0.03)	0.08
	Arteriolar calibre (per SD)	0.11 (0.03, 0.19)	**0.010**	0.04 (-0.04, 0.12)	0.34	0.09 (-0.07, 0.25)	0.28
	Venular calibre (per SD)	0.08 (0.00, 0.16)	**0.048**	0.02 (-0.06, 0.10)	0.65	0.13 (-0.02, 0.29)	0.10
	Fractal dimension (per SD)	-0.17 (-0.24, -0.11)	**2.4×10^{-7}**	-0.05 (-0.11, 0.02)	0.14	-0.11 (-0.24, 0.02)	0.10
	Fractal dimension (VAMPIRE) (per SD)	-0.27 (-0.35, -0.19)	**1.1×10^{-10}**	-0.14 (-0.22, -0.05)	**0.001**	-0.05 (-0.21, 0.11)	0.56
	Vessel density (per SD)	-0.15 (-0.22, -0.09)	**1.3×10^{-7}**	-0.06 (-0.12, 0.01)	0.11	-0.09 (-0.23, 0.05)	0.21
	Distance tortuosity (per SD)	0.02 (-0.05, 0.09)	0.60	0.00 (-0.01, 0.15)	0.96	-0.04 (-0.21, 0.07)	0.55
	Tortuosity density (per SD)	0.12 (0.05, 0.20)	**0.002**	0.07 (-0.02, 0.14)	0.08	0.05 (-0.11, 0.20)	0.55
OCT	RNFL (µm)	-0.37 (-1.49, 0.75)	0.52	-0.29 (-1.41, 0.84)	0.61	-1.02 (-3.22, 1.18)	0.36
	mGC-IPL (µm)	-4.87 (-6.22, -3.51)	**2.1×10^{-12}**	-4.05 (-5.40, -2.69)	**5.4×10^{-9}**	-3.99 (-6.67, -1.30)	**0.004**

Table 24: Adjusted associations between prevalent schizophrenia and retinal oculomic biomarkers from colour fundus photography and optical coherence tomography.

[1]Adjusted for age, sex, socioeconomic status, and image quality. [2]Adjusted for age, sex, socioeconomic status, diabetes mellitus, hypertension and image quality. [3]For AutoMorph and TABS, this was 121 individuals with schizophrenia and 75,627 without. For VAMPIRE, this was 104 (165 eyes) individuals with schizophrenia and 67,416 (111,915 eyes) controls. Adjustment is the same as for model 2 without diabetes mellitus. CDR: cup-disc ratio, CFP: colour fundus photography, mGC-IPL: macular ganglion cell-inner plexiform layer, OCT: optical coherence tomography, RNFL: retinal nerve fibre layer, SD: standard deviation.

mGCIPL		No schizophrenia		Schizophrenia	
		Regression coefficient (95% CI)	***p* value**	**Regression coefficient (95% CI)**	***p* value**
Age	Per decile	-2.54 (-2.62, -2.46)	**$<2.0 \times 10^{-16}$**	-3.20 (-4.40, -1.99)	**3.4×10^{-7}**
Sex	Female	**Reference**		**Reference**	
	Male	0.71 (0.52, 0.89)	**1.4×10^{-13}**	-0.88 (-3.77, 2.02)	0.56
Socioeconomic status	Per decile	0.22 (0.18, 0.26)	**$<2.0 \times 10^{-16}$**	-0.05 (-0.66, 0.56)	0.87
Hypertension	Absent	**Reference**		**Reference**	
	Present	-1.23 (-1.45, -1.00)	**$<2.0 \times 10^{-16}$**	4.14 (0.23, 8.03)	**0.039**
Diabetes mellitus	Absent	**Reference**		**Reference**	
	Present	-0.84 (-1.08, -0.60)	**2.9×10^{-12}**	-1.47 (-4.72, 1.78)	0.38
Image quality	Per SD increase	1.05 (0.97, 1.13)	**$<2.0 \times 10^{-16}$**	0.23 (-0.94, 1.40)	0.70

Table 25: Adjusted regression coefficients for secondary exposure variables stratified by those with schizophrenia versus those without schizophrenia.

CI: confidence interval, mGCIPL: macular ganglion cell-inner plexiform layer, SD: standard deviation

Increasing age was associated with thinner mGC-IPL in both the schizophrenia and control groups. In those with schizophrenia, mGC-IPL was 3.20 microns (95% CI: -4.40, -1.99, $p=3.4 \times 10^{-7}$) thinner while in those without schizophrenia, the mGC-IPL was 2.54 microns (95% CI: -2.62, -2.46, $p <2.0 \times 10^{-16}$, Table *25*) thinner per ten years of age. On adjusted analysis, I found no significant difference in RNFL between those with schizophrenia and those without.

Restricting the analysis to individuals without diabetes mellitus left a sample of 121 individuals (192 eyes) with schizophrenia and 73,574 controls (122,673 eyes, Table *26*). A strong association persisted between mGC-IPL and schizophrenia (-3.99 microns,

95% CI: -6.67, -1.30, *p*=0.004); the schizophrenia group no longer had enlarged CDR.

No retinovascular indices were associated with schizophrenia in this subgroup.

	Characteristic	Schizophrenia (*n*=121)	No schizophrenia (*n*=73,574)	*p*-value[1]
Demographics	**Age (years)**	66.6 +/- 12.9	64.5 +/- 12.0	0.09
	Female sex (*n* (%))	67 (55.4)	39,250 (53.3)	0.70
	Socioeconomic status (1=most deprived)	4.3 +/- 2.4	5.5 +/- 2.7	<0.001
Comorbidity	**Hypertension (*n* (%))**	94 (77.7)	24,754 (33.6)	<0.001
	Glaucoma (n (%))	10 (8.2)	5,416 (7.4)	0.87
	Age-related macular degeneration (n (%))	8 (6.6)	4,404 (6.0)	1
	Cataract (n (%))	31 (25.6)	13,034 (17.7)	0.033
CFP	**Image quality**	0.88 +/- 0.13	0.91 +/- 0.12	0.008
	Cup-disc ratio[2]	0.47 +/- 0.10	0.45 +/- 0.09	0.029
	Arteriolar calibre (µm)	64.3 +/- 8.5	63.2 +/- 8.0	0.13
	Venular calibre (µm)	73.7 +/- 9.9	71.4 +/- 9.1	0.009
	Fractal dimension	1.46 +/- 0.06	1.48 +/- 0.05	0.002
	Fractal dimension (VAMPIRE)[3]	1.51 +/- 0.04	1.52 +/- 0.03	0.16
	Vessel density	0.065 +/- 0.015	0.069 +/- 0.014	0.004
	Distance tortuosity	3.46 +/- 1.6	3.37 +/- 1.2	0.57
	Tortuosity density	0.70 +/- 0.04	0.70 +/- 0.03	0.07
OCT	**RNFL (µm)**	25.9 +/- 15.1	26.8 +/- 13.1	0.003
	mGC-IPL (µm)	77.9 +/- 20.9	83.3 +/- 16.0	<0.001

Table 26: Characteristics of the subgroup without diabetes mellitus.

[1] p-values were obtained using the Mann-Whitney-Wilcoxon test for continuous variables and the U-Statistic permutation test of independence for categorical variables. [2] Optic nerve measurements were available for 106 individuals with schizophrenia and 65,241 without. [3] Note that for VAMPIRE, data from 104 individuals with schizophrenia and 67,416 controls were available. CFP: color fundus photography, mGC-IPL: macular ganglion cell-inner plexiform layer, OCT: optical coherence tomography, RNFL: retinal nerve fibre layer.

I next stratified the cohort into those aged <55 and ≥55 years (Table *27*). Regardless of age, mGC-IPL was reduced in those with schizophrenia; however, the effect estimate was more extreme for older patients (younger group: -2.90 microns, 95% CI: -5.55, -0.24, p=0.033, older group: -4.43 microns, 95% CI: -6.00, -2.85, $p=3.6 \times 10^{-8}$, Table *28*). Reduced fractal dimension (VAMPIRE system) was seen in those with schizophrenia in both the older (-0.11 per SD increase, 95% CI: -0.20, -0.01, p=0.027) and younger (-0.23 per SD increase, 95% CI: -0.41, -0.04, p=0.016) subgroups.

	Characteristic	Schizophrenia (*n*=111)	No schizophrenia (*n*=24,847)	*p*-value[1]
Demographics	**Age (years)**	48.0 +/- 5.4	47.2 +/- 5.2	0.06
	Female sex (*n* (%))	44 (39.6)	10,842 (43.6)	0.43
	Socioeconomic status (1=most deprived)	4.0 +/- 2.3	4.9 +/- 2.6	<0.001
Comorbidity	**Hypertension (*n* (%))**	83 (74.8)	4,643 (18.7)	<0.001
	Diabetes mellitus (*n* (%))	84 (75.7)	4,183 (16.8)	<0.001
	Glaucoma (n (%))	*	*	0.85
	Age-related macular degeneration (n (%))	*	*	0.48
	Cataract (n (%))	12 (10.8)	1,885 (7.6)	0.26
CFP	**Image quality**	0.91 +/- 0.13	0.95 +/- 0.09	<0.001
	Cup-disc ratio[2]	0.48 +/- 0.07	0.45 +/- 0.08	<0.001
	Arteriolar calibre (µm)	66.0 +/- 10.1	63.6 +/- 7.7	0.006
	Venular calibre (µm)	73.2 +/- 12.5	70.1 +/- 8.4	0.013
	Fractal dimension	1.48 +/- 0.05	1.50 +/- 0.05	<0.001
	Fractal dimension (VAMPIRE)[3]	1.52 +/- 0.03	1.54 +/- 0.03	<0.001
	Vessel density	0.07 +/- 0.01	0.08 +/- 0.01	<0.001
	Distance tortuosity	3.23 +/- 1.0	3.07 +/- 0.9	0.11
	Tortuosity density	0.69 +/- 0.03	0.69 +/- 0.02	0.36
OCT	**RNFL (µm)**	27.5 +/- 25.5	26.6 +/- 11.5	0.022
	mGC-IPL (µm)	81.7 +/- 15.4	87.1 +/- 14.5	<0.001

Table 27: Characteristics of the young subgroup (<55 years of age).

[1] p-values were obtained using the Mann-Whitney-Wilcoxon test for continuous variables and the U-Statistic permutation test of independence for categorical variables. [2] Optic nerve measurements were available for 106 individuals with schizophrenia and 65,241 without. [3] Note that for VAMPIRE, data from 104 individuals with schizophrenia and 67,416 controls were available. *Raw values suppressed due to small numbers. CFP: colour fundus photography, mGC-IPL: macular ganglion cell-inner plexiform layer, OCT: optical coherence tomography, RNFL: retinal nerve fibre layer.

		Younger subgroup[1]		Older subgroup[2]	
Modality	**Characteristic**	**Regression coefficient**	***p*-value**	**Regression coefficient**	***p*-value**
CFP	**CDR (ratio)**	0.01 (0.00, 0.03)	0.19	0.01 (0.00, 0.02)	0.12
	Arteriolar calibre (per SD)	0.17 (0.00, 0.34)	**0.046**	0.01 (-0.09, 0.10)	0.87
	Venular calibre (per SD)	0.09 (-0.08, 0.25)	0.31	-0.01 (-0.10, 0.08)	0.89
	Fractal dimension (per SD)	0.14 (-0.01, 0.28)	0.06	-0.09 (-0.16, -0.01)	**0.025**
	Fractal dimension (VAMPIRE) (per SD)	-0.23 (-0.41, -0.04)	**0.016**	-0.11 (-0.20, -0.01)	**0.027**
	Vessel density (per SD)	0.08 (-0.07, 0.23)	0.28	-0.08 (-0.16, -0.01)	0.037
	Distance tortuosity (per SD)	-0.02 (-0.17, 0.13)	0.79	0.00 (-0.09, 0.08)	0.95
	Tortuosity density (per SD)	-0.01 (-0.26, 0.06)	0.23	0.11 (0.02, 0.20)	**0.017**
OCT	**RNFL (µm)**	-0.08 (-2.11, 1.96)	0.94	-0.48 (-1.82, 0.86)	0.48
	mGC-IPL (µm)	-2.90 (-5.55, -0.24)	**0.033**	-4.43 (-6.00, -2.85)	**3.6×10^{-8}**

Table 28: Adjusted associations between prevalent schizophrenia and retinal oculomic biomarkers from colour fundus photography and optical coherence tomography stratified by age.

Models were adjusted for age, sex, socioeconomic status, diabetes mellitus, hypertension and image quality.[1]For AutoMorph and TABS, this was 111 individuals (181 eyes) with schizophrenia and 24,847 (44,159) without. For VAMPIRE, this was 100 (166 eyes) with schizophrenia and 23,657 (41,984 eyes) controls. [2]For AutoMorph and TABS, this was 342 individuals (566 eyes) with schizophrenia and 66,761 (121,241 eyes) without. For VAMPIRE, this was 308 individuals (466 eyes) with schizophrenia and 67,760 (106,958 eyes) controls. CDR: cup-disc ratio, CFP: colour fundus photography, mGC-IPL: macular ganglion cell-inner plexiform layer, OCT: optical coherence tomography, RNFL: retinal nerve fibre layer, SD: standard deviation

6.2.4 Discussion

Among the AlzEye cohort of 101,416 individuals who had eye imaging of sufficient quality for analysis, people with schizophrenia had thinner mGC-IPL and slightly enlarged CDR compared to those without schizophrenia after adjustment for multiple demographic and medical factors, suggesting retinal neural atrophy. However, associations with retinovascular morphology could be explained by the increased prevalence of hypertension and diabetes mellitus among those with schizophrenia. My report is the largest to date to examine multimodal retinal oculomics in individuals with schizophrenia and supports evidence of heightened retinal neurodegeneration in this disease that accelerates with advanced age.

Retino-neural associations with schizophrenia

I report evidence of reduced thickness of the inner retinal layers, which would be consistent with a neurodegenerative process in schizophrenia. The effect size for mGC-IPL thickness was similar to what has been reported in the literature on Alzheimer's disease[139,343] and prominent even when people with diabetes mellitus were excluded. A link between schizophrenia and mGC-IPL has been proposed but with inconsistent evidence thus far. In a meta-analysis of seven studies comprising 453 participants, thinner mGC-IPL was associated with schizophrenia but only in right eyes[331]. In another meta-analysis of three studies comprising 169 participants with SSD, mGC-IPL thickness was reduced but significance was lost when excluding one published report and the overall quality of evidence was deemed to be very low[332].

There are several biologically plausible reasons for the thinner mGC-IPL I observed in schizophrenia. Firstly, mGC-IPL thinning may result from a central neurodegeneration which, through retrograde trans-synaptic degeneration (RTSD), manifests as inner retinal thinning, such as that found in multiple sclerosis, ischaemic stroke and chiasmal compression[4–6]. Some have advocated RTSD as the mechanism for inner retinal thinning in Alzheimer's disease and other forms of dementia, diseases which are more common in people with schizophrenia, however conclusive evidence for this in schizophrenia is lacking[312,344–346].My subgroup analysis showed a more modest reduction in mGC-IPL among younger individuals with schizophrenia compared to those older in the cohort corroborating evidence from other disciplines of accelerated neurodegeneration. Affected individuals have progressive grey and white matter volume loss, beyond that of healthy controls[347] and gene expression patterns suggest accelerated molecular ageing[348]. Even in the absence of confounding anti-psychotic therapy, individuals with schizophrenia show exaggerated cognitive decline[349]. Further evidence for a neurodegenerative phenomenon in schizophrenia comes from data on a different biomarker for neurodegeneration, neurofilaments, which were significantly increased in the blood of affected individuals[350,351]. Findings on retinoneural structure in those presenting with a first episode of psychosis have thus far been conflicting. While some have found no observable differences in retinal sublayer thicknesses[352], others have identified reductions in total retinal thickness and visual cortex grey matter volume in small samples[353]. Future work should assess the relationship between mGC-IPL thinning and other indices of accelerated ageing in schizophrenia, such as gene expression and blood neurofilament protein levels.

Alternatively, mGC-IPL thinning may result from bidirectional multisystemic associations with schizophrenia. Chronic psychosis is associated with a greater prevalence of systemic comorbidities, such as hypertension, which influence mGC-IPL thickness[354] and adjustment for medical comorbidities and age diminishes effect estimates between retinal thickness and schizophrenia[355]. Furthermore, schizophrenia has well-established epidemiological and genetic co-distribution with metabolic dysfunction[310,325,326] and there is increasing evidence that retinal thinning may pre-date overt diabetes mellitus[356,357]. In my sensitivity analysis, I excluded all patients with diabetes mellitus during the study period to mitigate this; however, it is conceivable that individuals within our population had early or undiagnosed metabolic syndrome. The finding that individuals with first-episode psychosis exhibit an initially accelerated but self-limiting decline in retinal thinning and brain grey matter has also led some to hypothesise a pharmacological aetiology for degeneration[358]. Finally, even certain health behaviours and lifecourse exposures, which may be more frequent in schizophrenia, are linked with reduced mGC-IPL. For example, alcohol misuse is highly prevalent among those with schizophrenia [359] and is known to lead to thinner mGC-IPL[15].

Retinovascular associations with schizophrenia

I noted an apparent association between schizophrenia and reduced fractal dimension, increased tortuosity and increased vascular calibre; however, these differences were mostly accounted for by diabetes mellitus and hypertension. Appaji and Rao also noted increased tortuosity and wider venules, but found increased retinal fractal dimension

and narrower arterioles[338,360,361]. The reasons likely relate to our contrasting study populations. While my cohort consisted of older patients (mean age 64.9 years) attending an ophthalmic hospital, Appaji et al studied younger participants (early 30s) in a community setting and excluded those with significant medical comorbidity. Retinal metrics are known to differ between those with chronic disease and those recovering from a first episode of psychosis[352]. Recent investigations using OCT angiography (OCTA), a newer modality providing visualisation of retinal vessel density and perfusion, highlight the complex relationship between disease duration and retinovascular indices. While several reports have shown reduced microvascular vessel density in schizophrenia[333,334,362], another has shown increased superficial vessel density in early-course patients[363] leading some to hypothesise that layer-specific changes may occur as disease progresses[335]. Further analyses should investigate the association between retinovascular and retinal layer changes. Incorporating longitudinal analyses would shed light on the temporal dynamics of retinovascular changes in psychosis.

A novel aspect of my work was the use of state-of-the-art retinal image analysis tools for fully automated extraction of retinovascular features in schizophrenia. I used two separate deep learning-based models - the VAMPIRE fractal dimension estimation module, based on a robustly validated U-Net segmentation algorithm developed by the Universities of Dundee and Edinburgh[364,365] and AutoMorph, an openly available fully automated pipeline for the extraction of retinal features[193]. Rejection rate based on image quality was similar to previous reports using retinal imaging[126,366]. Given the challenges in the agreement between different segmentation tools[75], I can have greater

confidence in my findings on retinal fractal dimension where results by two independent fully automated segmentation systems.

This study should be considered within the broader limitations of retrospective observational research. Firstly, there are likely confounders which I could not adjust due to a lack of data. For example, smoking is more prevalent among individuals with psychosis[367] and is known to affect retinal vasculature[368]. Secondly, my case definition of schizophrenia was based on ICD codes from hospital admissions data which may be prone to misclassification bias. However, my strategy for identifying individuals with schizophrenia was such that any misclassification bias would likely underestimate my effect measure[182]. Thirdly, the average age and prevalence of medical comorbidities, such as diabetes mellitus, of individuals with schizophrenia was relatively high in my study and as such my findings may not reflect the situation in younger patients without other systemic diseases presenting with a first episode of psychosis[333]. However, given the corroboration of my results with other studies where similar associations were found in younger groups and those with medical comorbidities excluded, the possibility of a unique sample effect seems unlikely.

6.2.5 Summary

In conclusion, I show that individuals with schizophrenia have both altered retinovascular indices and thinner mGC-IPL. While the former was accounted for by comorbid diabetes mellitus and hypertension, I found independent associations with thinner inner retinal features similar to those observed in other neurodegenerative

conditions, such as multiple sclerosis and Alzheimer's disease[369]. The absence of some of these findings in younger individuals presenting with a first episode of psychosis supports a neurodegenerative mechanism which could relate to a primary degenerative phenomenon or secondary to metabolic impairment. Longitudinal analyses, which incorporate multimodal imaging and ancillary investigations of neurodegeneration, such as the blood neurofilament protein concentration and gene expression, are needed to elucidate the developmental course of these changes[333,352]. Further investigations are warranted into whether oculomic biomarkers could help characterise disease course, predict treatment response or even risk-stratify those patients most at risk of developing cognitive decline, cardiovascular disease and other devastating sequelae of schizophrenia.

6.3 Parkinson's disease

6.3.1 Introduction

Parkinson's disease is a heterogenous progressive movement disorder characterised by a loss of nigrostriatal dopaminergic neurons.[370] Dopaminergic degeneration is detectable early with multimodal brain imaging, suggesting some striatal territories are affected decades before diagnosis.[371,372] Individuals with prodromal Parkinson's disease have increased nigral iron deposition on susceptibility magnetic resonance imaging (MRI) and accelerated dopaminergic dysfunction on serial dopamine transport (DAT) scanning.[373,374] However, brain imaging for diagnosis and disease monitoring in Parkinson's disease is limited as a scalable resource. DAT imaging is relatively costly, has modest availability, and requires intravenous contrast. MRI has shown promise for disease diagnosis and monitoring but has not yet been validated for these purposes.

Another attractive location for interrogation of dopaminergic pathology is the eye. Embryologically derived from the primitive forebrain, the retina provides a minimally invasive window into the central nervous system and can be imaged rapidly using modern high-resolution devices. The dopaminergic cells of the neurosensory retina are located in the inner plexiform (IPL) and inner nuclear layers (INL), where they mediate intercellular coupling between AII amacrine cells, horizontal cells and retinal ganglion cells (*Figure 32*).[136,375,376] Stimulated by the postmortem finding of reduced dopamine content in the retina of people with Parkinson's disease,[314] researchers have sought evidence of retinal changes on in vivo imaging techniques, most notably optical coherence tomography (OCT). These have revealed several potential morphological

differences associated with Parkinson's disease but with inconsistency between studies.[314,377] In a systematic review of ten studies including a total of 690 participants, Parkinson's disease was associated with reduced thickness of the macular ganglion cell-inner plexiform layer (GCIPL) and retinal nerve fibre layer (mRNFL). There was, however, a significant publication bias noted and some studies did not report key details, such as the age of controls.[378] The cell bodies of dopaminergic neurons sit at the border of INL and inner plexiform layer,[134] however the two studies reporting significant associations in a recent meta-analysis showed opposite directions of effect of Parkinson's disease with the INL.[379–381] Most studies also exclude individuals with other medical comorbidities but the natural history of Parkinson's disease may differ in individuals with other diseases, such as diabetes mellitus thus limiting the external validity of these findings to the wider patient group encountered by neurologists.[382]

In this report, I leveraged a bidirectional approach analysing retinal imaging data from individuals with Parkinson's disease both prior to and post diagnosis. My aims were firstly, to characterise inner retinal anatomy, as measured using OCT, in individuals with prevalent Parkinson's disease from a large ethnically diverse real-world population study (AlzEye); and secondly to test the utility of OCT-based measures as prognostic factors for the development of Parkinson's disease using the deeply phenotyped prospective UK Biobank (UKBB) cohort. I hypothesised that individuals with prevalent Parkinson's disease would exhibit thinner GCIPL, mRNFL and INL and that this difference would be associated with incident disease.

6.3.2 Methods

This cross-sectional analysis used data from the AlzEye and UKBB studies to explore retinal morphology in prevalent and incident Parkinson's disease respectively. AlzEye and UKBB have been described previously (section 4.1 The AlzEye project, section 4.2 UK Biobank).

Retinal imaging

Macula-centred OCT imaging was acquired from participants in both AlzEye and UKBB using Topcon imaging devices (Topcon Corporation, Tokyo, Japan). While the AlzEye study included imaging from five separate Topcon devices, UKBB exclusively used the 3D OCT-1000. In AlzEye, for those individuals who underwent imaging on more than one date during the study period, I chose images from the earliest date following a diagnosis of Parkinson's disease. Among those who had multiple images on that same date, I chose the image with the highest image quality score. All images covered a 6.0 mm × 6.0 mm^2 area and had 128 horizontal B scans and 512 A scans per B scan. Images from both eyes, where available, were used. In UKBB, I only included participants who had retinal imaging acquired at the initial assessment visit (baseline instance) as this corresponded to the same time as their touchscreen questionnaire response. mRNFL, GCIPL and INL thicknesses were estimated from OCT using the Topcon Advanced Boundary Segmentation Tool (TABS), a software providing automated segmentation of retinal sublayers using dual-scale gradients.[185] Given previous evidence of parafoveal spatially-relevant differences in Parkinson's disease and other neurodegenerative conditions, I investigated retinal sublayers for the four

parafoveal subfields, as defined by the Early Treatment for Diabetic Retinopathy Study (ETDRS), as well as averages for the four inner subfields.[200] The Topcon Advanced Boundary Segmentation Tool (TABS) provides automated segmentation of retinal sublayers using dual-scale gradients. TABS provides additional metadata for each image to establish scan quality based on segmentation error, movement artifact and poor quality. I used a quantile approach excluding the poorest 20% of images for the following metadata variables: quality, the minimum motion correlation, maximum motion delta, maximum motion factor and inner limiting membrane indicator. The motion indicators are based on the Pearson correlations and absolute differences between the thickness data of the entire retina and retinal nerve fiber layer from each set of consecutive B-scans. The lowest correlation and the highest absolute difference in a scan serve as the resulting indicator scores and identify blinks, eye motion artifacts, and segmentation failures. The inner limiting membrane indicator is a measure of the minimum localized edge strength around the inner limiting membrane boundary across the entire scan; this is useful for identifying blinks, scans that contain regions of severe signal fading, and segmentation errors.

Systemic and ocular disease variables

Parkinson's disease was defined using hospital admissions data from Hospital Episode Statistics (HES), a national repository of all hospital admissions in England under the provisions of the NHS (at least 97% of hospital admissions in England[144]). HES is coded using the 10th revision of the International Classification of Diseases (ICD-10).[145]

Parkinson's disease was defined as a HES episode with ICD-10 code G20. HES-based diagnostic codes for Parkinson's disease have recently been validated in a subset of 20,000 participants of UKBB and had a positive predictive value of 0.84 (95% CI: 0.68, 0.94).[383] For investigating retinal markers in prevalent Parkinson's disease, eligible cases were defined as images after the relevant ICD-10 code. Given previous evidence of reduced thickness of the GCIPL and mRNFL in dementia, I excluded individuals with ICD-10 codes for all-cause dementia (E512, F00, F01, F02, F03, F106, F107, G30, G310).[143] For defining incident Parkinson's disease in UKBB, I excluded those who self-reported having Parkinson's disease at their initial assessment visit when they had retinal imaging and then used the first hospital admission with an ICD-10 code indicating Parkinson's disease as the time of disease onset. I additionally excluded those who self-reported eye disease at the initial assessment visit. Secondary exposure variables included age, sex, ethnicity, hypertension (ICD: I10, I15) and diabetes mellitus (ICD: E10, E11). Ethnicity, as self-reported by participants, was aggregated into four groups as defined by the UK Census (Table *29*).[384] Glaucoma was defined as any patient attending the glaucoma clinic three or more times with ongoing follow-up as previously described.[165] Hypertension and diabetes mellitus were defined using HES diagnostic codes for the AlzEye analysis and through self-report at the initial assessment visit touchscreen questionnaire for UKBB. Further details regarding the Data Fields are in *Table 30.*

Ethnic Category	Ethnic Group
South Asian	Asian or Asian British
	Indian
	Pakistani
	Bangladeshi
	Any other Asian Background
Black	Black of Black British
	Caribbean
	African
	Any other Black Background
Other/Mixed	White and Black Caribbean
	Mixed
	White and Black African
	White and Asian
	Any other mixed background
	Chinese
	Other ethnic group
White	White
	British
	Irish
	Any other White Background

Table 29: Ethnic categories grouping for both AlzEye and UK Biobank, as per the UK Census categories.

Variable	UK Biobank Data Field	AlzEye Definition
Parkinson's disease (self report)	20002	NA
Parkinson's disease (Hospital admission)	41270	ICD-10: G20
Age	21003	NA
Sex	31	NA
Ethnicity	21000	NA
Presence of any eye disease	6148	NA
Hypertension	20002	ICD-10: I10, I15
Diabetes mellitus	20002	ICD-10: E10, E11

Table 30: Table of variables used as exposure variables.

Further information can be found at https://biobank.ndph.ox.ac.uk/showcase/.

Statistical analysis

Initial data distributions were analysed visually and statistically. Continuous variables were compared between groups using Student's *t* test and categorical variables through the *U*-Statistic permutation test of independence.[282] To examine the association between prevalent Parkinson's disease and retinal morphology, I fitted linear mixed effects models with a random intercept at the individual level to account for the

multilevel structure of eyes nested in participants. Models were fitted through maximum likelihood estimation and adjusted for age, sex, ethnicity group, diabetes mellitus and hypertension. To assess the risk of residual confounding (e.g. spuriously reduced retinal thickness due to individuals with Parkinson's disease having more advanced diabetic eye disease), I also performed a sensitivity analysis excluding all individuals with diabetes mellitus. Degrees of freedom were estimated using Satterthwaite's approximation.[215] Data on self-reported ethnicity were missing for 19.4% subjects in the AlzEye cohort. Given previous evidence on the determinants of missingness of self-reported demographic data in healthcare, I assumed ethnicity data was missing at random[385–387]. I therefore performed conditional multiple imputation with chained equations ten times with five iterations using multinomial logistic regression models on all exposure and outcome variables, in their raw form, and pooled adjusted regression coefficients using Rubin's rule.[216,388]

To examine the association between retinal morphology and incident Parkinson's disease, I estimated cause-specific adjusted hazard ratios (HR) fitting survival models including a gamma-distributed random effect on the intercept representing frailty at the individual level.[217,218] The at-risk period was defined from the time of retinal imaging acquisition (the UKBB initial assessment visit data) until the earliest of death, hospital admission with a Parkinson's disease diagnostic code or conclusion of the data refresh date for our UKBB application (1st December 2020). I conducted survival analysis using a complete-case approach given the small amount of missingness for ethnicity in UKBB after image quality control (<0.3% of total). Given that previous evidence has shown

HES-based codes for other neurodegenerative diseases can post-date their appearance in primary care, I additionally performed a sensitivity analysis excluding all incident cases within 24 months of retinal imaging.[151] Statistical significance was set at $p<0.05$. All analyses were conducted in R version 4.1.0 (R Core Team, 2021. R Foundation for Statistical Computing, Vienna, Austria) and used the `mice`, `survival` and `lmer` packages.[219–221]

Reporting is in line with the guidelines set by the Strengthening the Reporting of Observational Studies in Epidemiology (STROBE) and its extension, the REporting of studies Conducted using Observational Routinely-Collected health Data (RECORD) statements.[14,15]

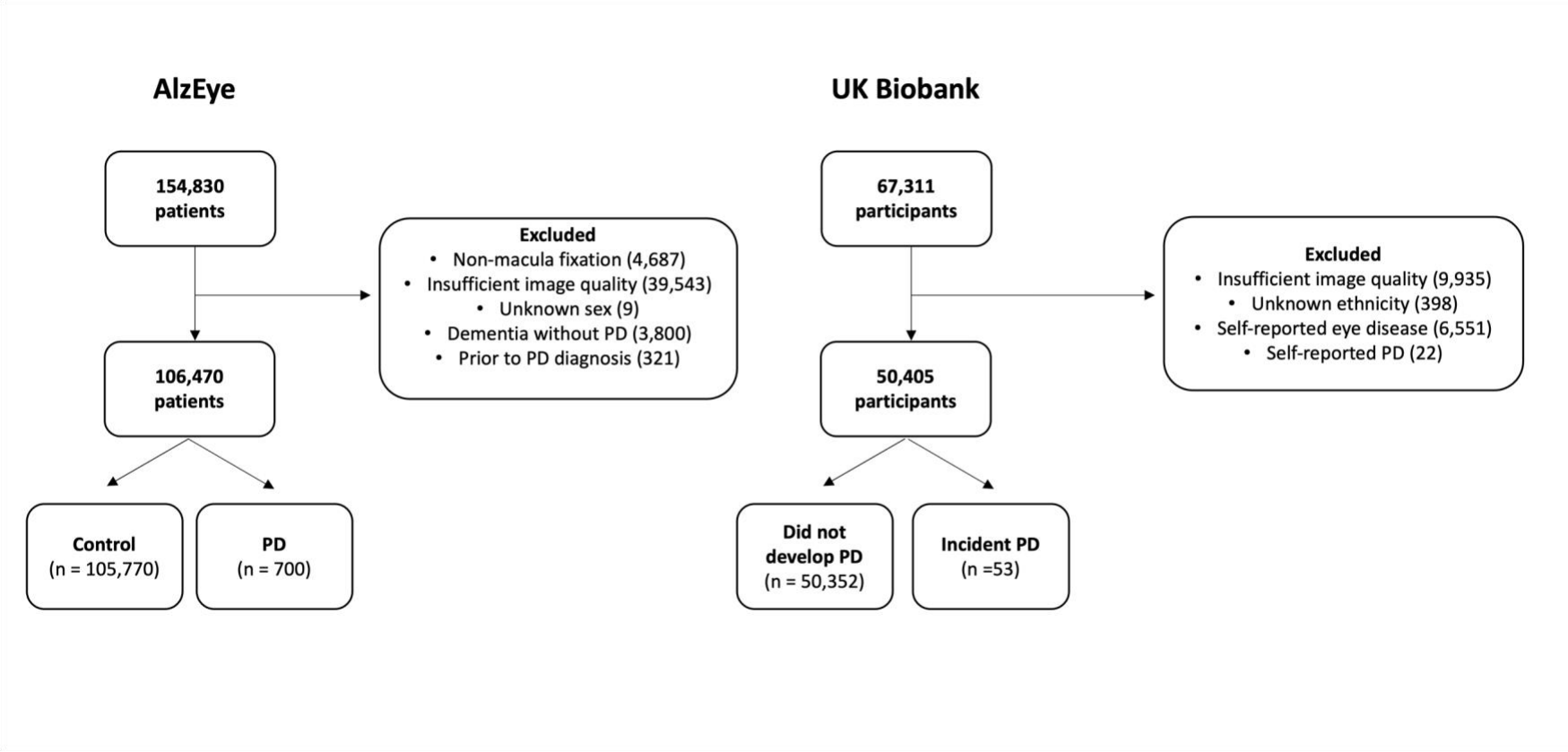

Figure 29: Flow chart detailing inclusion and exclusion of participants in both AlzEye and UK Biobank.

PD: Parkinson's disease.

6.3.3 Results

Retinal morphology in prevalent Parkinson's disease

From the AlzEye cohort of 154,830 with retinal imaging, there were 700 individuals (0.45%) who had prevalent Parkinson's disease and 105,770 controls (*Figure 29*). Those with Parkinson's disease were older, more likely to be male, hypertensive and have diabetes mellitus (Table *31*, all p <0.001). In unadjusted analysis, GCIPL and INL were significantly thinner across all parafoveal locations in patients with Parkinson's disease compared to controls (all p < 0.001, *Figure 30*). mRNFL was also thinner in individuals with Parkinson's disease in all regions except the nasal subfield.

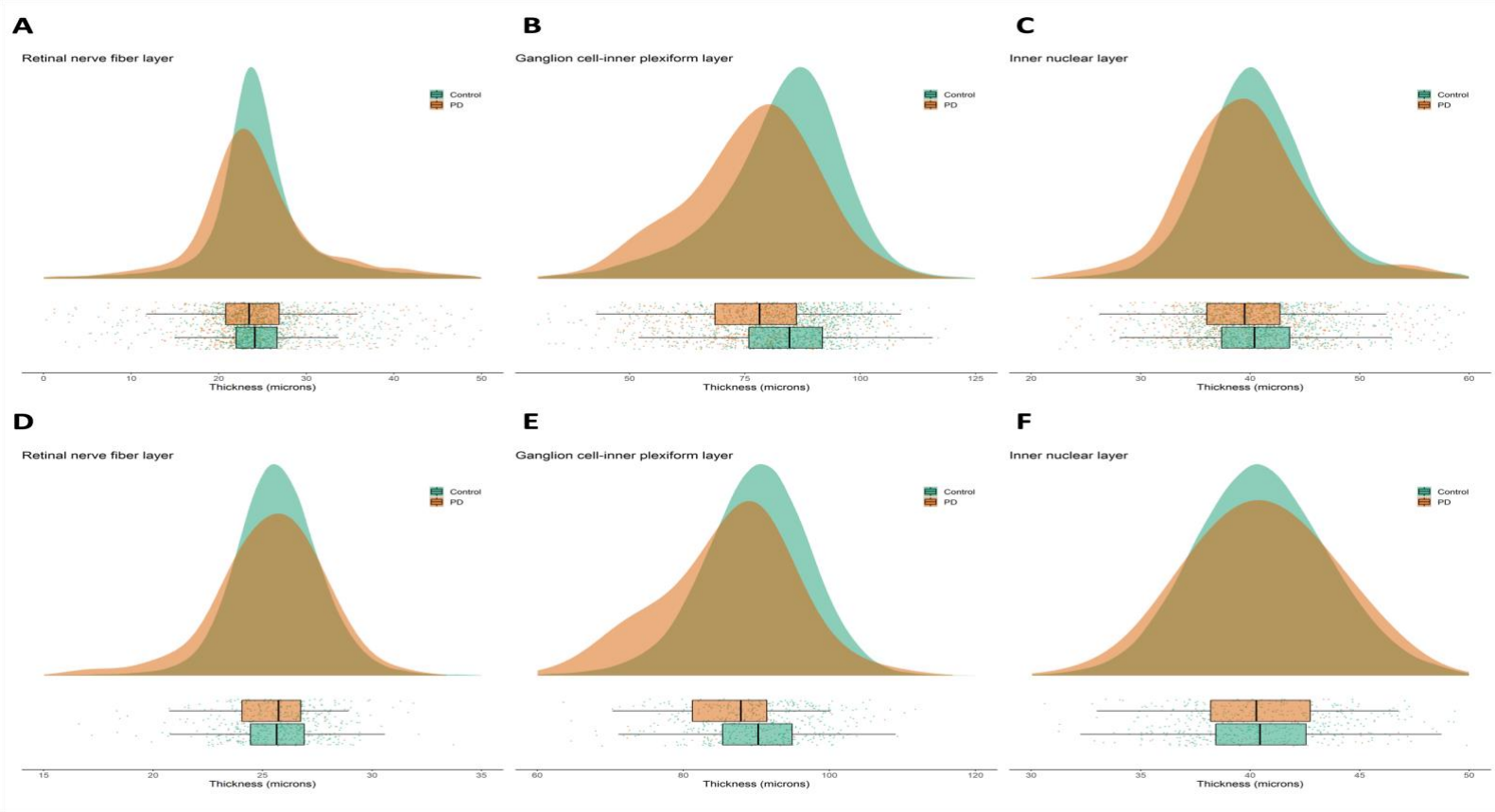

Figure 30: Distribution of retinal sublayer thicknesses in AlzEye and UK Biobank.

Raincloud plots consisting of a density, box-whisker, and scatter plots for AlzEye (A-C) and UK Biobank (D-F) for individual retinal sublayers. Scatter points represent the mean of both eyes (where available) per participant. To improve visibility, a random 2% of control participants are illustrated.

Characteristic		Parkinson's disease (*n*=700)	Controls (*n*=105,770)	*p*-value
Age (years)		77.5 +/- 8.0	65.4 +/- 13.5	**<0.001**
Women (*n* (%))		292 (41.7)	54,717 (51.7)	**<0.001**
Ethnicity (*n* (%))	**South Asian**	154 (22.0)	18,188 (17.2)	**0.026**
	Black	55 (7.9)	9,249 (8.7)	
	Other/Mixed	99 (14.1)	17,510 (16.6)	
	White	292 (41.7)	40,316 (38.1)	
	Unknown	100 (14.3)	20,507 (19.4)	
Hypertension (*n* (%))		558 (79.7)	53,010 (50.1)	**<0.001**
Diabetes mellitus (*n* (%))		356 (50.9)	31,365 (29.7)	**<0.001**
Glaucoma (n (%))		59 (8.4)	7,964 (7.5)	0.39
mRNFL (µm)	**All inner subfields**	24.7 +/- 8.0	25.4 +/- 8.4	**<0.001**
	Inner superior	26.6 +/- 9.8	27.0 +/- 9.5	**0.017**
	Inner nasal	25.0 +/- 9.3	25.2 +/- 10.0	0.21
	Inner temporal	19.9 +/- 8.0	21.0 +/- 8.7	**<0.001**
	Inner inferior	27.4 +/- 9.6	28.5 +/- 9.6	**<0.001**
GCIPL (µm)	**All inner subfields**	77.1 +/- 15.0	82.9 +/- 13.9	**<0.001**
	Inner superior	76.9 +/- 17.0	83.0 +/- 15.4	**<0.001**
	Inner nasal	78.0 +/- 16.0	84.0 +/- 15.1	**<0.001**
	Inner temporal	76.6 +/- 15.5	81.4 +/- 14.0	**<0.001**
	Inner inferior	76.9 +/- 16.9	83.3 +/- 15.3	**<0.001**
INL (µm)	**All inner subfields**	39.9 +/- 6.3	41.1 +/- 6.8	**<0.001**
	Inner superior	40.0 +/- 7.7	41.5 +/- 8.0	**<0.001**
	Inner nasal	41.0 +/- 7.0	42.1 +/- 7.8	**<0.001**
	Inner temporal	37.9 +/- 8.0	39.2 +/- 7.9	**<0.001**
	Inner inferior	40.5 +/- 7.7	41.8 +/- 7.9	**<0.001**

Table 31: Baseline characteristics of the AlzEye cohort by Parkinson's disease status.

Note that all results are at the level of the individual with the summary values for retinal imaging representing the means of the two eyes. Except where indicated, all characteristic results are shown as mean +/- standard deviation. INL: inner nuclear layer, GCIPL: macular ganglion cell-inner plexiform layer, mRNFL: macular retinal nerve fibre layer, SD: standard deviation.

Examination of those with missing ethnicity data showed that individuals, who chose not to self-report their ethnicity, were less likely to have Parkinson's disease. They were also younger and less likely to have hypertension, diabetes mellitus and glaucoma. (Table *32*).

Characteristic		Known ethnicity (*n* = 85,863)	Unknown ethnicity (*n* = 20,607)	*p*-value
Parkinson's disease (*n* (%))		600 (0.7)	100 (0.5)	**<0.001**
Age (years)		65.8 +/- 13.5	64.1 +/- 13.5	**<0.001**
Women (*n* (%))		44,470 (51.8)	10,539 (51.1)	0.10
Hypertension (*n* (%))		44,810 (52.2)	8,758 (42.5)	**<0.001**
Diabetes mellitus (*n* (%))		26,271 (30.6)	5,450 (26.4)	**<0.001**
Glaucoma (n (%))		7,363 (8.6)	660 (3.2)	**<0.001**
mRNFL (µm)	**All inner subfields**	25.5 +/- 8.5	25.0 +/- 7.6	**<0.001**
	Inner superior	27.1 +/- 9.6	26.5 +/- 8.8	**<0.001**
	Inner nasal	25.4 +/- 10.2	24.5 +/- 8.9	**<0.001**
	Inner temporal	21.1 +/- 8.8	20.7 +/- 7.8	**<0.001**
	Inner inferior	28.6 +/- 9.8	28.1 +/- 8.6	**<0.001**
GCIPL (µm)	**All inner subfields**	82.7 +/- 14.0	83.7 +/- 13.6	**<0.001**
	Inner superior	82.8 +/- 15.5	83.8 +/- 15.0	**<0.001**
	Inner nasal	83.7 +/- 15.2	84.7 +/- 14.7	**<0.001**
	Inner temporal	81.2 +/- 14.1	82.1 +/- 13.7	**<0.001**
	Inner inferior	83.0 +/- 15.4	84.2 +/- 14.8	**<0.001**
INL (µm)	**All inner subfields**	41.2 +/- 6.9	41.0 +/- 6.2	0.20
	Inner superior	41.5 +/- 8.1	41.3 +/- 7.3	1.0
	Inner nasal	42.1 +/- 7.9	41.9 +/- 7.1	0.12
	Inner temporal	39.2 +/- 8.0	39.0 +/- 7.2	0.61
	Inner inferior	41.8 +/- 8.1	41.6 +/- 7.2	0.84

Table 32: Summary characteristics of the AlzEye cohort stratified by those with missing ethnicity data.

INL: inner nuclear layer, GCIPL: macular ganglion cell-inner plexiform layer, mRNFL: macular retinal nerve fibre layer.

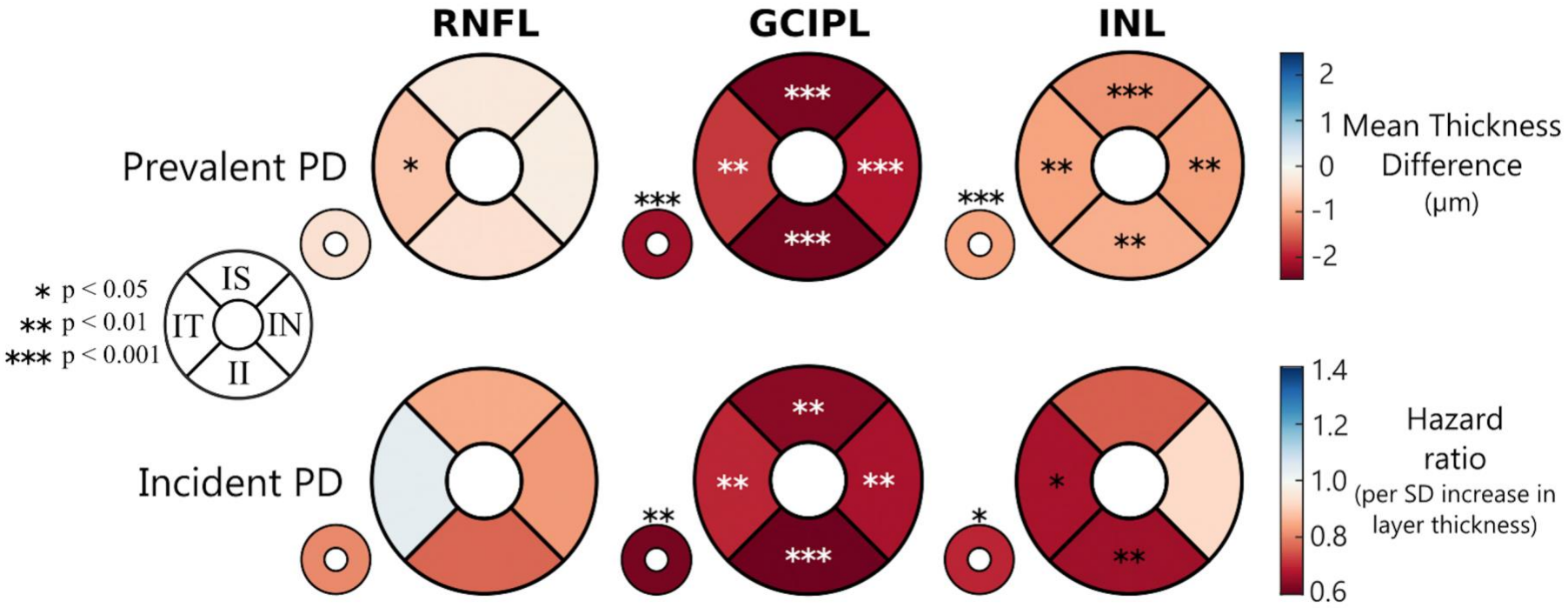

Figure 31: Summary of findings for prevalent and incident Parkinson's disease.

Values are shown per parafoveal region and for the average of all inner segments (small donut). The effect measure corresponds to a colour scale with warm colours indicating lower numbers.

II: inner inferior, IN: inner nasal, IS: inner superior, IT: inner temporal INL: inner nuclear layer, GCIPL: macular ganglion cell-inner plexiform layer, mRNFL: macular retinal nerve fibre layer.

After adjustment for age, sex, ethnicity, hypertension and diabetes mellitus, individuals with prevalent Parkinson's disease had significantly thinner GCIPL across all parafoveal subfields (all inner: -2.12 μm, 95% CI: -3.17, -1.07, $p = 8.2 \times 10^{-5}$). Thickness point estimates were most reduced in the inferior subfield (-2.38 μm, 95% CI: -3.54, -1.22, $p = 6.0 \times 10^{-5}$) and least reduced in the temporal subfield (-1.75 μm, 95% CI: -2.82, -0.68, $p = 0.001$). Individuals with Parkinson's disease also had significantly reduced thickness of the INL across all subfields (all inner: -0.99 μm, 95% CI: -1.52, -0.47, $p = 2.1 \times 10^{-4}$), most marked at the superior subfield (-1.09 μm, 95% CI: -1.70, -0.47, $p = 5.9 \times 10^{-4}$, *Figure 31*). There was limited evidence of reduced mRNFL thickness and prevalent Parkinson's disease with only a weak association seen for the inner temporal subfield (-0.69 μm, 95% CI: -1.37, -0.02, $p = 0.045$, Table *33*).

Exclusion of all individuals with diabetes mellitus left a cohort of 344 individuals with Parkinson's disease and 74,405 controls. Effect measures were slightly reduced but significant associations were still seen between Parkinson's disease and the thickness of both the GCIPL (all inner: -1.79 μm, 95% CI: -3.30, -0.27, $p = 0.020$) and INL (all inner: -0.85 μm, 95% CI: -1.58, -0.13, $p = 0.022$). There were no associations between mRNFL and prevalent Parkinson's disease in this restricted group (all inner: -0.36 μm, 95% CI: -1.30, 0.57, $p = 0.45$).

Prevalent Parkinson's disease		AlzEye – all		AlzEye – no diabetes mellitus	
Characteristic		Layer thickness difference (95% CI)	*p*-value	Layer thickness difference (95% CI)	*p*-value
mRNFL (µm)	**All subfields**	-0.39 (-1.04, 0.26)	0.24	-0.36 (-1.30, 0.57)	0.45
	Inner superior	-0.26 (-1.00, 0.47)	0.48	-0.36 (-1.41, 0.69)	0.50
	Inner nasal	-0.19 (-0.97, 0.59)	0.63	-0.02 (-1.16, 1.12)	0.97
	Inner temporal	-0.69 (-1.37, -0.02)	**0.045**	-0.78 (-1.73, 0.17)	0.11
	Inner inferior	-0.41 (-1.16, 0.34)	0.28	-0.26 (-1.33, 0.82)	0.64
GCIPL (µm)	**All subfields**	-2.12 (-3.17, -1.07)	**8.2×10^{-5}**	-1.79 (-3.30, -0.27)	**0.020**
	Inner superior	-2.36 (-3.52, -1.19)	**7.2×10^{-5}**	-2.07 (-3.73, -0.41)	**0.015**
	Inner nasal	-2.01 (-3.15, -0.87)	**5.6×10^{-4}**	-1.54 (-3.18, 0.09)	0.06
	Inner temporal	-1.75 (-2.82, -0.68)	**0.001**	-1.49 (-3.03, 0.04)	0.06
	Inner inferior	–2.38 (-3.54, -1.22)	**6.0×10^{-5}**	-1.90 (-3.56, -0.24)	**0.025**
INL (µm)	**All subfields**	-0.99 (-1.52, -0.47)	**2.1×10^{-4}**	-0.85 (-1.58, -0.13)	**0.022**
	Inner superior	-1.09 (-1.70, -0.47)	**5.9×10^{-4}**	-1.06 (-1.92, -0.21)	**0.015**
	Inner nasal	-1.00 (-1.61, -0.39)	**0.001**	-0.79 (-1.63, 0.05)	0.07
	Inner temporal	-0.99 (-1.60, -0.38)	**0.001**	-1.00 (-1.83, -0.16)	**0.019**
	Inner inferior	-0.89 (-1.51, -0.28)	**0.004**	-0.59 (-1.44, 0.26)	0.18

Table 33: Pooled adjusted regression coefficients estimated using linear mixed effects modelling retinal layer thickness against Parkinson's disease.

All models are adjusted for age, sex, ethnicity, diabetes mellitus and hypertension. CI: confidence interval, INL: inner nuclear layer, GCIPL: macular ganglion cell-inner plexiform layer, mRNFL: macular retinal nerve fibre layer

Retinal markers and incident Parkinson's disease

From 67,311 participants in UKBB who underwent extended ophthalmic assessment as part of their baseline visit, 50,405 individuals had images of sufficient quality for analysis and fit the inclusion criteria (*Figure 29*). The cohort had a mean age of 56.1 ± 8.2 years, 54.7% were women and people were predominantly of White self-reported ethnicity (91.4%). Fifty-three individuals developed Parkinson's disease during the study period (Table *34*).

Characteristic		UK Biobank (*n*= 50,405)
Age (years)		56.1 +/- 8.2
Female sex (*n* (%))		27,581 (54.7)
Ethnicity (*n* (%))	**South Asian**	1,412 (2.8)
	Black	1,500 (3.0)
	Other/Mixed	1,413 (2.8)
	White	46,084 (91.4)
Hypertension (*n* (%))		12,381 (24.6)
Diabetes mellitus (*n* (%))		1,933 (3.8)
Incident Parkinson's disease (*n* (%))		53 (0.1)

Table 34: Summary characteristics of the UK Biobank cohort following exclusion of insufficient quality images and confounding conditions.

Among those with incident Parkinson's disease, the average time between retinal imaging and clinical presentation was 2653 ± 851 days. On adjusted survival analysis, age and male sex were significantly associated with incident Parkinson's disease (Table *35*). Regarding retinal markers, reduced thickness of the GCIPL was associated with incident Parkinson's disease (HR = 0.62 95% CI: 0.46, 0.84 per SD increase, $p = 0.002$, *Figure 31*). There was also some evidence that thinner INL was associated with incident Parkinson's disease, especially at the inferior subfield (HR = 0.66, 95% CI: 0.51, 0.86, $p = 0.002$). The key findings of thinner GCIPL and INL being associated with greater likelihood of developing Parkinson's disease, persisted even when all those who developed Parkinson's disease in the first 24 months after having had retinal imaging were excluded (Table *36*).

Variable		Incident Parkinson's disease					
		mRNFL (all inner subfields)		GCIPL (all inner subfields)		INL (all inner subfields)	
		HR (95% CI)	*p*-value	HR (95% CI)	*p*-value	HR (95% CI)	*p*-value
Retinal sublayer	Per SD increase	0.81 (0.60, 1.11)	0.19	0.62 (0.46, 0.84)	0.002	0.70 (0.51, 0.96)	0.026
Age	Per decile	1.21 (1.15, 1.28)	4.6×10^{-13}	6.10 (3.62, 10.28)	1.2×10^{-11}	1.22 (1.15, 1.28)	1.7×10^{-13}
Sex	Female	Reference		Reference		Reference	
	Male	3.91 (2.11, 7.24)	1.5×10^{-5}	4.11 (2.21, 7.66)	8.4×10^{-6}	4.54 (2.39, 8.60)	3.5×10^{-6}
Ethnicity	Asian (South)	Reference		Reference		Reference	
	Black	2.74 (0.12, 62.90)	0.53	2.12 (0.09, 52.5)	0.65	3.26 (0.14, 76.77)	0.46
	White	1.45 (0.12, 18.15)	0.77	1.52 (0.11, 20.2)	0.75	1.48 (0.11, 19.28)	0.77
	Other/Mixed	0.98 (0.03, 32.57)	0.99	1.03 (0.11, 20.24)	0.99	1.01 (0.03, 35.25)	1.0
Diabetes mellitus	Absent	Reference		Reference		Reference	
	Present	1.15 (0.25, 5.28)	0.86	1.04 (0.22, 4.80)	0.96	1.08 (0.23, 4.99)	0.92
Hypertension	Absent	Reference		Reference		Reference	
	Present	0.77 (0.39, 1.54)	0.46	0.77 (0.38, 1.55)	0.46	0.76 (0.38, 1.52)	0.43

Table 35: Hazard ratios for all exposures variables derived from multivariable frailty models.

Models for average inner subfield thickness for the macular retinal nerve fibre, ganglion cell-inner plexiform and inner nuclear layers are shown.

GCIPL: ganglion cell-inner plexiform layer, HR: hazard ratio, INL: inner nuclear layer, mRNFL: macular retinal nerve fibre layer, SD: standard deviation

Incident Parkinson's disease		Unadjusted		Adjusted		Adjusted - late diagnosis	
		HR (95% CI)	*p* value	HR (95% CI)	*p*-value	HR (95% CI)	*p*-value
mRNFL (µm) (per SD increase)	All subfields	0.81 (0.62, 1.06)	0.13	0.81 (0.60, 1.11)	0.19	0.83 (0.61, 1.12)	0.23
	Inner superior	0.85 (0.65, 1.10)	0.21	0.85 (0.62, 1.15)	0.29	0.86 (0.63, 1.16)	0.32
	Inner nasal	0.87 (0.64, 1.18)	0.37	0.83 (0.58, 1.19)	0.31	0.85 (0.60, 1.20)	0.36
	Inner temporal	0.96 (0.74, 1.23)	0.73	1.04 (0.79, 1.35)	0.80	1.05 (0.80, 1.37)	0.73
	Inner inferior	0.79 (0.63, 1.00)	0.047	0.77 (0.60, 1.00)	0.05	0.78 (0.60, 1.01)	0.06
GCIPL (µm) (per SD increase)	All inner subfields	0.54 (0.42, 0.71)	8.0×10^{-6}	0.62 (0.46, 0.84)	0.002	0.64 (0.48, 0.87)	0.004
	Inner superior	0.57 (0.45, 0.74)	1.5×10^{-5}	0.64 (0.48, 0.85)	0.002	0.65 (0.49, 0.87)	0.004
	Inner nasal	0.54 (0.42, 0.71)	5.5×10^{-6}	0.67 (0.50, 0.90)	0.008	0.69 (0.52, 0.93)	0.014
	Inner temporal	0.66 (0.51, 0.87)	0.003	0.70 (0.51, 0.94)	0.019	0.73 (0.54, 0.98)	0.038
	Inner inferior	0.57 (0.45, 0.72)	2.7×10^{-6}	0.61 (0.47, 0.81)	4.9×10^{-4}	0.62 (0.47, 0.82)	7.6×10^{-4}
INL (µm) (per SD increase)	All subfields	0.85 (0.66, 1.11)	0.24	0.70 (0.51, 0.96)	0.026	0.70 (0.51, 0.97)	0.032
	Inner superior	0.88 (0.68, 1.14)	0.32	0.76 (0.56, 1.04)	0.08	0.76 (0.56, 1.04)	0.09
	Inner nasal	1.07 (0.82, 1.39)	0.62	0.92 (0.67, 1.26)	0.61	0.94 (0.67, 1.29)	0.70
	Inner temporal	0.80 (0.62, 1.05)	0.11	0.67 (0.49, 0.92)	0.013	0.67 (0.48, 0.92)	0.013
	Inner inferior	0.79 (0.63, 0.99)	0.037	0.66 (0.51, 0.86)	0.002	0.66 (0.50, 0.86)	0.002

Table 36: Hazard ratios derived from mixed effects Cox proportional hazards modelling time to diagnosis of Parkinson's disease against retinal layer thicknesses.

Adjusted models control for age, sex, ethnicity, diabetes mellitus and hypertension. Late diagnosis model excludes all individuals developing Parkinson's disease within 2 years of retinal imaging. CI: confidence interval, HR: hazard ratio, INL: inner nuclear layer, GCIPL: macular ganglion cell-inner plexiform layer, mRNFL: macular retinal nerve fibre layer

6.3.4 Discussion

In this cross-sectional analysis of the AlzEye and UKBB cohorts, I first confirm earlier reports that individuals with Parkinson's disease have significantly thinner GCIPL. Secondly, prevalent Parkinson's disease is also associated with thinner INL, which is a novel finding. This is relevant because the INL represents the hub of dopaminergic activity in the neurosensory retina. Thirdly, I found evidence that reduced thickness of the GCIPL and, to some extent, the INL is also associated with an increased chance of developing Parkinson's disease beyond that which is conferred by age, sex, ethnicity, hypertension and diabetes mellitus. Collectively, these findings strengthen the argument that neurodegenerative pathology in Parkinson's disease involves the GCIPL and INL and that these retinal layers may have prognostic clinical relevance.

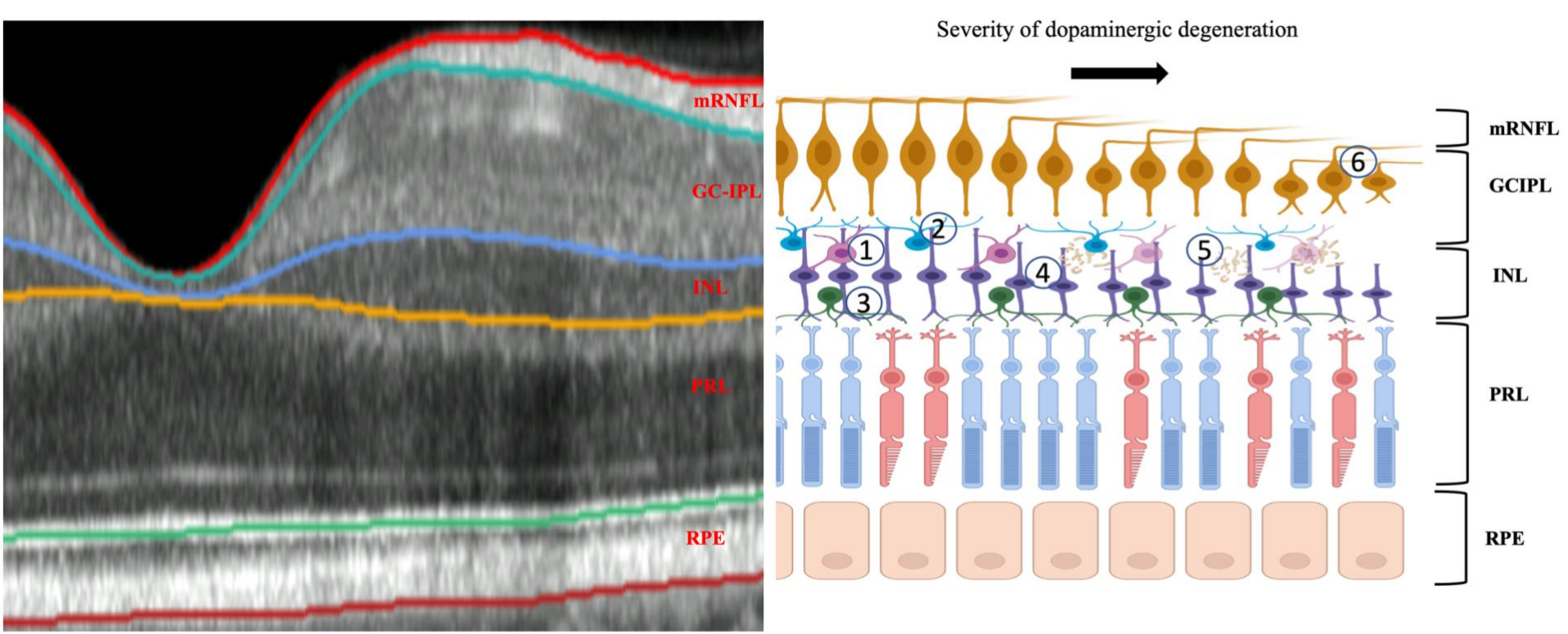

Figure 32: Illustration of cell type distribution in the retina. An example optical coherence tomography scan of the nasal macula adjacent to a schematic detailing interactions with dopaminergic amacrine cells.

Dopaminergic cells (1) have dense plexi positioned throughout the inner plexiform and inner nuclear layers. They are pre-synaptic to amacrine AII cells (2) and some dopaminergic processes project towards the photoreceptor layer where they interact with horizontal cells (3). They are postsynaptic to bipolar cells (4). Previous work has demonstrated aggregation of proteins, including α synuclein, within the inner nuclear layer (5), which could result in impairment of

nearby ganglion cells. INL: inner nuclear layer, GCIPL: macular ganglion cell-inner plexiform layer, PRL: photoreceptor layer, RPE: retinal pigment epithelium, RNFL: retinal nerve fibre layer

Prevalent Parkinson's disease and INL thickness

The INL acts as a barrier to propagation of retrograde trans-synaptic axonal degeneration (RTSD) from the brain to the eye. [389] The anatomical reason for this is the network function of the INL which involves horizontal connections of bipolar cells with amacrine and horizontal cells. Data on the preservation of INL thickness have been confirmed in the second of two large meta-analyses in multiple sclerosis (MS).[6,390] In contrast to the INL, there is atrophy of the peripapillary RNFL which is robust on repeat meta-analyses over two decades and different OCT devices. Therefore, the finding of reduced INL thickness in the present cohort is not only novel, but also permits formulation of a new hypothesis of retinal neurodegeneration in Parkinson's disease (*Figure 32*). Although the effect measure was modest (~ 1 µm), I found reduced INL thickness consistently across all parafoveal segments in prevalent Parkinson's disease and in the inferior and temporal subfields in incident Parkinson's disease. Studies thus far have likely been underpowered to detect this new effect. In a 2021 meta-analysis of a total of 387 participants across four reports, only two showed significant associations between INL thickness and prevalent Parkinson's disease but with opposite directions of effect.[378] While Schneider et al found a reduction in INL thickness (mean: 1.2 µm) when comparing 65 patients with Parkinson's disease against age and sex-matched controls,[391] Albrecht et al noted a mean increase of 4 µm.[380] Participants in the latter work were younger on average (61.2 $\pm$ 2.0 versus 66.2 $\pm$ 12) but both had similar disease duration and severity. Dopaminergic activity in the inner retina predominantly comes from the amacrine cells,[136] which interface with retinal ganglion and AII amacrine cells. Intracellular alpha-synuclein aggregates have been found in the INL[392] and individuals with Parkinson's disease have significantly reduced dopaminergic amacrine cells in the

retina on immunohistochemistry.[393] Inner retinal accumulation of toxic protein aggregates provide a plausible explanation for reduced INL thickness (*Figure 32*). On a molecular level, toxic protein aggregates lead to increase of free radicals and oxidative stress, mitochondrial damage, and dysfunction, Ca^{2+} influx all of which lead to energy deficiency and neurodegeneration. Thus, a biologically plausible explanation for my finding could be a primary inner retinal Parkinson's disease-related dopaminergic degeneration manifesting as INL thinning on OCT. This explanation reconciles my data on reduced INL thickness in Parkinson's disease with the general absence of INL atrophy in non-dopaminergic neurological disorders, where inner retinal change arises from RTSD.[390]

Prevalent Parkinson's disease and GCIPL thickness

I found individuals with Parkinson's disease had significantly thinner GCIPL, most prominent at the superior and inferior subfields and persisting when excluding all patients with diabetes. For context, my effect estimate (-2.12 μm) equates to approximately 14 years of age in a recent UKBB cohort analysis.[15] Across 690 participants in 10 studies, Huang et al found that people with Parkinson's disease had on average 3.17 μm (95% CI: -5.07, -1.26) thinner GCIPL compared to controls, with the inferior subfield exhibiting the greatest difference (-7.86 μm). GCIPL thinning has similarly been reported in Alzheimer's disease and following ischaemic stroke mediated through RTSD.[4,139] Even among neurologically healthy older individuals, a thinner GCIPL is associated with grey matter volume and brain atrophy.[394] Grey matter atrophy is found in patients with Parkinson's disease, but it is heterogenous and inconsistent,[395] possibly because grey matter atrophy represents neuronal cell death[396] which is a relatively late event in Parkinson's disease. Instead, animal

models suggest that axonal changes are likely to be earlier events[397] and this is supported by degeneration of white matter brain connections prior to cortical atrophy in Parkinson's disease.[398] In the retina, dopaminergic cell bodies are found at the border of the INL and inner plexiform layer, with axons projecting along the GCIPL. I can consider two potential mechanistic explanations for the reduced GCIPL thickness I have observed in Parkinson's disease. Firstly, cerebral neurodegeneration in Parkinson's disease may induce GCIPL thinning through RTSD given similar mechanisms seen in other neurodegenerative diseases. An alternative possibility is a local effect originating with dopaminergic dysfunction in the INL, or in situ axonal degeneration of the retinal ganglion cell. Although dopaminergic neurons represent <1% of all amacrine cells in the INL (density of 10-100/mm^2)[399], they reach their peak density in the parafoveal region in healthy primates (corresponding to the 1-3mm ETDRS area investigated in this report)[393]. Moreover, retinal dopaminergic dysfunction in humans with Parkinson's disease has previously been linked with death of adjacent cells, particularly ganglion cells. The dopaminergic amacrine cells couple to melanopsin-sensitive retinal ganglion cells in the GCIPL and immunohistochemistry shows that reduced dopaminergic plexi in individuals with Parkinson's disease are accompanied by abnormal retinal ganglion cell morphology.[393] Immunohistochemical staining for dopamine was almost absent from the INL in Parkinson's disease. Therefore, while the GCIPL and INL atrophy observed in the parafoveal region may predominantly involve other cell types, it is likely to be pathophysiologically related to dopaminergic cell death or dysfunction. Future studies are needed to determine whether progression of GCIPL atrophy in Parkinson's disease is driven by retrograde mechanism from the posterior thalamus

(e.g. lateral geniculate nucleus atrophy precedes GCIPL atrophy) or anterograde from the INL (INL thinning precedes GCIPL atrophy).

Incident Parkinson's disease and GCIPL thickness

In my report, thinner INL and GCIPL were also associated with a higher risk of developing Parkinson's disease. However, it should be noted that the effect sizes, especially for the INL, are small, so the practical value for an individual as a marker of early Parkinson's disease is currently limited. The association between retinal layer thicknesses and incident Parkinson's disease had not yet been explored; however, findings in early and prodromal Parkinson's disease do corroborate my results. Reduced thickness of the GCIPL has been described in individuals with drug-naive Parkinson's disease and is related to severity of disease.[400,401] Individuals with idiopathic rapid eye movement sleep behaviour disorder, a variant of prodromal Parkinson's disease where >70% of affected individuals may convert to a Lewy body disease,[402] have thinner ganglion cell complexes on OCT with the severity related to the degree of nigrostriatal dopaminergic degeneration.[403] Epidemiological patterns in other neurodegenerative diseases have also suggested inner retinal changes may occur early. In the Rotterdam Study, Mutlu et al found that individuals with thinner mRNFL on OCT had an increased risk of developing Alzheimer's dementia.[143] Another neurodegenerative explanation for the reduced inner retinal thickness observed could be glaucomatous optic neuropathy. The association between glaucoma and Parkinson's disease is conflicting and a recent meta-analysis concluded that glaucoma was not associated with an increased risk of Parkinson's disease [404]. In the AlzEye cohort, the prevalence of glaucoma was relatively similar in those with Parkinson's disease (8.4%) and controls (7.5%) despite the group with

Parkinson's disease being 12 years older on average. For the UKBB analysis, I excluded all individuals with previously diagnosed glaucoma, however, it is conceivable that individuals at risk of Parkinson's disease may have either undiagnosed and/or early-stage glaucoma. Ophthalmic deep phenotyping in for example, prodromal Parkinson's disease would help identify the interplay between development of glaucoma and progression to a synucleinopathy.

Limitations

Firstly, for my prevalent Parkinson's disease analysis, I did not have detailed clinical information about Parkinson's disease status, such as diagnosis date, treatment patterns or current therapy. I was therefore not able to relate retinal morphology to disease duration or severity, although retinal thicknesses have not been shown to differ between individuals with treated and untreated Parkinson's disease.[405] Secondly, my case definition of Parkinson's disease was based on ICD-10 codes rather than a Parkinson's disease-specific reference standard. ICD-10 codes from HES for Parkinson's disease have been validated in a subset of 20,000 UKBB participants and shown to have a positive predictive value of 0.84 (0.68-0.94).[383] A separate report at a large tertiary NHS hospital showed 27% of hospital admissions of individuals with Parkinson's disease did not have Parkinson's disease recorded (i.e. sensitivity of 0.73).[406] Thus, my effect sizes are likely to be biased towards the null as controls may in fact have Parkinson's disease. Finally, I do not have correlative OCT and retinal histology data on the proposed protein aggregation hypothesis in the INL. Such data will depend on tissue donation for research purposes by individuals with Parkinson's disease who have had in-vivo OCT, such as the UK Parkinson's disease Brain Bank.

6.3.5 Summary

In conclusion, my report demonstrates that individuals with Parkinson's disease have significantly thinner GCIPL and the INL. These differences appear early, being discernible several years prior to clinical presentation. It remains unclear whether such changes relate to the increased neurodegeneration found in the brains of individuals with Parkinson's disease and resulting RTSD or could represent a primary dopaminergic degeneration focused within the inner retina with anterior propagation of neurodegeneration. Further studies exploring the chronological sequence of retinal sublayer thickness would help elucidate the mechanism and determine whether retinal imaging could support the diagnosis, prognosis, and complex management of patients affected by Parkinson's disease.

6.4 Periodontitis

6.4.1 Introduction

Periodontal diseases, a group of chronic inflammatory conditions of the gums and bones surrounding the teeth, affect approximately 50% of adults worldwide[407]. Presenting initially with bleeding and swelling of the gums, gingivitis, if left untreated will progress from Stage I (mild) to Stage II (moderate), Stage III (severe) and ultimately Stage IV (very severe periodontitis), with associated tissue loss, including hidden epithelial micro-ulcers that facilitate entry of oral microorganisms into the systemic circulation and a corresponding surge in inflammatory mediators[408].

A substantial body of biochemical and epidemiological evidence suggests a link between periodontal disease, systemic inflammation and non-communicable diseases[409–412]. Periodontitis is associated with increased hazards of incident stroke (both ischaemic and haemorrhagic), myocardial infarction, cardiac arrhythmias [316–318] and dementia[319], consequences attributed to heightened chronic inflammation and periodontal bacteraemia. Individuals with periodontitis have elevated inflammatory biomarkers, such as C-reactive protein[413,414] and periodontal-linked pathogens have been identified in atheromatous plaques of the heart and brain[415–417] and levels of antibody against oral micro-organisms are strongly associated with carotid vascular disease[418]. Addressing periodontitis through treatments, such as subgingival root surface treatment and oral prophylaxis leads to reduced biochemical systemic inflammation and cardiovascular events[419–423].

Allowing direct visualization of the central nervous system and microvascular tissue, the retina represents an accessible *in vivo* model for characterizing neurodegenerative and cardiovascular disease risk. For example, thinner retinal

nerve fibre layer is associated with an increased risk of cognitive decline and Alzheimer's dementia[139,143,424] while wider retinal venules are found in those with cardiovascular disease and rheumatoid arthritis[425–427]. Given the systemic implications of periodontitis, it is credible that affected individuals have alterations in retinal structure consistent with chronic inflammation, cardiovascular dysfunction and neurodegeneration. Several epidemiological reports have also suggested an association between periodontitis and age-related macular degeneration (AMD)[428–432] and glaucoma[433,434], disorders intimately linked with systemic inflammation, but assessments of retinal morphology and the neurosensory retina are scarce. Increased retinal venular, but not arteriolar, calibre has been reported among those with periodontitis without diabetes mellitus[435]. Given that both retinal venular dilatation and periodontitis are associated with incident diabetes mellitus, retinal venular differences may simply indicate a predisposition to incipient metabolic syndrome[436–439]. To date, there has been no investigation of in-vivo imaging of the inner retina in periodontitis, despite the association between Alzheimer's dementia and glaucoma with periodontitis. In this report, I cross-sectionally analysed multimodal retinal imaging of participants in the UK Biobank cohort to assess whether retinovascular and inner retinal indices differed between those with very severe periodontitis and those without. I then investigated whether participants with very severe periodontitis within my cohort had a greater propensity towards several non-communicable diseases. I hypothesised that individuals with very severe periodontitis would exhibit retinal morphological features typically seen in chronic inflammation and neurodegeneration.

6.4.2 Methods

Data and Design

This cross-sectional analysis used data from the United Kingdom Biobank (UKBB), which has been described previously (section 4.2 UK Biobank). At the initial assessment, participants were asked about oral/dental problems experienced within the last year through touchscreen questionnaires. A subset of 67,311 UKBB participants attending six assessment centres additionally underwent a detailed ophthalmic assessment including retinal imaging with both colour fundus photography (CFP) and optical coherence tomography (OCT) at the initial visit[184,185].

Macula-centred CFP and OCT was acquired using the Topcon 3D-OCT 1000 device (Topcon Corporation, Tokyo, Japan). OCTs covered a 6.0 mm × 6.0 mm area and had 128 horizontal B scans and 512 A scans per B scan. Images from both eyes, where available, were used. Only participants who had completed the touchscreen questionnaire and undergone retinal imaging were included.

Outcome variables

The primary outcome measures were retinal vascular (arteriolar and venular) calibre derived from CFP, and macular retinal nerve fibre layer (mRNFL) and mGC-IPL thickness derived from OCT (*Figure 33*). Secondary outcome measures included retinal fractal dimension, retinal vascular distance tortuosity and optic nerve cup-disc ratio (CDR). Automated image analysis of CFPs was performed through the open-source fully-automated deep learning-based model, AutoMorph[193](section 4.3.1 Colour fundus photography). CDR was calculated as the ratio between vertical cup and disc sizes. OCTs were segmented using the Topcon Advanced Boundary

Segmentation Tool (TABS, version 1.6.2.6, section 4.3.2 Optical coherence tomography), a software leveraging dual-scale gradient information for automated segmentation of retinal sublayers[185]. mRNFL and mGC-IPL thickness were defined according to the lexicon proposed by the International Nomenclature for OCT panel[130]. Retinal sublayers for the four parafoveal subfields, as defined through the Early Treatment Diabetic Retinopathy Study[440], were averaged for analysis (*Figure 33*).

Occurrence of non-communicable disease was defined using the Admitted Patient Care hospital admissions data derived from Hospital Episode Statistics (HES), a repository of all hospital admissions in England under the provisions of the NHS (section 2.4 Hospital Episode Statistics[144]). I used UKBB HES data, which was coded using the 10th revision of the International Classification of Diseases (ICD-10)[145]. All-cause dementia was defined as codes E512, F00, F01, F02, F03, F106, F107, G30, G310[151]; major adverse cardiovascular events (MACE) as I20-I25, I60-I64, I50, I70-I74[441,442]; and diabetes mellitus as codes E10, E11, E13, E14[443];

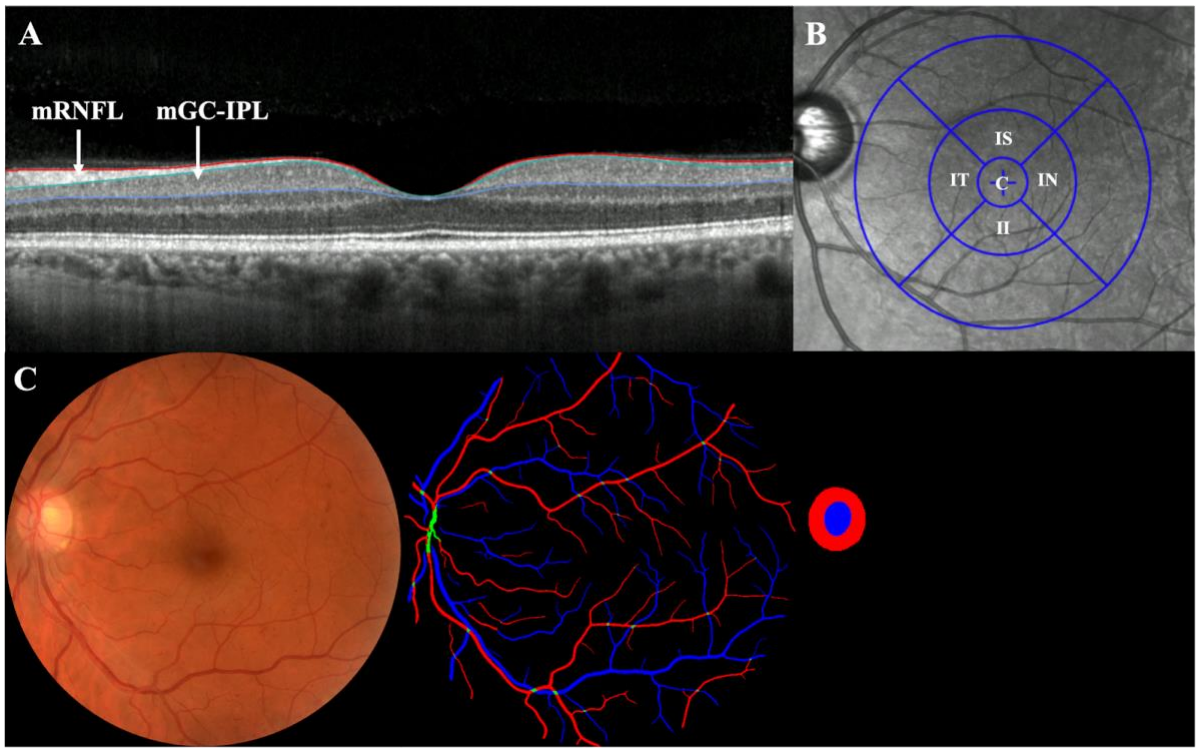

Figure 33: Example retinal images.

Macula-centred optical coherence tomography with the retinal nerve fibre (mRNFL) and ganglion cell-inner plexiform layer indicated (mGC-IPL) (A). Sublayer thicknesses were averaged across the four parafoveal grids (IS - Inner Superior region; IN - Inner Nasal region; II - Inner Inferior region; IT - Inner Temporal Region) (B). Retinal vasculature and the optic nerve were segmented from raw colour fundus photographs by AutoMorph to derive vessel maps, from which morphometric indices were estimated (C).

Image quality

Image quality was assessed through two means. Firstly, AutoMorph outputs an image quality metric of the CFP based on a convolutional neural network trained using two human expert gradings. I only included images considered of sufficient quality for analysis (output as ‘good’ or ‘ok’ by AutoMorph[193]). Secondly, TABS generates specific image quality metadata for each OCT scan. Standard criteria for quality assessment of OCT using TABS metadata have been previously

described[15,184]. I excluded the most extreme 10% of OCT images based on specific image quality metadata (inner limiting membrane indicator, motion indicators and quality) generated by TABS for each scan. The inner limiting membrane indicator is a measure of the minimum localized edge strength around the inner limiting membrane boundary across the entire scan; this is useful for identifying blinks, scans that contain regions of severe signal fading, and segmentation errors. The motion indicators are based on the Pearson correlations and absolute differences between the thickness data of the entire retina and retinal nerve fibre layer from each set of consecutive B-scans. The lowest correlation and the highest absolute difference in a scan serve as the resulting indicator scores and identify blinks, eye motion artifacts, and segmentation failures. Image quality was considered at the patient-eye level i.e. if either the OCT or CFP was deemed poor quality, both were removed. This was to harmonize the participants across both CFP and OCT analyses.

Exposure variables

Individuals reporting painful gums or loose teeth in the previous 12 months on the touchscreen questionnaire were considered as having very severe periodontitis (primary exposure), based on previous validity studies[444–446]. A meta-analysis indicated self-report of painful gums and loose teeth had a pooled specificity of 91.9 (95% CI: 88.5, 94.6) and 94.7 (95% CI: 92.5, 96.4) for moderate periodontitis and 91.9 (95% CI: 89.8, 93.7) and 90.3 (95% CI: 87.3, 92.8) for severe periodontitis respectively, as defined by the US Centers for Disease Control and Presentation and the American Academy of Periodontology[447]. The CDC case definitions were superseded in 2018 by the International Classification of Periodontal Diseases and Conditions and tooth mobility (which leads to tooth migration and bite collapse) is a

feature of Stage IV (very severe) periodontitis[448]. Individuals reporting other symptoms associated with oral disease which were not part of the case definition (e.g. mouth ulcers, dentures and toothache) were excluded. Secondary exposure variables were defined *a priori* and included age, sex, ethnicity, socioeconomic deprivation, hypertension, diabetes mellitus, smoking status, alcohol drinker status and refractive error. Ethnicity was self-reported by the patient according to groups, as per the UK Census. Socioeconomic deprivation was measured using the Index of Multiple Deprivation (IMD) 2010. Hypertension and diabetes mellitus were self-reported by the participant through touchscreen questionnaire. For hypertension, all those who reported having either hypertension or essential hypertension were categorised as hypertension and otherwise considered absent. For diabetes mellitus, all those reporting diabetes, type 1 or type 2 diabetes mellitus were categorised into a binary variable of diabetic/non-diabetic. Smoking status was self-reported as never, previous, or current. The few who preferred not to answer this question at the initial visit were excluded (499,461/501,518, 99.6% complete). Alcohol drinker status was self-reported as never, previous, or current and was available for 500,757 of 501,512 participants (99.8%). Refractive error, as measured using the spherical equivalent on autorefraction, is a source of magnification error resulting in strong associations with retinal thicknesses on OCT and measurements of retinal vascular calibre[15,71].

Data analysis

Distribution of data was visualised using quantile-quantile plots and assessed statistically. Continuous variables were summarised using mean +/- standard deviation and categorical variables through percentages. Comparison of continuous

variables between groups was assessed using the independent samples t test. Chi-squared testing was used to assess the association between very severe periodontitis and categorical secondary exposure variables. For unadjusted comparisons of eye-level data to describe baseline characteristics, I averaged the measurements of both eyes where data were available. For adjusted analysis, I fitted linear mixed effects regression models using maximum likelihood estimation with a random effect on the intercept to account for the multilevel data structure of eyes nested within participants. Degrees of freedom for multilevel modelling were estimated using Satterthwaite's approximation[215]. Retinal vascular calibre was standardised (mean-normalised) for adjusted analyses (raw values are less interpretable for these features). To assess for interaction between age and OCT layer thickness, I compared models with and without an interaction term using the likelihood ratio test/Wilks test (LRT) to compare model fit[449]. For investigating the association between very severe periodontitis and time to non-communicable disease (all-cause dementia, MACE and diabetes mellitus), I estimated cause-specific adjusted hazard ratios (HR) using Cox proportional hazards models. The at-risk period was defined from the time of retinal imaging acquisition (the UKBB initial assessment visit data) until the earliest of death, hospital admission with a relevant diagnostic code or conclusion of the data refresh date for our UKBB application (1st December 2020). Individuals with a relevant code pre-dating the time of retinal imaging were excluded. All models were adjusted for age, sex, ethnicity, socioeconomic deprivation, hypertension, diabetes mellitus, smoking status and alcohol drinker status. Models examining retinal outcome variables were additionally adjusted for refractive error. The level of statistical significance was set at $p < 0.05$. All analyses were conducted in R version 4.1.0 (R Core Team, 2021. R Foundation

for Statistical Computing, Vienna, Austria) and used the `lme4` and l`mertest` packages[341,450,451].

6.4.3 Results

Of the 40,615 individuals included in the analysis based on my inclusion criteria and image quality control, there were 2,749 individuals (5,425 eyes) that had very severe periodontitis and 37,866 (76,055 eyes) did not (prevalence: 6.8%). Individuals with severe periodontitis were older (affected: 57.7 +/- 7.8 years, unaffected: 56.3 +/- 8.1 years, p<0.001), lived in areas of greater deprivation (affected: 20.6 +/- 13.8, unaffected: 16.6 +/- 12.0, p<0.001) and were more likely to be current smokers (affected: 19.8%, unaffected: 9.0%, p < 0.001), hypertensive (affected: 31.4%, unaffected: 24.3%, p < 0.001) and diabetic (affected: 9.3%, unaffected 4.5%, p < 0.001). The distribution of ethnicity also differed between groups with individuals with severe periodontitis more likely to be South Asian (affected: 7.0%, unaffected: 2.7%) or Black (affected: 5.6%, unaffected: 2.7%) . They were also less myopic (affected spherical equivalent: -0.03 +/- 2.5 dioptres, unaffected: -0.40 +/- 2.6 dioptres, p < 0.001).

Retinal morphology in very severe periodontitis

Individuals with severe periodontitis had wider arteriolar calibre (affected: 61.9 +/- 5.4 units, unaffected: 61.1 +/- 5.3 units, p < 0.001), wider venular calibre (affected: 68.5 +/- 6.6 units, unaffected: 67.2 +/- 6.2 units, p < 0.001) thinner mRNFL (affected: 25.3 +/- 2.9 µm, unaffected: 25.6 +/- 2.8 µm, p < 0.001) and thinner mGC-IPL (affected: 88.3 +/- 8.8 µm, unaffected: 89.4 +/- 8.2 µm, p < 0.001) than participants

without severe periodontitis. They also had lower retinal fractal dimension (affected: 1.487 +/- 0.03 dimensions, unaffected: 1.490 +/- 0.03, $p < 0.001$) but there was no difference in retinal vascular distance tortuosity or optic nerve CDR between groups (Table *37*).

Characteristic		No very severe periodontitis (*n*= 37,866)	Very severe periodontitis	*p*-value
Age (mean +/- SD)	**Years**	56.3 +/- 8.1	57.7 +/- 7.8	**<0.001**
Sex (*n* (%))	**Female**	20,340 (53.7)	1,484 (53.9)	0.82
	Male	17,564 (46.3)	1,269 (46.1)	
Ethnicity (*n* (%))	**South Asian**	1,040 (2.7)	192 (7.0)	**<0.001**
	Black	1,020 (2.7)	154 (5.6)	
	Other	1,145 (3.0)	187 (6.8)	
	White	34,699 (91.5)	2,220 (80.6)	
Socioeconomic deprivation (mean +/- SD)[1]	**IMD score**	16.6 +/- 12.0	20.6 +/- 13.8	**<0.001**
Smoking status (*n* (%))	**Never**	21,960 (57.9)	1,185 (43.0)	**<0.001**
	Previous	12,515 (33.0)	1,024 (37.2)	
	Current	3,429 (9.0)	544 (19.8)	
Alcohol drinker status (*n* (%))	**Never**	1,640 (4.3)	218 (7.9)	**<0.001**
	Previous	1,174 (3.1)	152 (5.5)	
	Current	35,090 (92.6)	2,383 (86.6)	
Hypertension (*n* (%))	**Absent**	28,701 (75.7)	1,888 (68.6)	**<0.001**
	Present	9,203 (24.3)	865 (31.4)	
Diabetes mellitus (*n* (%))	**Absent**	36,201 (95.5)	2,496 (90.7)	**<0.001**
	Present	1,703 (4.5)	257 (9.3)	
Refractive error (mean +/- SD)	**Dioptres**	-0.40 +/- 2.6	-0.03 +/- 2.5	**<0.001**
Retinal layer thicknesses (mean +- SD)	**mRNFL (µm)**	25.6 +/- 2.8	25.3 +/- 2.9	**<0.001**
	mGC-IPL (µm)	89.4 +/- 8.2	88.3 +/- 8.8	**<0.001**
Retinovascular indices (mean +- SD)	**Arteriolar calibre (µm)**	61.1 +/- 5.3	61.9 +/- 5.4	**<0.001**
	Venular calibre (µm)	67.2 +/- 6.2	68.5 +/- 6.6	**<0.001**
	Fractal dimension (units)	1.490 +/- 0.03	1.487 +/- 0.03	**<0.001**
	Distance tortuosity (units)	3.36 +/- 0.98	3.39 +/- 0.95	0.89
Optic nerve morphology (mean ± SD)[2]	**CDR (ratio)**	0.48 ± 0.07	0.48 ± 0.08	0.17

Table 37: Baseline characteristics of the cohort.

For ophthalmic variables, when data from both eyes were available, measurements were averaged. SD: standard deviation. [1]Note that for socioeconomic deprivation, a higher number indicates greater levels of deprivation. [2]Optic nerve segmentation, a more challenging task than retinovascular segmentation, was available for 1,625 participants with very severe periodontitis and 24,662 participants without severe periodontitis.

Neither fractal dimension nor distance tortuosity were associated with very severe periodontitis (Table *38*) nor was there an association with mRNFL (-0.12 μm, 95% CI: -0.26, 0.02, $p = 0.09$) or optic nerve CDR (β-0.02, 95% CI: -0.09, 0.04, $p = 0.46$, Table *39*). After adjustment for confounders, very severe periodontitis was significantly associated with larger arteriolar calibre (β 0.05 units per SD increase, 95% CI: 0.01, 0.09, $p = 0.021$) and larger venular calibre (β 0.09 units per SD increase, 95% CI: 0.05, 0.14, $p = 3.1 \times 10^{-5}$), without any interaction by age. Among the whole cohort, very severe periodontitis was not associated with thickness of the mGC-IPL (-0.30 μm, 95% CI: -0.61, 0.02, $p = 0.07$) however there was a significant interaction between mGC-IPL and age for the association with severe periodontitis (LRT $p = 0.005$). When stratified by decile age groups, mGC-IPL was significantly reduced among those aged 60-69 years (-0.67 μm, 95% CI: -1.14, -0.19, $p = 0.006$) but not among those aged 50-59 years or 40-49 years (Table *40*).

Very severe periodontitis and incident non-communicable disease

I next examined whether very severe periodontitis was associated with incident all-cause dementia, MACE and diabetes mellitus in my cohort. Excluding individuals with a previous diagnosis of the relevant disease left a cohort of 40,610 participants for incident all-cause dementia (2,824 with very severe periodontitis, total follow up: 434,075 years), 39,916 participants for MACE (2,753 with very severe periodontitis, total follow up: 421,576 years) and 39,703 participants for incident diabetes mellitus (2,522 with very severe periodontitis, total follow up: 406,996 years). During the study period, 279 participants developed all-cause dementia, 753 developed diabetes mellitus, and 1388 developed MACE. On adjusted analysis, very severe periodontitis was associated with greater hazards of developing diabetes mellitus

(HR: 1.38, 95% CI: 1.10, 1.74, p=0.006) and MACE (HR 1.40, 95% CI: 1.18, 1.66, $p = 1.0 \times 10^{-4}$) but not all-cause dementia (HR: 1.27, 95% CI: 0.86, 1.87, Table *41*).

Variable		Arteriolar calibre (μm)		Venular calibre (μm)		Fractal dimension (units)		Distance tortuosity (units)	
		Beta (95% CI)	***p*-value**	**Beta (95% CI)**	***p*-value**	**Beta (95% CI)**	***p*-value**	**Beta (95% CI)**	***p*-value**
Very severe periodontitis	Absent	**Reference**		**Reference**		**Reference**		**Reference**	
	Present	0.05 (0.01, 0.09)	**0.021**	0.09 (0.05, 0.14)	**3.1×10^{-5}**	-0.01 (-0.05, 0.04)	0.73	-0.04 (-0.08, 0.01)	0.09
Age	Per decile	-0.03 (-0.04, -0.02)	**1.0×10^{-5}**	0.17 (0.15, 0.19)	**$<1 \times 10^{-16}$**	-0.46 (-0.48, -0.45)	**$<1 \times 10^{-16}$**	0.17 (0.16, 0.19)	**$<1 \times 10^{-16}$**
Sex	Female	**Reference**		**Reference**		**Reference**		**Reference**	
	Male	-0.23 (-0.25, -0.21)	**$<1 \times 10^{-16}$**	-0.11 (-0.13, -0.09)	**$<1 \times 10^{-16}$**	0.13 (0.11, 0.15)	**$<1 \times 10^{-16}$**	-0.09 (-0.11, -0.07)	**$<1 \times 10^{-16}$**
Ethnicity	White	**Reference**		**Reference**		**Reference**		**Reference**	
	Asian (South)	0.05 (-0.02, 0.12)	0.15	-0.10 (-0.17, -0.03)	**0.006**	-0.05 (-0.12, 0.02)	0.17	-0.13 (-0.20, -0.06)	**2.7×10^{-4}**
	Black	0.04 (-0.03, 0.11)	0.28	-0.15 (-0.22, -0.08)	**0.006**	-0.14 (-0.21, -0.07)	**1.3×10^{-4}**	-0.12 (-0.19, -0.05)	**4.1×10^{-4}**
	Other	0.06 (-0.01, 0.12)	0.07	-0.10 (-0.16, -0.04)	**0.002**	0.03 (-0.03, 0.09)	0.35	-0.07 (-0.12, -0.01)	**0.031**
Socioeconomic deprivation	Per SD increase	0.01 (0.00, 0.02)	0.19	0.02 (0.00, 0.03)	**0.007**	-0.01 (-0.02, 0.00)	0.06	0.01 (0.00, 0.02)	0.12
Diabetes mellitus	Absent	**Reference**		**Reference**		**Reference**		**Reference**	
	Present	0.14 (0.09, 0.20)	**2.3×10^{-7}**	0.07 (0.02, 0.13)	**0.007**	-0.08 (-0.14, -0.03)	**0.002**	-0.03 (-0.08, 0.02)	0.31
Hypertension	Absent	**Reference**		**Reference**		**Reference**		**Reference**	
	Present	-0.14 (-0.16, -0.11)	**$<1 \times 10^{-16}$**	0.02 (0.00, 0.05)	0.07	-0.13 (-0.16, -0.11)	**$<1 \times 10^{-16}$**	0.04 (0.01, 0.06)	**0.003**
Alcohol drinker status	Never	**Reference**		**Reference**		**Reference**		**Reference**	
	Previous	0.02 (-0.06, 0.10)	0.64	-0.03 (-0.10, 0.05)	0.53	0.04 (-0.04, 0.12)	0.34	0.07 (-0.01, 0.14)	0.07
	Current	-0.09 (-0.14, -0.03)	**0.001**	-0.05 (-0.11, 0.00)	**0.048**	-0.03 (-0.08, 0.03)	0.33	0.05 (0.00, 0.10)	0.07
Smoking status	Never	**Reference**		**Reference**		**Reference**		**Reference**	
	Previous	0.01 (-0.01, 0.04)	0.25	0.03 (0.01, 0.06)	**0.007**	0.01 (-0.02, 0.03)	0.56	0.00 (-0.02, 0.02)	0.92
	Current	0.19 (0.16, 0.23)	**$<1 \times 10^{-16}$**	0.22 (0.18, 0.26)	**$<1 \times 10^{-16}$**	0.05 (0.01, 0.09)	**0.006**	0.00 (-0.03, 0.04)	0.93
Spherical equivalent	Per dioptre	0.34 (0.33, 0.35)	**$<1 \times 10^{-16}$**	0.27 (0.26, 0.28)	**$<1 \times 10^{-16}$**	0.05 (0.05, 0.05)	**$<1 \times 10^{-16}$**	-0.01 (-0.02, -0.01)	**2.8×10^{-10}**

Table 38: Standardised differences in retinovascular indices between those with and without very severe periodontitis.

Values are standardized regression coefficients estimated through linear mixed effects. CI: confidence interval, IMD: index of multiple deprivation, SD: standard deviation.

Variable		mRNFL (µm)		mGC-IPL (µm)		CDR (ratio)	
		Thickness difference (95% CI)	***p*-value**	**Thickness difference (95% CI)**	***p*-value**	**Beta (95% CI)**	***p*-value**
Very severe periodontitis	Absent	**Reference**		**Reference**		**Reference**	
	Present	-0.09 (-0.19, 0.02)	0.09	-0.30 (-0.61, 0.02)	0.07	0.00 (-0.05, 0.05)	0.92
Age	Per decile	-0.19 (-0.23, -0.16)	**<1 x 10^{-16}**	-2.27 (-2.37, -2.16)	**<1 x 10^{-16}**	0.02 (0.01, 0.04)	**0.004**
Sex	Female	**Reference**		**Reference**		**Reference**	
	Male	0.53 (0.48, 0.58)	**<1 x 10^{-16}**	0.85 (0.69, 1.01)	**<1 x 10^{-16}**	0.03 (0.00, 0.05)	0.021
Ethnicity	White	**Reference**		**Reference**		**Reference**	
	Asian (South)	-0.80 (-0.96, -0.64)	**<1 x 10^{-16}**	-2.94 (-3.42, -2.46)	**<1 x 10^{-16}**	0.49 (0.41, 0.57)	**<1 x 10^{-16}**
	Black	-1.26 (-1.43, -1.10)	**<1 x 10^{-16}**	-3.65 (-4.13, -3.17)	**<1 x 10^{-16}**	0.70 (0.63, 0.78)	**<1 x 10^{-16}**
	Other	-0.27 (-0.42, -0.12)	**3.8 x 10^{-4}**	-0.79 (-1.24, -0.34)	**5.2 x 10^{-4}**	0.26 (0.19, 0.32)	**3.8 x 10^{-14}**
Socioeconomic deprivation	Per SD increase	-0.08 (-0.10, -0.05)	**1.1 x 10^{-8}**	-0.27 (-0.35, -0.19)	**8.7 x 10^{-11}**	-0.01 (-0.02, 0.01)	0.31
Diabetes mellitus	Absent	**Reference**		**Reference**		**Reference**	
	Present	-0.15 (-0.27, -0.02)	**0.022**	-1.49 (-1.86, -1.11)	**1.1 x 10^{-14}**	0.00 (-0.06, 0.06)	0.97
Hypertension	Absent	**Reference**		**Reference**		**Reference**	
	Present	-0.13 (-0.19, -0.07)	**7.0 x 10^{-5}**	-1.03 (-1.22, -0.84)	**<1 x 10^{-16}**	-0.01 (-0.04, 0.02)	0.64
Alcohol drinker status	Never	**Reference**		**Reference**		**Reference**	
	Previous	-0.06 (-0.25, 0.13)	0.54	-0.18 (-0.76, 0.40)	0.54	-0.01 (-0.10, 0.08)	0.84
	Current	0.12 (-0.02, 0.25)	0.09	0.18 (-0.22, 0.57)	0.37	-0.01 (-0.07, 0.05)	0.83
Smoking status	Never	**Reference**		**Reference**		**Reference**	
	Previous	-0.02 (-0.08, 0.04)	0.55	-0.22 (-0.40, -0.05)	**0.012**	0.02 (-0.01, 0.04)	0.13
	Current	-0.07 (-0.16, 0.02)	0.14	-0.43 (-0.71, -0.16)	**0.002**	-0.01 (-0.05, 0.03)	0.67
Spherical equivalent	Per dioptre	-0.19 (-0.20, -0.18)	**<1 x 10^{-16}**	0.28 (0.25, 0.30)	**<1 x 10^{-16}**	0.00 (0.00, 0.01)	0.72

Table 39: Thickness difference estimates for retinal sublayers between those with and without very severe periodontitis and other exposure variables.

Estimates are derived from multivariable linear mixed effects models. CDR: cup-to-disc ratio, CI: confidence interval, mGC-IPL: macular ganglion cell-inner plexiform layer, mRNFL: macular retinal nerve fibre layer, SD: standard deviation.

mGC-IPL Thickness		40-49 age group (*n* affected = 511)		50-59 age group (*n* affected = 903)		60-69 age group (*n* affected = 1,335)	
		Thickness difference (95% CI)	*p*-value	Thickness difference (95% CI)	*p*-value	Thickness difference (95% CI)	*p*-value
Very severe periodontitis	Absent	**Reference**		**Reference**		**Reference**	
	Present	-0.24 (-0.92, 0.43)	0.48	0.20 (-0.34, 0.75)	0.47	-0.67 (-1.14, -0.19)	**0.006**
Age	Per decile	-0.92 (-1.45, -0.39)	**6.2×10^{-4}**	-1.91 (-2.38, -1.44)	**1.6×10^{-15}**	-3.94 (-4.40, -3.48)	**$<1 \times 10^{-16}$**
Sex	Female	**Reference**		**Reference**		**Reference**	
	Male	2.28 (1.99, 2.58)	**$<1 \times 10^{-16}$**	0.68 (0.41, 0.95)	**1.2×10^{-6}**	0.26 (0.01, 0.52)	**0.042**
Ethnicity	White	**Reference**		**Reference**		**Reference**	
	Asian (South)	-2.58 (-3.32, -1.85)	**5.3×10^{-12}**	-3.07 (-3.87, -2.27)	**6.6×10^{-14}**	-3.17 (-4.10, -2.23)	**3.0×10^{-11}**
	Black	-2.62 (-3.29, -1.96)	**1.5×10^{-14}**	-3.62 (-4.42, -2.81)	**$<1 \times 10^{-16}$**	-6.03 (-7.19, -4.86)	**$<1 \times 10^{-16}$**
	Other	-0.64 (-1.32, 0.03)	0.06	-0.77 (-1.52, -0.03)	0.042	-0.80 (-1.68, 0.09)	0.08
Socioeconomic deprivation	Per SD increase	-0.31 (-0.46, -0.16)	**7.4×10^{-5}**	-0.19 (-0.33, -0.06)	**0.006**	-0.28 (-0.40, -0.15)	**1.4×10^{-5}**
Diabetes mellitus	Absent	**Reference**		**Reference**		**Reference**	
	Present	-1.71 (-2.72, -0.70)	**7.4×10^{-5}**	-1.06 (-1.75, -0.37)	**0.003**	-1.42 (-1.93, -0.90)	**7.2×10^{-8}**
Hypertension	Absent	**Reference**		**Reference**		**Reference**	
	Present	-0.85 (-1.32, -0.38)	**4.1×10^{-4}**	-1.30 (-1.63, -0.96)	**2.9×10^{-14}**	-0.87 (-1.13, -0.60)	**3.2×10^{-10}**
Alcohol drinker status	Never	**Reference**		**Reference**		**Reference**	
	Previous	-0.35 (-1.41, 0.70)	0.51	-0.63 (-1.64, 0.37)	0.22	0.15 (-0.78, 1.08)	0.75
	Current	-0.35 (-1.06, 0.36)	0.33	0.43 (-0.29, 1.14)	0.24	0.28 (-0.34, 0.91)	0.37
Smoking status	Never	**Reference**		**Reference**		**Reference**	
	Previous	0.11 (-0.25, 0.46)	0.55	0.00 (-0.30, 0.30)	0.98	-0.46 (-0.72, -0.19)	7.5×10^{-4}
	Current	-0.29 (-0.73, 0.15)	0.19	-0.12 (-0.59, 0.34)	0.61	-0.93 (-1.44, -0.42)	**3.6×10^{-4}**
Spherical equivalent	Per dioptre	0.24 (0.19, 0.29)	**$<1 \times 10^{-16}$**	0.25 (0.21, 0.30)	**$<1 \times 10^{-16}$**	0.31 (0.27, 0.36)	**$<1 \times 10^{-16}$**

Table 40: Thickness difference estimates stratified by age groups for the macular ganglion cell-inner plexiform layer.

A significant association was only seen for the group aged 60-69 years. CI: confidence interval, IMD: index of multiple deprivation, mGC-IPL: macular ganglion cell-inner plexiform layer, SD: standard deviation.

		Incident dementia (*n*=40,610)		Incident MACE (*n*=39,916)		Incident diabetes mellitus (*n*=39,703)	
		HR (95% CI)	***p*-value**	**HR (95% CI)**	***p*-value**	**HR (95% CI)**	***p*-value**
Very severe periodontitis	Absent	**Reference**		**Reference**		**Reference**	
	Present	1.27 (0.86, 1.87)	0.23	1.40 (1.18, 1.66)	**1.0×10^{-4}**	1.38 (1.10, 1.74)	**0.006**
Age	Per decile	5.95 (4.59, 7.72)	**1.0×10^{-16}**	2.34 (2.15, 2.55)	**1.0×10^{-16}**	1.47 (1.33, 1.63)	**1.3×10^{-13}**
Sex	Female	**Reference**		**Reference**		**Reference**	
	Male	1.51 (1.17, 1.94)	**0.001**	2.19 (1.95, 2.47)	**1×10^{-16}**	1.45 (1.25, 1.69)	**8.9×10^{-7}**
Ethnicity	White	**Reference**		**Reference**		**Reference**	
	Asian (South)	0.60 (0.24, 1.49)	0.27	0.97 (0.70, 1.33)	0.84	3.05 (2.25, 4.14)	**6.8×10^{-13}**
	Black	1.01 (0.44, 2.31)	0.98	0.83 (0.58, 1.20)	0.33	2.49 (1.83, 3.38)	**5.9×10^{-9}**
	Other	1.09 (0.54, 2.23)	0.80	0.82 (0.58, 1.17)	0.28	1.70 (1.20, 2.41)	**0.003**
Socioeconomic deprivation	Per SD increase	1.13 (1.01, 1.27)	**0.037**	1.15 (1.09, 1.21)	**5.1×10^{-8}**	1.27 (1.20, 1.36)	**5.3×10^{-14}**
Diabetes mellitus	Absent	**Reference**		**Reference**		*	
	Present	2.01 (1.42, 2.85)	**7.7×10^{-5}**	1.86 (1.59, 2.19)	**3.0×10^{-14}**		
Hypertension	Absent	**Reference**		**Reference**		**Reference**	
	Present	1.33 (1.04, 1.70)	**0.025**	1.82 (1.63, 2.04)	**1.0×10^{-16}**	2.23 (1.92, 2.59)	**1.0×10^{-16}**
Alcohol drinker status	Never	**Reference**		**Reference**		**Reference**	
	Previous	1.60 (0.81, 3.14)	0.18	1.34 (0.96, 1.87)	0.09	1.27 (0.85, 1.91)	0.25
	Current	0.74 (0.43, 1.24)	0.25	0.79 (0.61, 1.02)	0.07	0.74 (0.55, 1.01)	0.06
Smoking status	Never	**Reference**		**Reference**		**Reference**	
	Previous	0.90 (0.69, 1.17)	0.43	1.00 (0.89, 1.13)	0.95	1.26 (1.07, 1.48)	**0.006**
	Current	1.46 (0.98, 2.18)	0.06	1.64 (1.38, 1.93)	**7.6×10^{-9}**	1.63 (1.30, 2.05)	**2.3×10^{-5}**

Table 41: Association between very severe periodontitis and incident dementia, major adverse cardiovascular events and diabetes mellitus.

HR: hazard ratio, MACE: major adverse cardiovascular event, SD: standard deviation

* Participants with prevalent diabetes mellitus were excluded for this analysis.

6.4.4 Discussion

In this cross-sectional analysis of multimodal retinal imaging of 39,353 participants in the UKBB cohort, I report the following key findings. Firstly, very severe periodontitis is associated with increased retinal arteriolar and venular calibre in all age groups. Secondly, very severe periodontitis is associated with thinner mGC-IPL but the association was only significant among those aged 60 years and over. Thirdly, differences in retinal fractal dimension were explained by greater medical comorbidity (hypertension, diabetes mellitus) among those with very severe periodontitis. Fourthly, affected individuals in my cohort were more likely to develop diabetes mellitus and MACE but not dementia. My results highlight that individuals with very severe periodontitis have measurable differences in retinal morphology and sublayer thicknesses consistent with chronic inflammation, cardiovascular dysfunction and neurodegeneration.

Retinal vascular calibre

The effect size of the association between increased retinal venular calibre and very severe periodontitis (0.09 units per SD increase in calibre) was similar to that of diabetes mellitus (0.07 units) and nearly half of the estimate for current smoking (0.22 units). The association was not modified by age. Interestingly, similar relative effect estimates have been found on mortality in individuals with chronic kidney disease. Sharma et al found periodontitis and diabetes mellitus to have similar hazard estimates and current smoking to have approximately double the hazards of periodontitis for all-cause death in the US-based National Health and Nutrition Examination Survey[452]. Although not my primary question, my observed positive association of retinal venular calibre with age, diabetes mellitus and smoking and a

negative association with current alcohol consumption is consistent with previous studies[427,453,454]. However, evidence into any potential association of very severe periodontitis with retinal structure is limited. A cross-sectional analysis of the Studies of Health in Pomeria-TREND cohort of 3,183 participants found that central retinal vein equivalent (CRVE) was associated with increased mean attachment level and mean probing depth (features of periodontitis) but only among men[455]. Similarly, CRVE was increased among those with periodontitis, defined using CDC/AAP criteria on oral health examination, in the Dental ARIC study; however, this was only significant among those with diabetes mellitus and the numbers were relatively small (n = 66). A key limitation of both these studies is that they were not able to adjust for refractive error. Variability in optical magnification owing to heterogenous refractive error poses methodological challenges with retinal vascular calibre measurement. Although the retinal arteriole-to-venule ratio (AVR) appears relatively robust to refractive error, measurements of the retinal vessel diameters are significantly affected unless correction formulae based on spherical equivalent data are used[71]. Highlighting this, I found significant differences in refractive error between groups with individuals with severe periodontitis being less myopic. I hypothesise that the established positive association between myopia and educational experience and attainment underlie this as periodontitis is more prevalent among those with lower levels of education[456–458]. In light of these two issues, I advocate that future studies of retinal morphology in individuals with periodontitis account for refractive error to avoid biased effect estimates.

There are several biologically plausible mechanisms for my finding of increased retinal venular calibre in very severe periodontitis. Beyond an increased

cardiovascular disease burden, retinal venular dilatation is typically seen with increased systemic inflammation. Venular calibre is increased in individuals with autoimmune disorders, such as rheumatoid and psoriatic arthritis[459], and positively associated with serum pro-inflammatory markers, such as C-reactive protein and interleukin-6[460,461], many of which are concurrently elevated in severe periodontitis[422,462,463]. Retinal venular calibre enlargement seen in patients admitted with sepsis significantly reduced following intravenous antibiotics and normalisation of inflammatory markers[464]. Another potential contributor may relate to incipient metabolic syndrome. Venular calibre is increased in incident diabetes mellitus and mounting evidence suggests gingivitis and periodontitis may be harbingers of emerging diabetes mellitus[437–439]. Individuals with very severe periodontitis in my cohort had 38% greater risk of developing diabetes mellitus and 40% greater risk of developing a MACE during the study period, even after adjusting for shared risk factors. Whether venular calibre might have prognostic value in discriminating between those individuals with very severe periodontitis who are more likely to develop diabetes mellitus and MACE warrants further investigation.

Ganglion cell-inner plexiform layer

A novel finding of my report was that older individuals with very severe periodontitis have thinner mGC-IPL. Compared to another report examining the determinants of mGC-IPL thickness in UKBB, my estimate for very severe periodontitis in those aged 60-69 years (-0.67 μm) was greater than that attributed to daily alcohol consumption (-0.46 μm) or diabetes mellitus (-0.34 μm)[15]. The fact that this association was only significant among those aged 60-69 years points to the need for longitudinal studies to confirm the finding, but I speculate that these results may indicate that cumulative

exposure to chronic inflammation and repeated bacteraemia affects the mGC-IPL late resulting in heightened neurodegeneration, a phenomenon supported by a growing literature base. Individuals with periodontitis have a greater risk of developing Alzheimer's disease and bacterial microorganisms, typically associated with severe periodontitis, can induce a rise in systemic beta-amyloid peptides[465,466]. Even among cognitively normal individuals, severity of periodontitis is associated with brain amyloid accumulation[467]. Accelerated cerebral neurodegeneration and consequent retrograde trans-synaptic degeneration manifesting with thinner mGC-IPL is therefore a plausible mechanism for my finding. Evidence of a higher risk of primary open-angle glaucoma in those with periodontitis[433,434] may also explain my finding though, countering this, I did not find an association between very severe periodontitis and CDR or RNFL. Probing further into the biological causes of degeneration is beyond the scope of my study but inflammation resulting from chronic exposure to periodontal microorganisms has been shown to induce colonisation and induction of microglia-mediated neuroinflammation with resulting cognitive impairment in mice[468]. However, another consideration, as with retinal venular calibre, is metabolic syndrome. The macular ganglion cell complex is thinner in individuals with pre-diabetes[469] and a recent meta-analysis across 15 cohort studies including 114,361 individuals with periodontitis, showed risk of incident diabetes mellitus was 26% higher (95% CI: 12%, 41%) than in unaffected controls[470]. Moreover, I found that individuals with very severe periodontitis in my imaging cohort had 38% greater hazards of developing diabetes mellitus during the study period. Future work should examine whether thinner mGC-IPL in individuals with periodontitis can distinguish between individuals who develop cognitive decline, dementia, and diabetes mellitus.

My findings of retinal morphological differences in individuals with very severe periodontitis are important in the context of the growing motivation to develop retinal imaging-based risk stratification tools for non-communicable diseases, such as cardiovascular disease and dementia. Increased retinal venular calibre is associated with a higher risk of cardiovascular events and vascular dementia[425,471] – conditions which have similarly been described to have greater incidence in those with very severe periodontitis[472,473]. Similarly, thinner mGC-IPL has been described in both prevalent and incident Alzheimer's disease, Parkinson's disease, and vascular dementia. Accordingly, several prediction models for cardiovascular and neurodegenerative events using retinal imaging data have now been described and extensively externally validated[238,474,475]. Further investigation into the discrimination and calibration performance of these prediction models in those with periodontitis, a group with an enriched non-communicable disease burden, is needed.

Strengths and limitations

Strengths of my study include the large sample size, adjustment for multiple important confounders and use of data and artificial-intelligence based segmentation models, most of which are openly available for researchers[193]. However, there are some limitations. Oral health status in UK Biobank is limited to self-reported data on touchscreen questionnaires rather than a clinical assessment. I considered those reporting 'painful gums' or 'loose teeth' as affected individuals but mobile teeth are typically associated with very severe (Stage IV) periodontitis[448], drawing on the meta-analysis of Abbood et al which showed high specificity for loose teeth (pooled specificity of 94.7 and 91.9 for moderate and severe periodontitis). However, the low

pooled sensitivity of loose teeth (moderate: 28.3 and severe: 54.9) and painful gums (moderate disease: 17.1 and severe disease: 22.6) suggests that many of my unaffected controls may indeed have periodontitis[445]. Misclassification bias is thus likely to bias towards the null underestimating the true association. As with any observational study, I cannot exclude the possibility of residual confounding.

6.4.5 Summary

In conclusion, I report that individuals with very severe periodontitis exhibit wider retinal venules and thinner mGC-IPL, which is not explained by sociodemographic profile, lifestyle behaviours and cardiovascular risk factors. Corroborated by evidence from other epidemiological and biochemical reports, I suggest my findings highlight a periodontal-oculomic axis, such that retinal imaging has value for in vivo assessment of the non-communicable disease burden imparted by very severe periodontitis. Prospective studies examining oral health and systemic should consider retinal imaging-based features as adjunct outcome measures.

6.5 Amblyopia

6.5.1 Introduction

Amblyopia (“lazy eye”), a developmental disorder of vision classically involving one eye, affects 1-3% of children globally[320]. Resulting from limited or asymmetric visual experience during the critical period of neuroplasticity, amblyopia is characterised by aberrant competitive interaction between the cortical afferents of the two eyes[476]. Despite considerable improvements in visual outcomes owing to whole population screening programs and ophthalmic intervention (e.g. refractive correction or optical penalization of the contralateral eye), many individuals nonetheless develop longstanding monocular visual impairment, which persists into adulthood (persisting unilateral amblyopia)[477–479]. A relationship between the intrauterine environment, neurodevelopment, and non-communicable disease (NCD) in later life has garnered interest since David Barker proposed his *Fetal Origins (thrifty phenotype)* hypothesis in 1990[480]. Although his observations initially focused on the associations between early-life environmental influences and ischaemic heart disease in adulthood, similar detrimental associations with neurodevelopment have been subsequently described[481–485]. Intrinsically a neurodevelopmental disease, amblyopia has also been directly and indirectly (through ocular risk factors of strabismus and refractive error) linked with adverse parent-origin factors[486], including increased maternal age[487–489], maternal smoking[490,491] and alcohol consumption and lower socioeconomic status[491,492]. Consistent associations between these perinatal risk factors and the development of cardiometabolic disease in adulthood across several population-based studies in low, middle and high income countries[493–498], lends plausibility to an association between amblyopia and NCDs. However, evidence in this area is scarce. Adults with persisting unilateral amblyopia reported poorer

general health, mental health and overall wellbeing in a UK-based cross-sectional analysis[477] however no systematic investigation into the epidemiology of NCDs in adult amblyopes yet exists. The finding that even the unaffected 'normal' eye in individuals with unilateral amblyopia demonstrate retinal morphological differences further support a more generalised phenomenon of systemic dysregulation in amblyopia[321,322].

In this report, I leveraged a multimodal approach comprising classical epidemiological and retinal imaging analyses to investigate whether individuals with persisting unilateral amblyopia demonstrate evidence of heightened systemic dysregulation in adulthood. With collaborator Dr Vasiliki Bountziouka (Section 8. Author contribution statement), I firstly characterised cardiometabolic disease prevalence in affected individuals and, secondly, examined retinal morphology of both the affected and unaffected eyes. Given previous findings of adverse self-reported overall health among individuals with amblyopia, I hypothesised that affected individuals would exhibit a greater burden of NCDs in later life.

6.5.2 Methods

Participants and data collection

I utilised data from 126,399 UK Biobank (UKBB) participants, aged 40 years or older, eligible for an ophthalmic examination with visual acuity and refractive error measured in both eyes. Participants went through a detailed assessment using questionnaires, physical measurements, biological assays and longitudinal linkage with multiple health record systems, and self-reported whether they have been diagnosed with chronic disease and eye conditions, including amblyopia, and

whether they had treatment for them. A subset of 67,321 participants attending seven UKBB assessment centres additionally underwent retinal imaging in the form of colour fundus photography (CFP) and optical coherence tomography (OCT). Baseline data were collected from 2006 to 2010, with subsequent ongoing cycles, whilst to maximise the use of available data we utilised data until the end of 2017. Detailed information regarding the enhanced ophthalmic examination, other physical assessments, and biological samples are available at the UKBB website (https://www.ukbiobank.ac.uk/). Objective data on ophthalmic diagnoses were also provided through record linkage for all participants to the United Kingdom's National Health Service health administrative data set (Hospital Episode Statistics [HES]). My primary objective was to assess whether individuals with persisting unilateral amblyopia had a greater prevalence of cardiovascular disease and metabolic syndrome compared to controls. My secondary objective was to investigate whether affected and unaffected fellow eyes of individuals with persisting unilateral amblyopia had retinal and optic nerve morphological differences on in-vivo imaging compared to healthy controls.

Classification of amblyopia

According to a previously described hierarchical approach[477], participants were classified as having amblyopia if they self-reported amblyopia or treatment, and they also reported evidence of: (1) strabismus, (2) significant anisometropia (difference of at least -1.00 D/+1.00 D between eyes), (3) significant astigmatism (cylinder power ≥1.00 D), (4) significant refractive error per se (i.e., -3.00 D/+3.00 D or more extreme), (5) less severe refractive error but visual impairment without any other underlying eye disease (such as stimulus deprivation amblyopia or cataract), and (6)

current emmetropia (absence of refractive error, -0.99 D to +0.99 D) but self-reported glasses worn for hypermetropia in childhood and at least mild visual impairment with no other eye disease. Participants who did not self-report amblyopia were also identified through record linkage to treatment codes using HES data. "Resolved" amblyopia was considered if current near normal acuity (<0.06 logMAR), whilst "persisting" amblyopia was defined as residual acuity deficit despite treatment in childhood (also including bilateral amblyopia and visual impairment/ blindness). Participants with "optimal" vision, i.e. with bilateral normal visual acuity (i.e. 0.0 logMAR) and without primary refractive error (i.e. emmetropia) or any other eye disease or amblyogenic factors (using self–report, ophthalmic examination and HES data), were the comparator group.

Clinical outcomes

We used self-reported data on whether participants were diagnosed by their doctor for i) diabetes (UKBB field "2443"), ii) high blood pressure (derived from field "6150"), iii) vascular/ heart disease, namely angina, heart attack, stroke (all derived from field "6150"), and iv) cancer (field "2453"). Participants' body weight and height were measured using standard procedures during the initial assessment, and body mass index (BMI, kg/m^2) was then calculated. Obesity was defined as BMI > $30kg/m^2$. The co-existence of diabetes, high blood pressure and obesity was used to define the presence of metabolic syndrome[499].

Imaging outcomes

Macula-centred 45-degree colour fundus photography (CFP) and optical coherence tomography (OCT) were acquired using the Topcon 3D-OCT 1000 MKII (Topcon

Corporation, Tokyo, Japan)[184,185]. OCTs covered a 6.0 mm × 6.0 mm area and had 128 horizontal B scans and 512 A scans per B scan. Retinal imaging features pertaining to the retinal vasculature (arteriolar and venular calibre, fractal dimension, distance tortuosity and vessel density) and optic nerve (cup-disc ratio [CDR]) were extracted using the open-source deep learning-based pipeline, AutoMorph (section 4.3.1 Colour fundus photography). OCTs were segmented using the Topcon Advanced Boundary Segmentation Tool (TABS, version 1.6.2.6, section 4.3.2 Optical coherence tomography) . RNFL and mGC-IPL thickness were defined according to the lexicon proposed by the International Nomenclature for OCT panel[130]. Retinal sublayers for the four parafoveal subfields, as defined through the Early Treatment Diabetic Retinopathy Study, were averaged for analysis.

For imaging features, I considered individuals with valid eye data, confirmed amblyopia and no other eye disease as cases. My controls were individuals with valid eye data, no eye disease, no amblyopia and no amblyogenic factors. I firstly compared the affected eye of individuals with persisting unilateral amblyopia against one randomly chosen eye of controls, stratifying into those considered ‘resolved’ (i.e. <0.06 logMAR) and those ‘persisting’. Secondly, I compared the fellow eye of individuals with unilateral amblyopia (i.e. the normal eye) with one randomly chosen eye of individuals with optimal vision.

Statistical analysis

Descriptive statistics are shown as mean or frequencies alongside 95% confidence intervals (CI). The t-test was used to assess differences in the distribution of age, whilst the two-proportion z-test was used to assess differences in the distribution of

demographic (sex, ethnicity, deprivation) and clinical outcomes, between amblyopic and non-amblyopic participants.

For the epidemiological approach, we used logistic regression models, adjusted for age, sex (females/ males), ethnic background (white ethnic background/ other than white ethnic background), and deprivation (fifths of Townsend index of deprivation), to investigate the association between amblyopia and the number of components of metabolic syndrome (multinomial regression), and the individual diseases (binary regression). Therefore, estimates are reported as relative risk ratios (RRR) or odds ratios (OR) respectively, alongside 95% CIs. We undertook a matching analysis, using propensity score matching, implementing the nearest neighbour algorithm with no caliper, to account for confounding and differences between participants with amblyopia or optimal vision, and to estimate treatment effects for the treated (ATET). We matched participants with amblyopia (treated) and participants with optimal vision (untreated) based on age, sex, ethnic background and deprivation.

For the adjusted analysis of retinal imaging, I used nested logistic regression to investigate the association between persisting unilateral amblyopia and retinal features. The base model, similar to the epidemiological approach, was adjusted for age, sex, ethnicity, deprivation and additionally for spherical error (given its association with both retinovascular indices and inner retinal sublayer thicknesses). The full model was additionally adjusted for smoking status, alcohol consumption, hypertension, BMI and diabetes mellitus given previous evidence of their association with retinal markers. Retinovascular features were scaled (z-score) for model fitting to aid interpretability. All tests were two-sided, and the significance level was set to

0.05. Analyses were performed using Stata version 17.0 (StataCorp. 2021. Stata Statistical Software: Release 17. College Station, TX: StataCorp LLC) and R version 4.1.0 (R Core Team, 2021. R Foundation for Statistical Computing, Vienna, Austria).

6.5.3 Results

Epidemiological approach

Participants included in the clinical analysis sample (n=22,007) were on average younger (mean (95% CI): 52.2 (52.1, 52.3) vs 57.1 (57.0, 57.1)) compared to participants excluded due to eye conditions not relevant to amblyopia (n=89,453), whilst no major differences were observed in the distribution of sex (47.1% males (46.4%, 47.8%) vs 45.5% (45.2%, 45.9%)), ethnic background (10% other than white ethnic background (9.6%, 10.4%) vs 8.7% (8.5%, 8.9%)) and deprivation (23.0% from most deprived areas (22.4%, 23.5%) vs 21.4% (21.1%, 21.7%)). The analysis drew on data from 21,858 participants with complete ophthalmic and demographic data. Amblyopia was confirmed in 3,377 participants (15.4%), whilst it was persisting in 81.4% (2,750) of them. Compared to participants with optimal vision, participants with amblyopia were older by about 6 years on average, mainly of white ethnic background (97%), and self-reported higher disease prevalence, with similar distributions between those with resolved and persisting amblyopia (Table *42*).

	Control (unaffected vision)	Amblyopia		
		All	Resolved	Persisting
n (%)	18,481 (84.6)	3,377 (15.4)	627 (18.6)	2,750 (81.4)
Age at recruitment	51.3 (51.2; 51.4)	57.1 (56.8; 57.4)	56.3 (55.7; 57)	57.3 (57.0; 57.5)
Male participants, %	47.2 (46.5; 47.9)	47.1 (45.4; 48.9)	50.2 (46.1; 54.3)	46.5 (44.6; 48.4)
Other than white ethnic background, %	11.2 (10.8; 11.7)	3.0 (2.4; 3.6)	2.8 (1.4; 4.1)	3.1 (2.4; 3.7)
Live in a highly deprived area, %	46.3 (45.6; 47.0)	44.4 (42.7; 46.1)	42.3 (38.3; 46.4)	44.9 (43.0; 46.8)
Obesity (BMI >30kg/m^2), %	22.3 (21.7; 22.9)	25.4 (23.9; 26.9)	25.1 (21.6; 28.7)	25.4 (23.8; 27.1)
Missing, n (%)	*79 (0.43)*	*8 (0.25)*	*1 (0.17)*	*7 (0.26)*
Diabetes mellitus, %	2.8 (2.6; 3.1)	4.5 (3.7; 5.2)	3.8 (2.3; 5.4)	4.6 (3.8; 5.4)
Missing, n (%)	*72 (0.39)*	*8 (0.25)*	*0 (0.0)*	*8 (0.30)*
High blood pressure, %	19.0 (18.5; 19.6)	28.0 (26.5; 29.6)	26.2 (22.5; 29.8)	28.4 (26.7; 30.2)
Missing, n (%)	*332 (1.8)*	*94 (2.9)*	*20 (3.5)*	*74 (2.8)*
Vascular disease, %	3.0 (2.7; 3.2)	5.6 (4.8; 6.4)	5.9 (4.0; 7.9)	5.5 (4.6; 6.4)
Missing, n (%)	*48 (0.26)*	*5 (0.16)*	*2 (0.35)*	*3 (0.11)*
Metabolic Syndrome, %	0.9 (0.8; 1.1)	1.6 (1.2; 2.1)	1.3 (0.3; 2.2)	1.7 (1.2; 2.2)
Missing, n (%)	*457 (2.5)*	*110 (3.4)*	*21 (3.7)*	*89 (3.4)*

Table 42: Participants' demographic and clinical characteristics by vision status.

High deprived areas defined as being in the 4th or 5th quintile of the Townsend index of deprivation (2011). Metabolic syndrome was defined as the co-existence of medically diagnosed diabetes mellitus, high blood pressure, and obesity. Results are mean values, unless otherwise indicated, followed by 95% confidence interval.

In models adjusted for age, sex, ethnic background and deprivation participants with amblyopia had higher relative risk ratio of self-reporting one (RRR (95% CI): 1.23

(1.13; 1.34)) or two components of metabolic syndrome (1.30 (1.14; 1.49)), with highly significant associations retained for the “persisting amblyopia” group (Table *43*). Participants with “persisting amblyopia” had higher odds of self-reporting diabetes (1.26 (1.02; 1.56)) and high blood pressure (1.25 (1.14; 1.38)) and being classified as obese (1.17 (1.06; 1.28)), but no significant associations with metabolic syndrome per se were found (Table *44*). Overall confirmed amblyopia was also associated with higher odds of self-reporting diagnosis for vascular problems, with the association with “persisting amblyopia” retained significance at 0.10 level, but no associations with cancer were found for any of the groups (Table *45*).

	Number of metabolic syndrome components		
	One vs None	**Two vs None**	**Three vs None**
	RRR (95% CI)	**RRR (95% CI)**	**RRR (95% CI)**
All confirmed amblyopia vs normal vision	**1.22 (1.12; 1.34)**	**1.29 (1.13; 1.48)**	**1.40 (1.00; 1.95)**
50-59 years vs 40-49 years	**1.40 (1.30; 1.51)**	**2.18 (1.92; 2.48)**	**3.48 (2.38; 5.10)**
60-75 years vs 40-49 years	**1.87 (1.72; 2.04)**	**3.48 (3.03; 4.01)**	**6.62 (4.46; 9.82)**
Male vs Female	**1.25 (1.18; 1.34)**	**1.40 (1.26; 1.55)**	**1.88 (1.43; 2.48)**
Other than white ethnic background vs white	**1.42 (1.28; 1.58)**	**1.98 (1.68; 2.33)**	**1.82 (1.17; 2.82)**
Townsend index vs 1st quintile (least deprived)			
2nd quintile	0.93 (0.84; 1.04)	**1.31 (1.09; 1.58)**	1.00 (0.59; 1.69)
3rd quintile	1.05 (0.95; 1.17)	**1.36 (1.12; 1.64)**	1.28 (0.77; 2.12)
4th quintile	**1.12 (1.01; 1.24)**	**1.56 (1.30; 1.87)**	1.56 (0.97; 2.51)
5th quintile (most deprived)	**1.23 (1.11; 1.36)**	**2.02 (1.69; 2.41)**	**2.82 (1.79; 4.43)**
Resolved amblyopia vs normal vision	**1.26 (1.04; 1.53)**	1.18 (0.87; 1.59)	1.10 (0.51; 2.38)
50-59 years vs 40-49 years	**1.42 (1.31; 1.53)**	**2.15 (1.88; 2.46)**	**3.60 (2.39; 5.44)**
60-75 years vs 40-49 years	**1.90 (1.73; 2.08)**	**3.56 (3.07; 4.14)**	**8.07 (5.28; 12.34)**
Male vs Female	**1.25 (1.17; 1.34)**	**1.43 (1.28; 1.60)**	**1.97 (1.44; 2.68)**
Other than white ethnic background vs white	**1.43 (1.28; 1.60)**	**1.97 (1.66; 2.34)**	**2.05 (1.31; 3.21)**
Townsend index vs 1st quintile (least deprived)			
2nd quintile	0.94 (0.84; 1.06)	**1.35 (1.10; 1.66)**	1.35 (0.74; 2.48)
3rd quintile	1.08 (0.96; 1.21)	**1.38 (1.12; 1.69)**	1.62 (0.90; 2.91)
4th quintile	**1.15 (1.03; 1.28)**	**1.59 (1.30; 1.93)**	**1.81 (1.03; 3.19)**
5th quintile (most deprived)	**1.24 (1.11; 1.39)**	**2.02 (1.66; 2.47)**	**3.53 (2.06; 6.07)**
Persisting amblyopia vs normal vision	**1.22 (1.11; 1.34)**	**1.31 (1.14; 1.52)**	**1.45 (1.02; 2.05)**
50-59 years vs 40-49 years	**1.39 (1.29; 1.50)**	**2.19 (1.93; 2.50)**	**3.47 (2.36; 5.10)**
60-75 years vs 40-49 years	**1.86 (1.70; 2.02)**	**3.46 (3.00; 3.99)**	**6.77 (4.54; 10.1)**
Male vs Female	**1.26 (1.18; 1.34)**	**1.42 (1.27; 1.57)**	**1.80 (1.36; 2.37)**
Other than white ethnic background vs white	**1.42 (1.27; 1.58)**	**1.95 (1.65; 2.30)**	**1.87 (1.20; 2.91)**
Townsend index vs 1st quintile (least deprived)			
2nd quintile	0.93 (0.83; 1.04)	**1.29 (1.06; 1.56)**	0.96 (0.57; 1.63)
3rd quintile	1.06 (0.95; 1.18)	**1.35 (1.12; 1.64)**	1.27 (0.77; 2.10)
4th quintile	**1.12 (1.02; 1.25)**	**1.53 (1.28; 1.84)**	1.48 (0.92; 2.39)
5th quintile (most deprived)	**1.23 (1.10; 1.36)**	**2.04 (1.70; 2.44)**	**2.62 (1.66; 4.14)**

Table 43: Association between classification of amblyopia (i.e. i) all, ii) resolved, iii) persisting) and number of components relevant to the metabolic syndrome.

Results are relative risk ratios (95% confidence intervals)) derived from multinomial logistic regression models, adjusted for all the covariates shown in table. Estimates in bold are significant at $p < 0.05$.

	Diabetes	High blood pressure	Obesity	Metabolic syndrome	Vascular/ heart problems
	OR (95% CI)	OR (95% CI)	OR (95% CI)	OR (95% CI)	OR (95% CI)
All confirmed amblyopia vs normal vision	**1.27 (1.04; 1.55)**	**1.23 (1.13; 1.35)**	**1.16 (1.06; 1.27)**	1.27 (0.92; 1.77)	**1.19 (0.99; 1.43)**
50-59 years vs 40-49 years	**1.91 (1.56; 2.35)**	**2.20 (2.02; 2.40)**	**1.22 (1.13; 1.32)**	**2.97 (2.04; 4.35)**	**2.75 (2.18; 3.48)**
60-75 years vs 40-49 years	**3.76 (3.04; 4.65)**	**3.94 (3.59; 4.32)**	**1.18 (1.08; 1.29)**	**4.90 (3.31; 7.24)**	**7.79 (6.21; 9.76)**
Male vs Female	**1.50 (1.28; 1.76)**	**1.39 (1.30; 1.49)**	**1.16 (1.08; 1.23)**	**1.70 (1.29; 2.23)**	**2.41 (2.05; 2.83)**
Other than white ethnic background vs white	**2.63 (2.10; 3.28)**	**1.58 (1.41; 1.78)**	**1.26 (1.13; 1.40)**	1.51 (0.98; 2.34)	**1.44 (1.09; 1.89)**
Townsend index vs 1st quintile (least deprived)					
2nd quintile	1.04 (0.78; 1.40)	1.03 (0.91; 1.16)	1.11 (0.98; 1.25)	1.00 (0.59; 1.69)	**1.31 (1.00; 1.72)**
3rd quintile	1.12 (0.84; 1.50)	**1.13 (1.01; 1.27)**	**1.15 (1.02; 1.30)**	1.23 (0.74; 2.03)	1.24 (0.94; 1.63)
4th quintile	1.22 (0.93; 1.61)	**1.25 (1.11; 1.39)**	**1.28 (1.14; 1.43)**	1.44 (0.90; 2.32)	**1.42 (1.09; 1.84)**
5th quintile (most deprived)	**1.92 (1.48; 2.50)**	**1.37 (1.22; 1.53)**	**1.55 (1.38; 1.73)**	**2.46 (1.57; 3.86)**	**2.12 (1.64; 2.73)**
Resolved amblyopia vs normal vision	1.13 (0.72; 1.76)	1.16 (0.95; 1.41)	1.15 (0.95; 1.40)	1.00 (0.46; 2.15)	1.33 (0.92; 1.92)
50-59 years vs 40-49 years	**1.92 (1.54; 2.39)**	**2.21 (2.02; 2.42)**	**1.22 (1.13; 1.32)**	**3.07 (2.04; 4.62)**	**2.75 (2.15; 3.52)**
60-75 years vs 40-49 years	**3.97 (3.17; 4.98)**	**3.98 (3.60; 4.39)**	**1.23 (1.12; 1.35)**	**5.94 (3.90; 9.04)**	**8.25 (6.50; 10.5)**
Male vs Female	**1.55 (1.30; 1.84)**	**1.37 (1.28; 1.48)**	**1.19 (1.11; 1.27)**	**1.78 (1.31; 2.42)**	**2.20 (1.84; 2.62)**
Other than white ethnic background vs white	**2.67 (2.12; 3.36)**	**1.60 (1.42; 1.80)**	**1.28 (1.15; 1.42)**	1.70 (1.09; 2.66)	**1.53 (1.16; 2.03)**
Townsend index vs 1st quintile (least deprived)					
2nd quintile	1.14 (0.82; 1.60)	1.06 (0.93; 1.21)	1.10 (0.98; 1.23)	1.34 (0.73; 2.45)	**1.36 (1.00; 1.84)**
3rd quintile	1.24 (0.89; 1.72)	**1.18 (1.03; 1.34)**	**1.16 (1.04; 1.30)**	1.54 (0.85; 2.76)	**1.39 (1.03; 1.89)**
4th quintile	**1.35 (0.99; 1.84)**	**1.26 (1.12; 1.43)**	**1.26 (1.13; 1.40)**	1.66 (0.94; 2.93)	**1.40 (1.04; 1.88)**

5th quintile (most deprived)	**2.16 (1.60; 2.92)**	**1.36 (1.20; 1.55)**	**1.54 (1.38; 1.72)**	3.09 (1.80; 5.30)	**2.23 (1.68; 2.98)**
Persisting amblyopia vs normal vision	**1.29 (1.04; 1.59)**	**1.25 (1.13; 1.38)**	**1.16 (1.05; 1.28)**	1.32 (0.93; 1.86)	1.15 (0.95; 1.40)
50-59 years vs 40-49 years	**1.91 (1.55; 2.35)**	**2.21 (2.02; 2.41)**	**1.22 (1.13; 1.32)**	**2.97 (2.02; 4.36)**	**2.78 (2.19; 3.53)**
60-75 years vs 40-49 years	**3.80 (3.07; 4.71)**	**3.93 (3.58; 4.32)**	**1.17 (1.07; 1.28)**	**5.03 (3.38; 7.47)**	**8.06 (6.40; 10.1)**
Male vs Female	**1.47 (1.25; 1.72)**	**1.40 (1.30; 1.50)**	**1.16 (1.09; 1.24)**	**1.62 (1.23; 2.13)**	**2.40 (2.04; 2.83)**
Other than white ethnic background vs white	**2.65 (2.12; 3.32)**	**1.58 (1.40; 1.78)**	**1.26 (1.13; 1.40)**	**1.56 (1.00; 2.42)**	**1.44 (1.09; 1.90)**
Townsend index vs 1st quintile (least deprived)					
2nd quintile	1.01 (0.75; 1.36)	1.00 (0.89; 1.13)	1.10 (0.98; 1.23)	0.96 (0.57; 1.63)	**1.33 (1.01; 1.75)**
3rd quintile	1.08 (0.81; 1.45)	**1.13 (1.01; 1.28)**	**1.16 (1.04; 1.30)**	1.21 (0.73; 2.01)	1.23 (0.93; 1.63)
4th quintile	1.16 (0.88; 1.53)	**1.24 (1.11; 1.39)**	**1.26 (1.13; 1.40)**	1.37 (0.85; 2.22)	**1.39 (1.06; 1.82)**
5th quintile (most deprived)	**1.85 (1.42; 2.41)**	**1.37 (1.22; 1.53)**	**1.54 (1.38; 1.72)**	**2.29 (1.45; 3.61)**	**2.14 (1.65; 2.77)**

Table 44: Association between classification of amblyopia (i.e. i) all, ii) resolved, iii) persisting) and cardiometabolic diseases diagnosed by medical doctor.

Results are odds ratios (95% confidence intervals)) derived from binary logistic regression models, adjusted for all the covariates shown in table. Estimates in bold are significant at p <0.05. Metabolic syndrome was not medically diagnosed but was defined as being medically diagnosed with diabetes, high blood pressure and obesity.

	Body mass index, kg/m2	Systolic blood pressure, mmHg	Diastolic blood pressure, mmHg	Glycated haemoglobin, mmol/mol
	b (95% CI)	b (95% CI)	b (95% CI)	b (95% CI)
All confirmed amblyopia vs normal	**0.41 (0.23; 0.59)**	**0.66 (0.02; 1.29)**	-0.02 (-0.40; 0.37)	**0.48 (0.26; 0.70)**
50-59 yrs vs 40-49 yrs	**0.50 (0.35; 0.64)**	**6.87 (6.36; 7.37)**	**2.39 (2.08; 2.70)**	**1.80 (1.62; 1.97)**
60-75 yrs vs 40-49 yrs	**0.60 (0.44; 0.77)**	**14.0 (13.5; 14.6)**	**2.36 (2.00; 2.71)**	**2.99 (2.79; 3.20)**
Male vs Female	**0.99 (0.87; 1.12)**	**6.65 (6.21; 7.08)**	**3.83 (3.57; 4.10)**	**0.58 (0.43; 0.73)**
Other than white ethnic background	**0.56 (0.35; 0.78)**	**1.63 (0.87; 2.39)**	**1.95 (1.50; 2.41)**	**2.84 (2.56; 3.11)**
Townsend index vs 1st quintile (least				
2nd quintile	**0.21 (0.00; 0.43)**	-0.47 (-1.21; 0.27)	-0.23 (-0.67; 0.22)	**0.23 (-0.03; 0.49)**
3rd quintile	**0.39 (0.18; 0.60)**	-0.02 (-0.75; 0.72)	0.14 (-0.31; 0.58)	**0.32 (0.06; 0.57)**
4th quintile	**0.50 (0.30; 0.71)**	-0.42 (-1.13; 0.29)	-0.02 (-0.44; 0.41)	**0.28 (0.03; 0.52)**
5th quintile (most deprived)	**0.94 (0.73; 1.15)**	-0.21 (-0.93; 0.52)	**0.43 (-0.01; 0.87)**	**0.83 (0.58; 1.08)**
Resolved amblyopia vs normal	**0.46 (0.07; 0.84)**	-0.21 (-1.57; 1.15)	-0.24 (-1.07; 0.59)	**0.48 (0.02; 0.94)**
50-59 yrs vs 40-49 yrs	**0.49 (0.34; 0.64)**	**6.91 (6.38; 7.43)**	**2.42 (2.10; 2.74)**	**1.81 (1.62; 1.99)**
60-75 yrs vs 40-49 yrs	**0.64 (0.46; 0.82)**	**13.8 (13.2; 14.5)**	**2.40 (2.01; 2.79)**	**2.92 (2.70; 3.14)**
Male vs Female	**1.07 (0.94; 1.20)**	**6.85 (6.39; 7.31)**	**3.86 (3.58; 4.14)**	**0.63 (0.47; 0.79)**
Other than white ethnic background	**0.57 (0.35; 0.80)**	**1.79 (1.02; 2.56)**	**2.00 (1.54; 2.47)**	**2.83 (2.56; 3.11)**
Townsend index vs 1st quintile (least				
2nd quintile	0.19 (-0.03; 0.42)	-0.60 (-1.39; 0.18)	-0.28 (-0.76; 0.20)	**0.24 (-0.03; 0.51)**
3rd quintile	**0.37 (0.15; 0.60)**	-0.07 (-0.85; 0.71)	0.04 (-0.43; 0.52)	**0.29 (0.02; 0.56)**
4th quintile	**0.50 (0.28; 0.71)**	-0.54 (-1.29; 0.21)	-0.09 (-0.55; 0.36)	**0.32 (0.06; 0.58)**
5th quintile (most deprived)	**0.91 (0.69; 1.13)**	-0.41 (-1.18; 0.36)	0.35 (-0.12; 0.82)	**0.84 (0.57; 1.10)**
Persisting amblyopia vs normal	**0.40 (0.20; 0.60)**	**0.83 (0.14; 1.51)**	0.02 (-0.39; 0.44)	**0.48 (0.24; 0.73)**
50-59 yrs vs 40-49 yrs	**0.50 (0.35; 0.64)**	**6.83 (6.32; 7.34)**	**2.38 (2.07; 2.69)**	**1.79 (1.61; 1.97)**
60-75 yrs vs 40-49 yrs	**0.60 (0.43; 0.77)**	**14.2 (13.6; 14.8)**	**2.40 (2.04; 2.76)**	**2.99 (2.78; 3.20)**
Male vs Female	**1.02 (0.89; 1.14)**	**6.77 (6.33; 7.21)**	**3.89 (3.62; 4.16)**	**0.59 (0.43; 0.74)**
Other than white ethnic background	**0.55 (0.33; 0.76)**	**1.64 (0.88; 2.40)**	**1.96 (1.50; 2.42)**	**2.80 (2.53; 3.08)**
Townsend index vs 1st quintile (least				
2nd quintile	**0.22 (0.01; 0.44)**	-0.51 (-1.26; 0.24)	-0.24 (-0.69; 0.22)	0.20 (-0.06; 0.46)
3rd quintile	**0.40 (0.18; 0.61)**	0.00 (-0.74; 0.75)	0.13 (-0.32; 0.58)	**0.30 (0.04; 0.56)**
4th quintile	**0.50 (0.29; 0.70)**	-0.41 (-1.13; 0.31)	0.01 (-0.42; 0.45)	0.22 (-0.03; 0.47)
5th quintile (most deprived)	**0.96 (0.75; 1.17)**	-0.16 (-0.90; 0.57)	**0.47 (0.03; 0.91)**	**0.80 (0.54; 1.05)**

Table 45: Association between classification of amblyopia (i.e. i) all, ii) resolved, iii) persisting) with cardiometabolic biomarkers.

Results are beta coefficients (95% confidence intervals) derived from linear regression models, adjusted for all the covariates shown in table. Estimates in bold are significant at $p < 0.05$.

Results from the propensity score matching, to account for the observed differences in age and ethnic background and marginal differences in sex and deprivation between the amblyopia and optimal vision groups, indicate a significant difference in the probability of self-reporting diagnosis of high blood pressure or being classified as an obese participant between the two groups. In particular, the probability remained higher for participants in the amblyopia group, with percentage point differences between amblyopia and optimal vision of about 4 units for self-reporting diagnosis for high blood pressure and about 3 units for being classified as obese. Participants with amblyopia had increased risk of MI (HR 1.38 (1.11; 1.72)), and all-cause death (HR: 1.36 (1.15; 1.60)) but no significant association with stroke was found (1.20 (0.89; 1.62), Table *46* and Table *47*).

		Amblyopia		
	Control (unaffected vision)	**All**	**Resolved**	**Persisting**
n (%)	17,860 (84.5)	3,269 (15.5)	605 (18.5)	2,664 (81.5)
Age, years	51.3	57.1	56.3	57.3
	(51.2; 51.4)	(56.8; 57.3)	(55.7; 57.0)	(57.0; 57.5)
Male participants, n (%)	8,491 (47.5)	1,535 (47.0)	298 (49.3)	1,237 (46.4)
	(46.8; 47.5)	(45.2; 48.7)	(45.2; 53.3)	(44.5; 48.4)
Other than white ethnic background, n (%)	1,985 (11.1)	100 (3.1)	16 (2.6)	84 (3.2)
	(10.7; 11.6)	(2.5; 3.7)	(1.6; 4.4)	(2.5; 3.9)
Live in a highly deprived area, n (%)	7,179 (40.2)	1273 (38.9)	220 (36.4)	1053 (39.5)
	(39.5; 40.9)	(37.3; 40.6)	(35.5; 40.4)	(37.7; 41.4)
Previous myocardial infarction, n (%)	207 (1.2)	63 (1.9)	9 (1.5)	54 (2.0)
	(1.0; 1.3)	(1.5; 2.5)	(0.7; 2.9)	(1.5; 2.7)
Incident myocardial infarction, n (%)[1]	326 (1.8)	120 (3.7)	25 (4.2)	95 (3.6)
	(1.7; 2.1)	(3.1; 4.5)	(2.8; 6.2)	(3.0; 4.5)
Previous stroke, n (%)	169 (0.9)	49 (1.5)	9 (1.5)	40 (1.5)
	(0.8; 1.1)	(1.1; 2.0)	(0.8; 2.9)	(1.1; 2.1)
Incident stroke, n (%)[1]	182 (1.0)	64 (2.0)	6 (1.0)	58 (2.2)
	(0.9; 1.2)	(1.5; 2.5)	(0.4; 2.3)	(1.7; 2.9)
Died during study period, n (%)	516 (2.9)	215 (6.6)	26 (4.3)	189 (7.1)
	(2.7; 3.1)	(5.8; 7.5)	(2.9; 6.3)	(6.2; 8.2)

Table 46**:** Baseline characteristics of the cohort for survival analysis.

Highly deprived areas defined as being in the 4th or 5th quintile of the Townsend index of deprivation (2011). [1]Proportions for incident disease take, as denominator, those without a previous event.

	Myocardial infarction	All-cause stroke	All-cause death
	HR (95% CI)	**HR (95% CI)**	**HR (95% CI)**
All confirmed amblyopia vs normal vision	**1.38 (1.11; 1.72)**	1.20 (0.89; 1.62)	**1.36 (1.15; 1.60)**
Per 10-year increase in age	**2.08 (1.83; 2.36)**	**2.58 (2.16; 3.09)**	**2.80 (2.52; 3.11)**
Male vs Female	**3.03 2.45; 3.74)**	**1.20 (0.89; 1.62)**	**1.50 (1.29; 1.74)**
Other than white ethnic background vs white	0.98 (0.67; 1.44)	1.31 (0.80; 2.14)	**1.33 (1.00; 1.77)**
Townsend index vs 1st quintile (least deprived)			
2nd quintile	0.92 (0.69; 1.23)	1.22 (0.83; 1.78)	1.15 (0.92; 1.45)
3rd quintile	0.81 (0.60; 1.09)	1.15 (0.78; 1.70)	1.11 (0.88; 1.41)
4th quintile	0.98 (0.73; 1.32)	0.95 (0.62; 1.45)	1.25 (0.98; 1.58)
5th quintile (most deprived)	**1.35 (1.02; 1.79)**	1.34 (0.89; 1.99)	**1.65 (1.31; 2.07)**
Resolved amblyopia vs normal vision	**1.56 (1.03; 2.36)**	0.62 (0.27; 1.40)	0.91 (0.61; 1.36)
Per 10-year increase in age	**2.01 (1.75; 2.31)**	**2.62 (2.15; 3.19)**	**2.78 (2.47; 3.12)**
Male vs Female	**1.56 (1.03; 2.36)**	**1.62 (1.20; 2.17)**	**1.42 (1.20; 1.68)**
Other than white ethnic background vs white	1.02 (0.69; 1.51)	1.33 (0.80; 2.21)	1.25 (0.92; 1.70)
Townsend index vs 1st quintile (least deprived)			
2nd quintile	0.93 (0.67; 1.30)	1.02 (0.66; 1.58)	1.08 (0.83; 1.41)
3rd quintile	0.85 (061; 1.20)	0.95 (0.61, 1.49)	1.05 (0.80; 1.37)
4th quintile	1.02 (0.73; 1.42)	0.94 (0.59; 1.49)	1.18 (0.90; 1.55)
5th quintile (most deprived)	1.32 (0.96; 1.83)	1.24 (0.79; 1.96)	1.53 (1.17; 1.99)
Persisting amblyopia vs normal vision	**1.36 (1.07; 1.72)**	1.33 (0.98; 1.81)	**1.45 (1.21; 1.72)**
Per 10-year increase in age	**2.06 (1.81; 2.35)**	**2.58 (2.15; 3.09)**	**1.11 (1.10; 1.12)**

Male vs Female	**3.03 (2.44; 3.76)**	**1.51 (1.16; 1.95)**	**1.47 (1.26; 1.71)**
Other than white ethnic background vs white	1.01 (0.69; 1.48)	1.31 (0.80; 2.15)	1.33 (1.00; 1.77)
Townsend index vs 1st quintile (least deprived)			
2nd quintile	0.94 (0.70; 1.26)	1.23 (0.84; 1.80)	1.14 (0.90; 1.44)
3rd quintile	0.80 (0.59; 1.10)	1.09 (0.73; 1.63)	1.06 (0.83; 1.35)
4th quintile	0.99 (0.73; 1.34)	0.93 (0.61; 1.44)	1.22 (0.96; 1.56)
5th quintile (most deprived)	1.29 (0.96; 1.72)	1.32 (0.88; 1.97)	**1.60 (1.27; 2.02)**

Table 47: Association between classification of amblyopia (i.e. i) all, ii) resolved, iii) persisting) and incident cardiovascular events and dementia.

Results are hazard ratios (95% confidence intervals)) derived from Cox proportional hazards models. The full model adjusted for all the covariates shown in table. Estimates in bold are significant at $p < 0.05$.

Imaging outcomes

From an initial cohort of 67,272 participants who underwent retinal imaging in UKBB at the baseline visit, there were 35,061 controls (35,061 eyes), and 831 individuals with unilateral amblyopia included in the image analyses (Table *48*). Affected individuals in the complete cases analysis contributed 623 eyes with amblyopia and 663 fellow eyes to analysis. Individuals with amblyopia were older and more likely to self-report white ethnic background. Compared to control eyes, affected eyes had have worse visual acuity (0.38 (0.37) versus 0.00 (0.19) LogMAR, p<0.001) , were more hyperopic (1.68 (3.9) versus -0.46 (2.40) dioptres, p<0.001) and had thinner mRNFL (25.2 (5.5) versus 25.8 (2.8) microns, p<0.001) and mGC-IPL (87.9 (8.7) versus 90.1 (8.1) microns, p<0.001) and increased arteriolar calibre (63.7 (6.9) versus 61.7 (5.9) units, p<0.001) venular calibre (71.9 (8.8) versus 68.0 (7.1), p<0.001) and retinal fractal dimension (1.478 (0.04) versus 1.484 (0.04), p<0.001). Optic nerve height was also smaller (130.5 (20.5) versus 132.2 (19.2), p = 0.035). Compared to control eyes, fellow (unaffected) eyes of individuals with persisting unilateral amblyopia had slightly worse visual acuity (0.01 (0.17) versus 0.00 (0.19) logMAR, p = 0.027) and were more hyperopic (0.83 (3.1) versus 1.68 (3.9) dioptres, p <0.001). Fellow eyes also exhibited thinner mRNFL (25.4 (2.4) versus 25.8 (2.8) microns, p <0.001) and mGC-IPL (89.2 (7.6) versus 90.1 (8.1) microns, p =0.002) and greater arteriolar calibre (62.7 (6.3) versus 61.7 (5.9) units, p <0.001) and venular calibre (69.7 (7.4) versus 68.0 (7.1), p<0.001). There was no difference in fractal dimension or optic nerve morphology between fellow and control eyes (Table *49*).

	Control	Amblyopia	Fellow
	(n=35,061)	**(n=623)**	**(n=663)**
Age, years	54.9	55.7	55.6
	(54.8; 55.0)	(55.1; 56.3)	(55.0; 56.2)
Male participants, n (%)	15,650 (44.6)	262 (42.1)	271 (40.9)
	(44.1; 45.2)	(38.1; 46.0)	(37.1; 44.7)
Other than white ethnic background, n (%)	32,272 (92.0)	602 (96.6)	646 (97.4)
	(91.7; 92.3)	(94.9; 97.9)	(95.9; 98.5)
Live in a highly deprived area, n (%)	9,579 (27.3)	179 (28.7)	195 (29.4)
	(26.8; 27.8)	(25.2; 32.5)	(26.0; 33.0)
Smoking status, n (%)			
Previous	11,662 (33.2)	214 (34.3)	216 (32.6)
	(32.8; 33.8)	(30.6; 38.2)	(29.0; 36.3)
Current	3,332 (9.5)	62 (10.0)	75 (11.3)
	(9.2; 9.8)	(7.7; 12.8)	(9.0; 14.0)
Alcohol drinking status, n (%)			
Previous	32,402 (92.4)	580 (93.1)	620 (93.5)
	(92.1; 92.7)	(90.8; 95.0)	(91.4; 95.3)
Current	26,792 (76.4)	467 (75.0)	498 (75.1)
	(76.0; 76.7)	(71.4; 78.3)	(71.6; 78.4)
Body mass index, kg/m^2	27.1	27.3	27.3
	(27.0; 27.2)	(26.9; 27.7)	(26.9; 27.7)
Diabetes mellitus, n (%)	1,219 (3.5)	20 (3.2)	24 (3.6)
	(3.3; 3.7)	(2.0; 4.9)	(2.3; 5.3)
High blood pressure, n (%)	8,269 (23.6)	156 (25.0)	165 (24.9)
	(23.1; 24.0)	(21.7; 28.6)	(21.6; 28.4)
Refractive error, dioptres (D)	-0.46	1.68	0.83
	(-0.48; -0.44)	(1.37; 1.99)	(0.69; 1.07)
Visual acuity, logMAR	0.00	0.38	0.01
	(-0.002; 0.002)	(0.35; 0.41)	(-0.003; 0.02)
Retinal layer thicknesses			
mRNFL, µm	25.8	25.2	25.4 (2.4)
	(25.7; 25.8)	(24.8; 25.6)	(25.2; 25.6)
mGC-IPL, µm	90.1	87.9	89.2
	(90.0; 90.2)	(87.2; 88.6)	(88.2; 89.8)
Retinovascular indices			
Arteriolar calibre, µm	61.7	63.7	62.7
	(61.6; 61.8)	(63.2; 64.2)	(62.2; 63.2)
Venular calibre, µm	68	71.9	69.7
	(67.9; 68.1)	(61.6; 61.8)	(69.1; 70.3)
Fractal dimension, units	1.484	1.478	1.482
	(1.484; 1.484)	(1.475; 1.481)	(1.479; 1.485)
Distance tortuosity, units	3.43	3.61	3.43
	(3.42; 3.44)	(3.49; 3.73)	(3.32; 3.54)
Optic nerve morphology			
Cup height, units	62.9	61.8	62
	(62.7; 63.1)	(60.4; 63.2)	(60.7; 63.3)
Cup width, units	60.4	59.7	60

	(60.2; 60.6)	(61.6; 61.8)	(58.6; 61.4)
Disc height, units	132.2	130.5	131.3
	(132.0; 132.4)	(128.8; 132.2)	(129.6; 133.0)
Disc width, units	125.1	123.6	124.6
	(124.9; 125.3)	(121.8; 125.4)	(122.9; 126.3)

Table 48: Baseline characteristics of the cohort with retinal imaging data.

High deprived areas defined as being in the 4th or 5th quintile of the Townsend index of deprivation (2011). Data for optic nerve morphology were available for 32,525 controls, 544 cases and 583 fellow eyes. Results are mean values, unless otherwise indicated, followed by 95% confidence interval.

	Affected eye		Fellow/ Unaffected eye	
Outcomes	**Base model**	**Full model**	**Base model**	**Full model**
	b (95% CI)	**b (95% CI)**	**b (95% CI)**	**b (95% CI)**
Retinovascular				
Arteriolar calibre, per SD	0.04 (-0.03; 0.12)	0.05 (-0.03; 0.12)	-0.01 (-0.09; 0.06)	-0.01 (-0.09; 0.06)
p-value	0.27	0.23	0.72	0.70
Venular calibre, per SD	0.29 (0.21; 0.36)	0.29 (0.21; 0.36)	0.07 (0.00; 0.15)	0.07 (0.00; 0.14)
p-value	$8.7x10^{-14}$	4.3x10-14	0.048	0.06
Distance tortuosity, per SD	0.11 (0.03; 0.19)	0.11 (0.03; 0.19)	-0.01 (-0.08; 0.07)	-0.01 (-0.08; 0.07)
p-value	0.005	0.005	0.84	0.84
Fractal dimension, per SD	-0.23 (-0.30; -0.16)	-0.23 (-0.30; -0.16)	-0.08 (-0.15; -0.01)	-0.08 (-0.15; -0.01)
p-value	$8.4x10^{-10}$	$9.1x10^{-10}$	0.025	0.027
Retinal layer thickness				
mRNFL, per µm	-0.19 (-0.41; 0.04)	-0.19 (-0.41; 0.04)	-0.15 (-0.36; 0.06)	-0.15 (-0.36; 0.07)
p-value	0.10	0.10	0.16	0.18
mGC-IPL, per µm	-2.84 (-3.47; -2.22)	-2.85 (-3.47; -2.22)	-1.16 (-1.76; -0.55)	-1.14 (-1.74; -0.54)
p-value	$<1x10^{-16}$	$<1x10^{-16}$	$1.7x10^{-4}$	$2.0x10^{-4}$
Optic nerve morphology				
Cup height, per SD	-0.11 (-0.19; -0.02)	-0.11 (-0.19; -0.02)	-0.06 (-0.14; 0.02)	-0.06 (-0.14; 0.02)
p-value	0.013	0.014	0.14	0.14
Cup width, per SD	-0.05 (-0.14; 0.03)	-0.05 (-0.14; 0.03)	-0.01 (-0.09; 0.07)	-0.01 (-0.09; 0.07)
p-value	0.22	0.23	0.74	0.76
Disc height, per SD	-0.17 (-0.25; -0.08)	-0.17 (-0.25; -0.08)	-0.08 (-0.16; 0.00)	-0.08 (-0.16; 0.00)
p-value	$9.2x10^{-5}$	$1.0x10^{-6}$	0.06	0.07
Disc width, per SD	-0.13 (-0.21; -0.04)	-0.13 (-0.21; -0.04)	-0.05 (-0.13; 0.03)	-0.05 (-0.13; 0.03)
p-value	0.003	0.004	0.23	0.24

Table 49**:** Differences in retinal morphology between affected and unaffected (fellow) eyes of individuals with amblyopia compared to controls.

Results are beta coefficients (95% confidence intervals) derived from linear regression. Base model was adjusted for age, sex, ethnicity, socioeconomic deprivation and refractive error. Full model was the base model additionally adjusted for hypertension, diabetes mellitus, alcohol consumption, smoking history, and body mass index. mGC-IPL: macular ganglion cell-inner plexiform layer, mRFNL: macular retinal nerve fibre layer, SD: standard deviation.

On fully adjusted analysis, amblyopic eyes had significantly increased venular calibre (0.29 per SD (95% CI: 0.21, 0.36), p = 4.3 x 10-14) and distance tortuosity (0.11 per SD (0.03, 0.19), p=0.005) and lower fractal dimension (-0.23 per SD (-0.30, -0.16), p=9.1x10-10, Table *49*). They also had thinner mGC-IPL (-2.85 microns (-3.47, -2.22), p<1x10-16). Regarding optic nerve morphology, affected eyes had reduced disc height (-0.17 (-0.25, -0.08), p=1x10-6) and disc width (-0.13 (-0.21, -0.04), p=0.004) compared to controls. There was some evidence of decreased cup height (-0.11 (-0.19, -0.02), p=0.014).

When stratifying by visual acuity, both “persisting” and “resolved” cases had wider venular calibre and thinner mGC-IPL. However, only “persisting” eyes had significant differences in optic nerve morphology, including smaller cup height (-0.12 (-0.21, -0.02), p=0.017), disc height and disc width (both -0.17 (-0.27, -0.08), p= 3.6 x 10-4, Table *50*).

Unaffected fellow eyes also showed differences to controls. Fellow eyes had lower retinal fractal dimension (-0.08 per SD (-0.15, -0.01), p=0.027) and thinner mGC-IPL (-1.14 microns (-1.74, -0.54), p=2.0 x 10-4, Table *50*).

	Amblyopia			
Outcome	**Persisting (*n* cases = 483)**		**Resolved (*n* cases = 140)**	
	b (95% CI)	***p*-value**	**b (95% CI)**	***p*-value**
Retinovascular				
Arteriolar calibre, per SD	0.00 (-0.09; 0.08)	0.92	0.17 (0.01; 0.32)	0.033
Venular calibre, per SD	0.24 (0.16; 0.33)	$2.7x10^{-8}$	0.37 (0.22; 0.53)	$3.1x10^{-6}$
Distance tortuosity, per SD	0.14 (0.05; 0.23)	0.002	0.04 (-0.12; 0.20)	0.63
Fractal dimension, per SD	-0.20 (-0.28; -0.12)	$2.7x10^{-6}$	-0.30 (-0.45; -0.15)	$1.3x10^{-4}$
Retinal layer thickness				
mRNFL, per µm	-0.11 (-0.36; 0.14)	0.37	-0.50 (-0.95; -0.05)	0.029
mGC-IPL, per µm	-2.97 (-3.68; -2.27)	$1x10^{-16}$	-1.70 (-2.99; -0.40)	0.010
Optic nerve morphology				
Cup height, per SD	-0.12 (-0.21; -0.02)	0.017	-0.07 (-0.25; 0.11)	0.43
Cup width, per SD	-0.09 (-0.19; 0.00)	0.05	0.09 (-0.09; 0.27)	0.30
Disc height, per SD	-0.17 (-0.27; -0.08)	$3.6x10^{-4}$	-0.14 (-0.32; 0.03)	0.11
Disc width, per SD	-0.17 (-0.27; -0.08)	$3.6x10^{-4}$	0.04 (-0.14; 0.22)	0.64

Table 50: Association between amblyopia and retinal imaging outcome measures stratified into persisting (logMAR visual acuity ≥0.06) and resolved (logMAR visual acuity <0.06) amblyopia in the fully adjusted model.

All models were adjusted for age, sex, ethnicity, socioeconomic deprivation, refractive error, diabetes mellitus, alcohol consumption, smoking history, and body mass index. Results are beta coefficients (95% confidence interval) derived from linear regression models. mGC-IPL: macular ganglion cell-inner plexiform layer, mRFNL: macular retinal nerve fibre layer, SD: standard deviation.

6.5.4 Discussion

My report indicates that adults with persisting unilateral amblyopia have an increased burden of non-communicable disease beyond that which can be explained by sociodemographic profile. Affected individuals are more likely to report features suggestive of cardiovascular disease and metabolic syndrome and retinal morphological differences, typically seen in these systemic disorders, were observed in both the affected and putatively 'normal' fellow eye providing further evidence of more widespread dysregulation in amblyopia. In addition, amblyopic eyes with persisting visual deficit exhibit differences in optic nerve morphology compared to individuals with optimal vision. This is not the case for amblyopic eyes with resolved deficit (i.e. normal visual acuity).

In the absence of any similar-sized prospective cohort with retinal imaging and ophthalmic variables, I leveraged the population-based UKBB. Notwithstanding its strengths of large sample size and deep phenotyping data, there are some limitations with use of this cohort. The sociodemographic and lifestyle profile of UKBB recruits may not reflect that of the wider UK - compared to the general population, UKBB participants are less likely to smoke, drink alcohol, and suffer from obesity[158] prompting debate over the importance of representativeness in epidemiological analysis[500–502]. UKBB also had an exceptionally low response to invitation rate (5.5%) dwarfing that typically recommended[503,504]. Countering this is that risk factor associations estimated from UKBB do generalise well to nationwide registry and survey data for England and Scotland[505] and, in our previous report[477] investigating functional outcomes in individuals with persisting unilateral amblyopia in UKBB, I observed associations consistent with other prospective cohort

studies[478,506,507]. Our hierarchical approach for defining amblyopia and amblyogenic risk factors integrated the ophthalmic assessment, national health service data and self-reported outcomes to mitigate potential recall and misclassification bias. However, a sizeable proportion of the original cohort were excluded as a result, particularly due to the coexistence of other eye conditions. Given that our strategy has previously shown comparable estimates of amblyopia prevalence to that reported in other British population-based analyses[478,508], and most eye conditions, such as glaucoma, cataract and age-related macular degeneration all have strong associations with cardiometabolic disease[509–514], I argue that our approach mitigates confounding risk and more likely to estimate the true association between amblyopia and NCDs.

Amblyopia and non-communicable diseases

In my analysis, individuals with persisting amblyopia had greater odds of reporting diabetes mellitus, obesity, and hypertension on adjusted analysis. There are no studies to which I can directly compare my findings and only few reports have examined overall perception of general health in those with amblyopia in adulthood[477,478]. Participants in the 1958 British Birth Cohort with amblyopia were no more likely than those unaffected to report poor health[478]. However, it should be noted that the number affected was relatively small (51 individuals with moderate/severe amblyopia) and participants responded to this question aged 33, before most NCDs emerge. In contrast, our previous report examining health and well-being outcomes in adult life in UKBB (age range 40-69 years), found individuals with persisting unilateral amblyopia were more likely to report adverse general health although we did not examine individual diseases or risk factors[477]. What mediates

the association between persisting amblyopia and NCD burden in later life remains unclear however previous and the current work suggests psychosocial factors do not contribute significantly. Although affected individuals may exhibit worse motor skills and reading speed than those unaffected in childhood[515–517], educational and employment attainment as well as economic outcomes and socioeconomic status in adulthood appear similar[477,478,507]. Individuals with amblyopia do report poorer mental health and emotional wellbeing however, it is unknown whether this translates into harmful lifestyle behaviours[477,518,519]. In the current report, there were no differences in smoking status or alcohol consumption between those with amblyopia and those without and significant differences in retinal morphology persisted even after adjustment. Instead, one potential biological factor unifying amblyopia and NCDs may be shared early-life factors, as outlined by David Barker's hypothesis on the *developmental origins of adult disease*[520]. Individuals exposed to a harmful intrauterine environment or exhibiting features of restriction are more likely to develop both neurodevelopmental impairment and cardiometabolic disease in later life. Amblyopia may therefore simply represent an early consequence of an adverse perinatal environment which ultimately culminates in pathological cardiometabolic physiology (*Figure 34*). Due to the large amounts of missing data for perinatal data (e.g. birthweight data missing for 48%) and the risk of recall bias, I did not probe this potential link further although further work examining this association is warranted. A recent Mendelian Randomization experiment has suggested a causal link between low birthweight and self-reported amblyopia[521].

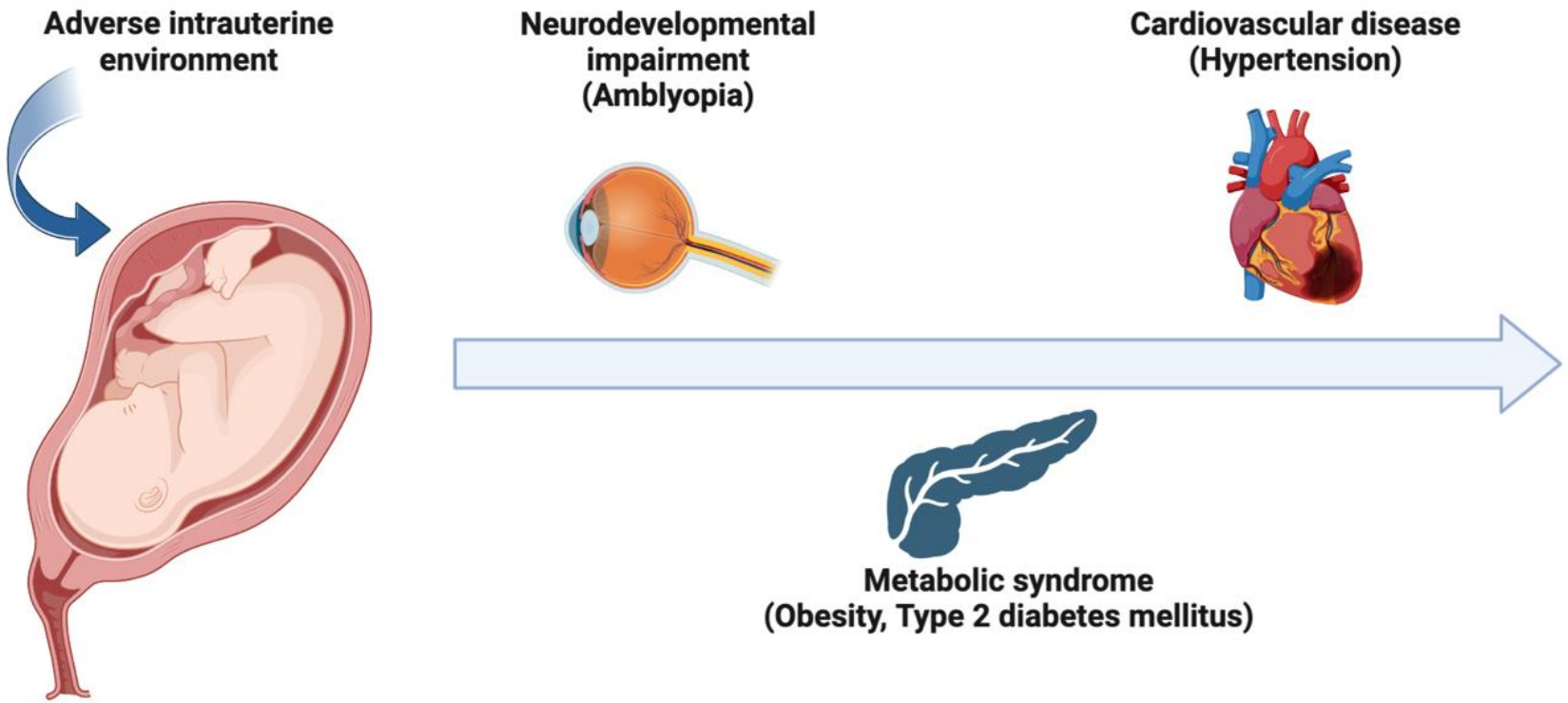

Figure 34: Fetal origins of adult disease as pertains to amblyopia.

Harmful intrauterine influences result in an increased risk of neurodevelopment impairment, such as amblyopia, in early life as well as cardiometabolic dysfunction manifesting in adulthood.

Differences in retinal morphology between individuals with and without amblyopia were seen in both the affected and unaffected fellow eye suggesting more diffuse impairment of the microvascular and central nervous systems. To contextualise my findings, the adjusted mGC-IPL thickness difference in the affected (-2.85 microns) and unaffected fellow (-1.14 microns) eye was similar to eighteen and eight years of older age respectively using a previous report using UKBB data[15]. On the one hand, a neurodevelopmental etiology seems most likely given the timing of amblyopia onset. Even children with unilateral amblyopia exhibit differences in both eyes[321,522] and a recent meta-analysis of OCT angiography, a newer modality capturing retinal vessel density, concluded that while amblyopic eyes have significantly different vessel density to healthy controls, there was no difference between affected and unaffected fellow eyes[322]. On the other hand, associations between retinal morphology and NCDs may also contribute. Individuals with incipient metabolic syndrome and cardiovascular disease exhibit thinner mGC-IPL[125,357]. Moreover, retinal fractal dimension, which was significantly lower in both eyes of individuals with unilateral amblyopia, is negatively associated with hypertension and cardiovascular disease[523,524] complementing my findings on NCD prevalence. Longitudinal studies are needed to determine whether degenerative mechanisms could partially account for my retinal findings.

Persisting visual deficit and optic nerve morphology

Optic disc size is known to vary with age, sex, and refractive error[525,526]. Adjusting for these and other factors, I found amblyopic eyes with persisting visual deficit exhibited significantly smaller optic disc height and width compared to healthy controls. This contrasted with ‘recovered’ (i.e. normal visual acuity) amblyopic eyes

where there was no difference. The natural question is whether these structural differences represent a primary cause of amblyopia (and therefore a potential prognostic factor for treatment success) or indicate a secondary consequence of visual deficit. Although foveal abnormalities of individuals with amblyopia are bilateral and symmetrical regardless of interocular differences in visual acuity[321], my evidence suggests this is not the case for the optic nerve. Structural abnormalities of the optic nerve, such as hypoplasia, are present from birth and are associated with low birthweight, maternal smoking and preterm birth[527]. Indeed, Lempert proposed that asymmetric neurodevelopment secondary to a gestational insult might result in asymmetric optic nerve hypoplasia and impaired binocular interactions[528]. Moreover, major risk factors for amblyopia, including strabismus and anisometropia, are also not typically present in a persistent form from birth and may result from a primary structural abnormality[321,529,530]. Collectively, these findings suggest eyes with persisting amblyopia may have subclinical or missed optic nerve hypoplasia. I advocate optic nerve imaging in studies examining outcomes of amblyopia treatment to ascertain whether disc morphology may discriminate between children likely to experience visual recovery.

6.5.5 Summary

My report shows that individuals with persisting unilateral amblyopia have an increased burden of NCD. This is corroborated by differences in retinal morphology, which resemble those seen in cardiometabolic disease, and are present in both the affected and unaffected fellow eye. The finding that amblyopic eyes with a persisting visual deficit have smaller optic disc size warrants further investigation as a potential predictor of amblyopia treatment response, especially given the growing offering of

sophisticated optic disc measurement algorithms twinned with minimally invasive retinal imaging technology. While a causal link cannot be established based on this report, healthcare professionals should be cognisant to the potential of more widespread systemic dysregulation in patients affected by childhood amblyopia.

7. Prediction

The association between retinal features and both neurodegenerative and cardiovascular diseases has been consistently reproduced across several population-based cohorts. However, translation of these group-level differences to individual-level prediction has been limited, especially for all-cause dementia. This chapter focuses on the utility of retinal imaging-derived features for individual-level prediction for all-cause dementia and major adverse cardiovascular events. In particular, I investigate whether retinal imaging confers additional benefits beyond traditional risk factors in discriminating those who go on to develop all-cause dementia or a cardiovascular event.

7.1 All-cause dementia

7.1.1 Introduction

Nearly ten million people develop dementia each year. From an estimated 57 million individuals affected in 2019[531], the World Health Organization estimates the total number to double every 20 years[532]. Yet, even in high income countries, 20-50% of those with dementia remain undiagnosed[533]. With growing evidence that lifestyle modification may prevent or delay up to 40% of dementia cases and the advent of novel therapies in early disease, motivation is greater than ever to identify those at risk or already affected by the disease[30,32]. Current approaches typically rely on cognitive questionnaires, blood tests and brain imaging but these have limitations for whole-population detection approaches given their cost, availability, invasiveness and need for expert interpretation[534]. Such strategies are even less feasible in low- and middle-income countries where 71% of new cases by 2050 are anticipated to occur[535].

Several retinal morphological associations with dementia have now been described using the two most common retinal imaging modalities – colour fundus photography (CFP) and optical coherence tomography (OCT). Individuals with Alzheimer's disease (AD), the most common form of dementia, have reduced thickness of the peripapillary retinal nerve fibre layer (RNFL) and ganglion cell-inner plexiform layer (GCIPL) on OCT[139]. Thinner RNFL is associated with greater risk of developing AD among healthy volunteers. Microvascular differences, which are typically quantified on CFP, are also evident in dementia. Calibre and fractal dimension of the retinal vessels are reduced in those with vascular dementia, a finding consistent with other forms of cerebrovascular disease[123,124].

However, translating the discovery of these potential prognostic factors into individual risk prediction has thus far been limited partly due to small numbers of cases, sociodemographically homogenous cohorts and single retinal imaging modalities. All models described thus far have focused on prevalent disease yet strategies for reducing the development of dementia are likely to be more effective when implemented early[474].

Leveraging the health informatic opportunity afforded by a unified single care provider (the UK National Health Service), I used AlzEye, a retinal imaging database linked with nationally collected systemic disease data from a large socio-demographically diverse cohort of patients attending a network of ophthalmic hospitals under the provisions of Moorfields Eye Hospital NHS Foundation Trust (MEH). Here, I report the development and validation of clinical prediction models for all-cause dementia using multimodal retinal imaging features extracted through automated segmentation methods, such as deep learning. I, firstly, investigate the incremental benefit of retinal imaging over traditional risk factors for all-cause dementia prediction. Secondly, I externally validate models in over 30,000 participants (0.6-4.1%) in both hospital eye and community-based settings. Finally, I characterise model fairness and robustness by examining discrimination in socially (e.g. ethnic minority, greater levels of deprivation) and clinically (e.g. AMD, glaucoma) meaningful subgroups.

7.1.2 Methods

Datasets and Participants

This study used data from two separate cohort studies – AlzEye and UKBB.

As described earlier, the AlzEye project is a retrospective cohort study of all patients aged 40 years and over who have attended the hospitals of Moorfields Eye Hospital NHS Foundation Trust (MEH) between January 1st 2008 and April 1st 2018. Further details about AlzEye are provided in section 4.1 The AlzEye project.

As described in more detail in section 4.2 UK Biobank, UKBB is a prospective population-based multicentre cohort study of approximately 500,000 participants residing in the UK, registered with the NHS and residing within 25 miles of a study assessment centre. Participants aged 40-69 years were initially recruited between 2006 and 2010 through postal invitation. In addition to questionnaires and physical measurements, a subset of 82,911 UKBB participants additionally retinal imaging at either the baseline visit (*n*=67,321) or the first repeat visit (*n*= 15,590).

Case definitions

All-cause dementia was defined as a hospital admission with one of the following ICD-10 codes: E51.2, F00, F01, F02, F03, F10.6, F10.7, G30, or G31.0 (Table *1*). This was derived from previous work by Brown et al evaluating the agreement between HES admitted patient care data and primary care data, through general practitioner surveys and the Clinical Practice Research Datalink (CPRD) where a positive predictive value of 0.85 (95% CI: 0.80, 0.89) was estimated[151]. For our

subgroup validation sets, I also explicitly defined Alzheimer's disease (F00, G30) and vascular dementia (F01).

Incident all-cause dementia cases and controls were defined using a rules-based approach at an image-level. The entry date was defined as the date of the respective retinal image which must have preceded a hospital admission where there was no recording of an all-cause dementia ICD-10 code. The at-risk period was then estimated from the aforementioned date until either i) a hospital admission where all-cause dementia was recorded (event) or ii) a hospital admission where all-cause dementia was not recorded (censored). Therefore, participants' at-risk period ended at the time of their last hospital admission as we could not guarantee that they had not developed all-cause dementia after this.

For the UKBB cohort, individuals having all-cause dementia at the time of retinal imaging were identified through both preceding hospital admissions data and the self-report on the touchscreen questionnaire. The at-risk period was from this date until either an all-cause dementia (defined algorithmically based on hospital admissions, death certificates and primary care records, UKBB field ID: 42018) or end of the available hospital admissions data (1st December 2020).

Retinal imaging including quality control

Retinal imaging in this study included macula-centred CFP and OCT. Candidate predictor variables were extracted from retinal images using two segmentation models. CFP images were processed using the openly available deep learning-based pipeline, AutoMorph (4.3.1 Colour fundus photography). AutoMorph

automatically assigns a categorical outcome of image quality as ‘good’, ‘okay’ or ‘poor’. For this study, I only included images categorised as ‘good’ or ‘ok’. Further details on AutoMorph have been previously published[193].

Retinal sublayer thicknesses were extracted from OCT images using the Topcon Advanced Boundary Segmentation (TABS) tool (version 1.6.2.6, section 4.3.2 Optical coherence tomography). TABS takes the OCT volume, in its proprietary file format, and outputs segmentations of individual retinal sublayers at the level of the B-scan using dual-scale gradients. I estimated sublayer thicknesses in spatially conventional macular regions, as defined by the Early Treatment for Diabetic Retinopathy Study (Figure *18*). With 9 relevant regions and 9 individual sublayers, tabular data from OCT included 81 continuous features. TABS provides additional metadata for each image to establish scan quality based on segmentation error, movement artifact and poor quality. For image quality control, I excluded the poorest 10% of images based on these specific image quality control metadata, applying the same method to both cohort datasets.

For the remaining images, multiple outliers were noted for most variables. Manual inspection of such images showed these almost always be segmentation errors when considering the most extreme 3% of sublayer thickness measurements. Therefore, I assigned the value as missing for subsequent multiple imputation methods for the 3% most extreme values for each retinal sublayer thickness. I did not opt for alternative strategies, such as trimming (i.e. removing the observation entirely) or winsorisation (i.e. replacing the outlier measurements traditionally with the respectively smallest/largest observation) for two primary reasons – firstly, due to

the greater risk of selection bias (older, multimorbid patients are more likely to have poor segmentation quality) and secondly, I noted on manual inspection that outlier values did not represent true extreme measurements but rather algorithmic errors and thus winsorisation was inappropriate.

Candidate predictors

Candidate predictors included demographics, clinical details, and retinal imaging-derived features (*Table 51*). Demographics included age, biological sex, ethnicity, and socioeconomic status. Ethnicity was self-reported by the individual according to categories defined by the UK Office for National Statistics. Response options were then aggregated into four groupings of Asian, Black, White and Other Ethnic Groups (*Table 29*). Socio-economic status (SES) was defined through the Index of Multiple Deprivation (IMD), a measure of relative deprivation across seven domains (income, employment, education, health, and barriers to housing and services, crime and living environment) within the United Kingdom provided by the Ministry of Housing, Communities & Local Government[162]. SES measures were estimated by converting the patient's postcode to Lower Super Output Areas (LSOA) and cross-referencing with tables for the IMD 2010. For UKBB, scores for the IMD are provided as part of the UKBB showcase.

Clinical details included diagnoses of diabetes mellitus and hypertension. For AlzEye, these were defined using ICD-10 (hypertension: I10, I15, diabetes mellitus, E10, E11) and coded as present if recorded on the hospital admission prior the retinal image date assuming that these diseases are chronic conditions, which are only rarely reversible. For UKBB, I used self-reported illness data from the

touchscreen questionnaire data for defining the presence of hypertension and diabetes mellitus as this was collected concurrently at the time of retinal imaging. Retinal imaging candidate predictors were chosen based on known associations from literature review (Table *51*). Among the 9 retinal sublayers segmented by TABS, I did not include the choroid as the accuracy of segmentation of this layer in older Topcon devices is unclear.

Demographics		Age	Continuous
		Biological sex	Binary
		Ethnicity	Categorical
		Socioeconomic status (IMD)	Continuous
Clinical		Diabetes mellitus	Binary
		Hypertension	Binary
Retinal imaging	Colour fundus photography	Disc height	Continuous
		Disc width	Continuous
		Cup height	Continuous
		Cup width	Continuous
		Cup-disc ratio	Discrete
		Calibre[1]	Continuous
		Fractal dimension[1]	Continuous
		Vessel density[1]	Continuous
		Distance tortuosity[1]	Continuous
		Squared curvature tortuosity[1]	Continuous
		Tortuosity density[1]	Continuous
	Optical coherence tomography	Total retinal thickness	Continuous
		Nerve fibre layer	Continuous
		Ganglion cell-inner plexiform layer	Continuous
		Inner nuclear layer	Continuous
		Outer plexiform layer	Continuous
		Myoid zone layer	Continuous
		Ellipsoid zone layer	Continuous
		Retinal pigment epithelium layer	Continuous
		Choroidal layer	Continuous

Table 51: Candidate predictor variables considered for all-cause dementia prediction models.

[1]Note that these indices were available separately for arteriolar and venular vessels.

Sample size

Estimation of sample size for clinical prediction model development was conducted using the work of Riley et al[226]. Further details are in Section 4.7.3 Sample size and Appendix 2: Sample size calculation.

Model development

Development and validation of all-cause dementia prediction models are reported in line with the recommendations of the Transparent Reporting of a multivariable prediction model for individual prognosis or diagnosis (TRIPOD) statement[536]. I used Cox proportional hazards to model time-to-event (all-cause dementia) against demographic, clinical and retinal imaging-based candidate predictor variables, which were defined a priori according to literature review and clinical applicability (Table 52). Models were developed separately for diabetic and non-diabetic participants, firstly due to the differing potential setting (e.g. diabetic screening programme versus community-based screening) and the known impact of diabetes on OCT and CFP-based indices. For each task, four models were developed.

- Traditional risk factors alone (TRF): age, sex, ethnicity, IMD, hypertension
- TRF and CFP-derived oculomic markers
- TRF and OCT-derived oculomic markers
- TRF, CFP-derived and OCT-derived oculomic markers

The assumption of proportional hazards was checked visually and statistically using scaled Schoenfeld residuals against transformed time[213].

Data reduction and collinearity

I used recommended techniques on redundancy analysis for variable reduction, examining predictors that could be predicted from others using the coefficient of determination (R^2) [537]. For both arteriolar and venular features from AutoMorph, the fractal dimension and vessel density were highly correlated as were the distance tortuosity and squared curvature tortuosity (*Figure 35*, *Figure 36*). The former variables in both pairs were retained given they have greater evidence in the literature for associations with all-cause dementia[22,23,119,123,124,128].

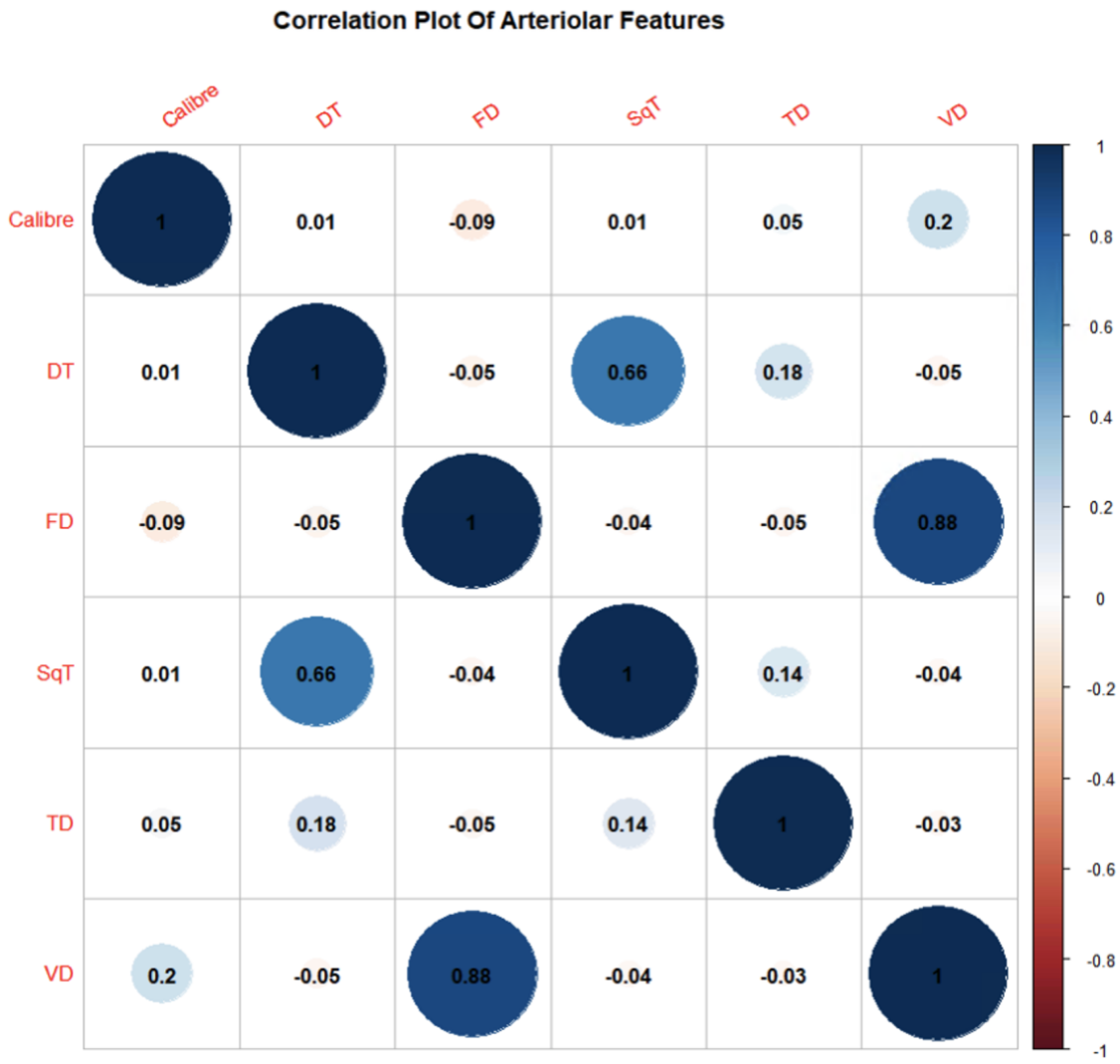

Figure 35: Correlation plot of arteriolar features derived from AutoMorph.

DT: distance tortuosity, FD: fractal dimension, SqT: squared curvature tortuosity, TD: tortuosity density, VD: vessel density.

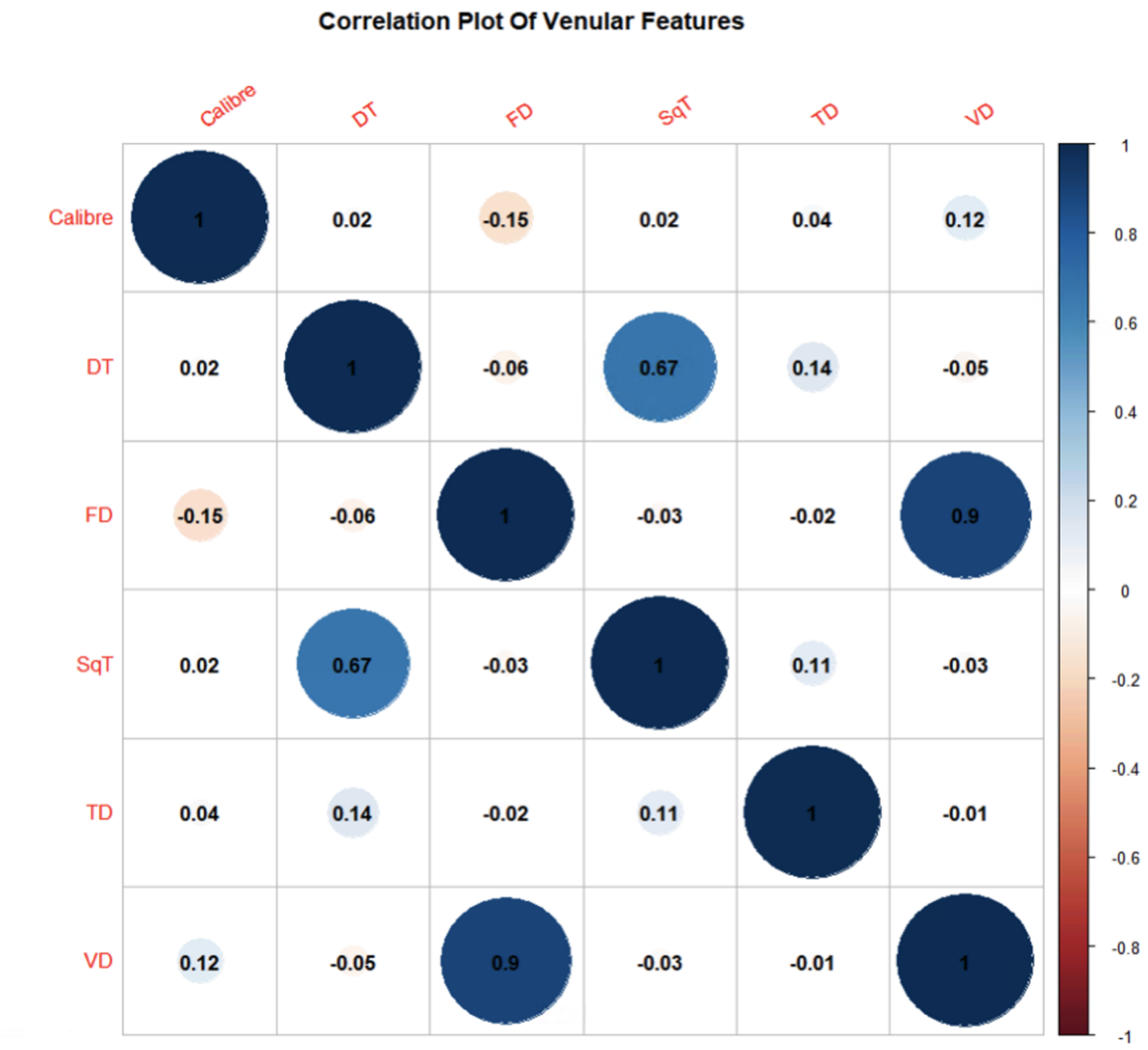

Figure 36: Correlation plot of venular features derived from AutoMorph.

DT: distance tortuosity, FD: fractal dimension, SqT: squared curvature tortuosity, TD: tortuosity density, VD: vessel density.

I next examined collinearity with overall retinovascular indices derived from the binary vessel map segmented by AutoMorph (e.g. fractal dimension of all vessels versus arteriolar fractal dimension). Calibre and fractal dimension from the binary vessel map (all vessels) highly correlated with their respective features from the arteriole-venule map (*Figure 37*). I therefore excluded these two features leaving ten included retinovascular features as:

- Arteriolar
    - Calibre
    - Distance tortuosity
    - Fractal dimension
    - Tortuosity density
- Venular
    - Calibre
    - Distance tortuosity
    - Fractal dimension
    - Tortuosity density
- All
    - Distance tortuosity
    - Tortuosity density

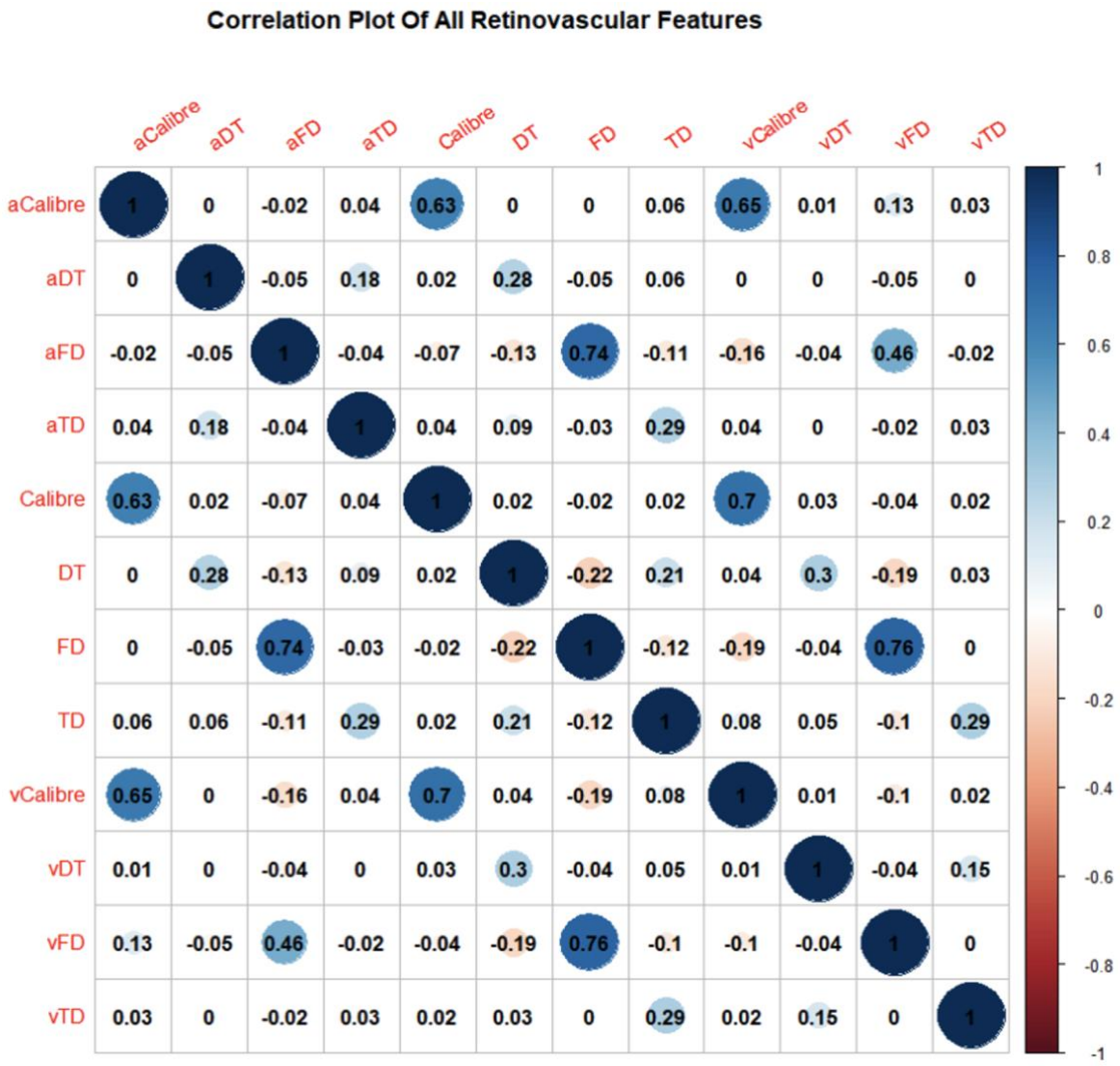

Figure 37: Correlation plot of all retinovascular features derived from AutoMorph.

aDT: arteriolar distance tortuosity, aFD: arteriolar fractal dimension, aTD: arteriolar tortuosity density, vDT: venular distance tortuosity, vFD: venular fractal dimension, TD: venular tortuosity density.

For sublayer thicknesses of TABS, the total retinal thickness was highly correlated with many other sublayers and I therefore did not include the total retinal thickness. Otherwise, correlation analysis of both the inner (*Figure 38*) and the outer ETDRS segments (*Figure 39*) revealed strong relationships between other spatial regions of the same sublayer but in general, not with other sublayers. Exceptions include the ellipzoid zone and RPE and nerve fibre layer and GCIPL for the inner subfields (*Figure 38*) and the nerve fibre layer and GCIPL for the outer layers (*Figure 39*). I opted not to exclude these layers because i) one would expect correlation in thicknesses between these different layers (e.g. the ellipsoid zone and RPE are intimately related in their structure and function), ii) differences in one sublayer provide additional information beyond that of an adjacent one as highlighted, for example by the GCIPL and inner nuclear layer in Parkinson's disease (Section 6.3 Parkinson's disease).

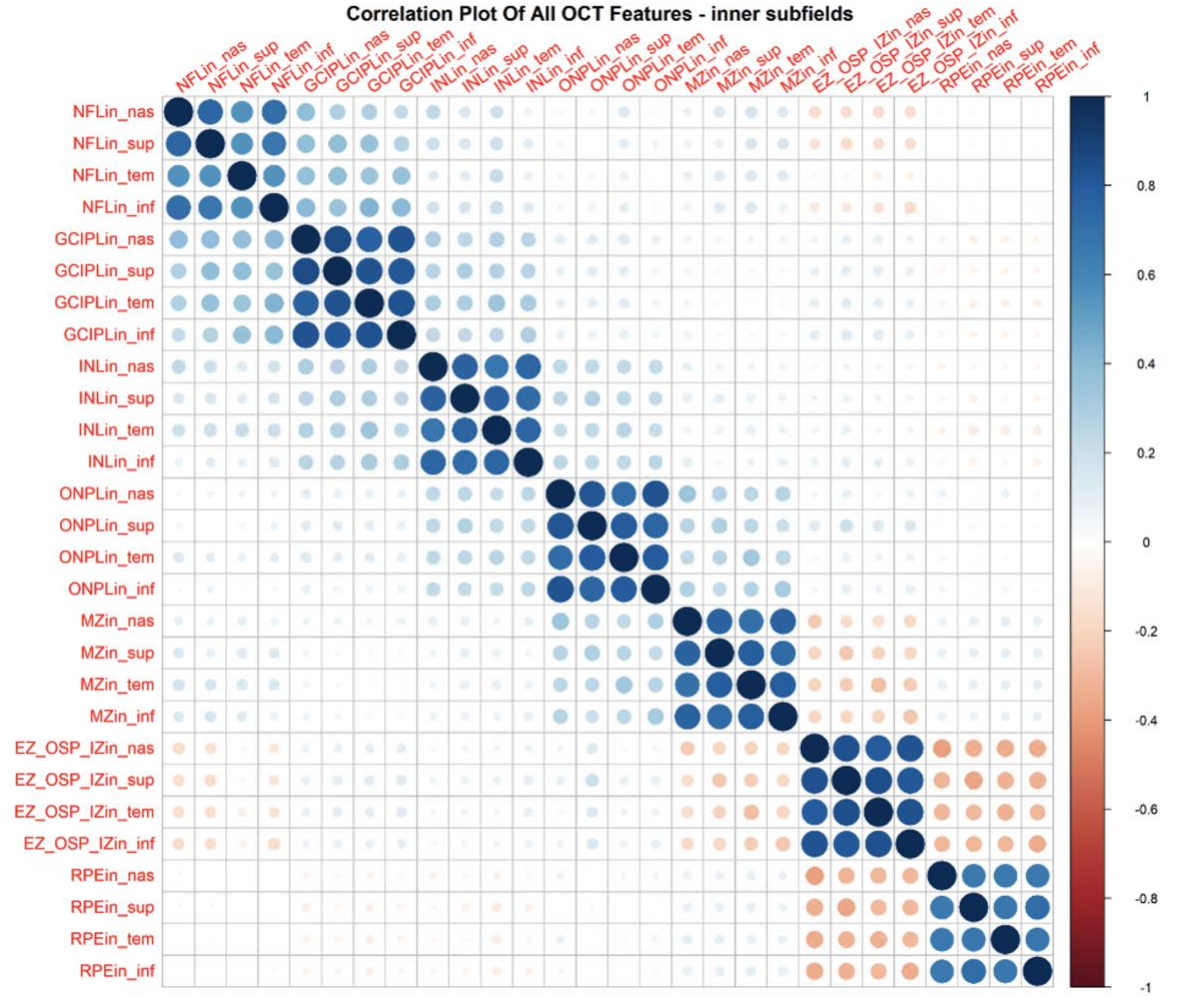

Figure 38: Correlation plot of retinal sublayer thicknesses from the inner ETDRS segments derived from the Topcon Advanced Boundary Segmentation tool.

NFL: nerve fibre layer, GCIPL: ganglion cell-inner plexiform layer, INL: inner nuclear layer, ONPL: outer plexiform layer, MZ: myoid zone, EZ_OSP_IZ: ellipsoid zone, RPE: retinal pigment epithelium

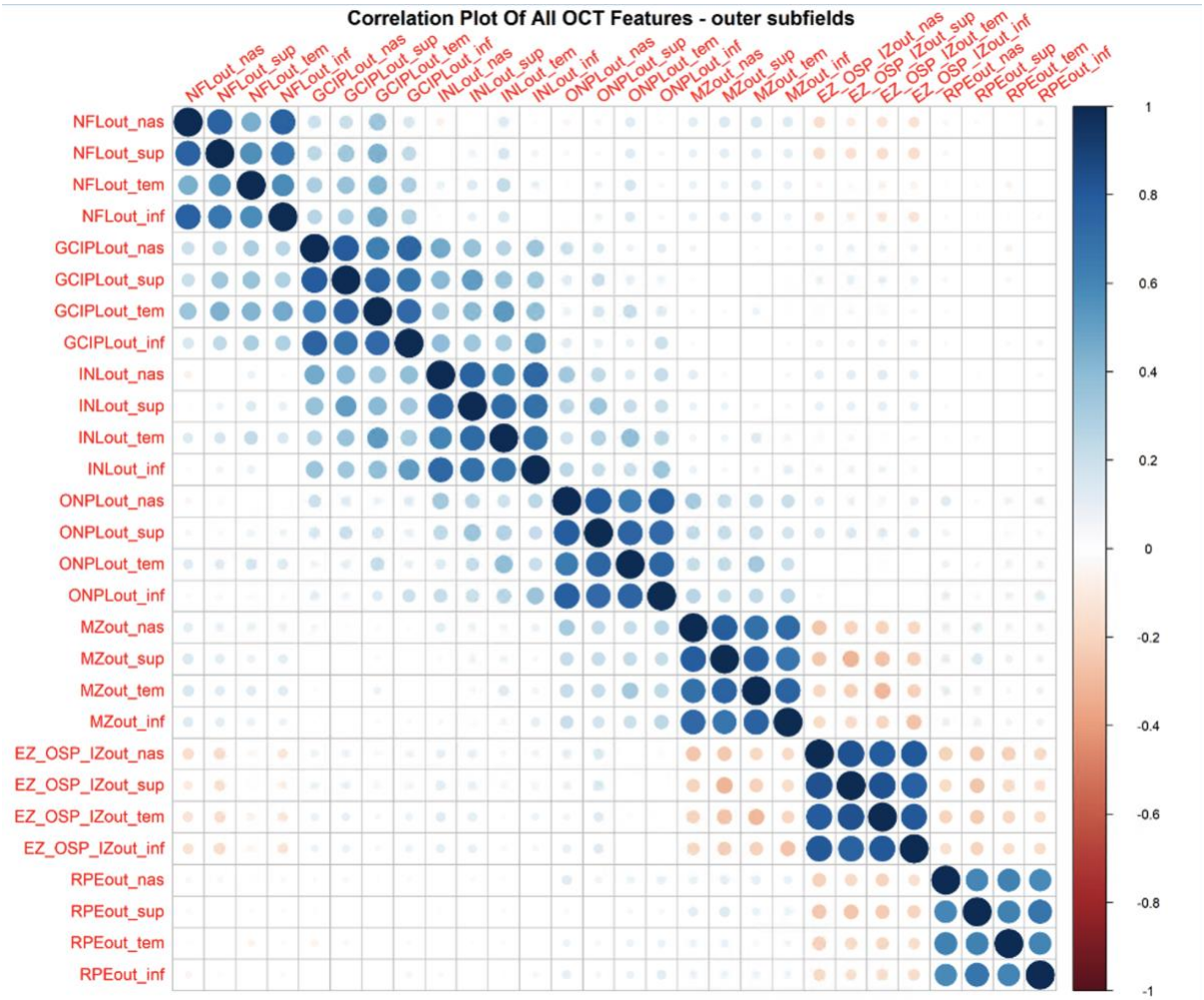

Figure 39: Correlation plot of retinal sublayer thicknesses from the outer ETDRS segments derived from the Topcon Advanced Boundary Segmentation tool.

NFL: nerve fibre layer, GCIPL: ganglion cell-inner plexiform layer, INL: inner nuclear layer, ONPL: outer plexiform layer, MZ: myoid zone, EZ_OSP_IZ: ellipsoid zone, RPE: retinal pigment epithelium

Variable transformations, non-linear relationships and interactions

Most retinal imaging-based predictor variables were normally distributed. However, distance tortuosity required log-transformation. Fractal dimension was negatively skewed and therefore subtracted from a constant and a log-transformation subsequently applied. I modelled non-linear relationships between the outcome and predictor variables using restricted cubic splines, a flexible function defined by polynomials (*Figure 40*). I assessed fit visually and statistically using the Akaike Information Criterion (AIC) and the Bayesian Information Criteria (BIC, *Table 52*). I used a default of four knots (this provided visually and statistically the best fit) with locations defined using percentiles of the marginal distribution[537–539].

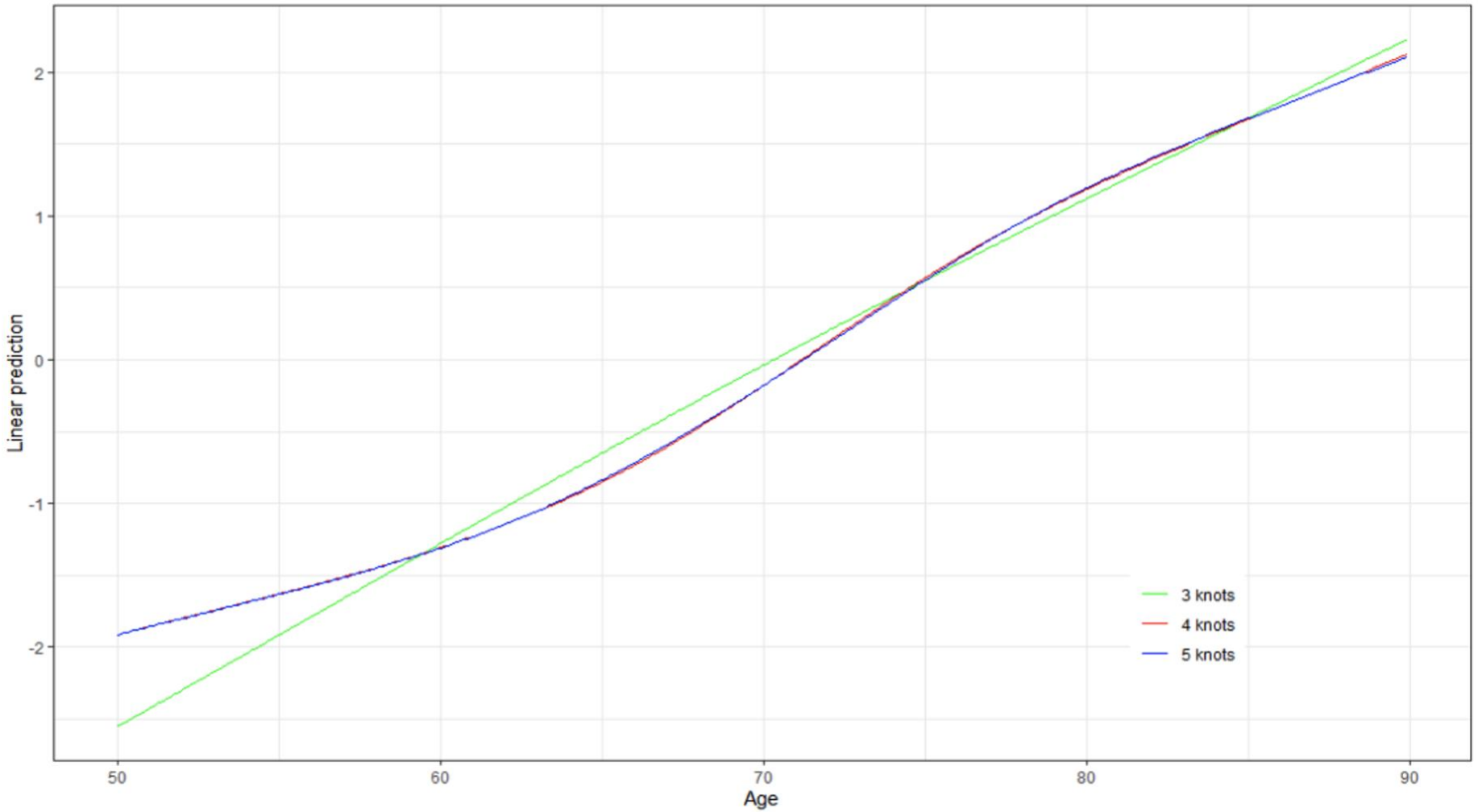

Figure 40: Restricted cubic splines modelling incident all-cause dementia against age with 3, 4 or 5 knots.

		AIC	BIC
Continuous		118480.3	118486.9
RCS (Number of knots)	3	118479.2	118492.6
	4	**118441.2**	**118461.2**
	5	118441.7	118468.3

Table 52: Goodness-of-fit assessed through the Akaike Information Criterion (AIC) and the Bayesian Information Criterion (BIC) for models of all-cause dementia and age, the latter as a continuous variable and using restricted cubic splines.

The lowest numbers, indicating the most preferable models, are in bold.

Missing data

There was missing data for retinal imaging variables and for ethnicity (*Figure 41*). For retinal imaging variables, this resulted either from general segmentation error and therefore no output for certain sublayer thicknesses or because thicknesses were in the outlier distribution and therefore replaced as missing. I assumed these were missing at random given i) previous evidence on the determinants of missingness of self-reported demographic data in healthcare[387] and ii) missing retinal imaging features are strongly associated with various sociodemographic and clinical features and image quality. Most frequently, this was for metrics regarding optic nerve morphology (~19%) followed by ethnicity (~10%). For OCT, this was approximately 6%. I performed conditional multi-level (respecting clustering by eye and by patient) multiple imputation using chained equations for sporadic and systematically missing data ten times with ten iterations (model convergence

observed at this level for all retinal imaging variables) using multinomial logistic regression models for ethnicity and predictive mean matching for continuous variables[220,540–543]. Imputation was performed using all exposure and outcome variables, in their raw form. Pooled adjusted regression coefficients and their respective standard errors were estimated using Rubin's rule.[216]

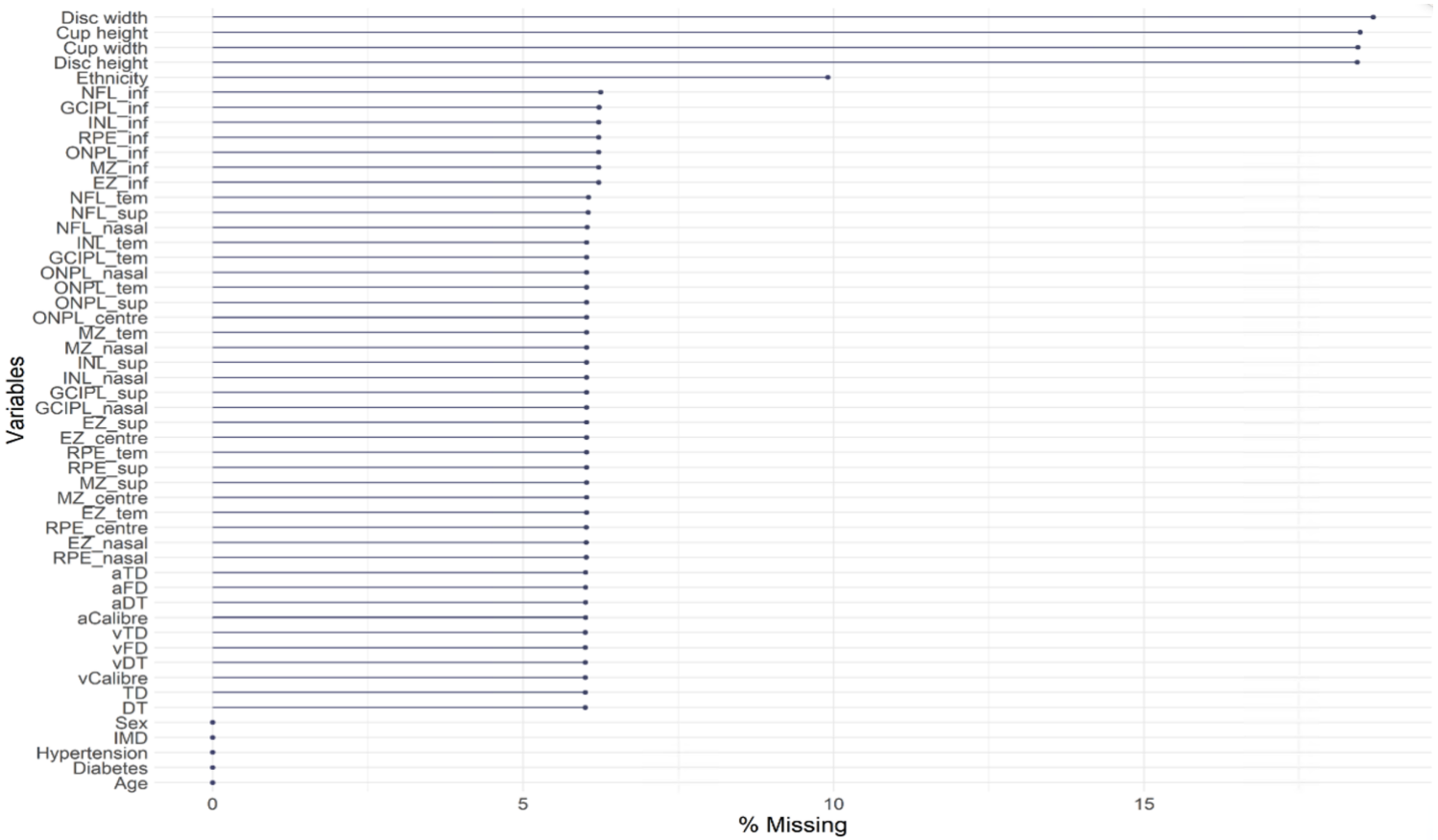

Figure 41: Distribution of missingness in predictor variables.

NFL: nerve fibre layer, GCIPL: ganglion cell-inner plexiform layer, INL: inner nuclear layer, ONPL: outer plexiform layer, MZ: myoid zone, EZ: ellipsoid zone, RPE: retinal pigment epithelium. aTD: arteriolar tortuosity density, aFD: arteriolar fractal dimension, aDT: arteriolar distance tortuosity, vTD: venular tortuosity density, vFD: venular fractal dimension, vDT: venular distance tortuosity, IMD: index of multiple deprivation

Performance

Model performance was first investigated in the development dataset (apparent performance) and then further assessed using bootstrap resampling (internal performance) with the difference between the two representing the 'optimism' in performance. Performance was then assessed on a further split-sample validation (internal test). Discrimination for time-to-event model was through Harrell's concordance (*C*) statistic and Uno's *C* statistic (a variant of Harrell's which incorporates a time dependent weighting to more fully account for censoring)[544]. 95% confidence intervals were estimated through bootstrapping. Calibration was assessed through two means – i) mean calibration was estimated using the expected (average predicted risk of event at fixed time point) and observed (complementary to the Kaplan-Meier curve) ratio at 5 years and ii) and visually through calibration slopes.

I externally validated all models in test sets from five separate cohorts. Four cohorts (External validation Moorfields - Croydon, St Ann's, Mile End and Sir Ludwig Guttman) were derived from hospital eye settings while the fifth dataset, UKBB (External validation UKBB), was a population-based prospective cohort study of healthy volunteers. All external test sets included only one image per individual with the laterality chosen randomly.

Sensitivity analyses

I investigated model discrimination across several clinically important subgroups to assess for any differential performance in the MEH external validation cohort. I evaluated all models in test sets stratified into groups of the following variables – i)

Age deciles (50-59, 60-69, 70-79, 80-89), ii) biological sex, iii) ethnicity, iv) socioeconomic status as defined by the IMD less deprived and more deprived using the median, v) age-related macular degeneration presence, vi) glaucoma presence and v) subtypes of dementia stratified into Alzheimer's disease versus vascular dementia.

All analyses were conducted in R version 4.1.0 (R Core Team, 2021. R Foundation for Statistical Computing, Vienna, Austria) and used the `survival`, `survminer`, `boot`, and `riskRegression` packages[221,545–547]. I followed published guidance and adapted code on assessing the performance of Cox's proportional hazards model from McLernon et al and the STRATOS initiative[548].

7.1.3 Results

Description of dataset

For the development dataset, 27,472 patients with a median follow-up of 679 (164.5-1193.5) days and a median age of 71.9 (64.2-79.6) years were included. During the study period, 1,419 patients (5.2%) developed all-cause dementia (*Figure 42*). The internal test set included 6,837 patients (median age 71.8 [64.1-79.5] years), of which 352 (5.1%) developed all-cause dementia. The median follow-up time was 683 (175.5-1190.5) days.

The Moorfields external validation cohort had a median age of 73.0 (15.1) years and among 3,408 patients, 141 (4.1%) developed incident all-cause dementia during the study period (*Figure 43*). The UKBB external validation cohort was significantly younger than the development and other validation cohorts – a total of 29,206 participants had a median age of 56.0 (14.0) years and an event proportion of 0.6% (171 participants). Median follow-up time was much higher in the UKBB cohort at 3,867 (3,777-3.957) days owing to the initial retinal imaging visit being in the 2006-2010 period (*Figure 44*).

There were many key differences in the sociodemographic and clinical profile of the Moorfields cohorts versus those of UKBB. As well as UKBB participants being substantially younger, they were also predominantly White (92.2%) and they were less likely to be diabetic (3.8%) or hypertensive (22.2%, *Table 53*).

		Development (*n*=27,472)	Internal test (*n*=6,837)	External validation Moorfields (*n*=3,408)	External validation Biobank (*n*=29,206)
Age median (IQR)		71.9 (15.4)	71.8 (15.4)	73.0 (15.1)	56.0 (14.0)
Sex *n* (%)	**Female**	13,903 (50.6)	3,463 (50.7)	1,790 (52.5)	15,893 (54.4)
	Male	13,569 (49.4)	3,374 (49.3)	1,618 (47.5)	13,313 (45.6)
Ethnicity *n* (%)	**Asian (South)**	6,272 (22.8)	1,530 (22.4)	531 (15.6)	708 (2.4)
	Black	2,335 (8.5)	607 (8.9)	480 (14.1)	686 (2.3)
	White	11,226 (40.9)	2,809 (41.1)	1,443 (42.3)	26,929 (92.2)
	Other/Mixed	3,967(14.4)	989 (14.5)	242 (7.1)	883 (3.0)
	Unknown	3,672 (13.4)	902 (13.2)	712 (20.9)	-
IMD median (IQR)		20.7 (19.5)	21.1 (19.7)	24.7 (22.6)	13.1 (14.5)
Hypertension *n* (%)		16,610 (60.5)	4,064 (59.5)	2,280 (66.9)	6,472 (22.2)
Diabetes mellitus *n* (%)		10,290 (37.5)	2,553 (37.3)	1,346 (39.5)	1,109 (3.8)
Incident all-cause dementia *n* (%)		1,419 (5.2)	352 (5.1)	141 (4.1)	171 (0.6)

Table 53: Baseline characteristics of the development, internal and external test sets for all-cause dementia prediction.

IMD: index of multiple deprivation, IQR: interquartile range.

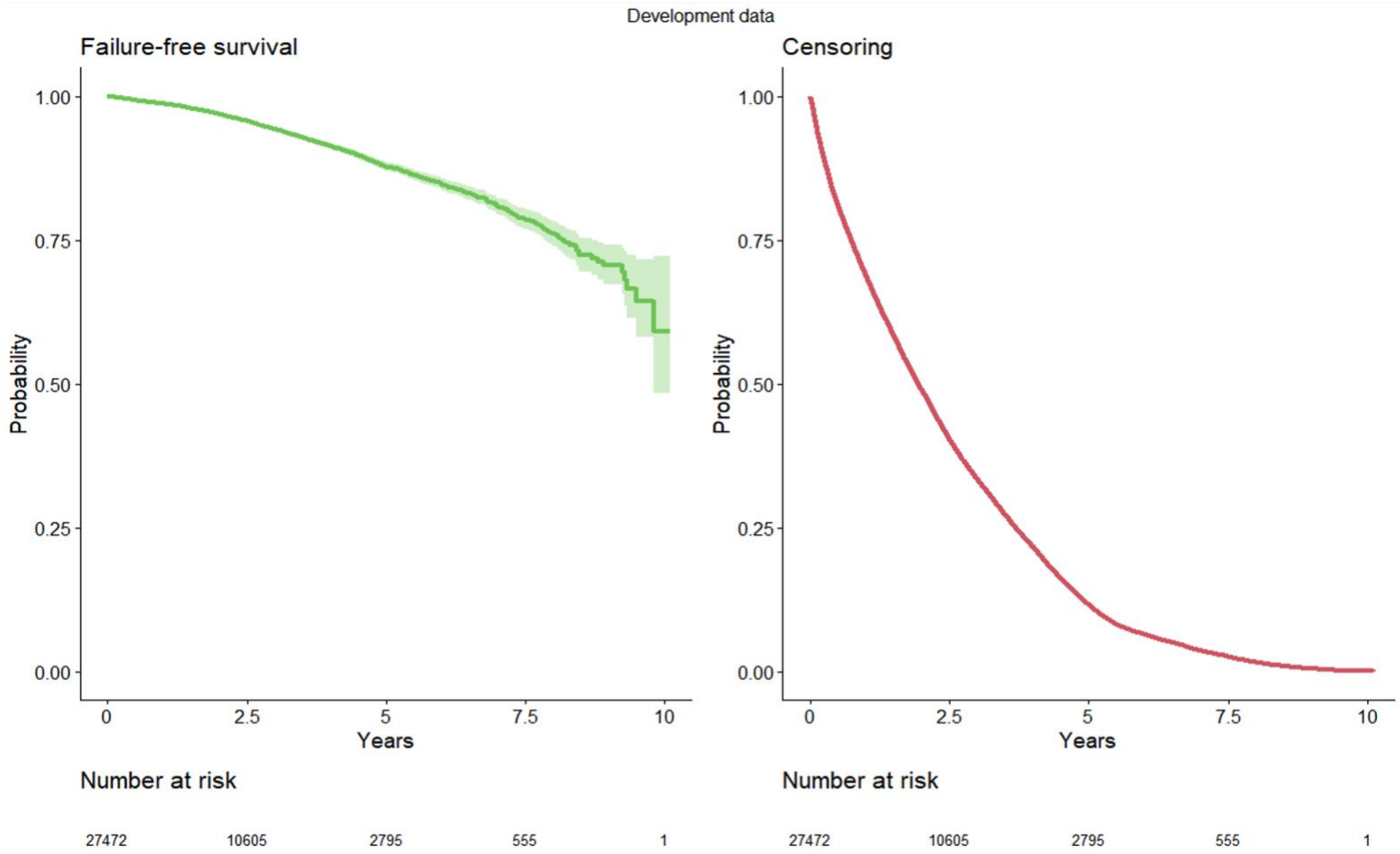

Figure 42: Failure-free survival and censoring curves for the development dataset.

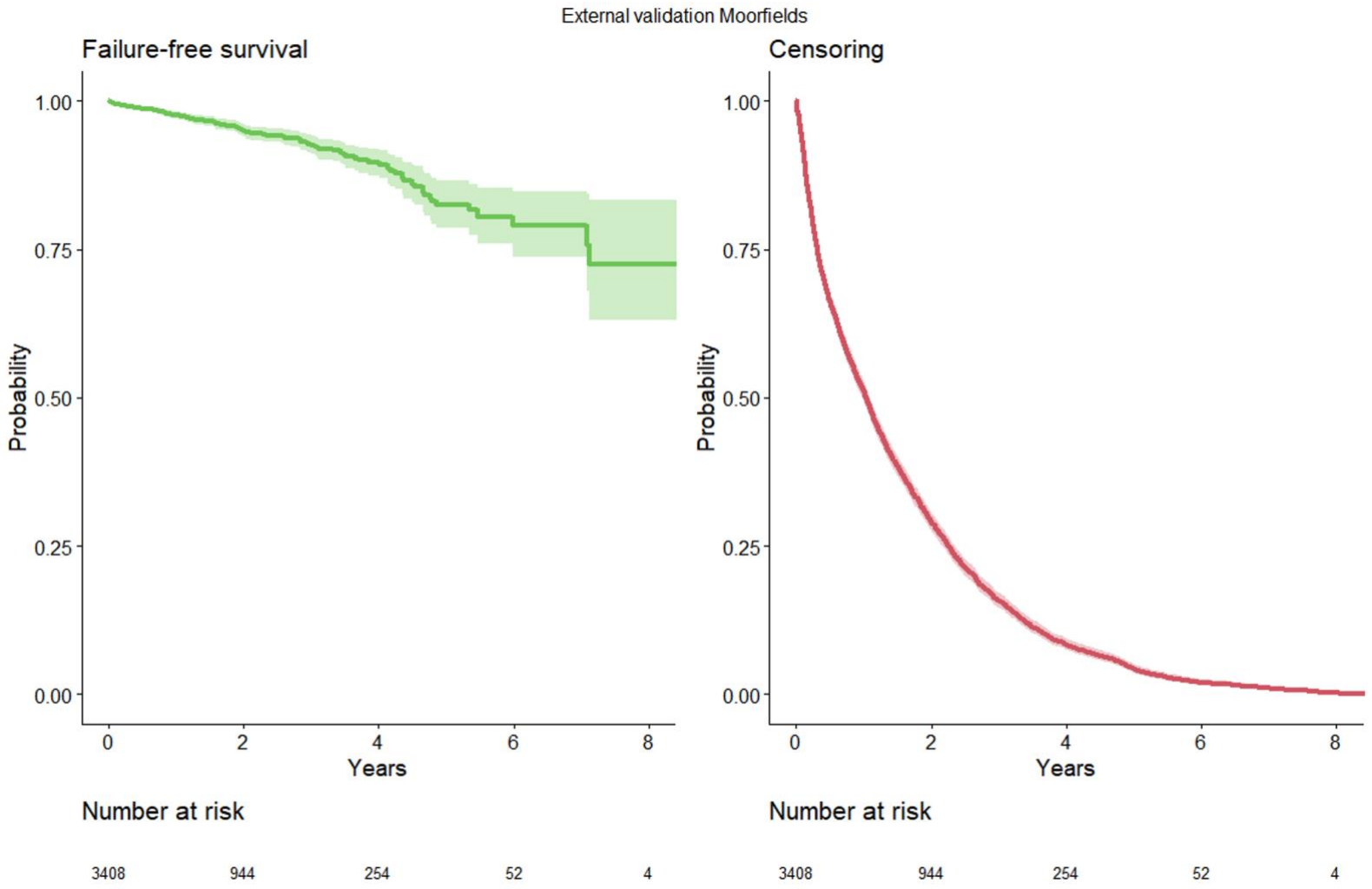

Figure 43: Failure-free survival and censoring curves for the Moorfields external validation cohort.

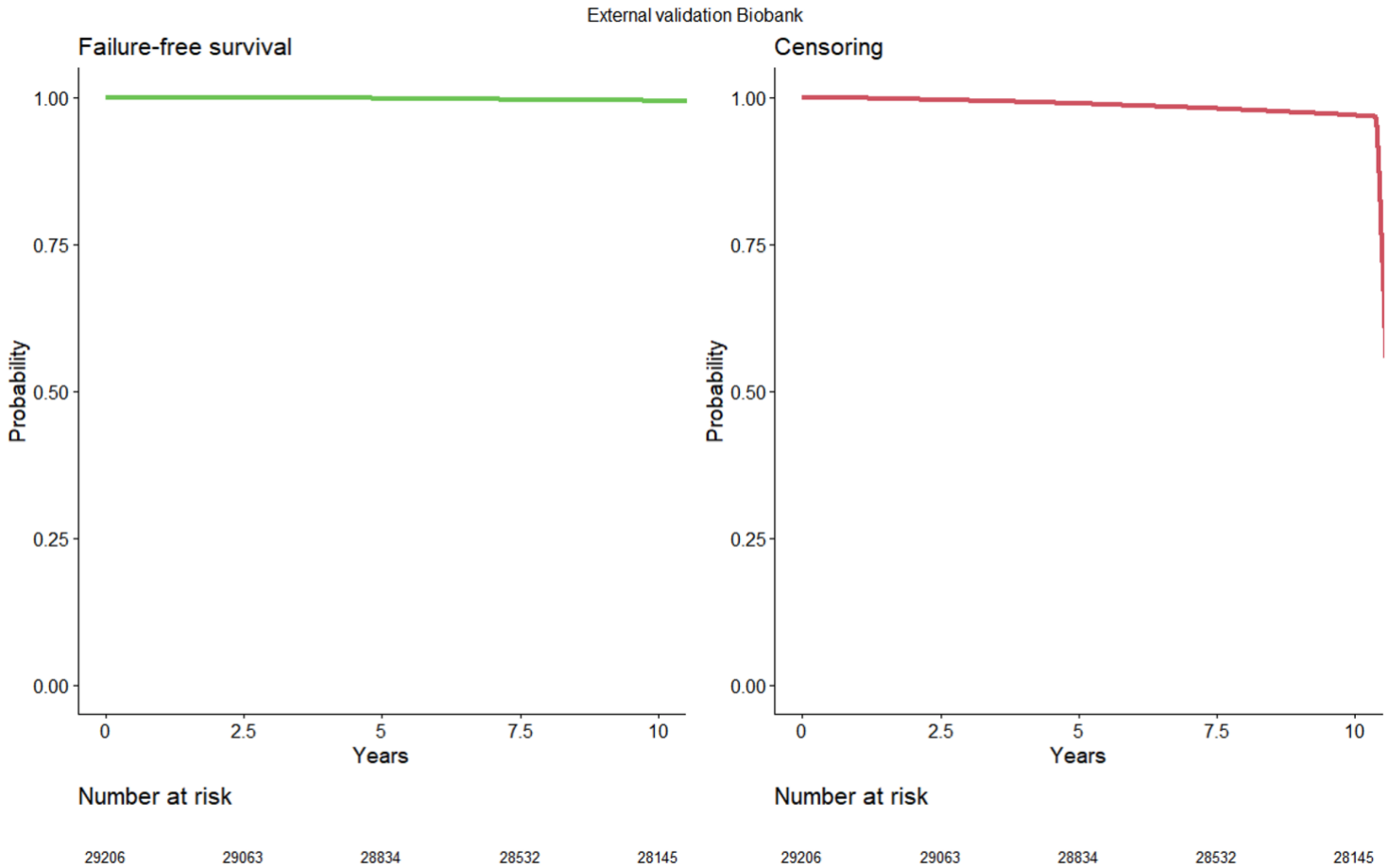

Figure 44: Failure-free survival and censoring curves for the Biobank external validation cohort.

Note the contrast with the internal and Moorfields external validation cohorts due to most Biobank imaging taking place 2006-2010 and the younger age group.

		Chi-squared value	Degrees of freedom	*p*-value
Non-diabetic	**TRF + CFP**	13.3	15	0.58
	TRF + OCT	69.1	37	0.001
	TRF + CFP + OCT	836	51	0.003
Diabetic	**TRF + CFP**	38.0	15	9.1×10^{-4}
	TRF + OCT	55.3	37	0.027
	TRF + CFP + OCT	89.9	51	6.3×10^{-4}

Table 54: Measures of model fit including oculomic markers.

Comparison is made to a base model of traditional risk factors alone. *p*-values are derived from the likelihood ratio test.

CFP: colour fundus photography, OCT: optical coherence tomography, TRF: traditional risk factors.

Addition of oculomic markers

I first investigated whether model fit improved with the addition of oculomic markers from CFP and OCT. For the models for non-diabetic individuals, compared to a base model consisting of TRF only, addition of CFP-derived oculomic markers conferred no difference in model fit (*Table 54*). However, addition of OCT-derived oculomic markers did provide significantly improved model fit ($p = 0.001$). A different pattern was seen for models for diabetic individuals. Compared to the base model, addition of CFP markers led to significantly improved model fit ($p = 9.1 \times 10^{-4}$) whereas OCT conferred only a modest benefit (*Table 54*).

Discrimination performance

Discriminative performance overall was high, even with just traditional risk factors of age, sex, ethnicity, socioeconomic status, and hypertension (*Table 55*). For the non-diabetes model, TRFs alone had an Uno's *C* ranging from 0.775 (0.719, 0.830) on the MEH external validation cohort to 0.819 (0.774, 0.864) on UKBB. In general, drops in performance were seen in the MEH external validation cohort compared to the internal test set – for example, the full TRF+CFP+OCT model achieved a Harrell's *C* of 0.770 (0.740, 0.801) on the internal test set and 0.726 (0.662, 0.789) on the MEH external test set. However, performance was higher on the UKBB external validation set overall, especially for the TRF model.

		Internal test		External validation Moorfields		External validation Biobank	
		Harrell's *C*	**Uno's *C***	**Harrell's *C***	**Uno's *C***	**Harrell's *C***	**Uno's *C***
Non-diabetic	**TRF**	0.775 (0.744, 0.805)	0.778 (0.747, 0.809)	0.731 (0.665, 0.796)	0.775 (0.719, 0.830)	0.819 (0.774, 0.864)	0.819 (0.774, 0.864)
	TRF + CFP	0.774 (0.743, 0.806)	0.779 (0.750, 0.809)	0.740 (0.671, 0.808)	0.788 (0.734, 0.843)	0.802 (0.754, 0.850)	0.802 (0.754, 0.850)
	TRF + OCT	0.769 (0.739, 0.798)	0.771 (0.738, 0.803)	0.719 (0.658, 0.779)	0.770 (0.711, 0.829)	0.802 (0.758, 0.846)	0.802 (0.758, 0.846)
	TRF + CFP + OCT	0.770 (0.740, 0.801)	0.774 (0.743, 0.805)	0.726 (0.662, 0.789)	0.781 (0.726, 0.835)	0.787 (0.741, 0.834)	0.787 (0.741, 0.834)
Diabetic	**TRF**	0.718 (0.663, 0.773)	0.711 (0.658, 0.764)	0.805 (0.758, 0.851)	0.731 (0.636, 0.827)	0.852 (0.751, 0.953)	0.852 (0.752, 0.953)
	TRF + CFP	0.718 (0.666, 0.770)	0.713 (0.662, 0.765)	0.812 (0.763, 0.860)	0.740 (0.651, 0.829)	0.866 (0.788, 0.944)	0.866 (0.789, 0.944)
	TRF + OCT	0.726 (0.672, 0.780)	0.729 (0.679, 0.780)	0.800 (0.749, 0.851)	0.706 (0.613, 0.800)	0.838 (0.759, 0.916)	0.838 (0.759, 0.916)
	TRF + CFP + OCT	0.726 (0.673, 0.778)	0.733 (0.682, 0.784)	0.806 (0.756, 0.855)	0.729 (0.643, 0.815)	0.846 (0.751, 0.941)	0.845 (0.750, 0.940)

Table 55: Discrimination performance of all models on the internal and external test sets. Measures of discrimination include the Harrell's *C* index and Uno's *C* index. Note that the high discrimination values in Biobank likely reflect the low outcome proportion where the *C* index is known to be sensitive to class distribution.

CFP: colour fundus photography, OCT: optical coherence tomography, TRF: traditional risk factors.

For the models for diabetic individuals, discriminative performance was highest in the UKBB external validation cohort though confidence intervals were wide owing to small sample sizes. In contrast to the models for non-diabetes, discriminative performance on the MEH external validation cohort generally exceeded that of the internal test set. As an example, the TRF + CFP model achieved a Harrell's *C* of 0.718 (0.666, 0.770) in the internal test set and 0.812 (0.763, 0.860) on the MEH external validation set.

Overall, there was limited evidence that the models incorporating oculomic markers had superior discriminative performance to TRF alone. Discriminative performance generally increased over time for both the non-diabetes (*Figure 45*) and diabetes models (*Figure 46*).

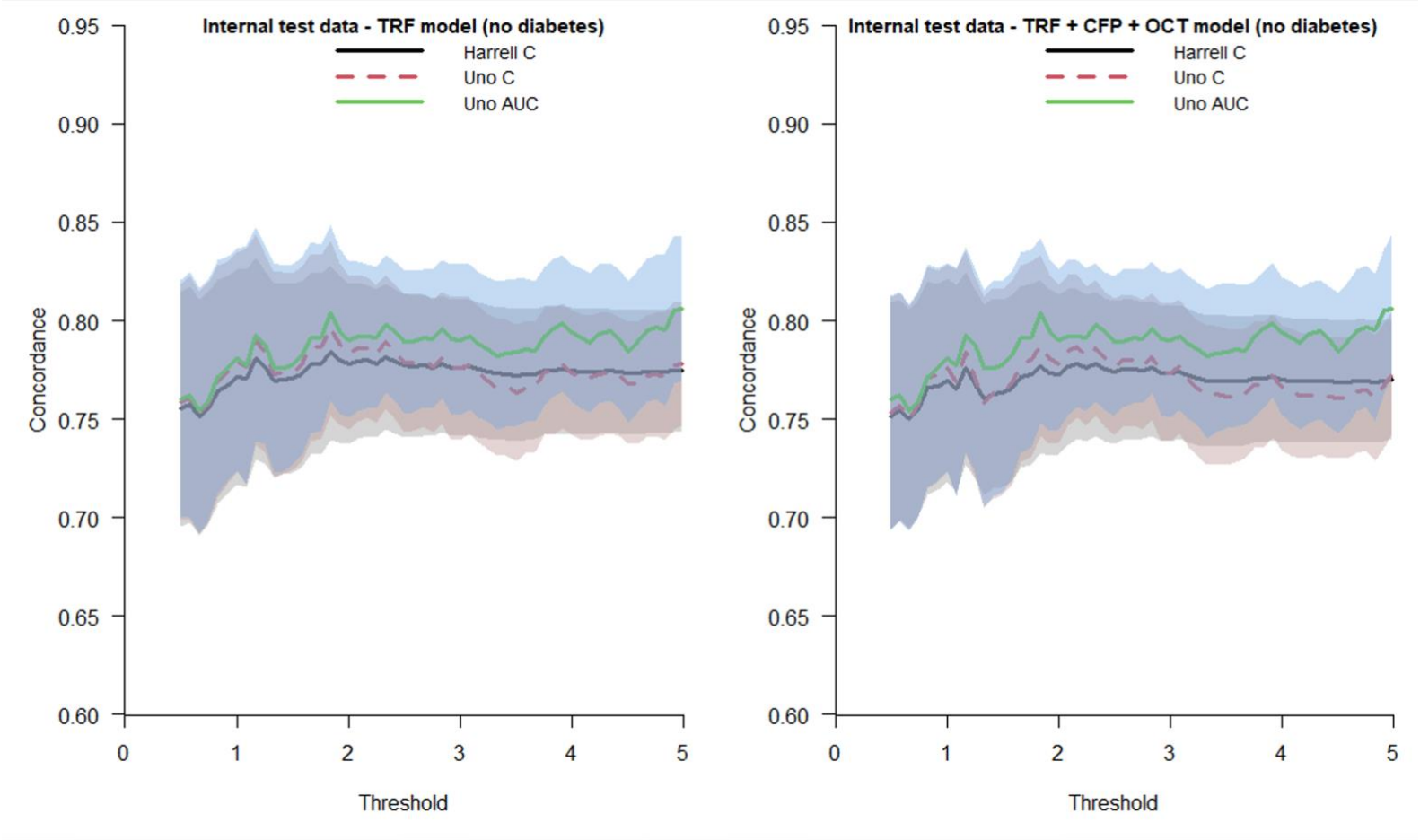

Figure 45: Plot of discrimination performance against time for the base and full model on the internal test set (non diabetics).

CFP: colour fundus photography, OCT: optical coherence tomography, TRF: traditional risk factors.

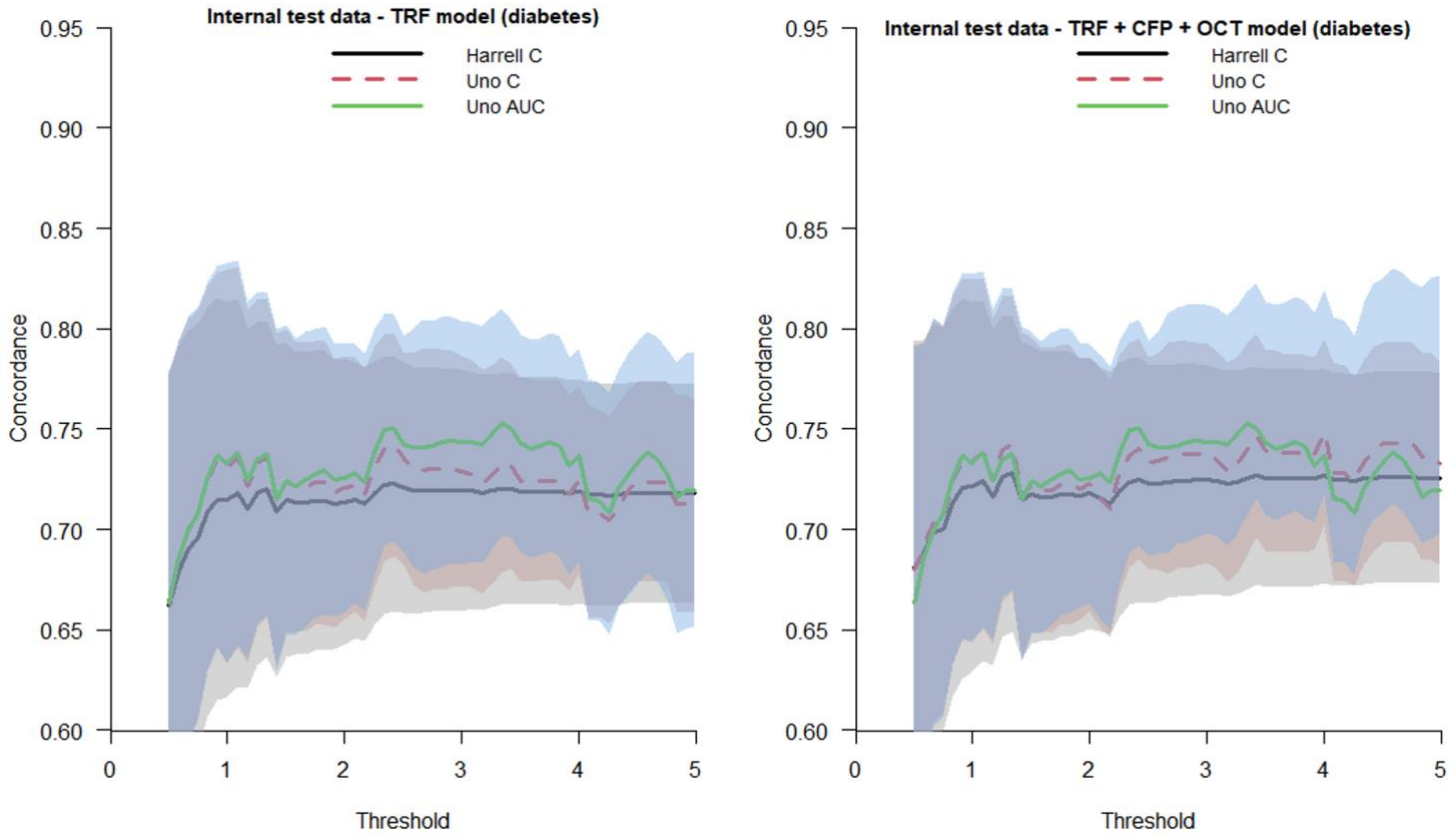

Figure 46: Plot of discrimination performance against time for the base and full model on the internal test set (diabetics).

CFP: colour fundus photography, OCT: optical coherence tomography, TRF: traditional risk factors.

Calibration performance

Calibration performance in shown in *Table 56, Figure 47, and Figure 48*. In general, mean calibration was similar, regardless of model complexity. In the internal test set, models tended to underestimate the risk of all-cause dementia for both the non-diabetic (observed/expected ratio range 0.89-0.91) and diabetic (0.84-0.85) samples. In contrast, the models tended to overestimate the risk in the Moorfields external validation cohort (non-diabetic model range 1.19-1.25, diabetic model range 1.26-1.31). Calibration in the UKBB external validation was poor ranging from 0.16-0.19 for the non-diabetic models and 0.17-0.22 for the diabetic models (i.e. gross underestimates of risk). Overall, there was no evidence that inclusion of oculomic markers improved the mean calibration of models.

		Internal test	External validation Moorfields	External validation Biobank
Non-diabetic	**TRF**	0.91 (0.78, 1.06)	1.22 (0.97, 1.54)	0.16 (0.12, 0.21)
	TRF + CFP	0.89 (0.77, 1.04)	1.19 (0.95, 1.51)	0.17 (0.13, 0.23)
	TRF + OCT	0.90 (0.77, 1.05)	1.25 (0.99, 1.57)	0.18 (0.13, 0.24)
	TRF + CFP + OCT	0.89 (0.76, 1.03)	1.22 (0.96, 1.54)	0.19 (0.14, 0.26)
Diabetic	**TRF**	0.84 (0.70, 1.01)	1.26 (0.99, 1.60)	0.17 (0.08, 0.36)
	TRF + CFP	0.83 (0.70, 0.99)	1.28 (1.00, 1.63)	0.19 (0.09, 0.40)
	TRF + OCT	0.85 (0.71, 1.01)	1.30 (1.02, 1.66)	0.19 (0.09, 0.41)
	TRF + CFP + OCT	0.83 (0.70, 1.00)	1.31 (1.03, 1.67)	0.22 (0.10, 0.45)

Table 56: Mean calibration, as measured through the expected/observed ratio for all models on the internal and external test sets.

CFP: colour fundus photography, OCT: optical coherence tomography, TRF: traditional risk factors.

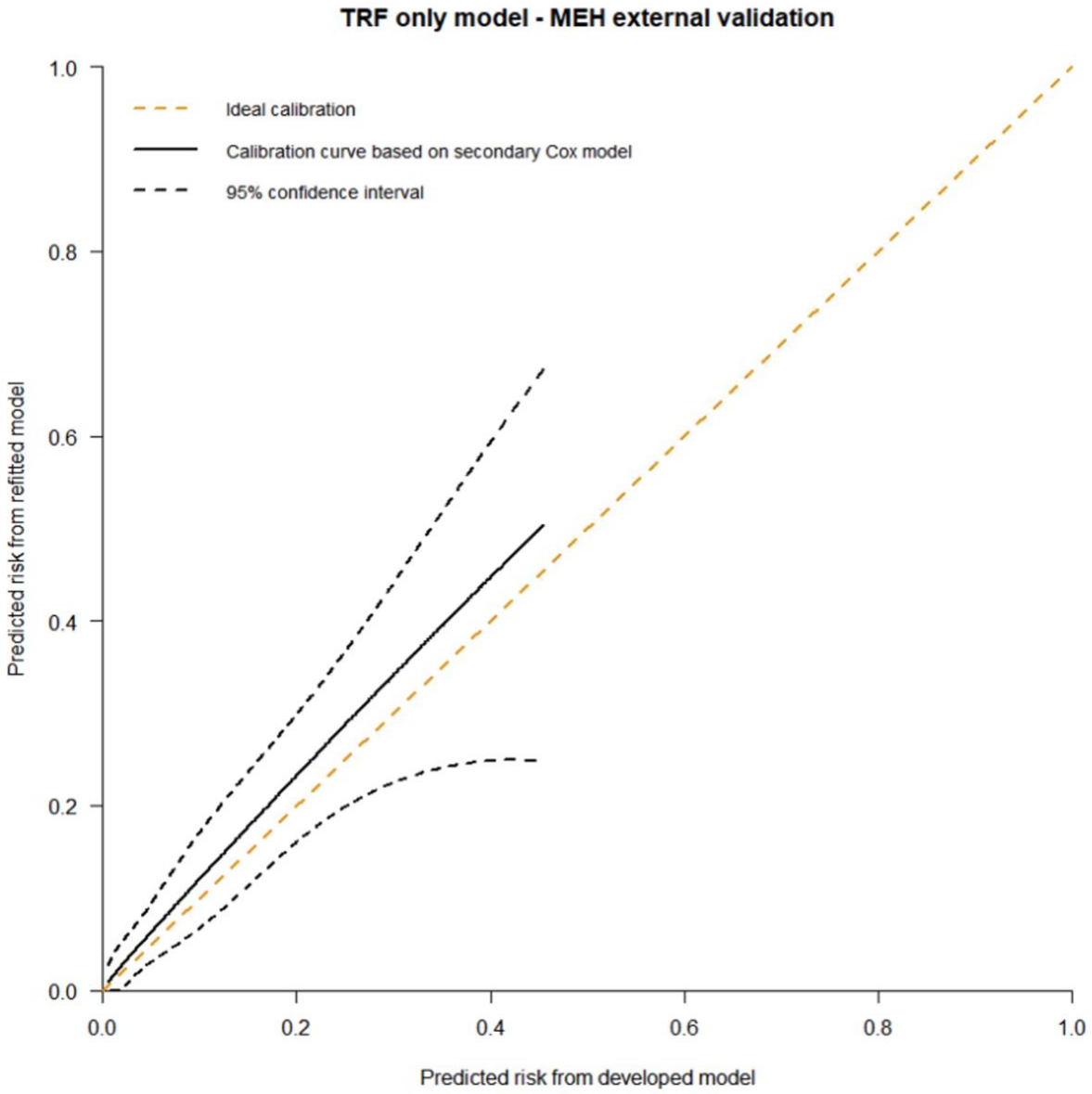

Figure 47: Calibration plot of the TRF model on the Moorfields external validation (non-diabetic).

MEH: Moorfields Eye Hospital, TRF: traditional risk factor

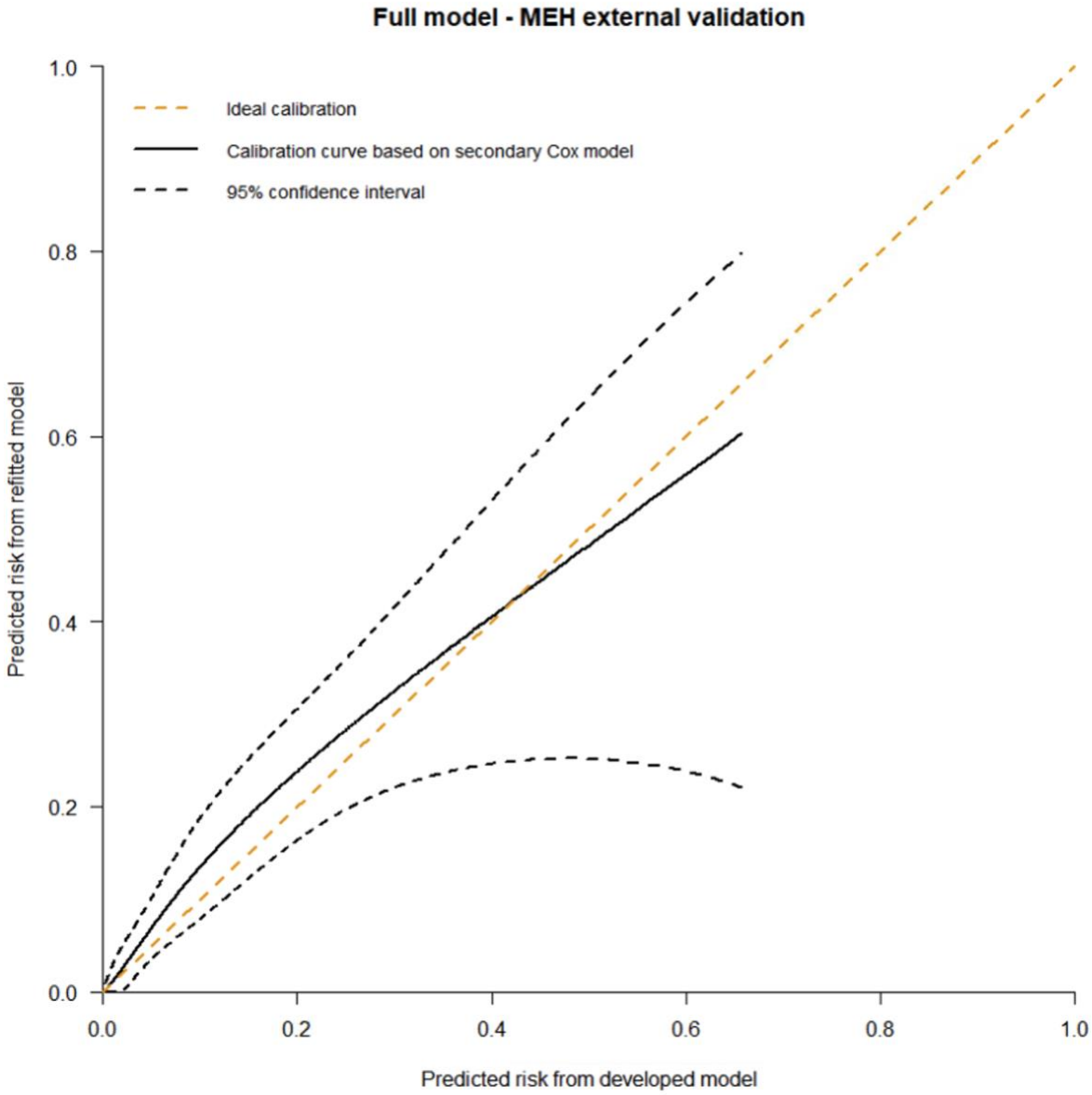

Figure 48: Calibration plot of the full model on the Moorfields external validation (non-diabetic).

MEH: Moorfields Eye Hospital

Sensitivity analysis

I then assessed model discrimination in clinically relevant subgroups (*Table 57 and Table 58*). Performance was lower in groups stratified by age deciles, dropping to a Harrell's *C* of 0.507 (0.400, 0.613) in the 80-89 years group for the TRF alone model in diabetic patients. Biological sex had a reversed pattern depending on diabetic status – for the non-diabetic model, performance was higher for men across all models. In contrast, for the diabetic model, performance was higher for women. Similar performance was seen among White and Black ethnic groups in both the non-diabetic and diabetic models but this was not the case for South Asians. Particularly high performance was seen among South Asians with the diabetic model whereas, lower performance was seen in the non-diabetic population. Large differences were also seen for both the non-diabetic models and diabetic models between groups with and without AMD and glaucoma.

Non-diabetic patients		*n*	TRF	TRF + CFP	TRF + OCT	TRF + CFP + OCT
Age	**50-59**	277	-	-	-	-
	60-69	488	0.564 (0.260, 0.868)	0.572 (0.271, 0.874)	0.639 (0.332, 0.947)	0.650 (0.348, 0.952)
	70-79	708	0.591 (0.436, 0.746)	0.597 (0.427, 0.767)	0.604 (0.485, 0.724)	0.594 (0.452, 0.736)
	80-89	589	0.565 (0.741, 0.658)	0.613 (0.513, 0.713)	0.523 (0.423, 0.622)	0.558 (0.460, 0.656)
Sex	**Female**	1,155	0.706 (0.610, 0.803)	0.712 (0.612, 0.811)	0.691 (0.599, 0.784)	0.685 (0.601, 0.789)
	Male	907	0.769 (0.687, 0.851)	0.782 (0.674, 0.871)	0.760 (0.688, 0.832)	0.770 (0.690, 0.850)
Ethnicity	**Asian (South)**	218	0.603 (0.363, 0.843)	0.635 (0.385, 0.886)	0.606 (0.340, 0.873)	0.625 (0.355, 0.895)
	Black	233	0.734 (0.500, 0.969)	0.752 (0.522, 0.982)	0.715 (0.525, 0.904)	0.727 (0.545, 0.909)
	White	1,031	0.735 (0.661, 0.810)	0.745 (0.665, 0.825)	0.718 (0.650, 0.786)	0.723 (0.652, 0.795)
SES	**Less deprived**	1,031	0.778 (0.709, 0.847)	0.789 (0.717, 0.861)	0.757 (0.684, 0.829)	0.766 (0.690, 0.842)
	More deprived	1,031	0.698 (0.602, 0.795)	0.706 (0.604, 0.807)	0.691 (0.604, 0.778)	0.695 (0.603, 0.786)
AMD	**Absent**	1.963	0.736 (0.665, 0.808)	0.745 (0.670, 0.821)	0.723 (0.657, 0.789)	0.730 (0.661, 0.799)
	Present	99	0.607 (0.435, 0.779)	0.606 (0.429, 0.783)	0.628 (0.422, 0.834)	0.620 (0.419, 0.820)
Glaucoma	**Absent**	1.862	0.708 (0.638, 0.779)	0.716 (0.642, 0.790)	0.699 (0.634, 0.765)	0.705 (0.636, 0.774)
	Present	200	0.857 (0.749, 0.965)	0.873 (0.760, 0.985)	0.833 (0.730, 0.936)	0.846 (0.738, 0.954)
Dementia type	**Alzheimer's disease**	2,050	0.725 (0.650, 0.800)	0.732 (0.653, 0.811)	0.716 (0.646, 0.785)	0.722 (0.649, 0.796)
	Vascular dementia	2,032	0.698 (0.600, 0.795)	0.703 (0.606, 0.800)	0.686 (0.594, 0.777)	0.690 (0.600, 0.781)

Table 57: Discrimination performance across pre-specified subgroups for all models in the non-diabetic cohort.

AMD: age-related macular degeneration, CFP: colour fundus photography, OCT: optical coherence tomography, SES: socioeconomic status, TRF: traditional risk factor

Diabetic patients		*n*	TRF	TRF + CFP	TRF + OCT	TRF + CFP + OCT
Age	**50-59**	241	-	-	-	-
	60-69	353	-	-	-	-
	70-79	500	0.592 (0.467, 0.716)	0.612 (0.481, 0.743)	0.563 (0.441, 0.685)	0.593 (0.468, 0.718)
	80-89	252	0.507 (0.400, 0.613)	0.556 (0.458, 0.653)	0.581 (0.473, 0.688)	0.585 (0.491, 0.680)
Sex	**Female**	635	0.828 (0.783, 0.873)	0.840 (0.797, 0.883)	0.822 (0.774, 0.871)	0.833 (0.790, 0.875)
	Male	711	0.748 (0.645, 0.851)	0.798 (0.632, 0.844)	0.751 (0.636, 0.867)	0.740 (0.625, 0.855)
Ethnicity	**Asian (South)**	323	0.918 (0.869, 0.967)	0.908 (0.858, 0.958)	0.884 (0.824, 0.944)	0.875 (0.820, 0.931)
	Black	259	0.864 (0.758, 0.971)	0.870 (0.748, 0.991)	0.801 (0.662, 0.940)	0.817 (0.669, 0.967)
	White	436	0.810 (0.746, 0.875)	0.839 (0.774, 0.904)	0.842 (0.781, 0.903)	0.860 (0.806, 0.914)
SES	**Less deprived**	673	0.814 (0.742, 0.887)	0.817 (0.744, 0.890)	0.828 (0.753, 0.904)	0.825 (0.754, 0.896)
	More deprived	673	0.803 (0.746, 0.860)	0.810 (0.748, 0.872)	0.783 (0.719, 0.846)	0.791 (0.725, 0.858)
AMD	**Absent**	1,329	0.807 (0.759, 0.855)	0.816 (0.766, 0.865)	0.811 (0.761, 0.861)	0.816 (0.768, 0.864)
	Present	18	0.574 (0.202, 0.945)	0.596 (0.240, 0.951)	0.532 (0.134, 0.930)	0.596 (0.280, 0.912)
Glaucoma	**Absent**	1,245	0.808 (0.760, 0.855)	0.817 (0.768, 0.866)	0.803 (0.752, 0.855)	0.810 (0.760, 0.861)
	Present	101	0.818 (0.655, 0.981)	0.773 (0.624, 0.922)	0.852 (0.718, 0.987)	0.818 (0.687, 0.949)
Dementia type	**Alzheimer's disease**	1,329	0.805 (0.759, 0.850)	0.820 (0.770, 0.870)	0.794 (0.740, 0.847)	0.809 (0.756, 0.862)
	Vascular dementia	1,323	0.834 (0.777, 0.890)	0.835 (0.776, 0.894)	0.830 (0.766, 0.894)	0.828 (0.765, 0.891)

Table 58: Discrimination performance across pre-specified subgroups for all models in the diabetic cohort.

AMD: age-related macular degeneration, CFP: colour fundus photography, OCT: optical coherence tomography, SES: socioeconomic status, TRF: traditional risk factor

7.1.4 Discussion

In this report, I developed clinical prediction models for all-cause dementia using sociodemographic and retinal imaging data from 27,242 patients in the AlzEye cohort. Models were then externally validated on >30,000 patients from both hospital-attending (MEH external validation) and community-based settings (Biobank external validation). Discriminative performance was generally high across all models even, in the absence of retinal imaging data. On the external validation in UK Biobank, discrimination of models was particularly high likely reflecting the low proportion of patients affected by dementia where the *C* index may be sensitive to class imbalance issues. There was no evidence that retinal markers conferred performance benefit beyond TRFs. This work highlights the challenges of transitioning from group-level differences to individual-level prediction with retinal imaging data.

Comparison of these results to current literature is limited as, at the time of this thesis, there had been no studies describing clinical prediction models for all-cause dementia using retinal imaging. There are, however, a few reports regarding diagnostic models for prevalent all-cause dementia. During the writing of is thesis, Cheung et al developed and validated a CFP-based model for detecting Alzheimer's disease (AD) using data from 648 affected patients in a multinational case-control design[474]. Their models achieved AUCs on a separate dataset incorporating a robust ground truth definition (additional confirmation on amyloid positron emission topography [amyloid-PET]) ranging from 0.68-0.86. Strengths of their work include the multi-centre international, the robust reference standard for some of the participants and the technical novelties around unsupervised domain adaptation for

improving generalisability and harmonising outputs from both eyes into a single patient-level prediction. However, they did not formally assess whether the CFP-based model confers performance benefit beyond simple risk factors. Indeed, their "risk factors alone" model achieved impressive discriminative performance with AUCs up to 0.91 on internal validation and 0.74 on the amyloid-PET subset. In several testing subsets, the risk factor alone model performance estimates exceeded that of the model combining risk factors and CFP (Supplementary Table 3 in their report). Dementia, in particular AD, is intimately related to age. While 3% of people aged 65-74 years are affected by AD, this rises to 17% for those aged 75-84 and 32% of those aged 85 or older[549]. Moreover, convolutional neural networks are capable of discerning age from a CFP alone with remarkable accuracy – Poplin et al showed in 2018 that age could be estimated from a single CFP alone with a mean absolute error of 3.3 years[237] and several reports subsequently have tightened the gap. In my report, the performance of the TRF model alone was high across both internal and external test sets (*Table 55*). Moreover, subgroup analysis in groups stratified by age deciles led to significant drops in performance for all models, both TRF alone and those incorporating retinal imaging data (*Table 57, Table 58*). Studies investigating the performance of AD detection or prediction models should incorporate explicit comparison to models of age alone or in tandem with other basic risk factors. While the observation that retinal features associate strongly with age has scientific interest, implementation of these models for patient care or screening will require a careful assessment of the benefit imaging brings in addition.

Models were stratified based on diabetic status for several reasons. Firstly, in the UK and increasingly in other high and middle income countries, individuals with diabetes

mellitus undergoing interval screening with CFP (and in some cases OCT) to identify retinopathy[550]. Therefore, there already exists a dedicated pathway for this patient group and ideally any deployed model would be optimised for the relevant population. Secondly, diabetes significantly affects both retinovascular and retinal sublayer indices, regardless of disease severity, and may modify the relationship between neurodegeneration and retinal morphology[453,551]. Prediction models in the diabetic group generally outperformed those on the non-diabetic group on external validation (*Table 55)* however discriminating between TRF only models and the full models were generally similar except for the non-diabetic model in the UKBB external validation where performance dropped. I hypothesised that retinal imaging markers would especially help in the diabetic population as retinovascular and OCT metrics may provide a surrogate for disease severity[552]. Specifically, duration of diabetes is not only intimately linked with retinal morphology but also the incidence of dementia[553]. This confounder could plausibly therefore lead to better discrimination of those at risk however this was not the case. Possible explanations include spurious measurements due to previous treatment, imprecise segmentation (though I sought to mitigate this through quality control processes) or simply that these differences are dwarfed by the discriminative strength of age. This contrasts with the findings of Doney et al – they developed logistic regression models for 10-year risk of dementia (defined through electronic medical record) using clinical variables, apolipoprotein E4 genotype, and retinal vascular indices from 6,111 patients with diabetes mellitus in the GoDARTS resource[554]. They found an improvement in discriminative performance of their model for the task of all-cause dementia though this was slight (AUC 0.7855 [0.7689, 0.8022] versus 0.7896 [0.7731, 0.8060), p = 0.022) and the estimate range suggests this may not be clinically significant.

While external validation performance was generally high, in terms of discrimination, the models were poorly calibrated for the UKBB population. In particular, the models tended to underestimate the risk in the UKBB population, likely reflecting the differing profile of study participants. Compared to AlzEye, UKBB is younger, much more likely to be White and has significantly less medical comorbidity, including hypertension and diabetes mellitus. Overfitting of the model is another possibility though this seems unlikely since i) sample size calculations prior to model development suggested sufficient power for several multiples of the predictor variables used, ii) large drops in discriminative performance in external validation sets were not seen, iii) the optimism, as assessed through internal bootstrapping was minimal and iv) even the TRF alone models (with just five covariates) had similar calibration to the more complex models. Prior to any deployment, such models would benefit from algorithmic updating (changing of the intercept has been proposed as a simple and useful first step[555]) or even full refitting[556].

Analysis of the model outputs across pre-specified subgroups revealed disparate performance characteristics (*Table 57 and Table 58*). As mentioned earlier, notable drops in performance of both non-diabetic and diabetic models were seen when stratifying by age. Similar drops were seen in the subgroup with AMD, likely due to the same reason. Stratifying for those with AMD present narrows the age group to those >55 years. Performance between patients identifying as White or Black was relatively similar however, opposite effects on performance were seen for those of South Asian ethnicity depending on diabetic status. In the non-diabetic cohort, there was a substantial drop in performance across all models, while the reverse was seen

in the diabetic cohort. The reason for this is unclear but one reason may be the higher prevalence of proliferative diabetic retinopathy among South Asian patients in AlzEye (*Table 9*). While 20.5% of the AlzEye cohort identify as South Asian, 33.7% of all individuals with proliferative diabetic retinopathy are South Asian, the highest of any ethnic group. Stratification by diabetic status is therefore likely to select out those with the most severe form of diabetic eye disease, which generally present at a younger age in AlzEye (*Table 3*, mean age of South Asians with proliferative diabetic retinopathy 61.6 years) and can therefore be discriminated from cases more easily.

Strengths of this report include the large sample size, the ethnic diversity of the patients and participants and availability of multimodal retinal imaging data. Moreover, several tools (e.g. AutoMorph) are freely available online supporting open science and reproducibility of this work. Several limitations, most of which have been discussed in the previous chapters, should be considered. Firstly, AlzEye is derived from a hospital-attending population and naturally exhibits higher medical comorbidity and socioeconomic deprivation than the general UK population[165]. As demonstrated by evaluation of predicted versus observed risks in UKBB for all-cause dementia, this can result in miscalibration of prediction models. Updating and refitting is likely to be necessary for any population or community-based setting of deployment. Secondly, the reference standard of all-cause dementia in AlzEye was defined through hospital admissions data, which has the potential for misclassification bias. Thirdly, retinal image quality control remains an under-researched area with the potential to affect the study findings in several ways, from inducing selection bias through exclusion of poor quality images to distorting

predictor variables through segmentation quality. I used widely adopted techniques applying a quantile approach based on image quality metadata on OCT[15,142,184] and the segmentation quality score of AutoMorph. Both methods are easily adopted by other groups but this approach may not be the most effective for delivering optimal prognostic model performance.

7.1.5 Summary

In conclusion, my analysis suggests that incorporation of retinal imaging-derived features does not significantly improve the discriminative or calibration performance of individual-level prediction models for all-cause dementia beyond traditional risk factors of age, sex, ethnicity, socioeconomic deprivation, hypertension, and diabetes. My approach is based on *a priori* definition of clinically meaningful retinal variables (e.g. vascular tortuosity, GCIPL thickness) and their spatial distribution (e.g. parafoveal regions). High dimensional approaches and alternative imaging modalities, beyond CFP and OCT, may be considered for identifying other potentially useful features.

8. Conclusions

This project represents a combined hypothesis and data-driven approach to understanding the associations between eye disease, retinal morphology and systemic health. Drawing on the establishment of a bespoke privacy-by-design health data resource, AlzEye, as its foundation, I have reported novel findings within three themes comprising *Description, Discovery and Prediction.*

Description

AlzEye includes data from a large ethnically and socioeconomically diverse cohort of patients attending Moorfields Eye Hospital. Within AlzEye, individuals with acute retinal artery occlusion and ocular cranial nerve palsies have an increased risk of stroke and death. Management pathways in acute and emergency ophthalmic care should reflect this; prompt engagement with stroke physicians is warranted. The association of non-arteritic ischaemic optic neuropathy with increased mortality requires further investigation.

Discovery

Individuals with schizophrenia have thinner ganglion cell-inner plexiform layer, a feature suggestive of neurodegeneration in the context of other research. They also exhibit retinovascular differences though these appear secondary to the increased prevalence of medical comorbidity, particularly hypertension and diabetes mellitus.

Reduced thickness of the ganglion cell-inner plexiform layer is also seen in individuals with Parkinson’s disease and can be observed, on average, seven years before diagnosis. In combination with a novel observation of reduced inner nuclear

layer thickness in both prevalent and incident disease, further work is justified into the role of retinal imaging for risk stratification and whether oculomic markers may be useful longitudinally in high-risk groups. The effect sizes, especially for the inner nuclear layer, are however small.

Gum disease is common. Those with the advanced disease, termed very severe periodontitis, have retinovascular differences consistent with inflammation. They also exhibit a thinner ganglion cell-inner plexiform layer which may echo the increased incidence of cardiometabolic and neurodegenerative disease in these patients. Gum disease was defined through questionnaire and subsequent work should investigate retinal morphology in conjunction with more granular and deeply phenotyped case definitions.

The finding that individuals with childhood unilateral amblyopia have bilateral retinal structural differences consistent with cardiometabolic disease, has been corroborated by a multimodal epidemiological investigation into physical measurements, biological measurements and incident risk of major adverse cardiovascular events and death. Healthcare professionals should be mindful of increased risk in these patients.

Prediction

Although group-level differences exist between those with and without all-cause dementia, the feasibility for individual-level prediction of this disease is limited currently with the data available and using the approach in this thesis. Modelling strategies will need to consider the overwhelming value of age in the likelihood of

dementia and, as with any prediction model, the heterogenous populations of the development and deployment settings.

In the context of the widespread availability of non-invasive high-resolution imaging, our growing catalogue of computational tools and the importance the public places on their vision, this thesis highlights the rich tapestry woven by the interplay of eye health and systemic disease. Retinal imaging should be investigated more widely across the life sciences landscape as an adjunct measure for further understanding comorbidity and informing the risk of chronic and complex non-communicable disease in patients.

9. References

1 Retief F, Stulting A, Cilliers L. The eye in antiquity. *S Afr Med J* 2008; **98**: 697–700.

2 Snell RS, Lemp MA. Clinical anatomy of the eye, 2nd edn. Malden, MA, USA: Blackwell Science, 1998.

3 Reh TA. Chapter 13 - The Development of the Retina. In: Ryan SJ, Sadda SR, Hinton DR, *et al.*, eds. Retina (Fifth Edition). London: W.B. Saunders, 2013: 330–41.

4 Jindahra P, Petrie A, Plant GT. The time course of retrograde trans-synaptic degeneration following occipital lobe damage in humans. *Brain* 2012; **135**: 534–41.

5 Lee G-I, Park K-A, Son G, Kong D-S, Oh SY. Optical coherence tomography analysis of inner and outer retinal layers in eyes with chiasmal compression caused by suprasellar tumours. *Acta Ophthalmol* 2020; **98**: e373–80.

6 Petzold A, de Boer JF, Schippling S, *et al.* Optical coherence tomography in multiple sclerosis: a systematic review and meta-analysis. *Lancet Neurol* 2010; **9**: 921–32.

7 Davis BM, Crawley L, Pahlitzsch M, Javaid F, Cordeiro MF. Glaucoma: the retina and beyond. *Acta Neuropathol* 2016; **132**: 807–26.

8 Murray CD. The Physiological Principle of Minimum Work: I. The Vascular System and the Cost of Blood Volume. *Proc Natl Acad Sci U S A* 1926; **12**: 207–14.

9 Taber LA. An optimization principle for vascular radius including the effects of smooth muscle tone. *Biophysical journal* 1998; **74**: 109–14.

10 Cogan DG, Kuwabara T. Comparison of retinal and cerebral vasculature in trypsin digest preparations. *Br J Ophthalmol* 1984; **68**: 10–2.

11 Medawar PB. Immunity to homologous grafted skin; the fate of skin homografts transplanted to the brain, to subcutaneous tissue, and to the anterior chamber of the eye. *Br J Exp Pathol* 1948; **29**: 58–69.

12 Lee RW, Nicholson LB, Sen HN, *et al.* Autoimmune and autoinflammatory mechanisms in uveitis. *Seminars in immunopathology* 2014; **36**: 581–94.

13 Lubs ML, Bauer MS, Formas ME, Djokic B. Lisch nodules in neurofibromatosis type 1. *N Engl J Med* 1991; **324**: 1264–6.

14 Pollack A, Rodov L, Greenwald Y. Elschnig spots. In: Encyclopedia of Ophthalmology. Berlin, Heidelberg: Springer Berlin Heidelberg, 2014: 1–2.

15 Khawaja AP, Chua S, Hysi PG, *et al.* Comparison of Associations with Different Macular Inner Retinal Thickness Parameters in a Large Cohort: The UK Biobank. *Ophthalmology* 2020; **127**: 62–71.

16 Owen CG, Rudnicka AR, Welikala RA, *et al.* Retinal Vasculometry Associations with Cardiometabolic Risk Factors in the European Prospective Investigation of Cancer-Norfolk Study. *Ophthalmology* 2019; **126**: 96–106.

17 Organisation, World Health. The top 10 causes of death. https://www.who.int/news-room/fact-sheets/detail/the-top-10-causes-of-death.

18 Bright R. Tabular view of the morbid appearances in 100 cases connected with albuminous urine. *Guy's Hospital reports* 1836; **1**.

19 Gunn RM. Ophthalmoscopic evidence of (1) arterial changes associated with chronic renal disease, and (2) of increased arterial tension. *Transactions of the Ophthalmological Society of the United Kingdom* 1892; **12**: 124–5.

20 Keith, M. N, Wagener, and Barker HP, W. N. Some Different Types of Essential Hypertension: Their Course and Prognosis. *The American Journal of the Medical Sciences* 1939; **197**: 332–43.

21 Downie LE, Hodgson LA, Dsylva C, *et al.* Hypertensive retinopathy: comparing the Keith-Wagener-Barker to a simplified classification. *J Hypertens* 2013; **31**: 960–5.

22 Cheung CY, Zheng Y, Hsu W, *et al.* Retinal vascular tortuosity, blood pressure, and cardiovascular risk factors. *Ophthalmology* 2011; **118**: 812–8.

23 Tapp RJ, Owen CG, Barman SA, *et al.* Associations of Retinal Microvascular Diameters and Tortuosity With Blood Pressure and Arterial Stiffness. *Hypertension* 2019; **74**: 1383–90.

24 Prince M, Bryce R, Albanese E, Wimo A, Ribeiro W, Ferri CP. The global prevalence of dementia: a systematic review and metaanalysis. *Alzheimers Dement* 2013; **9**: 63-75.e2.

25 International, Alzheimer's Disease. World Alzheimer Report 2015 The global impact of dementia: An analysis of prevalence, incidence, cost and trends. https://www.alzint.org/resource/world-alzheimer-report-2015/.

26 Statistics, Office for National. Deaths registered in England and Wales (series DR): 2015. https://www.ons.gov.uk/peoplepopulationandcommunity/birthsdeathsandmarriages/deaths/bulletins/deathsregisteredinenglandandwalesseriesdr/2015.

27 Stites SD, Karlawish J, Harkins K, Rubright JD, Wolk D. Awareness of Mild Cognitive Impairment and Mild Alzheimer's Disease Dementia Diagnoses Associated With Lower Self-Ratings of Quality of Life in Older Adults. *The Journals of Gerontology: Series B* 2017; **72**: 974–85.

28 Wilson JMG, Jungner G, World Health, Organization. Principles and practice of screening for disease / J. M. G. Wilson, G. Jungner. 1968. https://apps.who.int/iris/handle/10665/37650.

29 Ursin F, Timmermann C, Steger F. Ethical Implications of Alzheimer's Disease Prediction in Asymptomatic Individuals through Artificial Intelligence. *Diagnostics (Basel)* 2021; **11**. DOI:10.3390/diagnostics11030440.

30 Livingston G, Huntley J, Sommerlad A, *et al.* Dementia prevention, intervention, and care: 2020 report of the Lancet Commission. *Lancet* 2020; **396**: 413–46.

31 Association, Alzheimer's. Federal Alzheimer's and Dementia Research Funding Reaches $3.1 Billion Annually. https://www.alz.org/news/2020/federal-alzheimers-and-dementia-research-funding-r#:~:text=Federal%20Alzheimer's%20and%20Dementia%20Research%20Funding%20Reaches%20%243.1%20Billion%20Annually&text=WASHINGTON%2C%20D.C.%2C%20December%2028%2C,federal%20investment%20to%20%243.1%20billion.

32 van Dyck CH, Swanson CJ, Aisen P, *et al.* Lecanemab in early Alzheimer's disease. *N Engl J Med* 2023; **388**: 9–21.

33 Kim S, Sargent-Cox K, Cherbuin N, Anstey KJ. Development of the motivation to change lifestyle and health behaviours for dementia risk reduction scale. *Dement Geriatr Cogn Dis Extra* 2014; **4**: 172–83.

34 Smith BJ, Ali S, Quach H. The motivation and actions of Australians concerning brain health and dementia risk reduction. *Health Promotion Journal of Australia* 2015; **26**: 115–21.

35 Serrano-Pozo A, Frosch MP, Masliah E, Hyman BT. Neuropathological alterations in Alzheimer disease. *Cold Spring Harbor perspectives in medicine* 2011; **1**: a006189–a006189.

36 Cogan DG. Visual Disturbances With Focal Progressive Dementing Disease. *American Journal of Ophthalmology* 1985; **100**: 68–72.

37 Nissen MJ, Corkin S, Buonanno FS, Growdon JH, Wray SH, Bauer J. Spatial vision in Alzheimer's disease. General findings and a case report. *Arch Neurol* 1985; **42**: 667–71.

38 Hinton DR, Sadun AA, Blanks JC, Miller CA. Optic-nerve degeneration in Alzheimer's disease. *N Engl J Med* 1986; **315**: 485–7.

39 Koronyo Y, Biggs D, Barron E, *et al.* Retinal amyloid pathology and proof-of-concept imaging trial in Alzheimer's disease. *JCI insight* 2017; **2**: e93621.

40 Koronyo-Hamaoui M, Koronyo Y, Ljubimov AV, *et al.* Identification of amyloid plaques in retinas from Alzheimer's patients and noninvasive in vivo optical imaging of retinal plaques in a mouse model. *Neuroimage* 2011; **54 Suppl 1**: S204-17.

41 Alber J, Goldfarb D, Thompson LI, *et al.* Developing retinal biomarkers for the earliest stages of Alzheimer's disease: What we know, what we don't, and how to move forward. *Alzheimers Dement* 2020; **16**: 229–43.

42 Petzold A, de Boer JF, Schippling S, *et al.* Optical coherence tomography in multiple sclerosis: a systematic review and meta-analysis. *Lancet Neurol* 2010; **9**: 921–32.

43 Gabilondo I, Martínez-Lapiscina EH, Martínez-Heras E, *et al.* Trans-synaptic axonal degeneration in the visual pathway in multiple sclerosis. *Ann Neurol* 2014; **75**: 98–107.

44 Brewer A, Barton B. Visual cortex in aging and Alzheimer's disease: changes in visual field maps and population receptive fields. *Frontiers in Psychology* 2014; **5**: 74.

45 Biessels GJ. Alzheimer's disease, cerebrovascular disease and dementia: lump, split or integrate? Brain. 2022; **145**: 2632–4.

46 Launer LJ, Petrovitch H, Ross GW, Markesbery W, White LR. AD brain pathology: vascular origins? Results from the HAAS autopsy study. *Neurobiol Aging* 2008; **29**: 1587–90.

47 Schneider JA, Arvanitakis Z, Leurgans SE, Bennett DA. The neuropathology of probable Alzheimer disease and mild cognitive impairment. *Ann Neurol* 2009; **66**: 200–8.

48 Arvanitakis Z, Capuano AW, Leurgans SE, Bennett DA, Schneider JA. Relation of cerebral vessel disease to Alzheimer's disease dementia and cognitive function in elderly people: a cross-sectional study. *Lancet Neurol* 2016; **15**: 934–43.

49 Ossenkoppele R, Jansen WJ, Rabinovici GD, *et al.* Prevalence of amyloid PET positivity in dementia syndromes. *JAMA* 2015; **313**: 1939.

50 Barnes DE, Yaffe K. The projected effect of risk factor reduction on Alzheimer's disease prevalence. *Lancet Neurol* 2011; **10**: 819–28.

51 Jackman T WJD. Photographing the Eye of the Living Human Retina. *Photographic News* 1886; published online May 7.

52 Hildred RB. A brief history on the development of ophthalmic retinal photography into digital imaging. *Journal of Audiovisual Media in Medicine* 1990; **13**: 101–5.

53 Panwar N, Huang P, Lee J, *et al.* Fundus Photography in the 21st Century--A Review of Recent Technological Advances and Their Implications for Worldwide Healthcare. *Telemedicine journal and e-health : the official journal of the American Telemedicine Association* 2016; **22**: 198–208.

54 Torpy JM, Glass TJ, Glass RM. Retinopathy. *JAMA* 2007; **298**: 944–944.

55 Scanlon PH. The English National Screening Programme for diabetic retinopathy 2003-2016. *Acta diabetologica* 2017; **54**: 515–25.

56 Keith NM, Wagener HP, Barker NW. Some different types of essential hypertension: their course and prognosis. *Am J Med Sci* 1974; **268**: 336–45.

57 Yu T, Mitchell P, Berry G, Li W, Wang JJ. Retinopathy in Older Persons Without Diabetes and Its Relationship to Hypertension. *Archives of Ophthalmology* 1998; **116**: 83–9.

58 Palatini P, Penzo M, Bongiovì S, Canali C, Pessina AC. [Role of ophthalmoscopy in arterial hypertension: a problem revisited]. *Cardiologia* 1991; **36**: 713–22.

59 Besharati MR, Rastegar A, Shoja MR, Maybodi ME. Prevalence of retinopathy in hypertensive patients. *Saudi Med J* 2006; **27**: 1725–8.

60 Kim GH, Youn HJ, Kang S, Choi YS, Moon JI. Relation between grade II hypertensive retinopathy and coronary artery disease in treated essential hypertensives. *Clin Exp Hypertens* 2010; **32**: 469–73.

61 Cuspidi C, Macca G, Sampieri L, *et al.* High prevalence of cardiac and extracardiac target organ damage in refractory hypertension. *J Hypertens* 2001; **19**: 2063–70.

62 Doubal FN, Hokke PE, Wardlaw JM. Retinal microvascular abnormalities and stroke: a systematic review. *J Neurol Neurosurg Psychiatry* 2009; **80**: 158–65.

63 Dumitrascu OM, Demaerschalk BM, Valencia Sanchez C, *et al.* Retinal Microvascular Abnormalities as Surrogate Markers of Cerebrovascular Ischemic Disease: A Meta-Analysis. *J Stroke Cerebrovasc Dis* 2018; **27**: 1960–8.

64 Wong TY, Klein R, Nieto FJ, *et al.* Retinal microvascular abnormalities and 10-year cardiovascular mortality: A population-based case-control study. *Ophthalmology* 2003; **110**: 933–40.

65 Wong TY, Klein R, Sharrett AR, *et al.* Retinal Arteriolar Narrowing and Risk of Coronary Heart Disease in Men and WomenThe Atherosclerosis Risk in Communities Study. *JAMA* 2002; **287**: 1153–9.

66 Vermeer SE, Prins ND, den Heijer T, Hofman A, Koudstaal PJ, Breteler MM. Silent brain infarcts and the risk of dementia and cognitive decline. *N Engl J Med* 2003; **348**: 1215–22.

67 Schrijvers EMC, Buitendijk GHS, Ikram MK, *et al.* Retinopathy and risk of dementia: the Rotterdam Study. *Neurology* 2012; **79**: 365–70.

68 Cheung CY, Lamoureux E, Ikram MK, *et al.* Retinal vascular geometry in Asian persons with diabetes and retinopathy. *J Diabetes Sci Technol* 2012; **6**: 595–605.

69 Wong TY, Klein R, Couper DJ, *et al.* Retinal microvascular abnormalities and incident stroke: the Atherosclerosis Risk in Communities Study. *Lancet* 2001; **358**: 1134–40.

70 Hubbard LD, Brothers RJ, King WN, *et al.* Methods for evaluation of retinal microvascular abnormalities associated with hypertension/sclerosis in the Atherosclerosis Risk in Communities Study. *Ophthalmology* 1999; **106**: 2269–80.

71 Wong TY, Wang JJ, Rochtchina E, Klein R, Mitchell P. Does refractive error influence the association of blood pressure and retinal vessel diameters? The Blue Mountains Eye Study. *Am J Ophthalmol* 2004; **137**: 1050–5.

72 Fraz MM, Welikala RA, Rudnicka AR, Owen CG, Strachan DP, Barman SA. QUARTZ: Quantitative Analysis of Retinal Vessel Topology and size – An automated system for quantification of retinal vessels morphology. *Expert Systems with Applications* 2015; **42**: 7221–34.

73 Wei FF, Zhang ZY, Petit T, *et al.* Retinal microvascular diameter, a hypertension-related trait, in ECG-gated vs. non-gated images analyzed by IVAN and SIVA. *Hypertens Res* 2016; **39**: 886–92.

74 Yip W, Tham YC, Hsu W, *et al.* Comparison of Common Retinal Vessel Caliber Measurement Software and a Conversion Algorithm. *Transl Vis Sci Technol* 2016; **5**: 11.

75 McGrory S, Taylor AM, Pellegrini E, *et al.* Towards Standardization of Quantitative Retinal Vascular Parameters: Comparison of SIVA and VAMPIRE Measurements in the Lothian Birth Cohort 1936. *Transl Vis Sci Technol* 2018; **7**: 12.

76 Scheie HG. Evaluation of ophthalmoscopic changes of hypertension and arteriolar sclerosis. *AMA Arch Ophthalmol* 1953; **49**: 117–38.

77 Sharrett AR, Hubbard LD, Cooper LS, *et al.* Retinal arteriolar diameters and elevated blood pressure: the Atherosclerosis Risk in Communities Study. *Am J Epidemiol* 1999; **150**: 263–70.

78 McGeechan K, Liew G, Macaskill P, *et al.* Prediction of incident stroke events based on retinal vessel caliber: a systematic review and individual-participant meta-analysis. *Am J Epidemiol* 2009; **170**: 1323–32.

79 McGeechan K, Liew G, Macaskill P, *et al.* Meta-analysis: retinal vessel caliber and risk for coronary heart disease. *Ann Intern Med* 2009; **151**: 404–13.

80 Seidelmann SB, Claggett B, Bravo PE, *et al.* Retinal Vessel Calibers in Predicting Long-Term Cardiovascular Outcomes: The Atherosclerosis Risk in Communities Study. *Circulation* 2016; **134**: 1328–38.

81 Chandra A, Seidelmann SB, Claggett BL, *et al.* The association of retinal vessel calibres with heart failure and long-term alterations in cardiac structure and

function: the Atherosclerosis Risk in Communities (ARIC) Study. *Eur J Heart Fail* 2019; **21**: 1207–15.

82 Guo S, Yin S, Tse G, Li G, Su L, Liu T. Association Between Caliber of Retinal Vessels and Cardiovascular Disease: a Systematic Review and Meta-Analysis. *Current Atherosclerosis Reports* 2020; **22**: 16.

83 Berisha F, Feke GT, Trempe CL, McMeel JW, Schepens CL. Retinal abnormalities in early Alzheimer's disease. *Invest Ophthalmol Vis Sci* 2007; **48**: 2285–9.

84 Cheung CY, Ong YT, Ikram MK. Microvascular network al- terations in the retina of patients with Alzheimer's disease. *Alzheimers Dement* 2014; **10**: 135–42.

85 Liew G, Mitchell P, Wong TY, *et al.* Retinal microvascular signs and cognitive impairment. *J Am Geriatr Soc* 2009; **57**: 1892–6.

86 De Jong FJ, Schrijvers EM, Ikram MK. Retinal vascular calibre and risk of dementia: The rotterdam study. *Neurology* 2011; **76**: 816–21.

87 Lesage SR, Mosley TH, Wong TY. Retinal microvascular ab- normalities and cognitive decline: The ARIC 14-year follow-up study. *Neurology* 2009; **73**: 862–8.

88 Mandelbrot B. How long is the coast of britain? Statistical self-similarity and fractional dimension. *Science* 1967; **156**: 636–8.

89 Lipsitz LA, Goldberger AL. Loss of "complexity" and aging. Potential applications of fractals and chaos theory to senescence. *Jama* 1992; **267**: 1806–9.

90 Masters BR. Fractal analysis of the vascular tree in the human retina. *Annu Rev Biomed Eng* 2004; **6**: 427–52.

91 Mainster MA. The fractal properties of retinal vessels: Embryological and clinical implications. *Eye* 1990; **4**: 235–41.

92 Allen M, Brown GJ, Miles NJ. Measurement of boundary fractal dimensions: review of current techniques. *Powder Technology* 1995; **84**: 1–14.

93 Hao H, Sasongko MB, Wong TY, *et al.* Does Retinal Vascular Geometry Vary with Cardiac Cycle? *Investigative Ophthalmology & Visual Science* 2012; **53**: 5799–805.

94 Dumskyj MJ, Aldington SJ, Dore CJ, Kohner EM. The accurate assessment of changes in retinal vessel diameter using multiple frame electrocardiograph synchronised fundus photography. *Curr Eye Res* 1996; **15**: 625–32.

95 Knudtson MD, Klein BEK, Klein R, *et al.* Variation associated with measurement of retinal vessel diameters at different points in the pulse cycle. *The British journal of ophthalmology* 2004; **88**: 57–61.

96 Chen HC, Patel V, Wiek J, Rassam SM, Kohner EM. Vessel diameter changes during the cardiac cycle. *Eye* 1994; **8**: 97–103.

97 Aliahmad B, Kumar DK, Hao H, Kawasaki R. Does fractal properties of retinal vasculature vary with cardiac cycle? 2013.

98 Wainwright A, Liew G, Burlutsky G, *et al.* Effect of image quality, color, and format on the measurement of retinal vascular fractal dimension. *Invest Ophthalmol Vis Sci* 2010; **51**: 5525–9.

99 Lyu X, Jajal P, Tahir MZ, Zhang S. Fractal dimension of retinal vasculature as an image quality metric for automated fundus image analysis systems. *Sci Rep* 2022; **12**: 11868.

100 Family, Fereydoon, Masters BR, Platt DE. Fractal pattern formation in human retinal vessels. *Physica D: Nonlinear Phenomena* 1989; **38**: 98–103.

101 Masters B, Platt D. Development of human retinal vessels: a fractal analysis. *Invest Ophthalmol Vis Sci* 1989; **30**: 391.

102 Liew G, Wang JJ, Cheung N, *et al.* The retinal vasculature as a fractal: methodology, reliability, and relationship to blood pressure. *Ophthalmology* 2008; **115**: 1951–6.

103 Sng CC, Wong WL, Cheung CY, Lee J, Tai ES, Wong TY. Retinal vascular fractal and blood pressure in a multiethnic population. *J Hypertens* 2013; **31**: 2036–42.

104 Kurniawan ED, Cheung N, Cheung CY, Tay WT, Saw SM, Wong TY. Elevated blood pressure is associated with rarefaction of the retinal vasculature in children. *Invest Ophthalmol Vis Sci* 2012; **53**: 470–4.

105 Liew G, Mitchell P, Rochtchina E, *et al.* Fractal analysis of retinal microvasculature and coronary heart disease mortality. *Eur Heart J* 2011; **32**: 422–9.

106 Lemmens S, Devulder A, Van Keer K, Bierkens J, De Boever P, Stalmans I. Systematic Review on Fractal Dimension of the Retinal Vasculature in Neurodegeneration and Stroke: Assessment of a Potential Biomarker. *Front Neurosci* 2020; **14**: 16.

107 Ong YT, De Silva DA, Cheung CY, *et al.* Microvascular structure and network in the retina of patients with ischemic stroke. *Stroke* 2013; **44**: 2121–7.

108 Cheung CY, Tay WT, Ikram MK, *et al.* Retinal microvascular changes and risk of stroke: the Singapore Malay Eye Study. *Stroke* 2013; **44**: 2402–8.

109 Cheung N, Liew G, Lindley RI, *et al.* Retinal fractals and acute lacunar stroke. *Ann Neurol* 2010; **68**: 107–11.

110 McGrory S, Ballerini L, Doubal FN, *et al.* Retinal microvasculature and cerebral small vessel disease in the Lothian Birth Cohort 1936 and Mild Stroke Study. *Sci Rep* 2019; **9**: 6320.

111 Doubal FN, MacGillivray TJ, Patton N, Dhillon B, Dennis MS, Wardlaw JM. Fractal analysis of retinal vessels suggests that a distinct vasculopathy causes lacunar stroke. *Neurology* 2010; **74**: 1102–7.

112 Cheung CY, Ong YT, Ikram MK, *et al.* Microvascular network alterations in the retina of patients with Alzheimer's disease. *Alzheimers Dement* 2014; **10**: 135–42.

113 Taylor AM, MacGillivray TJ, Henderson RD, *et al.* Retinal Vascular Fractal Dimension, Childhood IQ, and Cognitive Ability in Old Age: The Lothian Birth Cohort Study 1936. *PLOS ONE* 2015; **10**: e0121119.

114 Benitez-Aguirre P, Craig ME, Sasongko MB, *et al.* Retinal vascular geometry predicts incident retinopathy in young people with type 1 diabetes: a prospective cohort study from adolescence. *Diabetes Care* 2011; **34**: 1622–7.

115 Zepeda-Romero LC, Martinez-Perez ME, Ruiz-Velasco S, Ramirez-Ortiz MA, Gutierrez-Padilla JA. Temporary morphological changes in plus disease induced during contact digital imaging. *EYE* 2011; **25**: 1337–40.

116 Mahal S, Strain WD, Martinez-Perez ME, Thom SAM, Chaturvedi N, Hughes AD. Comparison of the retinal microvasculature in European and African-Caribbean people with diabetes. *Clin Sci (Lond)* 2009; **117**: 229–36.

117 Hughes AD, Stanton AV, Jabbar AS, Chapman N, Martinez-Perez ME, McG Thom SA. Effect of antihypertensive treatment on retinal microvascular changes in hypertension. *J Hypertens* 2008; **26**: 1703–7.

118 Crosby-Nwaobi R, Heng LZ, Sivaprasad S. Retinal vascular calibre, geometry and progression of diabetic retinopathy in type 2 diabetes mellitus. *Ophthalmologica* 2012; **228**: 84–92.

119 Cheung CY, Tay WT, Mitchell P, *et al.* Quantitative and qualitative retinal microvascular characteristics and blood pressure. *J Hypertens* 2011; **29**: 1380–91.

120 Lim LS, Cheung CY-L, Lin X, Mitchell P, Wong TY, Mei-Saw S. Influence of refractive error and axial length on retinal vessel geometric characteristics. *Invest Ophthalmol Vis Sci* 2011; **52**: 669–78.

121 Kalitzeos AA, Lip GYH, Heitmar R. Retinal vessel tortuosity measures and their applications. *Exp Eye Res* 2013; **106**: 40–6.

122 Ong Y-T, De Silva DA, Cheung CY, *et al.* Microvascular structure and network in the retina of patients with ischemic stroke. *Stroke* 2013; **44**: 2121–7.

123 Biffi E, Turple Z, Chung J, Biffi A. Retinal biomarkers of Cerebral Small Vessel Disease: A systematic review. *PLoS One* 2022; **17**: e0266974.

124 Hilal S, Ong Y-T, Cheung CY, *et al.* Microvascular network alterations in retina of subjects with cerebral small vessel disease. *Neurosci Lett* 2014; **577**: 95–100.

125 Sandoval-Garcia E, McLachlan S, Price AH, *et al.* Retinal arteriolar tortuosity and fractal dimension are associated with long-term cardiovascular outcomes in people with type 2 diabetes. *Diabetologia* 2021; **64**: 2215–27.

126 Mordi IR, Trucco E, Syed MG, *et al.* Prediction of Major Adverse Cardiovascular Events From Retinal, Clinical, and Genomic Data in Individuals With Type 2 Diabetes: A Population Cohort Study. *Diabetes Care* 2022; **45**: 710–6.

127 Frost S, Kanagasingam Y, Sohrabi H, *et al.* Retinal vascular biomarkers for early detection and monitoring of Alzheimer's disease. *Transl Psychiatry* 2013; **3**: e233.

128 Williams MA, McGowan AJ, Cardwell CR, *et al.* Retinal microvascular network attenuation in Alzheimer's disease. *Alzheimers Dement (Amst)* 2015; **1**: 229–35.

129 Pead E, Thompson AC, Grewal DS, *et al.* Retinal vascular changes in Alzheimer's dementia and mild cognitive impairment: A pilot study using ultra-Widefield imaging. *Transl Vis Sci Technol* 2023; **12**: 13.

130 Staurenghi G, Sadda S, Chakravarthy U, Spaide RF, International Nomenclature for Optical Coherence Tomography (IN•OCT) Panel. Proposed lexicon for anatomic landmarks in normal posterior segment spectral-domain optical coherence tomography: the IN•OCT consensus. *Ophthalmology* 2014; **121**: 1572–8.

131 Amoaku WM, Ghanchi F, Bailey C, *et al.* Diabetic retinopathy and diabetic macular oedema pathways and management: UK Consensus Working Group. *Eye* 2020; **34**: 1–51.

132 Huang D, Swanson EA, Lin CP, *et al.* Optical coherence tomography. *Science* 1991; **254**: 1178–81.

133 van Munster CEP, Uitdehaag BMJ. Outcome Measures in Clinical Trials for Multiple Sclerosis. *CNS Drugs* 2017; **31**: 217–36.

134 Dacey DM. The dopaminergic amacrine cell. *J Comp Neurol* 1990; **301**: 461–89.

135 Frederick JM, Rayborn ME, Laties AM, Lam DM, Hollyfield JG. Dopaminergic neurons in the human retina. *J Comp Neurol* 1982; **210**: 65–79.

136 Witkovsky P. Dopamine and retinal function. *Doc Ophthalmol* 2004; **108**: 17–40.

137 Kergoat H, Kergoat M-J, Justino L, Chertkow H, Robillard A, Bergman H. An evaluation of the retinal nerve fiber layer thickness by scanning laser polarimetry in individuals with dementia of the Alzheimer type. *Acta Ophthalmologica Scandinavica* 2001; **79**: 187–91.

138 Mejia-Vergara AJ, Restrepo-Jimenez P, Pelak VS. Optical coherence tomography in mild cognitive impairment: A systematic review and meta-analysis. *Front Neurol* 2020; **11**: 578698.

139 Chan VTT, Sun Z, Tang S, *et al.* Spectral-domain OCT measurements in Alzheimer's disease: A systematic review and meta-analysis. *Ophthalmology* 2019; **126**: 497–510.

140 Costanzo E, Lengyel I, Parravano M, *et al.* Ocular biomarkers for Alzheimer disease dementia: An umbrella review of Systematic Reviews and Meta-analyses. *JAMA Ophthalmol* 2023; **141**: 84–91.

141 Wisely CE, Wang D, Henao R, *et al.* Convolutional neural network to identify symptomatic Alzheimer's disease using multimodal retinal imaging. *Br J Ophthalmol* 2020. DOI:10.1136/bjophthalmol-2020-317659.

142 Ko F, Muthy ZA, Gallacher J, *et al.* Association of Retinal Nerve Fiber Layer Thinning With Current and Future Cognitive Decline: A Study Using Optical Coherence Tomography. *JAMA Neurol* 2018; **75**: 1198–205.

143 Mutlu U, Colijn JM, Ikram MA, *et al.* Association of retinal neurodegeneration on optical coherence tomography with dementia: A population-based study. *JAMA Neurol* 2018; **75**: 1256–63.

144 Healthcare across the UK: A comparison of the NHS in England, Scotland, wales and northern Ireland - national audit office (NAO) report. National Audit Office. 2012; published online June 29. https://www.nao.org.uk/report/healthcare-across-the-uk-a-comparison-of-the-nhs-in-england-scotland-wales-and-northern-ireland/ (accessed Aug 9, 2022).

145 The web's free 2022 ICD-10-CM/PCS medical coding reference. https://www.icd10data.com/ (accessed Aug 2, 2022).

146 Hospital Episode Statistics (HES). NHS Digital. https://digital.nhs.uk/data-and-information/data-tools-and-services/data-services/hospital-episode-statistics (accessed June 8, 2022).

147 Burns EM, Rigby E, Mamidanna R, *et al.* Systematic review of discharge coding accuracy. *Journal of public health (Oxford, England)* 2012; **34**: 138–48.

148 Spencer SA, Davies MP. Hospital episode statistics: improving the quality and value of hospital data: a national internet e-survey of hospital consultants. *BMJ open* 2012; **2**: e001651.

149 Luben R, Hayat S, Khawaja A, Wareham N, Pharoah PP, Khaw K-T. Residential area deprivation and risk of subsequent hospital admission in a British population: the EPIC-Norfolk cohort. *BMJ Open* 2019; **9**: e031251.

150 Boyd A, Golding J, Macleod J, *et al.* Cohort Profile: the 'children of the 90s'--the index offspring of the Avon Longitudinal Study of Parents and Children. *International journal of epidemiology* 2013; **42**: 111–27.

151 Brown A, Kirichek O, Balkwill A, *et al.* Comparison of dementia recorded in routinely collected hospital admission data in England with dementia recorded in primary care. *Emerg Themes Epidemiol* 2016; **13**: 11.

152 Herrett E, Shah AD, Boggon R, *et al.* Completeness and diagnostic validity of recording acute myocardial infarction events in primary care, hospital care, disease registry, and national mortality records: cohort study. *BMJ : British Medical Journal* 2013; **346**: f2350.

153 Wood A, Denholm R, Hollings S, *et al.* Linked electronic health records for research on a nationwide cohort of more than 54 million people in England: data resource. *BMJ* 2021; **373**: n826.

154 Brenner H, Gefeller O. Use of the Positive Predictive Value to Correct for Disease Misclassification in Epidemiologic Studies. *American Journal of Epidemiology* 1993; **138**: 1007–15.

155 Greenland S. Variance estimation for epidemiologic effect estimates under misclassification. *Stat Med* 1988; **7**: 745–57.

156 Selén J. Adjusting for Errors in Classification and Measurement in the Analysis of Partly and Purely Categorical Data. *Journal of the American Statistical Association* 1986; **81**: 75–81.

157 Marshall RJ. Validation study methods for estimating exposure proportions and odds ratios with misclassified data. *J Clin Epidemiol* 1990; **43**: 941–7.

158 Fry A, Littlejohns TJ, Sudlow C, *et al.* Comparison of sociodemographic and health-related characteristics of UK Biobank participants with those of the general population. *Am J Epidemiol* 2017; **186**: 1026–34.

159 Justin BN, Turek M, Hakim AM. Heart disease as a risk factor for dementia. *Clinical epidemiology* 2013; **5**: 135–45.

160 de Bruijn RFAG, Ikram MA. Cardiovascular risk factors and future risk of Alzheimer's disease. *BMC Medicine* 2014; **12**: 130.

161 Wikipedia S, Books LLC. Lists of ethnic groups. Books LLC, Wiki Series, 2011.

162 The English Index of Multiple Deprivation (IMD) 2015 -guidance. https://assets.publishing.service.gov.uk/government/uploads/system/uploads/attachment_data/file/464430/English_Index_of_Multiple_Deprivation_2015_-_Guidance.pdf (accessed March 6, 2023).

163 Digital, NHS. https://digital.nhs.uk/services/data-access-request-service-dars. .

164 UK Government Web Archive. https://webarchive.nationalarchives.gov.uk/20200706184649/https://digital.nhs.uk/about-nhs-digital/corporate-information-and-documents/independent-group-advising-on-the-release-of-data (accessed March 6, 2023).

165 Wagner SK, Hughes F, Cortina-Borja M, *et al.* AlzEye: longitudinal record-level linkage of ophthalmic imaging and hospital admissions of 353 157 patients in London, UK. *BMJ Open* 2022; **12**: e058552.

166 Quartilho A, Simkiss P, Zekite A, Xing W, Wormald R, Bunce C. Leading causes of certifiable visual loss in England and Wales during the year ending 31 March 2013. *EYE* 2016; **30**: 602–7.

167 Pezzullo L, Streatfeild J, Simkiss P, Shickle D. The economic impact of sight loss and blindness in the UK adult population. *BMC Health Services Research* 2018; **18**: 63.

168 Pascolini D, Mariotti SP. Global estimates of visual impairment: 2010. *Br J Ophthalmol* 2012; **96**: 614–8.

169 Lee AJ, Wang JJ, Kifley A, Mitchell P. Open-angle glaucoma and cardiovascular mortality: the Blue Mountains Eye Study. *Ophthalmology* 2006; **113**: 1069–76.

170 Wang J, Xue Y, Thapa S, Wang L, Tang J, Ji K. Relation between Age-Related Macular Degeneration and Cardiovascular Events and Mortality: A Systematic Review and Meta-Analysis. *Biomed Res Int* 2016; **2016**: 8212063.

171 Hu WS, Lin CL, Chang SS, Chen MF, Chang KC. Increased risk of ischemic heart disease among subjects with cataracts: A population-based cohort study. *Medicine (Baltimore)* 2016; **95**: e4119.

172 Wong TY, Tikellis G, Sun C, Klein R, Couper DJ, Sharrett AR. Age-related macular degeneration and risk of coronary heart disease: the Atherosclerosis Risk in Communities Study. *Ophthalmology* 2007; **114**: 86–91.

173 Castells X, Alonso J, Ribó C, Nara D, Teixidó A, Castilla M. Factors associated with second eye cataract surgery. *British Journal of Ophthalmology* 2000; **84**: 9–12.

174 Laidlaw A, Harrad R. Can second eye cataract extraction be justified? *Eye* 1993; **7**: 680–6.

175 Claridge KG, Francis PJ, Bates AK. Should second eye cataract surgery be rationed? *Eye (Lond)* 1995; **9 (Pt 6 Su)**: 47–9.

176 Fasler K, Fu DJ, Moraes G, *et al.* Moorfields AMD database report 2: fellow eye involvement with neovascular age-related macular degeneration. *British Journal of Ophthalmology* 2020; **104**: 684.

177 Fasler K, Moraes G, Wagner S, *et al.* One- and two-year visual outcomes from the Moorfields age-related macular degeneration database: a retrospective cohort study and an open science resource. *BMJ Open* 2019; **9**: e027441.

178 Asaria P, Elliott P, Douglass M, *et al.* Acute myocardial infarction hospital admissions and deaths in England: a national follow-back and follow-forward record-linkage study. *The Lancet Public health* 2017; **2**: e191–201.

179 Nedkoff L, Lopez D, Goldacre M, Sanfilippo F, Hobbs M, Wright FL. Identification of myocardial infarction type from electronic hospital data in England and Australia: a comparative data linkage study. *BMJ Open* 2017; **7**: e019217.

180 Smolina K, Wright FL, Rayner M, Goldacre MJ. Incidence and 30-day case fatality for acute myocardial infarction in England in 2010: national-linked database study. *European Journal of Public Health* 2012; **22**: 848–53.

181 Definitions of stroke for UK biobank phase 1 outcomes adjudication. https://biobank.ndph.ox.ac.uk/ukb/ukb/docs/alg_outcome_stroke.pdf (accessed July 24, 2023).

182 Davis KAS, Bashford O, Jewell A, *et al.* Using data linkage to electronic patient records to assess the validity of selected mental health diagnoses in English Hospital Episode Statistics (HES). *PLoS One* 2018; **13**: e0195002.

183 Chua SYL, Thomas D, Allen N, *et al.* Cohort profile: design and methods in the eye and vision consortium of UK Biobank. *BMJ Open* 2019; **9**: e025077.

184 Patel PJ, Foster PJ, Grossi CM, *et al.* Spectral-domain optical coherence tomography imaging in 67 321 adults: Associations with macular thickness in the UK Biobank study. *Ophthalmology* 2016; **123**: 829–40.

185 Keane PA, Grossi CM, Foster PJ, *et al.* Optical coherence tomography in the UK Biobank study - rapid automated analysis of retinal thickness for large population-based studies. *PLoS One* 2016; **11**: e0164095.

186 Abel GA, Barclay ME, Payne RA. Adjusted indices of multiple deprivation to enable comparisons within and between constituent countries of the UK including an illustration using mortality rates. *BMJ Open* 2016; **6**: e012750.

187 Blane D, Townsend P, Phillimore P, Beattie A. Health and deprivation: Inequality and the north. *Br J Sociol* 1989; **40**: 344.

188 Data impact blog. https://blog.ukdataservice.ac.uk/deprived-or-live-in-poverty-1/ (accessed March 6, 2023).

189: Category 100006. https://biobank.ndph.ox.ac.uk/showcase/label.cgi?id=100006 (accessed March 7, 2023).

190 Biomarker data. https://www.ukbiobank.ac.uk/enable-your-research/about-our-data/biomarker-data (accessed March 7, 2023).

191 Health-related outcomes data. https://www.ukbiobank.ac.uk/enable-your-research/about-our-data/health-related-outcomes-data (accessed March 7, 2023).

192 Vampire. https://vampire.computing.dundee.ac.uk/ (accessed March 7, 2023).

193 Zhou Y, Wagner SK, Chia MA, *et al.* AutoMorph: Automated Retinal Vascular Morphology Quantification Via a Deep Learning Pipeline. *Transl Vis Sci Technol* 2022; **11**: 12.

194 Trucco E, Ballerini L, Relan D, *et al.* Novel VAMPIRE algorithms for quantitative analysis of the retinal vasculature. 2013.

195 Ronneberger O, Fischer P, Brox T. U-Net: Convolutional Networks for Biomedical Image Segmentation. In: Lecture Notes in Computer Science. Cham: Springer International Publishing, 2015: 234–41.

196 Zhou Y, Xu M, Hu Y, *et al.* Learning to address intra-segment misclassification in retinal imaging. In: Medical Image Computing and Computer Assisted Intervention – MICCAI 2021. Cham: Springer International Publishing, 2021: 482–92.

197 Fu H, Wang B, Shen J, *et al.* Evaluation of retinal image quality assessment networks in different color-spaces. In: Lecture Notes in Computer Science. Cham: Springer International Publishing, 2019: 48–56.

198 Galdran A, Anjos A, Dolz J, Chakor H, Lombaert H, Ayed IB. The little W-Net that could: State-of-the-art retinal vessel segmentation with minimalistic models. arXiv [eess.IV]. 2020; published online Sept 3. http://arxiv.org/abs/2009.01907.

199 Valdés A. retipy: A complete retipy application using docker. Github https://github.com/alevalv/retipy (accessed March 7, 2023).

200 Early Treatment Diabetic Retinopathy Study Research Group. Photocoagulation for diabetic macular edema. *Arch Ophthalmol* 1985; **103**: 1796–806.

201 Tuten WS, Harmening WM. Foveal vision. *Curr Biol* 2021; **31**: R701–3.

202 Hemingway H, Croft P, Perel P, *et al.* Prognosis research strategy (PROGRESS) 1: A framework for researching clinical outcomes. *BMJ : British Medical Journal* 2013; **346**: e5595.

203 Riley RD, Hayden JA, Steyerberg EW, *et al.* Prognosis Research Strategy (PROGRESS) 2: Prognostic Factor Research. *PLOS Medicine* 2013; **10**: e1001380.

204 Steyerberg EW, Moons KGM, van der Windt DA, *et al.* Prognosis Research Strategy (PROGRESS) 3: Prognostic Model Research. *PLOS Medicine* 2013; **10**: e1001381.

205 Cox DR. Regression Models and Life-Tables. *Journal of the Royal Statistical Society Series B (Methodological)* 1972; **34**: 187–220.

206 Fine JP, Gray RJ. A Proportional Hazards Model for the Subdistribution of a Competing Risk. *Journal of the American Statistical Association* 1999; **94**: 496–509.

207 Rosenbaum PR, Rubin DB. The central role of the propensity score in observational studies for causal effects. *Biometrika* 1983; **70**: 41.

208 Belitser SV, Martens EP, Pestman WR, Groenwold RHH, de Boer A, Klungel OH. Measuring balance and model selection in propensity score methods. *Pharmacoepidemiol Drug Saf* 2011; **20**: 1115–29.

209 Austin PC. Balance diagnostics for comparing the distribution of baseline covariates between treatment groups in propensity-score matched samples. *Stat Med* 2009; **28**: 3083–107.

210 Austin PC, Stuart EA. Moving towards best practice when using inverse probability of treatment weighting (IPTW) using the propensity score to estimate causal treatment effects in observational studies. *Stat Med* 2015; **34**: 3661–79.

211 Ho DE, Imai K, King G, Stuart EA. Matching as Nonparametric Preprocessing for Reducing Model Dependence in Parametric Causal Inference. *Polit Anal* 2007; **15**: 199–236.

212 Stensrud MJ, Hernán MA. Why Test for Proportional Hazards? *Jama* 2020; **323**: 1401–2.

213 Grambsch PM, Therneau TM. Proportional Hazards Tests and Diagnostics Based on Weighted Residuals. *Biometrika* 1994; **81**: 515–26.

214 Berrett TB, Samworth RJ. USP: an independence test that improves on Pearson's chi-squared and the G-test. *Proc Math Phys Eng Sci* 2021; **477**: 20210549.

215 Satterthwaite FE. An approximate distribution of estimates of variance components. *Biometrics* 1946; **2**: 110–4.

216 van Buuren S. Multiple imputation of discrete and continuous data by fully conditional specification. *Stat Methods Med Res* 2007; **16**: 219–42.

217 Aalen OO. Heterogeneity in survival analysis. *Stat Med* 1988; **7**: 1121–37.

218 Hens N, Wienke A, Aerts M, Molenberghs G. The correlated and shared gamma frailty model for bivariate current status data: an illustration for cross-sectional serological data. *Stat Med* 2009; **28**: 2785–800.

219 Bates D, Mächler M, Bolker B, Walker S. Fitting Linear Mixed-Effects Models Using**lme4**. Journal of Statistical Software. 2015; **67**. DOI:10.18637/jss.v067.i01.

220 van Buuren S, Groothuis-Oudshoorn K. mice: Multivariate Imputation by Chained Equations in R. *J Stat Softw* 2011; **45**: 1–67.

221 Therneau T, Lumley T. R survival package. *R Core Team* 2013. https://mran.revolutionanalytics.com/snapshot/2019-04-07/web/packages/survival/vignettes/survival.pdf.

222 van Smeden M, de Groot JAH, Moons KGM, *et al.* No rationale for 1 variable per 10 events criterion for binary logistic regression analysis. *BMC Medical Research Methodology* 2016; **16**: 163.

223 Peduzzi P, Concato J, Kemper E, Holford TR, Feinstein AR. A simulation study of the number of events per variable in logistic regression analysis. *Journal of clinical epidemiology* 1996; **49**: 1373–9.

224 Courvoisier DS, Combescure C, Agoritsas T, Gayet-Ageron A, Perneger TV. Performance of logistic regression modeling: beyond the number of events per variable, the role of data structure. *Journal of clinical epidemiology* 2011; **64**: 993–1000.

225 Vittinghoff E, McCulloch CE. Relaxing the rule of ten events per variable in logistic and Cox regression. *American journal of epidemiology* 2007; **165**: 710–8.

226 Riley RD, Snell KIE, Ensor J, *et al.* Minimum sample size for developing a multivariable prediction model: PART II - binary and time-to-event outcomes. *Statistics in Medicine* 2019; **38**: 1276–96.

227 Muzerengi S, Herd C, Rick C, Clarke CE. A systematic review of interventions to reduce hospitalisation in Parkinson's disease. *Parkinsonism Relat Disord* 2016; **24**: 3–7.

228 Mutlu U, Bonnemaijer PWM, Ikram MA, *et al.* Retinal neurodegeneration and brain MRI markers: the Rotterdam Study. *Neurobiol Aging* 2017; **60**: 183–91.

229 Hofman A, Brusselle GGO, Darwish Murad S, *et al.* The Rotterdam Study: 2016 objectives and design update. *Eur J Epidemiol* 2015; **30**: 661–708.

230 Ikram MA, Brusselle GGO, Murad SD, *et al.* The Rotterdam Study: 2018 update on objectives, design and main results. *Eur J Epidemiol* 2017; **32**: 807–50.

231 Majithia S, Tham Y-C, Chee M-L, *et al.* Cohort profile: The Singapore epidemiology of eye diseases study (SEED). *Int J Epidemiol* 2021; **50**: 41–52.

232 Khan SM, Liu X, Nath S, *et al.* A global review of publicly available datasets for ophthalmological imaging: barriers to access, usability, and generalisability. *Lancet Digit Health* 2021; **3**: e51–66.

233 2011 census. https://www.ons.gov.uk/census/2011census (accessed March 28, 2023).

234 Enoch J, McDonald L, Jones L, Jones PR, Crabb DP. Evaluating whether sight is the most valued sense. *JAMA Ophthalmol* 2019; **137**: 1317–20.

235 Sabanayagam C, Xu D, Ting DSW, *et al.* A deep learning algorithm to detect chronic kidney disease from retinal photographs in community-based populations. *Lancet Digit Health* 2020; **2**: e295–302.

236 Mitani A, Huang A, Venugopalan S, *et al.* Detection of anaemia from retinal fundus images via deep learning. *Nat Biomed Eng* 2020; **4**: 18–27.

237 Poplin R, Varadarajan AV, Blumer K, *et al.* Prediction of cardiovascular risk factors from retinal fundus photographs via deep learning. *Nat Biomed Eng* 2018; **2**: 158–64.

238 Cheung CY, Xu D, Cheng C-Y, *et al.* A deep-learning system for the assessment of cardiovascular disease risk via the measurement of retinal-vessel calibre. *Nat Biomed Eng* 2021; **5**: 498–508.

239 Xiao W, Huang X, Wang JH, *et al.* Screening and identifying hepatobiliary diseases through deep learning using ocular images: a prospective, multicentre study. *Lancet Digit Health* 2021; **3**: e88–97.

240 Deng J, Dong W, Socher R, Li L-J, Li K, Fei-Fei L. ImageNet: A large-scale hierarchical image database. In: 2009 IEEE Conference on Computer Vision and Pattern Recognition. IEEE, 2009. DOI:10.1109/cvpr.2009.5206848.

241 Sinha S, Peach G, Poloniecki JD. Studies using English administrative data (Hospital episode statistics) to assess health-care outcomes-systematic review and recommendations for reporting. *Eur J Public Health* 2013; **23**: 86–92.

242 Vetrano DL, Roso-Llorach A, Fernández S, *et al.* Twelve-year clinical trajectories of multimorbidity in a population of older adults. *Nat Commun* 2020; **11**. DOI:10.1038/s41467-020-16780-x.

243 Yamanouchi M, Mori M, Hoshino J, *et al.* Retinopathy progression and the risk of end-stage kidney disease: results from a longitudinal Japanese cohort of 232 patients with type 2 diabetes and biopsy-proven diabetic kidney disease. *BMJ Open Diabetes Res Care* 2019; **7**: e000726.

244 Lin H-T, Zheng C-M, Wu Y-C, *et al.* Diabetic retinopathy as a risk factor for chronic kidney disease progression: A multicenter Case⁻Control study in Taiwan. *Nutrients* 2019; **11**: 509.

245 Hu W-S, Lin C-L, Chang S-S, Chen M-F, Chang K-C. Increased risk of ischemic heart disease among subjects with cataracts: A population-based cohort study. *Medicine (Baltimore)* 2016; **95**: e4119.

246 Chen Y-Y, Hu H-Y, Chu D, Chen H-H, Chang C-K, Chou P. Patients with primary open-angle glaucoma may develop ischemic heart disease more often than those without glaucoma: An 11-year population-based cohort study. *PLoS One* 2016; **11**: e0163210.

247 Hiller R, Podgor MJ, Sperduto RD, Wilson PWF, Chew EY, D'Agostino RB. High intraocular pressure and survival: the Framingham studies. *Am J Ophthalmol* 1999; **128**: 440–5.

248 Biggerstaff KS, Frankfort BJ, Orengo-Nania S, *et al.* Validity of code based algorithms to identify primary open angle glaucoma (POAG) in Veterans Affairs (VA) administrative databases. *Ophthalmic Epidemiol* 2018; **25**: 162–8.

249 Gray B. cmprsk: Subdistribution Analysis of Competing Risks. 2020. https://CRAN.R-project.org/package=cmprsk.

250 T, Therneau. A Package for Survival Analysis in R. 2020. https://CRAN.R-project.org/package=survival.

251 Service, National Health. https://www.nhs.uk/live-well/healthy-body/look-after-your-eyes/. .

252 Service. , National Health. Diabetes Data. https://www.england.nhs.uk/statistics/statistical-work-areas/integrated-performance-measures-monitoring/diabetes-data/ (accessed June 29, 2021).

253 Hu FB, Hankinson SE, Stampfer MJ, *et al.* Prospective study of cataract extraction and risk of coronary heart disease in women. *Am J Epidemiol* 2001; **153**: 875–81.

254 Podgor MJ, Kannel WB, Cassel GH, Sperduto RD. Lens changes and the incidence of cardiovascular events among persons with diabetes. *Am Heart J* 1989; **117**: 642–8.

255 Hospital Outpatient Activity, 2017-18. https://digital.nhs.uk/data-and-information/publications/statistical/hospital-outpatient-activity/2017-18 (accessed Sept 8, 2020).

256 Robson J, Dostal I, Sheikh A, *et al.* The NHS Health Check in England: an evaluation of the first 4 years. *BMJ Open* 2016; **6**: e008840.

257 [No title]. https://d25d2506sfb94s.cloudfront.net/today_uk_import/yg-archives-salixconsulting-eyecare-220611.pdf (accessed Sept 28, 2020).

258 Biousse V, Trobe JD. Transient monocular visual loss. *Am J Ophthalmol* 2005; **140**: 717–21.

259 Biousse V, Newman N. Retinal and optic nerve ischemia. *Continuum (Minneap Minn)* 2014; **20**: 838–56.

260 Sacco RL, Kasner SE, Broderick JP, *et al.* An updated definition of stroke for the 21st century: a statement for healthcare professionals from the American Heart Association/American Stroke Association. *Stroke* 2013; **44**: 2064–89.

261 Biousse V, Nahab F, Newman NJ. Management of acute retinal ischemia: Follow the guidelines! *Ophthalmology* 2018; **125**: 1597–607.

262 Petzold A, Islam N, Hu H-H, Plant GT. Embolic and nonembolic transient monocular visual field loss: a clinicopathologic review. *Surv Ophthalmol* 2013; **58**: 42–62.

263 Zarkali A, Cheng SF, Dados A, Simister R, Chandratheva A. Atrial fibrillation: An underestimated cause of ischemic monocular visual loss? *J Stroke Cerebrovasc Dis* 2019; **28**: 1495–9.

264 Lauda F, Neugebauer H, Reiber L, Jüttler E. Acute silent brain infarction in monocular visual loss of ischemic origin. *Cerebrovasc Dis* 2015; **40**: 151–6.

265 Coutts SB. Diagnosis and Management of Transient Ischemic Attack. *Continuum* 2017; **23**: 82–92.

266 Tamhankar MA, Biousse V, Ying G-S, *et al.* Isolated third, fourth, and sixth cranial nerve palsies from presumed microvascular versus other causes: a prospective study. *Ophthalmology* 2013; **120**: 2264–9.

267 Oh SY. Clinical outcomes and etiology of acquired sixth cranial nerve palsy. *Medicine (Baltimore)* 2022; **101**. DOI:10.1097/MD.0000000000029102.

268 Kim K, Noh SR, Kang MS, Jin KH. Clinical Course and Prognostic Factors of Acquired Third, Fourth, and Sixth Cranial Nerve Palsy in Korean Patients. *Korean J Ophthalmol* 2018; **32**: 221–7.

269 Fang C, Leavitt JA, Hodge DO, Holmes JM, Mohney BG, Chen JJ. Incidence and etiologies of acquired third nerve palsy using a population-based method. *JAMA Ophthalmol* 2017; **135**: 23–8.

270 Jung EH, Kim S-J, Lee JY, Cho B-J. The incidence and etiology of sixth cranial nerve palsy in Koreans: A 10-year nationwide cohort study. *Sci Rep* 2019; **9**: 18419.

271 Dosunmu EO, Hatt SR, Leske DA, Hodge DO, Holmes JM. Incidence and etiology of presumed fourth cranial nerve palsy: A population-based study. *Am J Ophthalmol* 2018; **185**: 110–4.

272 Dotan G, Korczyn AD. Nonarteritic ischemic optic neuropathy and other vascular diseases. Neuroepidemiology. 2013; **40**: 225–6.

273 Chatziralli IP, Kazantzis D, Chatzirallis AP, *et al.* Cardiometabolic factors and risk of non-arteritic anterior ischemic optic neuropathy: a systematic review and meta-analysis. *Arbeitsphysiologie* 2022; **260**: 1445–56.

274 Hayreh SS. Ischemic optic neuropathies - where are we now? Graefe's Archive for. *Clinical and Experimental Ophthalmology* 2013; **251**: 1873–84.

275 Shir Yen W, Yathavan S, Ramli MA, Siu Wan F, Che Hamzah J. Bilateral sequential non-arteritic anterior ischemic optic neuropathy (NAION). *Cureus* 2021; **13**: e19408.

276 Miller NR, Arnold AC. Current concepts in the diagnosis, pathogenesis and management of nonarteritic anterior ischaemic optic neuropathy. *EYE* 2015; **29**: 65–79.

277 Liu B, Yu Y, Liu W, Deng T, Xiang D. Risk factors for non-arteritic anterior ischemic optic neuropathy: A large scale meta-analysis. *Front Med (Lausanne)* 2021; **8**: 618353.

278 Hayreh SS, Joos KM, Podhajsky PA, Long CR. Systemic diseases associated with nonarteritic anterior ischemic optic neuropathy. *J Neuroophthalmol* 1996; **16**: 59.

279 Sm C, Ca G, Ja M Iii. Nonarteritic ischemic optic neuropathy. The impact of tobacco use. *J Neuroophthalmol* 1994; **14**: 223.

280 Sakai T, Shikishima K, Matsushima M, Tsuneoka H. Genetic polymorphisms associated with endothelial function in nonarteritic anterior ischemic optic neuropathy. *Mol Vis* 2013; **19**: 213–9.

281 Clinical classifications. NHS Digital. https://digital.nhs.uk/services/terminology-and-classifications/clinical-classifications (accessed March 28, 2023).

282 Berrett TB, Samworth R. USP: an independence test that improves on Pearson's chi-squared and the G-test. 2021. DOI:10.17863/CAM.78074.

283 Rosenbaum PR, Rubin DB. The central role of the propensity score in observational studies for causal effects. *Biometrika* 1983; **70**: 41–55.

284 French DD, Margo CE, Greenberg PB. Ischemic stroke risk in medicare beneficiaries with central retinal artery occlusion: A retrospective cohort study. *Ophthalmol Ther* 2018; **7**: 125–31.

285 Park SJ, Choi N-K, Yang BR, *et al.* Risk and risk periods for stroke and acute myocardial infarction in patients with central retinal artery occlusion. *Ophthalmology* 2015; **122**: 2336-2343.e2.

286 Ferguson GG, Eliasziw M, Barr HWK, *et al.* The North American Symptomatic Carotid Endarterectomy Trial. *Stroke* 1999; **30**: 1751–8.

287 Furie KL, Kasner SE, Adams RJ, *et al.* Guidelines for the prevention of stroke in patients with stroke or transient ischemic attack: a guideline for healthcare professionals from the american heart association/american stroke association. *Stroke* 2011; **42**: 227–76.

288 Liapis CD, Bell PRF, Mikhailidis D, *et al.* ESVS guidelines. Invasive treatment for carotid stenosis: indications, techniques. *Eur J Vasc Endovasc Surg* 2009; **37**: 1–19.

289 Wolf PA, Abbott RD, Kannel WB. Atrial fibrillation as an independent risk factor for stroke: the Framingham Study. *Stroke* 1991; **22**: 983–8.

290 Martin DT, Bersohn MM, Waldo AL, *et al.* Randomized trial of atrial arrhythmia monitoring to guide anticoagulation in patients with implanted defibrillator and cardiac resynchronization devices. *Eur Heart J* 2015; **36**: 1660–8.

291 Mead GE, Lewis SC, Wardlaw JM, Dennis MS. Comparison of risk factors in patients with transient and prolonged eye and brain ischemic syndromes. *Stroke* 2002; **33**: 2383–90.

292 Volkers EJ, Donders RCJM, Koudstaal PJ, van Gijn J, Algra A, Jaap Kappelle L. Transient monocular blindness and the risk of vascular complications according to subtype: a prospective cohort study. *J Neurol* 2016; **263**: 1771–7.

293 Callizo J, Feltgen N, Ammermann A, *et al.* Atrial fibrillation in retinal vascular occlusion disease and non-arteritic anterior ischemic optic neuropathy. *PLoS One* 2017; **12**: e0181766.

294 Mac Grory B, Landman SR, Ziegler PD, *et al.* Detection of atrial fibrillation after central retinal artery occlusion. *Stroke* 2021; **52**: 2773–81.

295 Rim TH, Han J, Choi YS, Lee T, Kim SS. Stroke risk among adult patients with third, fourth or sixth cranial nerve palsy: a Nationwide Cohort Study. *Acta Ophthalmol* 2017; **95**: e656–61.

296 Hoi C-P, Chen Y-T, Fuh J-L, Yang C-P, Wang S-J. Increased risk of stroke in patients with isolated third, fourth, or sixth cranial nerve palsies: A nationwide cohort study. *Cerebrovasc Dis* 2016; **41**: 273–82.

297 Park SJ, Yang HK, Byun SJ, Park KH, Hwang J-M. Ocular motor cranial nerve palsy and increased risk of stroke in the general population. *PLoS One* 2018; **13**: e0205428.

298 Ueshima H, Sekikawa A, Miura K, *et al.* Cardiovascular disease and risk factors in Asia: a selected review. *Circulation* 2008; **118**: 2702–9.

299 Chou KL, Galetta SL, Liu GT, *et al.* Acute ocular motor mononeuropathies: prospective study of the roles of neuroimaging and clinical assessment. *J Neurol Sci* 2004; **219**: 35–9.

300 Chi SL, Bhatti MT. The diagnostic dilemma of neuro-imaging in acute isolated sixth nerve palsy. *Curr Opin Ophthalmol* 2009; **20**: 423–9.

301 Murchison AP, Gilbert ME, Savino PJ. Neuroimaging and acute ocular motor mononeuropathies: a prospective study. *Arch Ophthalmol* 2011; **129**: 301–5.

302 Appenzeller S, Veilleux M, Clarke A. Third cranial nerve palsy or pseudo 3rd nerve palsy of myasthenia gravis? A challenging diagnosis in systemic lupus erythematosus. *Lupus* 2009; **18**: 836–40.

303 Bertolet AN, Druckenbrod RC. Pseudopartial third nerve palsy as the presenting sign of ocular myasthenia gravis. *Optom Vis Sci* 2020; **97**: 377–82.

304 Bhatti MT, Eisenschenk S, Roper SN, Guy JR. Superior divisional third cranial nerve paresis: clinical and anatomical observations of 2 unique cases. *Arch Neurol* 2006; **63**: 771–6.

305 Smith SV, Lee AG. Update on ocular myasthenia gravis. *Neurol Clin* 2017; **35**: 115–23.

306 Guyer DR, Miller NR, Auer CL, Fine SL. The risk of cerebrovascular and cardiovascular disease in patients with anterior ischemic optic neuropathy. *Arch Ophthalmol* 1985; **103**: 1136–42.

307 Biousse V, Newman NJ. Diagnosis and clinical features of common optic neuropathies. *Lancet Neurol* 2016; **15**: 1355–67.

308 Hasanreisoglu M, Robenshtok E, Ezrahi D, Stiebel-Kalish H. Do patients with non-arteritic ischemic optic neuritis have increased risk for cardiovascular and cerebrovascular events? *Neuroepidemiology* 2013; **40**: 220–4.

309 Schizophrenia. https://www.who.int/news-room/fact-sheets/detail/schizophrenia (accessed June 9, 2023).

310 Pillinger T, Beck K, Gobjila C, Donocik JG, Jauhar S, Howes OD. Impaired Glucose Homeostasis in First-Episode Schizophrenia: A Systematic Review and Meta-analysis. *JAMA Psychiatry* 2017; **74**: 261–9.

311 Laursen TM, Nordentoft M, Mortensen PB. Excess early mortality in schizophrenia. *Annu Rev Clin Psychol* 2014; **10**: 425–48.

312 Ribe AR, Laursen TM, Charles M, *et al.* Long-term Risk of Dementia in Persons With Schizophrenia: A Danish Population-Based Cohort Study. *JAMA Psychiatry* 2015; **72**: 1095–101.

313 Dorsey ER, Bloem BR. The Parkinson pandemic-A call to action. *JAMA Neurol* 2018; **75**: 9–10.

314 Harnois C, Di Paolo T. Decreased dopamine in the retinas of patients with Parkinson's disease. *Invest Ophthalmol Vis Sci* 1990; **31**: 2473–5.

315 Nazir MA. Prevalence of periodontal disease, its association with systemic diseases and prevention. *Int J Health Sci (Qassim)* 2017; **11**: 72–80.

316 Qin X, Zhao Y, Guo Y. Periodontal disease and myocardial infarction risk: A meta-analysis of cohort studies. *Am J Emerg Med* 2021; **48**: 103–9.

317 Chen D-Y, Lin C-H, Chen Y-M, Chen H-H. Risk of Atrial Fibrillation or Flutter Associated with Periodontitis: A Nationwide, Population-Based, Cohort Study. *PLoS One* 2016; **11**: e0165601.

318 Lafon A, Pereira B, Dufour T, *et al.* Periodontal disease and stroke: a meta-analysis of cohort studies. *Eur J Neurol* 2014; **21**: 1155–61, e66-7.

319 Nadim R, Tang J, Dilmohamed A, *et al.* Influence of periodontal disease on risk of dementia: a systematic literature review and a meta-analysis. *Eur J Epidemiol* 2020; **35**: 821–33.

320 Fu Z, Hong H, Su Z, Lou B, Pan C-W, Liu H. Global prevalence of amblyopia and disease burden projections through 2040: a systematic review and meta-analysis. *Br J Ophthalmol* 2020; **104**: 1164–70.

321 Bruce A, Pacey IE, Bradbury JA, Scally AJ, Barrett BT. Bilateral changes in foveal structure in individuals with amblyopia. *Ophthalmology* 2013; **120**: 395–403.

322 Gao L, Gao Y, Hong F, Zhang P, Shu X. Assessment of foveal avascular zone and macular vascular plexus density in children with unilateral amblyopia: A systemic review and meta-analysis. *Front Pediatr* 2021; **9**: 620565.

323 GBD 2019 Mental Disorders Collaborators. Global, regional, and national burden of 12 mental disorders in 204 countries and territories, 1990-2019: a systematic analysis for the Global Burden of Disease Study 2019. *Lancet Psychiatry* 2022; **9**: 137–50.

324 Mitchell AJ, Dinan TG. Schizophrenia: a multisystem disease? *J Psychopharmacol* 2010; **24**: 5–7.

325 Garcia-Rizo C, Kirkpatrick B, Fernandez-Egea E, Oliveira C, Bernardo M. Abnormal glycemic homeostasis at the onset of serious mental illnesses: A common pathway. *Psychoneuroendocrinology* 2016; **67**: 70–5.

326 Hackinger S, Prins B, Mamakou V, *et al.* Evidence for genetic contribution to the increased risk of type 2 diabetes in schizophrenia. *Transl Psychiatry* 2018; **8**: 252.

327 De Hert MA, van Winkel R, Van Eyck D, *et al.* Prevalence of the metabolic syndrome in patients with schizophrenia treated with antipsychotic medication. *Schizophr Res* 2006; **83**: 87–93.

328 Kørner A, Lopez AG, Lauritzen L, Andersen PK, Kessing LV. Late and very-late first-contact schizophrenia and the risk of dementia--a nationwide register based study. *Int J Geriatr Psychiatry* 2009; **24**: 61–7.

329 Laursen TM, Munk-Olsen T, Nordentoft M, Mortensen PB. Increased mortality among patients admitted with major psychiatric disorders: a register-based study comparing mortality in unipolar depressive disorder, bipolar affective disorder, schizoaffective disorder, and schizophrenia. *J Clin Psychiatry* 2007; **68**: 899–907.

330 Kirkpatrick B, Messias E, Harvey PD, Fernandez-Egea E, Bowie CR. Is schizophrenia a syndrome of accelerated aging? *Schizophr Bull* 2008; **34**: 1024–32.

331 Gonzalez-Diaz JM, Radua J, Sanchez-Dalmau B, Camos-Carreras A, Zamora DC, Bernardo M. Mapping Retinal Abnormalities in Psychosis: Meta-analytical Evidence for Focal Peripapillary and Macular Reductions. *Schizophr Bull* 2022; : sbac085.

332 Komatsu H, Onoguchi G, Jerotic S, *et al.* Retinal layers and associated clinical factors in schizophrenia spectrum disorders: a systematic review and meta-analysis. *Mol Psychiatry* 2022; : 1–25.

333 Silverstein SM, Lai A, Green KM, Crosta C, Fradkin SI, Ramchandran RS. Retinal Microvasculature in Schizophrenia. *Eye Brain* 2021; **13**: 205–17.

334 Koman-Wierdak E, Róg J, Brzozowska A, *et al.* Analysis of the Peripapillary and Macular Regions Using OCT Angiography in Patients with Schizophrenia and Bipolar Disorder. *J Clin Med Res* 2021; **10**. DOI:10.3390/jcm10184131.

335 Green KM, Choi JJ, Ramchandran RS, Silverstein SM. OCT and OCT Angiography Offer New Insights and Opportunities in Schizophrenia Research and Treatment. *Front Digit Health* 2022; **4**: 836851.

336 Staurenghi, Sadda, Chakravarthy, Spaide. International Nomenclature for Optical Coherence Tomography (IN• OCT) Panel. Proposed lexicon for anatomic landmarks in normal posterior segment …. *Ophthalmology*.

337 Ministry of Housing, Communities, Local Government. English indices of deprivation 2015. 2015; published online Sept 30. https://www.gov.uk/government/statistics/english-indices-of-deprivation-2015 (accessed Oct 10, 2022).

338 Appaji A, Nagendra B, Chako DM, *et al.* Retinal vascular fractal dimension in bipolar disorder and schizophrenia. *J Affect Disord* 2019; **259**: 98–103.

339 Lizano P, Bannai D, Lutz O, Kim LA, Miller J, Keshavan M. A Meta-analysis of Retinal Cytoarchitectural Abnormalities in Schizophrenia and Bipolar Disorder. *Schizophr Bull* 2020; **46**: 43–53.

340 Cruz-Herranz A, Balk LJ, Oberwahrenbrock T, *et al.* The APOSTEL recommendations for reporting quantitative optical coherence tomography studies. *Neurology* 2016; **86**: 2303–9.

341 Kuznetsova A, Brockhoff PB, Christensen RHB. lmerTest Package: Tests in Linear Mixed Effects Models. *J Stat Softw* 2017; **82**: 1–26.

342 U-Statistic Permutation Tests of Independence for all Data Types. R package version 0. ; **1**.

343 Cheung CY-L, Ong YT, Hilal S, *et al.* Retinal ganglion cell analysis using high-definition optical coherence tomography in patients with mild cognitive impairment and Alzheimer's disease. *J Alzheimers Dis* 2015; **45**: 45–56.

344 Nishioka C, Liang H-F, Barsamian B, Sun S-W. Amyloid-beta induced retrograde axonal degeneration in a mouse tauopathy model. *Neuroimage* 2019; **189**: 180–91.

345 Cai L, Huang J. Schizophrenia and risk of dementia: a meta-analysis study. *Neuropsychiatr Dis Treat* 2018; **14**: 2047–55.

346 Silverstein SM, Rosen R. Schizophrenia and the eye. *Schizophr Res Cogn* 2015; **2**: 46–55.

347 Cropley VL, Klauser P, Lenroot RK, *et al.* Accelerated gray and white matter deterioration with age in schizophrenia. *Am J Psychiatry* 2017; **174**: 286–95.

348 Lin C-W, Chang L-C, Ma T, *et al.* Older molecular brain age in severe mental illness. *Mol Psychiatry* 2021; **26**: 3646–56.

349 Stone WS, Cai B, Liu X, *et al.* Association between the duration of untreated psychosis and selective cognitive performance in community-dwelling individuals with chronic untreated schizophrenia in rural China. *JAMA Psychiatry* 2020; **77**: 1116–26.

350 Bavato F, Cathomas F, Klaus F, *et al.* Altered neuroaxonal integrity in schizophrenia and major depressive disorder assessed with neurofilament light chain in serum. *J Psychiatr Res* 2021; **140**: 141–8.

351 Rodrigues-Amorim D, Rivera-Baltanás T, Del Carmen Vallejo-Curto M, *et al.* Plasma β-III tubulin, neurofilament light chain and glial fibrillary acidic protein are associated with neurodegeneration and progression in schizophrenia. *Sci Rep* 2020; **10**: 14271.

352 Lai A, Crosta C, Loftin M, Silverstein SM. Retinal structural alterations in chronic versus first episode schizophrenia spectrum disorders. *Biomarkers in Neuropsychiatry* 2020; **2**: 100013.

353 Zhuo C, Xiao B, Ji F, *et al.* Patients with first-episode untreated schizophrenia who experience concomitant visual disturbances and auditory hallucinations exhibit co-impairment of the brain and retinas-a pilot study. *Brain Imaging Behav* 2021; **15**: 1533–41.

354 Lim HB, Lee MW, Park JH, Kim K, Jo YJ, Kim JY. Changes in Ganglion Cell-Inner Plexiform Layer Thickness and Retinal Microvasculature in Hypertension: An Optical Coherence Tomography Angiography Study. *Am J Ophthalmol* 2019; **199**: 167–76.

355 Silverstein SM, Paterno D, Cherneski L, Green S. Optical coherence tomography indices of structural retinal pathology in schizophrenia. *Psychol Med* 2018; **48**: 2023–33.

356 De Clerck EEB, Schouten JSAG, Berendschot TTJM, *et al.* Macular thinning in prediabetes or type 2 diabetes without diabetic retinopathy: the Maastricht Study. *Acta Ophthalmol* 2018; **96**: 174–82.

357 Huru J, Leiviskä I, Saarela V, Liinamaa MJ. Prediabetes influences the structure of the macula: thinning of the macula in the Northern Finland Birth Cohort. *Br J Ophthalmol* 2021; **105**: 1731–7.

358 Zhuo C, Ji F, Xiao B, *et al.* Antipsychotic agent-induced deterioration of the visual system in first-episode untreated patients with schizophrenia maybe self-limited: Findings from a secondary small sample follow-up study based on a pilot follow-up study. *Psychiatry Res* 2020; **286**: 112906.

359 Hunt GE, Large MM, Cleary M, Lai HMX, Saunders JB. Prevalence of comorbid substance use in schizophrenia spectrum disorders in community and clinical settings, 1990-2017: Systematic review and meta-analysis. *Drug Alcohol Depend* 2018; **191**: 234–58.

360 Appaji A, Nagendra B, Chako DM, *et al.* Retinal vascular tortuosity in schizophrenia and bipolar disorder. *Schizophr Res* 2019; **212**: 26–32.

361 Appaji A, Nagendra B, Chako DM, *et al.* Retinal vascular abnormalities in schizophrenia and bipolar disorder: A window to the brain. *Bipolar Disord* 2019; **21**: 634–41.

362 Budakoglu O, Ozdemir K, Safak Y, Sen E, Taskale B. Retinal nerve fibre layer and peripapillary vascular density by optical coherence tomography angiography in schizophrenia. *Clin Exp Optom* 2021; **104**: 788–94.

363 Bannai D, Adhan I, Katz R, *et al.* Quantifying Retinal Microvascular Morphology in Schizophrenia Using Swept-Source Optical Coherence Tomography Angiography. *Schizophr Bull* 2022; **48**: 80–9.

364 VAMPIRE: Vessel assessment and measurement platform for images of the retina. In: Human Eye Imaging and Modeling. CRC Press, 2012: 39–54.

365 Perez-Rovira A, MacGillivray T, Trucco E, *et al.* VAMPIRE: Vessel assessment and measurement platform for images of the REtina. *Annu Int Conf IEEE Eng Med Biol Soc* 2011; **2011**: 3391–4.

366 MacGillivray TJ, Cameron JR, Zhang Q, *et al.* Suitability of UK Biobank Retinal Images for Automatic Analysis of Morphometric Properties of the Vasculature. *PLoS One* 2015; **10**: e0127914.

367 Myles N, Newall HD, Curtis J, Nielssen O, Shiers D, Large M. Tobacco use before, at, and after first-episode psychosis: a systematic meta-analysis. *J Clin Psychiatry* 2012; **73**: 468–75.

368 Lemmens S, Luyts M, Gerrits N, *et al.* Age-related changes in the fractal dimension of the retinal microvasculature, effects of cardiovascular risk factors and smoking behaviour. *Acta Ophthalmol* 2021; published online Nov 7. DOI:10.1111/aos.15047.

369 Hart NJ, Koronyo Y, Black KL, Koronyo-Hamaoui M. Ocular indicators of Alzheimer's: exploring disease in the retina. *Acta Neuropathol* 2016; **132**: 767–87.

370 Berg D, Lang AE, Postuma RB, *et al.* Changing the research criteria for the diagnosis of Parkinson's disease: obstacles and opportunities. *Lancet Neurol* 2013; **12**: 514–24.

371 Biondetti E, Santin MD, Valabrègue R, *et al.* The spatiotemporal changes in dopamine, neuromelanin and iron characterizing Parkinson's disease. *Brain* 2021; **144**: 3114–25.

372 Morrish PK, Sawle GV, Brooks DJ. An [18F]dopa–PET and clinical study of the rate of progression in Parkinson's disease. *Brain* 1996; **119**: 585–91.

373 Sun J, Lai Z, Ma J, *et al.* Quantitative evaluation of iron content in idiopathic rapid eye movement sleep behavior disorder. *Mov Disord* 2020; **35**: 478–85.

374 Iranzo A, Valldeoriola F, Lomeña F, *et al.* Serial dopamine transporter imaging of nigrostriatal function in patients with idiopathic rapid-eye-movement sleep behaviour disorder: a prospective study. *Lancet Neurol* 2011; **10**: 797–805.

375 Lee J-Y, Martin-Bastida A, Murueta-Goyena A, *et al.* Multimodal brain and retinal imaging of dopaminergic degeneration in Parkinson disease. *Nat Rev Neurol* 2022; **18**: 203–20.

376 Kolb H, Cuenca N, Wang HH, Dekorver L. The synaptic organization of the dopaminergic amacrine cell in the cat retina. *J Neurocytol* 1990; **19**: 343–66.

377 Archibald NK, Clarke MP, Mosimann UP, Burn DJ. The retina in Parkinson's disease. *Brain* 2009; **132**: 1128–45.

378 Huang L, Zhang D, Ji J, Wang Y, Zhang R. Central retina changes in Parkinson's disease: a systematic review and meta-analysis. *J Neurol* 2021; **268**: 4646–54.

379 Lee J-Y, Kim JM, Ahn J, Kim H-J, Jeon BS, Kim TW. Retinal nerve fiber layer thickness and visual hallucinations in Parkinson's Disease. *Mov Disord* 2014; **29**: 61–7.

380 Albrecht P, Müller A-K, Südmeyer M, *et al.* Optical coherence tomography in parkinsonian syndromes. *PLoS One* 2012; **7**: e34891.

381 Chrysou A, Jansonius NM, van Laar T. Retinal layers in Parkinson's disease: A meta-analysis of spectral-domain optical coherence tomography studies. *Parkinsonism Relat Disord* 2019; **64**: 40–9.

382 Komici K, Femminella GD, Bencivenga L, Rengo G, Pagano G. Diabetes Mellitus and Parkinson's Disease: A Systematic Review and Meta-Analyses. *J Parkinsons Dis* 2021; **11**: 1585–96.

383 Website. (https://biobank.ctsu.ox.ac.uk/crystal/ukb/docs/alg_outcome_pdp.

384 List of ethnic groups. https://www.ethnicity-facts-figures.service.gov.uk/style-guide/ethnic-groups (accessed Oct 28, 2022).

385 Suominen S, Koskenvuo K, Sillanmäki L, *et al.* Non-response in a nationwide follow-up postal survey in Finland: a register-based mortality analysis of respondents and non-respondents of the Health and Social Support (HeSSup) Study. *BMJ Open* 2012; **2**: e000657.

386 Guadagnoli E, Cleary PD. Age-related item nonresponse in surveys of recently discharged patients. *J Gerontol* 1992; **47**: P206-12.

387 Tsiampalis T, Panagiotakos DB. Missing-data analysis: socio- demographic, clinical and lifestyle determinants of low response rate on self- reported psychological and nutrition related multi- item instruments in the context of the ATTICA epidemiological study. *BMC Med Res Methodol* 2020; **20**: 148.

388 Roderick JA, Little DB. Statistical Analysis with Missing Data. .

389 Balk LJ, Steenwijk MD, Tewarie P, *et al.* Bidirectional trans-synaptic axonal degeneration in the visual pathway in multiple sclerosis. *J Neurol Neurosurg Psychiatry* 2015; **86**: 419–24.

390 Petzold A, Balcer LJ, Calabresi PA, *et al.* Retinal layer segmentation in multiple sclerosis: a systematic review and meta-analysis. *Lancet Neurol* 2017; **16**: 797–812.

391 Schneider M, Müller H-P, Lauda F, *et al.* Retinal single-layer analysis in Parkinsonian syndromes: an optical coherence tomography study. *J Neural Transm* 2014; **121**: 41–7.

392 Bodis-Wollner I, Kozlowski PB, Glazman S, Miri S. A-synuclein in the inner retina in parkinson disease. *Ann Neurol* 2014; **75**: 964–6.

393 Ortuño-Lizarán I, Sánchez-Sáez X, Lax P, *et al.* Dopaminergic Retinal Cell Loss and Visual Dysfunction in Parkinson Disease. *Ann Neurol* 2020; **88**: 893–906.

394 Mejia-Vergara AJ, Karanjia R, Sadun AA. OCT parameters of the optic nerve head and the retina as surrogate markers of brain volume in a normal population, a pilot study. *J Neurol Sci* 2021; **420**: 117213.

395 Weil RS, Hsu JK, Darby RR, Soussand L, Fox MD. Neuroimaging in Parkinson's disease dementia: connecting the dots. *Brain Commun* 2019; **1**: fcz006.

396 Rossor MN, Fox NC, Freeborough PA, Roques PK. Slowing the progression of Alzheimer disease: monitoring progression. *Alzheimer Dis Assoc Disord* 1997; **11 Suppl 5**: S6-9.

397 Chung CY, Koprich JB, Siddiqi H, Isacson O. Dynamic changes in presynaptic and axonal transport proteins combined with striatal neuroinflammation precede dopaminergic neuronal loss in a rat model of AAV alpha-synucleinopathy. *J Neurosci* 2009; **29**: 3365–73.

398 Zarkali A, McColgan P, Leyland L-A, Lees AJ, Weil RS. Visual Dysfunction Predicts Cognitive Impairment and White Matter Degeneration in Parkinson's Disease. *Mov Disord* 2021; **36**: 1191–202.

399 Popova E. Role of dopamine in retinal function. University of Utah Health Sciences Center, 2020.

400 Lee J-Y, Ahn J, Yoon EJ, Oh S, Kim YK, Jeon B. Macular ganglion-cell-complex layer thinning and optic nerve integrity in drug-naïve Parkinson's disease. *J Neural Transm* 2019; **126**: 1695–9.

401 Ahn J, Lee J-Y, Kim TW, *et al.* Retinal thinning associates with nigral dopaminergic loss in de novo Parkinson disease. *Neurology* 2018; **91**: e1003–12.

402 Postuma RB, Gagnon J-F, Bertrand J-A, Génier Marchand D, Montplaisir JY. Parkinson risk in idiopathic REM sleep behavior disorder: preparing for neuroprotective trials. *Neurology* 2015; **84**: 1104–13.

403 Lee J-Y, Ahn J, Oh S, *et al.* Retina thickness as a marker of neurodegeneration in prodromal lewy body disease. *Mov Disord* 2020; **35**: 349–54.

404 Zhao B, Cheung R, Malvankar-Mehta MS. Risk of Parkinson's disease in glaucoma patients: a systematic review and meta-analysis. *Curr Med Res Opin* 2022; **38**: 955–62.

405 Sen A, Tugcu B, Coskun C, Ekinci C, Nacaroglu SA. Effects of levodopa on retina in Parkinson disease. *Eur J Ophthalmol* 2014; **24**: 114–9.

406 Muzerengi S, Rick C, Begaj I, *et al.* Coding accuracy for Parkinson's disease hospital admissions: implications for healthcare planning in the UK. *Public Health* 2017; **146**: 4–9.

407 Kassebaum NJ, Bernabé E, Dahiya M, Bhandari B, Murray CJL, Marcenes W. Global burden of severe periodontitis in 1990-2010: a systematic review and meta-regression. *J Dent Res* 2014; **93**: 1045–53.

408 Hujoel PP, White BA, García RI, Listgarten MA. The dentogingival epithelial surface area revisited. *J Periodontal Res* 2001; **36**: 48–55.

409 Scannapieco FA, Bush RB, Paju S. Associations between periodontal disease and risk for atherosclerosis, cardiovascular disease, and stroke. A systematic review. *Ann Periodontol* 2003; **8**: 38–53.

410 Beck J, Garcia R, Heiss G, Vokonas PS, Offenbacher S. Periodontal Disease and Cardiovascular Disease. *J Periodontol* 1996; **67 Suppl 10S**: 1123–37.

411 Desvarieux M, Demmer RT, Rundek T, *et al.* Periodontal microbiota and carotid intima-media thickness: the Oral Infections and Vascular Disease Epidemiology Study (INVEST). *Circulation* 2005; **111**: 576–82.

412 Loesche WJ, Schork A, Terpenning MS, Chen YM, Kerr C, Dominguez BL. The relationship between dental disease and cerebral vascular accident in elderly United States veterans. *Ann Periodontol* 1998; **3**: 161–74.

413 Ebersole JL, Machen RL, Steffen MJ, Willmann DE. Systemic acute-phase reactants, C-reactive protein and haptoglobin, in adult periodontitis. *Clin Exp Immunol* 1997; **107**: 347–52.

414 Mustapha IZ, Debrey S, Oladubu M, Ugarte R. Markers of systemic bacterial exposure in periodontal disease and cardiovascular disease risk: a systematic review and meta-analysis. *J Periodontol* 2007; **78**: 2289–302.

415 Pucar A, Milasin J, Lekovic V, *et al.* Correlation between atherosclerosis and periodontal putative pathogenic bacterial infections in coronary and internal mammary arteries. *J Periodontol* 2007; **78**: 677–82.

416 Haraszthy VI, Zambon JJ, Trevisan M, Zeid M, Genco RJ. Identification of periodontal pathogens in atheromatous plaques. *J Periodontol* 2000; **71**: 1554–60.

417 Poole S, Singhrao SK, Kesavalu L, Curtis MA, Crean S. Determining the presence of periodontopathic virulence factors in short-term postmortem Alzheimer's disease brain tissue. *J Alzheimers Dis* 2013; **36**: 665–77.

418 Beck JD, Eke P, Lin D, *et al.* Associations between IgG antibody to oral organisms and carotid intima–medial thickness in community-dwelling adults. *Atherosclerosis* 2005; **183**: 342–8.

419 Lee Y-L, Hu H-Y, Huang N, Hwang D-K, Chou P, Chu D. Dental prophylaxis and periodontal treatment are protective factors to ischemic stroke. *Stroke* 2013; **44**: 1026–30.

420 Chen Z-Y, Chiang C-H, Huang C-C, *et al.* The association of tooth scaling and decreased cardiovascular disease: a nationwide population-based study. *Am J Med* 2012; **125**: 568–75.

421 de Oliveira C, Watt R, Hamer M. Toothbrushing, inflammation, and risk of cardiovascular disease: results from Scottish Health Survey. *BMJ* 2010; **340**: c2451.

422 de Pablo P, Serban S, Lopez-Oliva I, *et al.* Outcomes of periodontal therapy in rheumatoid arthritis: The OPERA feasibility randomized trial. *J Clin Periodontol* 2022; published online Nov 22. DOI:10.1111/jcpe.13756.

423 D'Aiuto F, Gkranias N, Bhowruth D, *et al.* Systemic effects of periodontitis treatment in patients with type 2 diabetes: a 12 month, single-centre, investigator-masked, randomised trial. *Lancet Diabetes Endocrinol* 2018; **6**: 954–65.

424 Ko F, Muthy ZA, Gallacher J, *et al.* Association of retinal nerve fiber layer thinning with current and future cognitive decline: A study using optical coherence tomography. *JAMA Neurol* 2018; **75**: 1198–205.

425 Wong TY, Kamineni A, Klein R, *et al.* Quantitative retinal venular caliber and risk of cardiovascular disease in older persons: the cardiovascular health study. *Arch Intern Med* 2006; **166**: 2388–94.

426 Van Doornum S, Strickland G, Kawasaki R, *et al.* Retinal vascular calibre is altered in patients with rheumatoid arthritis: a biomarker of disease activity and cardiovascular risk? *Rheumatology* 2011; **50**: 939–43.

427 Sun C, Wang JJ, Mackey DA, Wong TY. Retinal vascular caliber: systemic, environmental, and genetic associations. *Surv Ophthalmol* 2009; **54**: 74–95.

428 Lv X, Li W, Fang Z, Xue X, Pan C. Periodontal Disease and Age-Related Macular Degeneration: A Meta-Analysis of 112,240 Participants. *Biomed Res Int* 2020; **2020**: 4753645.

429 Karesvuo P, Gursoy UK, Pussinen PJ, *et al.* Alveolar Bone Loss Associated With Age-Related Macular Degeneration in Males. Journal of Periodontology. 2013; **84**: 58–67.

430 Wagley S, Marra KV, Salhi RA, *et al.* PERIODONTAL DISEASE AND AGE-RELATED MACULAR DEGENERATION. Retina. 2015; **35**: 982–8.

431 Shin YU, Lim HW, Hong EH, *et al.* The association between periodontal disease and age-related macular degeneration in the Korea National health and nutrition examination survey: A cross-sectional observational study. *Medicine* 2017; **96**: e6418.

432 Sun K-T, Hsia N-Y, Chen S-C, *et al.* RISK OF AGE-RELATED MACULAR DEGENERATION IN PATIENTS WITH PERIODONTITIS: A Nationwide Population-Based Cohort Study. *Retina* 2020; **40**: 2312–8.

433 Sun K-T, Shen T-C, Chen S-C, *et al.* Periodontitis and the subsequent risk of glaucoma: results from the real-world practice. *Sci Rep* 2020; **10**: 17568.

434 Pasquale LR, Hyman L, Wiggs JL, *et al.* Prospective Study of Oral Health and Risk of Primary Open-Angle Glaucoma in Men: Data from the Health Professionals Follow-up Study. *Ophthalmology* 2016; **123**: 2318–27.

435 Boillot A, Bouchard P, Moss K, Offenbacher S, Czernichow S. Periodontitis and retinal microcirculation in the Atherosclerosis Risk in Communities study. *J Clin Periodontol* 2015; **42**: 342–9.

436 Sabanayagam C, Lye WK, Klein R, *et al.* Retinal microvascular calibre and risk of diabetes mellitus: a systematic review and participant-level meta-analysis. *Diabetologia* 2015; **58**: 2476–85.

437 Saito T, Shimazaki Y, Kiyohara Y, *et al.* The severity of periodontal disease is associated with the development of glucose intolerance in non-diabetics: the Hisayama study. *J Dent Res* 2004; **83**: 485–90.

438 Demmer RT, Jacobs DR Jr, Desvarieux M. Periodontal disease and incident type 2 diabetes: results from the First National Health and Nutrition Examination Survey and its epidemiologic follow-up study. *Diabetes Care* 2008; **31**: 1373–9.

439 Morita I, Inagaki K, Nakamura F, *et al.* Relationship between periodontal status and levels of glycated hemoglobin. *J Dent Res* 2012; **91**: 161–6.

440 Grading diabetic retinopathy from stereoscopic color fundus photographs—an extension of the modified Airlie house classification. *Ophthalmology* 1991; **98**: 786–806.

441 Bosco E, Hsueh L, McConeghy KW, Gravenstein S, Saade E. Major adverse cardiovascular event definitions used in observational analysis of administrative databases: a systematic review. *BMC Med Res Methodol* 2021; **21**: 241.

442 Petermann-Rocha F, Deo S, Celis-Morales C, *et al.* An Opportunity for Prevention: Associations Between the Life's Essential 8 Score and Cardiovascular Incidence Using Prospective Data from UK Biobank. *Curr Probl Cardiol* 2022; **48**: 101540.

443 Eastwood SV, Mathur R, Atkinson M, *et al.* Algorithms for the Capture and Adjudication of Prevalent and Incident Diabetes in UK Biobank. *PLoS One* 2016; **11**: e0162388.

444 Eke PI, Dye BA, Wei L, *et al.* Self-reported measures for surveillance of periodontitis. *J Dent Res* 2013; **92**: 1041–7.

445 Abbood HM, Hinz J, Cherukara G, Macfarlane TV. Validity of self-reported periodontal disease: A systematic review and meta-analysis. *J Periodontol* 2016; **87**: 1474–83.

446 Sharma P, Kristunas C, Chapple IL, Dietrich T. Periodontal health and patient-reported outcomes: A longitudinal analysis of data from non-specialist practice settings. *J Clin Periodontol* 2023; published online Jan 15. DOI:10.1111/jcpe.13776.

447 Page RC, Eke PI. Case definitions for use in population-based surveillance of periodontitis. *J Periodontol* 2007; **78**: 1387–99.

448 Tonetti MS, Greenwell H, Kornman KS. Staging and grading of periodontitis: Framework and proposal of a new classification and case definition. *J Periodontol* 2018; **89 Suppl 1**: S159–72.

449 Wilks SS. The Large-Sample Distribution of the Likelihood Ratio for Testing Composite Hypotheses. *aoms* 1938; **9**: 60–2.

450 Bates D, Mächler M, Bolker B, Walker S. Fitting Linear Mixed-Effects Models using lme4. arXiv [stat.CO]. 2014; published online June 23. http://arxiv.org/abs/1406.5823.

451 Team. R: A language and environment for statistical computing. R Foundation for Statistical Computing, Vienna, Austria. *http://www R-project org/* https://ci.nii.ac.jp/naid/20001692429/.

452 Sharma P, Dietrich T, Ferro CJ, Cockwell P, Chapple ILC. Association between periodontitis and mortality in stages 3-5 chronic kidney disease: NHANES III and linked mortality study. *J Clin Periodontol* 2016; **43**: 104–13.

453 Wong TY, Islam FMA, Klein R, *et al.* Retinal vascular caliber, cardiovascular risk factors, and inflammation: the multi-ethnic study of atherosclerosis (MESA). *Invest Ophthalmol Vis Sci* 2006; **47**: 2341–50.

454 Owen CG, Rudnicka AR, Welikala RA, *et al.* Retinal vasculometry associations with cardiometabolic risk factors in the European prospective investigation of cancer—Norfolk study. *Ophthalmology* 2019; **126**: 96–106.

455 Samietz S, Jürgens C, Ittermann T, *et al.* Cross-sectional association between oral health and retinal microcirculation. *J Clin Periodontol* 2018; **45**: 404–12.

456 Cumberland PM, Bountziouka V, Hammond CJ, Hysi PG, Rahi JS, UK Biobank Eye and Vision Consortium. Temporal trends in frequency, type and severity of myopia and associations with key environmental risk factors in the UK: Findings from the UK Biobank Study. *PLoS One* 2022; **17**: e0260993.

457 Williams KM, Bertelsen G, Cumberland P, *et al.* Increasing Prevalence of Myopia in Europe and the Impact of Education. *Ophthalmology* 2015; **122**: 1489–97.

458 Eke PI, Dye BA, Wei L, Thornton-Evans GO, Genco RJ. Prevalence of Periodontitis in Adults in the United States: 2009 and 2010. Journal of Dental Research. 2012; **91**: 914–20.

459 Okada M, Wong TY, Kawasaki R, *et al.* Retinal venular calibre is increased in patients with autoimmune rheumatic disease: a case-control study. *Curr Eye Res* 2013; **38**: 685–90.

460 Ikram MK, de Jong FJ, Vingerling JR, *et al.* Are retinal arteriolar or venular diameters associated with markers for cardiovascular disorders? The Rotterdam Study. *Invest Ophthalmol Vis Sci* 2004; **45**: 2129–34.

461 de Jong FJ, Ikram MK, Witteman JCM, Hofman A, de Jong PTVM, Breteler MMB. Retinal vessel diameters and the role of inflammation in cerebrovascular disease. *Ann Neurol* 2007; **61**: 491–5.

462 Beck JD, Offenbacher S. Relationships among clinical measures of periodontal disease and their associations with systemic markers. *Ann Periodontol* 2002; **7**: 79–89.

463 Keles ZP, Keles GC, Avci B, Cetinkaya BO, Emingil G. Analysis of YKL-40 acute-phase protein and interleukin-6 levels in periodontal disease. *J Periodontol* 2014; **85**: 1240–6.

464 Fitt C, Luong TV, Cresp D, *et al.* Increased retinal venular calibre in acute infections. *Sci Rep* 2021; **11**: 17280.

465 Leira Y, Domínguez C, Seoane J, *et al.* Is Periodontal Disease Associated with Alzheimer's Disease? A Systematic Review with Meta-Analysis. *Neuroepidemiology* 2017; **48**: 21–31.

466 Leira Y, Iglesias-Rey R, Gómez-Lado N, *et al.* Porphyromonas gingivalis lipopolysaccharide-induced periodontitis and serum amyloid-beta peptides. *Arch Oral Biol* 2019; **99**: 120–5.

467 Kamer AR, Pirraglia E, Tsui W, *et al.* Periodontal disease associates with higher brain amyloid load in normal elderly. *Neurobiol Aging* 2015; **36**: 627–33.

468 Dominy SS, Lynch C, Ermini F, *et al.* Porphyromonas gingivalis in Alzheimer's disease brains: Evidence for disease causation and treatment with small-molecule inhibitors. *Sci Adv* 2019; **5**: eaau3333.

469 Şahin M, Şahin A, Kılınç F, *et al.* Early detection of macular and peripapillary changes with spectralis optical coherence tomography in patients with prediabetes. *Arch Physiol Biochem* 2018; **124**: 75–9.

470 Stöhr J, Barbaresko J, Neuenschwander M, Schlesinger S. Bidirectional association between periodontal disease and diabetes mellitus: a systematic review and meta-analysis of cohort studies. *Sci Rep* 2021; **11**: 13686.

471 de Jong FJ, Schrijvers EMC, Ikram MK, *et al.* Retinal vascular caliber and risk of dementia: the Rotterdam study. *Neurology* 2011; **76**: 816–21.

472 Choi S, Kim K, Chang J, *et al.* Association of Chronic Periodontitis on Alzheimer's Disease or Vascular Dementia. *J Am Geriatr Soc* 2019; **67**: 1234–9.

473 Demmer RT, Norby FL, Lakshminarayan K, *et al.* Periodontal disease and incident dementia: The Atherosclerosis Risk in Communities Study (ARIC). *Neurology* 2020; **95**: e1660–71.

474 Cheung CY, Ran AR, Wang S, *et al.* A deep learning model for detection of Alzheimer's disease based on retinal photographs: a retrospective, multicentre case-control study. *Lancet Digit Health* 2022; **4**: e806–15.

475 Rim TH, Lee CJ, Tham Y-C, *et al.* Deep-learning-based cardiovascular risk stratification using coronary artery calcium scores predicted from retinal photographs. *Lancet Digit Health* 2021; **3**: e306–16.

476 Holmes JM, Clarke MP. Amblyopia. *Lancet* 2006; **367**: 1343–51.

477 Bountziouka V, Cumberland PM, Rahi JS. Impact of persisting amblyopia on socioeconomic, health, and well-being outcomes in adult life: Findings from the UK Biobank. *Value Health* 2021; **24**: 1603–11.

478 Rahi JS, Cumberland PM, Peckham CS. Does amblyopia affect educational, health, and social outcomes? Findings from 1958 British birth cohort. *BMJ* 2006; **332**: 820–5.

479 Solebo AL, Cumberland PM, Rahi JS. Whole-population vision screening in children aged 4-5 years to detect amblyopia. *Lancet* 2015; **385**: 2308–19.

480 Barker DJ, Winter PD, Osmond C, Margetts B, Simmonds SJ. Weight in infancy and death from ischaemic heart disease. *Lancet* 1989; **2**.

481 McCarton CM, Wallace IF, Divon M, Vaughan HG Jr. Cognitive and neurologic development of the premature, small for gestational age infant through age 6: Comparison by birth weight and gestational age. *Pediatrics* 1996; **98**: 1167–78.

482 Low JA, Handley-Derry MH, Burke SO. Association of intrauterine foetal growth retardation and learning deficits at age 9-11 years. *Am J Obstet Gynecol* 1992; **167**: 1499–505.

483 Robertson CM, Etches PC, Kyle JM. Eight-year school performance and growth of preterm, small for gestational age infants: a comparative study with subjects matched for birth weight or for gestational age. *J Pediatr* 1990; **116**: 19–26.

484 Smedler AC, Faxelius G, Bremme K, Lagerström M. Psychological development in children born with very low birth weight after severe intrauterine growth retardation: a 10-year follow-up study. *Acta Paediatr* 1992; **81**: 197–203.

485 Sung I-K, Vohr B, Oh W. Growth and neurodevelopmental outcome of very low birth weight infants with intrauterine growth retardation: Comparison with control subjects matched by birth weight and gestational age. *J Pediatr* 1993; **123**: 618–24.

486 Torp-Pedersen T, Boyd HA, Poulsen G, *et al.* Perinatal risk factors for strabismus. *Int J Epidemiol* 2010; **39**: 1229–39.

487 Lingham G, Mackey DA, Sanfilippo PG, *et al.* Influence of prenatal environment and birth parameters on amblyopia, strabismus, and anisometropia. *J AAPOS* 2020; **24**: 74.e1-74.e7.

488 Chew E, Remaley NA, Tamboli A, Zhao J, Podgor MJ, Klebanoff M. Risk factors for esotropia and exotropia. *Arch Ophthalmol* 1994; **112**: 1349–55.

489 Robaei D, Rose KA, Kifley A, Cosstick M, Ip JM, Mitchell P. Factors associated with childhood strabismus: findings from a population-based study. *Ophthalmology* 2006; **113**: 1146–53.

490 Torp-Pedersen T, Boyd HA, Poulsen G, *et al.* In-utero exposure to smoking, alcohol, coffee, and tea and risk of strabismus. *Am J Epidemiol* 2010; **171**: 868–75.

491 Pathai S, Cumberland PM, Rahi JS. Prevalence of and early-life influences on childhood strabismus: findings from the Millennium Cohort Study. *Arch Pediatr Adolesc Med* 2010; **164**: 250–7.

492 Williams C, Northstone K, Howard M, Harvey I, Harrad RA, Sparrow JM. Prevalence and risk factors for common vision problems in children: data from the ALSPAC study. *Br J Ophthalmol* 2008; **92**: 959–64.

493 de Mendonça ELSS, de Lima Macêna M, Bueno NB, de Oliveira ACM, Mello CS. Premature birth, low birth weight, small for gestational age and chronic non-communicable diseases in adult life: A systematic review with meta-analysis. *Early Hum Dev* 2020; **149**: 105154.

494 Järvelin M-R, Sovio U, King V, *et al.* Early life factors and blood pressure at age 31 years in the 1966 northern Finland birth cohort. *Hypertension* 2004; **44**: 838–46.

495 Tikanmäki M, Tammelin T, Vääräsmäki M, *et al.* Prenatal determinants of physical activity and cardiorespiratory fitness in adolescence – Northern Finland Birth Cohort 1986 study. *BMC Public Health* 2017; **17**. DOI:10.1186/s12889-017-4237-4.

496 Knop MR, Geng T-T, Gorny AW, *et al.* Birth weight and risk of type 2 diabetes mellitus, cardiovascular disease, and hypertension in adults: A meta-analysis of 7 646 267 participants from 135 studies. *J Am Heart Assoc* 2018; **7**: e008870.

497 Curhan GC, Chertow GM, Willett WC, *et al.* Birth weight and adult hypertension and obesity in women. *Circulation* 1996; **94**: 1310–5.

498 Chen W, Srinivasan SR, Yao L, *et al.* Low birth weight is associated with higher blood pressure variability from childhood to young adulthood: the Bogalusa Heart Study. *Am J Epidemiol* 2012; **176 Suppl 7**: S99-105.

499 Beilby J. Definition of Metabolic Syndrome: Report of the National Heart, Lung, and Blood Institute/American Heart Association Conference on Scientific Issues Related to Definition. *Clin Biochem Rev* 2004; **25**: 195–8.

500 Swanson JM. The UK Biobank and selection bias. Lancet. 2012; **380**: 110.

501 Keyes KM, Westreich D. UK Biobank, big data, and the consequences of non-representativeness. *Lancet* 2019; **393**: 1297.

502 Richiardi L, Pizzi C, Pearce N. Commentary: Representativeness is usually not necessary and often should be avoided. Int. J. Epidemiol. 2013; **42**: 1018–22.

503 Fincham JE. Response rates and responsiveness for surveys, standards, and the Journal. Am. J. Pharm. Educ. 2008; **72**: 43.

504 Evans SJ. Good surveys guide. *BMJ* 1991; **302**: 302–3.

505 Batty GD, Gale CR, Kivimäki M, Deary IJ, Bell S. Comparison of risk factor associations in UK Biobank against representative, general population based studies with conventional response rates: prospective cohort study and individual participant meta-analysis. *BMJ* 2020; **368**: m131.

506 Gitsels LA, Cortina-Borja M, Rahi JS. Is amblyopia associated with school readiness and cognitive performance during early schooling? Findings from the Millennium Cohort Study. *PLoS One* 2020; **15**: e0234414.

507 Wilson GA, Welch D. Does amblyopia have a functional impact? Findings from the Dunedin Multidisciplinary Health and Development Study. *Clin Experiment Ophthalmol* 2013; **41**: 127–34.

508 Williams C, Northstone K, Harrad RA, Sparrow JM, Harvey I. ALSPAC Study Team. Amblyopia treatment outcomes after preschool screening v school entry screening: observational data from a prospective cohort study. *Br J Ophthalmol* 2003; **87**: 988–93.

509 Ritland JS, Egge K, Lydersen S, Juul R, Semb SO. Exfoliative glaucoma and primary open-angle glaucoma: associations with death causes and comorbidity. *Acta Ophthalmol Scand* 2004; **82**: 401–4.

510 Newman-Casey PA, Talwar N, Nan B, Musch DC, Stein JD. The relationship between components of metabolic syndrome and open-angle glaucoma. *Ophthalmology* 2011; **118**: 1318–26.

511 Sabanayagam C, Wang JJ, Mitchell P, *et al.* Metabolic syndrome components and age-related cataract: the Singapore Malay eye study. *Invest Ophthalmol Vis Sci* 2011; **52**: 2397–404.

512 Ghaem Maralani H, Tai BC, Wong TY, *et al.* Metabolic syndrome and risk of age-related macular degeneration. *Retina* 2015; **35**: 459–66.

513 Hyman L, Schachat AP, He Q, Leske MC. Hypertension, cardiovascular disease, and age-related macular degeneration. Age-Related Macular Degeneration Risk Factors Study Group. *Arch Ophthalmol* 2000; **118**: 351–8.

514 Younan C, Mitchell P, Cumming R, Rochtchina E, Panchapakesan J, Tumuluri K. Cardiovascular disease, vascular risk factors and the incidence of cataract and cataract surgery: the Blue Mountains Eye Study. *Ophthalmic Epidemiol* 2003; **10**: 227–40.

515 Hrisos S, Clarke MP, Kelly T, Henderson J, Wright CM. Unilateral visual impairment and neurodevelopmental performance in preschool children. *Br J Ophthalmol* 2006; **90**: 836–8.

516 Kelly KR, Jost RM, De La Cruz A, Birch EE. Amblyopic children read more slowly than controls under natural, binocular reading conditions. *J AAPOS* 2015; **19**: 515–20.

517 Stifter E, Burggasser G, Hirmann E, Thaler A, Radner W. Monocular and binocular reading performance in children with microstrabismic amblyopia. *Br J Ophthalmol* 2005; **89**: 1324–9.

518 Kumaran SE, Rakshit A, Hussaindeen JR, Khadka J, Pesudovs K. Does non-strabismic amblyopia affect the quality of life of adults? Findings from a qualitative study. *Ophthalmic Physiol Opt* 2021; **41**: 996–1006.

519 Carlton J, Kaltenthaler E. Health-related quality of life measures (HRQoL) in patients with amblyopia and strabismus: a systematic review. *Br J Ophthalmol* 2011; **95**: 325–30.

520 Barker DJ, Osmond C. Infant mortality, childhood nutrition, and ischaemic heart disease in England and Wales. *Lancet* 1986; **1**: 1077–81.

521 Lee J-Y, Lee S, Park SK. Genetic causal inference between amblyopia and perinatal factors. *Sci Rep* 2022; **12**: 18050.

522 Pineles SL, Demer JL. Bilateral abnormalities of optic nerve size and eye shape in unilateral amblyopia. *Am J Ophthalmol* 2009; **148**: 551-557.e2.

523 Cheung CY, Thomas GN, Tay W, *et al.* Retinal vascular fractal dimension and its relationship with cardiovascular and ocular risk factors. *Am J Ophthalmol* 2012; **154**: 663-674.e1.

524 Cheung CY-L, Ong S, Ikram MK, *et al.* Retinal vascular fractal dimension is associated with cognitive dysfunction. *J Stroke Cerebrovasc Dis* 2014; **23**: 43–50.

525 Ramrattan RS, Wolfs RC, Jonas JB, Hofman A, de Jong PT. Determinants of optic disc characteristics in a general population: The Rotterdam Study. *Ophthalmology* 1999; **106**: 1588–96.

526 Rudnicka AR, Frost C, Owen CG, Edgar DF. Nonlinear behavior of certain optic nerve head parameters and their determinants in normal subjects. *Ophthalmology* 2001; **108**: 2358–68.

527 Tornqvist K, Ericsson A, Källén B. Optic nerve hypoplasia: Risk factors and epidemiology. *Acta Ophthalmol Scand* 2002; **80**: 300–4.

528 Lempert P. Optic disc area and retinal area in amblyopia. *Semin Ophthalmol* 2008; **23**: 302–6.

529 Nixon RB, Helveston EM, Miller K, Archer SM, Ellis FD. Incidence of strabismus in neonates. *Am J Ophthalmol* 1985; **100**: 798–801.

530 Archer SM, Sondhi N, Helveston EM. Strabismus in infancy. *Ophthalmology* 1989; **96**: 133–7.

531 GBD 2019 Dementia Forecasting Collaborators. Estimation of the global prevalence of dementia in 2019 and forecasted prevalence in 2050: an analysis for the Global Burden of Disease Study 2019. *Lancet Public Health* 2022; **7**: e105–25.

532 Dua T, Seeher KM, Sivananthan S, Chowdhary N, Pot AM, Saxena S. [FTS5–03–01]: WORLD HEALTH ORGANIZATION's GLOBAL ACTION PLAN ON THE PUBLIC HEALTH RESPONSE TO DEMENTIA 2017–2025. *Alzheimers Dement* 2017; **13**: P1450–1.

533 Bradford A, Kunik ME, Schulz P, Williams SP, Singh H. Missed and delayed diagnosis of dementia in primary care: prevalence and contributing factors. *Alzheimer Dis Assoc Disord* 2009; **23**: 306–14.

534 Overview | Dementia: assessment, management and support for people living with dementia and their carers | Guidance | NICE. https://www.nice.org.uk/guidance/ng97 (accessed May 31, 2023).

535 Kenne Malaha A, Thébaut C, Achille D, Preux P-M, Guerchet M. Costs of dementia in low- and middle-income countries: A systematic review. *J Alzheimers Dis* 2023; **91**: 115–28.

536 Collins GS, Reitsma JB, Altman DG, Moons KGM, TRIPOD Group. Transparent reporting of a multivariable prediction model for individual prognosis or diagnosis

(TRIPOD): the TRIPOD statement. The TRIPOD Group. *Circulation* 2015; **131**: 211–9.

537 Harrell FE Jr. Regression modeling strategies. Cham, Switzerland: Springer International Publishing, 2016.

538 Durrleman S, Simon R. Flexible regression models with cubic splines. *Stat Med* 1989; **8**: 551–61.

539 Stone CJ. [Generalized Additive Models]: Comment. *Stat Sci* 1986; **1**: 312–4.

540 Resche-Rigon M, White IR. Multiple imputation by chained equations for systematically and sporadically missing multilevel data. *Stat Methods Med Res* 2018; **27**: 1634–49.

541 Enders CK, Mistler SA, Keller BT. Multilevel multiple imputation: A review and evaluation of joint modeling and chained equations imputation. *Psychol Methods* 2016; **21**: 222–40.

542 Lüdtke O, Robitzsch A, Grund S. Multiple imputation of missing data in multilevel designs: A comparison of different strategies. *Psychol Methods* 2017; **22**: 141–65.

543 White IR, Royston P, Wood AM. Multiple imputation using chained equations: Issues and guidance for practice. *Stat Med* 2011; **30**: 377–99.

544 Uno H, Cai T, Pencina MJ, D'Agostino RB, Wei LJ. On the C-statistics for evaluating overall adequacy of risk prediction procedures with censored survival data. *Stat Med* 2011; **30**: 1105–17.

545 Ozenne B, Sørensen A, Scheike T, Torp-Pedersen C, Gerds T. RiskRegression: Predicting the risk of an event using cox regression models. *R J* 2017; **9**: 440.

546 Canty A, Ripley BD. boot: Bootstrap R (S-Plus) Functions. 2022.

547 Alboukadel Kassambara and Marcin Kosinski and Przemyslaw Biecek. survminer: Drawing Survival Curves using "ggplot2." 2021.

548 McLernon DJ, Giardiello D, Van Calster B, *et al.* Assessing performance and clinical usefulness in prediction models with survival outcomes: Practical guidance for Cox proportional hazards models. *Ann Intern Med* 2023; **176**: 105–14.

549 2020 Alzheimer's disease facts and figures. *Alzheimers Dement* 2020; **16**: 391–460.

550 Huemer J, Wagner SK, Sim DA. The evolution of diabetic retinopathy screening programmes: A chronology of retinal photography from 35 mm slides to artificial intelligence. *Clin Ophthalmol* 2020; **14**: 2021–35.

551 Ikram MK, Cheung CY, Lorenzi M, *et al.* Retinal vascular caliber as a biomarker for diabetes microvascular complications. *Diabetes Care* 2013; **36**: 750–9.

552 Klein R, Klein BEK, Moss SE, *et al.* The relation of retinal vessel caliber to the incidence and progression of diabetic retinopathy: XIX: the Wisconsin Epidemiologic Study of Diabetic Retinopathy. *Arch Ophthalmol* 2004; **122**: 76–83.

553 Reinke C, Buchmann N, Fink A, Tegeler C, Demuth I, Doblhammer G. Diabetes duration and the risk of dementia: a cohort study based on German health claims data. *Age Ageing* 2022; **51**. DOI:10.1093/ageing/afab231.

554 Doney ASF, Nar A, Huang Y, *et al.* Retinal vascular measures from diabetes retinal screening photographs and risk of incident dementia in type 2 diabetes: A GoDARTS study. *Front Digit Health* 2022; **4**: 945276.

555 Steyerberg EW, Borsboom GJJM, van Houwelingen HC, Eijkemans MJC, Habbema JDF. Validation and updating of predictive logistic regression models: a study on sample size and shrinkage. *Stat Med* 2004; **23**: 2567–86.

556 Su T-L, Jaki T, Hickey GL, Buchan I, Sperrin M. A review of statistical updating methods for clinical prediction models. *Stat Methods Med Res* 2018; **27**: 185–97.

8. Author contribution statement

Some information in this thesis has been obtained with the help of others; I confirm that any such aid is as indicated below:

- Dr Vasiliki Bountziouka carried out cross-sectional analysis for the physical measurements and biological markers data in section 6.4.
- Mr David Romero-Bascones, Dr Robbert Struyven, Mr Dominic Williamson and Mr Yukun Zhou are computer scientists who extracted features from retinal imaging that were used for analysis in the project.
- Parts of Section 6.3 contributed to my MSc in Epidemiology at the LSTHM. However, that focus was predominantly focused on outer retinal thicknesses, which have not been included in this report. Analyses were also re-run following discussions with collaborators with dental expertise.

9. Appendices

Appendix 1: Search strategies

The following search strategies were performed to inform this report, executed on November 11, 2020, using the MEDLINE (National Library of Medicine) database and updated on April 9th 2023.

Cardiovascular diseases

(cardi* OR myocardi* OR stroke OR CVA) AND (retin*)

(cardio* OR myocardial OR stroke OR CVA OR heart attack) AND (retin* OR fundus) AND (sensitivity OR specificity OR prediction OR validation OR development OR model) AND (calib* OR tortuos* OR fractal*)

Dementia

((dementia[MeSH Terms]) OR (Alzheimer disease[MeSH Terms]) OR (dementia, vascular[MeSH Terms]) OR (dementia, multi infarct[MeSH Terms]) OR (Lewy body disease[MeSH Terms]) OR (mild cognitive impairment[MeSH Terms])) AND ((tomography[MeSH Terms]) AND (tomography, optical coherence[MeSH Terms]))

(dementia OR cognitive OR Alzheimer*) AND (retin*)

(dementia OR cognitive OR Alzheimer*) AND (retin*) AND (sensitivity OR specificity OR prediction OR validation OR development OR model OR prognos*) AND (OCT OR optical coherence)

Appendix 2: Sample size calculation

Sample sizes were calculated for clinical prediction model development using the work of Riley et al[226]. Performance metrics, event numbers and sample size from previous studies were used to inform the estimation[141,237]. Given the emphasis on the AUC measure, which is analogous to the c statistic for binary outcomes, the calculation is convoluted. Further details are given here.

There are limited reports of clinical prediction models using OCT imaging as predictor variables for dementia. The work from Wisely et al demonstrated an AUC of 0.809 (0.700-0.919) when using GC-IPL en-face maps alone, rising to 0.841 (0.739, 0.943) when additionally incorporating patient data and other quantitative metrics from OCTA.

Step 1: Derive Royston's D using the c statistic

$$D = 5.50(C - 0.5) + 10.26(C - 0.5)^3$$

Where c = 0.81[141]

Step 2: Estimate $R^2_{D\_app}$ using D

$$R^2_{D\_app} = \frac{\frac{\pi}{8}D^2}{\frac{\pi^2}{6} + \frac{\pi}{8}D^2}$$

Step 3: Estimate O'Quigley's R^2 using $R^2_{D\_app}$

$$R^2_{O'Quigley\_app} = -\frac{\frac{\pi^2}{6}R^2 D_{app}}{\left(1 - \frac{\pi^2}{6}\right)R^2 D_{app} - 1}$$

Step 4: Estimate the Likelihood Ratio using O'Quigley's R^2 and the number of events (E)

$$LR = -E\ln(1 - R^2_{O'Quigley_{app}})$$

Where E = 62 events

Step 5: Estimate an approximate of the Cox-Snell R^2 value using LR and sample size

$$R^2_{CS_{app}} = 1 - \exp\left(-\frac{LR}{n}\right)$$

Where n = 284

Step 6: The approximate Cox-Snell R^2 can be easily converted to the adjusted Cox-Snell R^2 using the heuristic shrinkage factor of Van Houwelingen (desired = 0.9).

$$R^2_{CS_{adj}} = \frac{R^2_{CSapp}}{S_{VH}}$$

Where S_{VH} = 0.9

Step 7: Finally, the sample size can be estimated using the anticipated number of predictor variables, adjusted Cox-Snell R^2 and heuristic shrinkage factor.

$$n = \frac{p}{(S_{VH} - 1)\ln\left(1 - \frac{R^2_{CSadj}}{S_{VH}}\right)}$$

Appendix 3: Health Research Authority Approval

Ymchwil Iechyd a Gofal Cymru
Health and Care Research Wales

NHS
Health Research Authority

Mr Pearse Keane
NIHR Clinician Scientist
Honorary Consultant Ophthalmologist
University College London
Moorfields Eye Hospital NHS Foundation Trust
162 City Road
London EC1V 2PD

Email: hra.approval@nhs.net
Research.permissions@wales.nhs.uk

13 September 2018

Dear Mr Keane,

HRA and Health and Care Research Wales (HCRW) Approval Letter

Study title:	**Detection Dementia from Retinal Morphology: a Big Data Machine Learning based Retrospective Case-Control Study**
IRAS project ID:	**233974**
REC reference:	**18/LO/1163**
Sponsor:	**Moorfields Eye Hospital NHS Foundation Trust**

I am pleased to confirm that **HRA and Health and Care Research Wales (HCRW) Approval** has been given for the above referenced study, on the basis described in the application form, protocol, supporting documentation and any clarifications received. You should not expect to receive anything further relating to this application.

How should I continue to work with participating NHS organisations in England and Wales?
You should now provide a copy of this letter to all participating NHS organisations in England and Wales, as well as any documentation that has been updated as a result of the assessment.

This is a single site study sponsored by the site. The sponsor R&D office will confirm to you when the study can start following issue of HRA and HCRW Approval.

It is important that you involve both the research management function (e.g. R&D office) supporting each organisation and the local research team (where there is one) in setting up your study. Contact details of the research management function for each organisation can be accessed here.

How should I work with participating NHS/HSC organisations in Northern Ireland and Scotland?
HRA and HCRW Approval does not apply to NHS/HSC organisations within the devolved administrations of Northern Ireland and Scotland.

Appendix 4: Confidential Advisory Group recommendation

Health Research Authority

Skipton House
80 London Road
London
SE1 6LH

Telephone: 0207 972 2557
Email: hra.cag@nhs.net

13 September 2018

Mr Pearse Keane
Moorfields Eye Hospital NHS Foundation Trust
Moorfields Eye Hospital
162 City Road
London
EC1V2PD

Dear Mr Keane

Application title:	**Detection Dementia from Retinal Morphology: a Big Data Machine Learning based Retrospective Case-Control Study**
CAG reference:	**18/CAG/0111**
IRAS project ID:	**233974**
REC reference:	**18/LO/1163**

Thank you for your research application, submitted for approval under Regulation 5 of the Health Service (Control of Patient Information) Regulations 2002 to process patient identifiable information without consent. Approved applications enable the data controller to provide specified information to the applicant for the purposes of the relevant activity, without being in breach of the common law duty of confidentiality, although other relevant legislative provisions will still be applicable.

The role of the Confidentiality Advisory Group (CAG) is to review applications submitted under these Regulations and to provide advice to the Health Research Authority on whether an application should be approved, and if so, any relevant conditions. This application was considered at the CAG meeting held on 05 July 2018. The response to the provisionally supported outcome was considered by a Sub-Committee of the main CAG in correspondence.

Health Research Authority decision

The Health Research Authority, having considered the advice from the Confidentiality Advisory Group as set out below, has determined the following:

1. The application is conditionally approved, subject to compliance with the standard and specific conditions of approval outlined below.

Please note that the legal basis to allow access to the specified confidential patient information without consent is now in effect.

This outcome should be read in conjunction with the letter dated 19 July 2018.

Appendix 5: Research Ethics Committee Recommendation

NHS
Health Research Authority

London - Central Research Ethics Committee
3rd Floor, Barlow House
4 Minshull Street
Manchester
M1 3DZ

Telephone: 0207 1048 007

Please note: This is the favourable opinion of the REC only and does not allow you to start your study at NHS sites in England until you receive HRA Approval

01 August 2018

Mr Pearse Keane, NIHR Clinician Scientist and Honorary Consultant Ophthalmologist
NIHR Biomedical Resource Centre
Moorfields Eye Hospital NHS Foundation Trust
162 City Road, London
EC1V 2PD

Dear Mr Keane

Study title:	**Detection Dementia from Retinal Morphology: a Big Data Machine Learning based Retrospective Case-Control Study**
REC reference:	**18/LO/1163**
IRAS project ID:	**233974**

The Research Ethics Committee reviewed the above application at the meeting held on 25 July 2018. Thank you for attending the meeting with your colleagues to discuss the application.

We plan to publish your research summary wording for the above study on the HRA website, together with your contact details. Publication will be no earlier than three months from the date of this favourable opinion letter. The expectation is that this information will be published for all studies that receive an ethical opinion but should you wish to provide a substitute contact point, wish to make a request to defer, or require further information, please contact hra.studyregistration@nhs.net outlining the reasons for your request.Under very limited circumstances (e.g. for student research which has received an unfavourable opinion), it may be possible to grant an exemption to the publication of the study.

Appendix 6: PPIE survey

Results: Survey on the acceptable use of anonymised patient data

---

Survey open: 28.10.17 to 13.11.17
Total number of people approached: 483 (388 by email; 95 by post)
Total number of responses: 102 (71 online; 31 by post); 21%

Summary:

On the whole the response was positive. The few caveats were:

- People were more likely to prefer consent when data specifically referred to the individual rather than a population.
- Data leakages and the insurance of this not happening.
- The purpose of use and the meaning of the study outcomes raised some questions.

Q1. Would you be happy for a scan of your eye, taken as part of a routine or emergency hospital appointment, to later be used anonymously for research purposes?

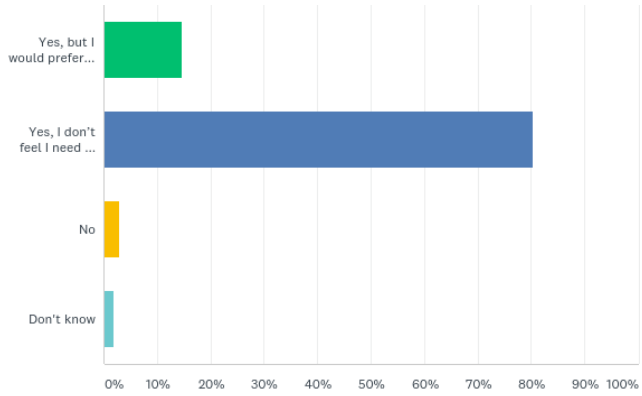

ANSWER CHOICES	RESPONSES	
Yes, but I would prefer to give consent	14.71%	15
Yes, I don't feel I need to consent to this	80.39%	82
No	2.94%	3
Don't know	1.96%	2
TOTAL		102

Q2. If a friend/family member was unable to give consent for themselves, either because they did not have the capacity to do so or they were deceased, would you be happy for a past eye scan of theirs to be used anonymously for research purposes?

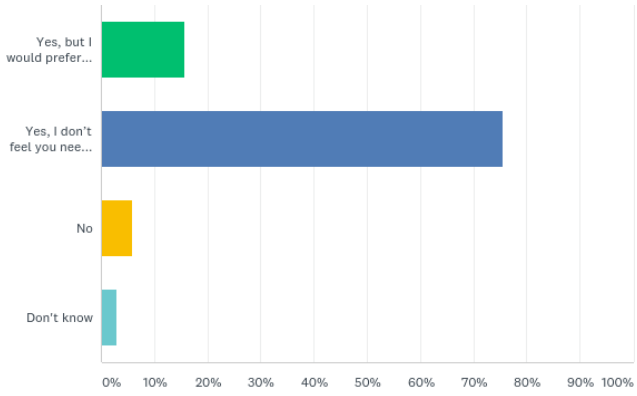

ANSWER CHOICES	RESPONSES	
Yes, but I would prefer it if someone was asked to consent to this	15.69%	16
Yes, I don't feel you need consent for this	75.49%	77
No	5.88%	6
Don't know	2.94%	3
TOTAL		102

Q3. In areas where we have large sets of patient data on file, do you think it is acceptable for us to anonymise this data and use it, without having patient consent, to search for patterns in diseases that in the future may help us with the diagnosis, management and treatment of disease?

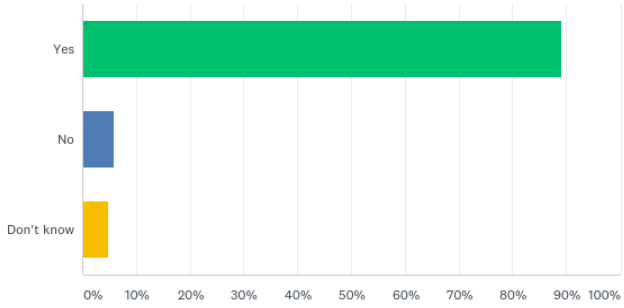

ANSWER CHOICES	RESPONSES	
Yes	89.22%	91
No	5.88%	6
Don't know	4.90%	5
TOTAL		102

Q4. Do you have any further thoughts you would like to share with us?

Total number of responses relevant to the survey: 42; 41%

- 27 (64%) people commented positively on the use of anonymised patient data without consent.
- 5 (12%) people made positive comments but raised additional concerns:
    - Potential for data to be passed to third parties eg; insurance companies or pharma
    - Can consent for this type of research not be taken as standard during clinical data collection.
    - Happy for one's own data to be used but not comfortable speaking for others.
- 5 (12%) were against.
    - Should get consent at time of data collection.
    - Concerns over data leaks and true anonymisation.
    - Taking away freedom of choice, particularly when people are vulnerable.

- Because the survey is not study specific, questions around data protection and anonymisation were raised along with the purpose of use and the meaning of the study outcomes.

Q5. Would you be happy to be contacted in the future to discuss this topic in more detail? If so, please provide your name and contact information below. We will remove this information before we collate the results of this survey.

Total number of responses: 79 (78%)

Appendix

Context given for the survey:

The eye and the brain contain many of the same types of cells and tissues and therefore degenerate in a similar way. Several studies have now demonstrated that changes occur in the eyes of patients a number of years before the brain shows signs of change.

Over the last 10 years at Moorfields Eye Hospital we have collected a database of over 2 million high quality eye scans from 200,000 patients. Researchers at Moorfields would like to analyse these 2 million images to determine if we can identify any features in these eye scans which are common to people who have gone on to develop a neurodegenerative condition but are absent in the scans of those who have not. Researchers plan to match scans to hospital patient records to determine which belong to people who went on to develop a neurodegenerative condition. After this step, as we are only seeking to establish patterns within scans at this stage of research many years after the scans were taken, scans will be anonymised so it will be impossible to know who they came from.

Due to the large number of scans researchers need to use for this study and because some of the scans will be from patients who perhaps are now deceased or have advanced neurodegenerative disease, it will not be possible to seek consent to use people's eye scan data.

We would like to know your thoughts around using people's anonymised data for research. We would be grateful if you could take a few minutes to answer some short questions. Your responses will be anonymised.

Appendix 7: Propensity-matching quality for retinal artery occlusion

CENTRAL RETINAL ARTERY OCCLUSION (N=190)

	Cases (n=190)	Pre-match controls (n=347,353)				Post-match controls (n=760)			
	Mean/prop	**Mean/prop**	**SMD**	**Variance ratio**	**eCDF mean**	**Mean/prop**	**SMD**	**Variance ratio**	**eCDF mean**
AGE	68.7	61.6	0.57	0.82	0.12	69.7	-0.08	1.01	0.02
FEMALE SEX	0.36	0.54	-0.38	*	0.18	0.39	-0.08	*	0.04
HYPERTENSION	0.59	0.43	0.34	*	0.17	0.59	0.01	*	0.01
DIABETES MELLITUS	0.22	0.20	0.05	*	0.02	0.24	-0.05	*	0.02

BRANCH RETINAL ARTERY OCCLUSION

	Cases (n=178)	Pre-match controls (n=347,366)				Post-match controls (n=712)			
	Mean/prop	**Mean/prop**	**SMD**	**Variance ratio**	**eCDF mean**	**Mean/prop**	**SMD**	**Variance ratio**	**eCDF mean**
AGE	67.9	61.6	0.48	0.93	0.10	67.2	0.05	1.02	0.01
FEMALE SEX	0.34	0.54	-0.42	*	0.20	0.35	-0.01	*	0.01
HYPERTENSION	0.53	0.43	0.21	*	0.10	0.46	0.14	*	0.07
DIABETES MELLITUS	0.13	0.20	-0.19	*	0.06	0.08	0.17	*	0.06

TRANSIENT MONOCULAR VISUAL LOSS

	Cases (n=205)	Pre-match controls (n=347,339)				Post-match controls (n=820)			
	Mean/prop	**Mean/prop**	**SMD**	**Variance ratio**	**eCDF mean**	**Mean/prop**	**SMD**	**Variance ratio**	**eCDF mean**
AGE	68.3	61.6	0.53	0.83	0.11	67.9	0.03	0.99	0.01
FEMALE SEX	0.53	0.54	-0.02		0.01	0.55	-0.03		0.01
HYPERTENSION	0.52	0.43	0.18		0.09	0.56	-0.08		0.04
DIABETES MELLITUS	0.16	0.20	-0.12		0.04	0.13	0.08		0.03